STRUCTURAL AND SPECTROSCOPIC STUDIES ON CEFALEXIN AND METHYLDOPA USING QUANTUM MECHANICAL METHODS

A THESIS SUBMITTED TO THE

CENTRAL DEPARTMENT OF PHYSICS

INSTITUTE OF SCIENCE AND TECHNOLOGY

TRIBHUVAN UNIVERSITY

NEPAL

FOR THE AWARD OF

DOCTOR OF PHILOSOPHY

IN PHYSICS

BY

TARUN CHAUDHARY

JANUARY 2024

STRUCTURAL AND SPECTROSCOPIC STUDIES ON CEFALEXIN AND METHYLDOPA USING QUANTUM MECHANICAL METHODS

A THESIS SUBMITTED TO THE

CENTRAL DEPARTMENT OF PHYSICS

INSTITUTE OF SCIENCE AND TECHNOLOGY

TRIBHUVAN UNIVERSITY

NEPAL

FOR THE AWARD OF

DOCTOR OF PHILOSOPHY

IN PHYSICS

BY

TARUN CHAUDHARY

JANUARY 2024

TRIBHUVAN UNIVERSITY

Institute of Science and Technology

DEAN'S OFFICE

Kirtipur, Kathmandu, Nepal

Reference No.:

Institute of Science & Technology
Dean's Office
Kirtipur 2045

EXTERNAL EXAMINERS

The Title of Ph.D. Thesis: "Structural and spectroscopic studies on cefalexin and methyldopa using quantum mechanical methods "

Name of Candidate: Tarun Chaudhary

External Examiners:

(1) Prof. Dr. Rajendra Parajuli
Amrit Campus
Tribhuvan University, NEPAL

(2) Prof. Dr. Archana Gupta
M.J.P. Rohilkhand University
Bareilly, INDIA

(3) Prof. Dr. Alejandro Pecro Ayala
Federal University of Ceara
Fortaleza, BRAZIL

January 29, 2024

(Dr. Surendra Kumar Gautam)
Asst. Dean

DECLARATION

Thesis entitled **"STRUCTURAL AND SPECTROSCOPIC STUDIES ON CEFALEXIN AND METHYLDOPA USING QUANTUM MECHANICAL METHODS"** which is being submitted to the Central Department of Physics, Institute of Science and Technology (IOST), Tribhuvan University, Nepal for the award of the degree of Doctor of Philosophy (Ph.D.), is a research work carried out by me under the supervision of Prof. Dr. Bhawani Datt Joshi, Department of Physics, Siddhanath Science Campus, Tribhuvan University, Mahendranagar, Nepal.

This research is original and has not been submitted earlier in part or full in this or any other form to any university or institute, here or elsewhere, for the award of any degree.

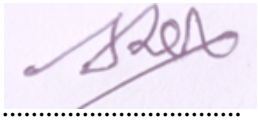

.....

Tarun Chaudhary

RECOMMENDATION

This is to recommend that **Mr. Tarun Chaudhary** has carried out research entitled **"STRUCTURAL AND SPECTROSCOPIC STUDIES ON CEFALEXIN AND METHYLDOPA USING QUANTUM MECHANICAL METHODS"** for the award of Doctor of Philosophy (Ph.D.) in **Physics** under my supervision. In my knowledge, this work has not been submitted for any other degree.

He has fulfilled all the requirements laid down by the Institute of Science and Technology (IOST), Tribhuvan University, Kirtipur for the submission of the thesis for the award of Ph.D. degree.

. . . . . .

Dr. Bhawani Datt Joshi
Supervisor
(Professor)
Department of Physics
Siddhanath Science Campus
Tribhuvan University
Mahendranagar, Nepal

JULY 2023

TRIBHUVAN UNIVERSITY
CENTRAL DEPARTMENT OF PHYSICS
Kirtipur, Kathmandu, Nepal

☎ 4331054
www.tucdp.edu.np

Ref. No.: (F. No ... .) CDP ..... Date: .....

LETTER OF APPROVAL

[Date: 14/07/2023]

On the recommendation of Prof. Dr. **Bhawani Datt Joshi**, Department of Physics, Siddhanath Science Campus, Tribhuvan University, Mahendranagar, Nepal, this Ph.D. thesis submitted by **Tarun Chaudhary**, entitled **"STRUCTURAL AND SPECTROSCOPIC STUDIES ON CEFALEXIN AND METHYLDOPA USING QUANTUM MECHANICAL METHODS"** is forwarded by Central Department Research Committee (CDRC) to the Dean, IOST, T.U.

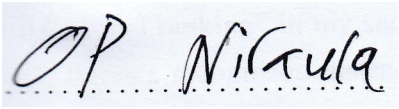

Dr. Om Prakash Niraula
Professor
Head
Central Department of Physics
Tribhuvan University
Kirtipur, Kathmandu
Nepal

ACKNOWLEDGMENTS

I would like to express my sincere gratitude to my supervisor, Prof. Dr. Bhawani Datt Joshi, for providing me with invaluable guidance to complete the research work. Also, I would like to extend my sincere gratitude to Prof. Dr. Om Prakash Niraula, the head of the Central Department of Physics (CDP),CDRC members as well as the entire CDP family for their encouragement and assistance.

I am greatly indebted to Prof. Dr. Narayan Prasad Adhikari, Prof. Dr. Binil Aryal, Dean of IOST, Tribhuvan University, Prof. Dr. Raju Khanal, Prof. Dr. Ishwar Koirala, Dr. Bal Ram Ghimire, Prof. Dr. H. Lamichhane, Dr. H. S. Mallik Dr. Gopi Chandra Kaphle for their profound inspiration and encouragement.

Further, I would like to convey my heartfelt appreciation to Prof. Dr. Ragnar Fjelland (University of Bergen, Norway), Prof. Dr. Shankar Pd. Khanal, Prof. Dr. Srijan Lal Shrestha, and Assoc. Prof. Dr. Chitra Bd. Baniya for providing philosophical ideas and approaches to research.

I sincerely acknowledge Prof. Dr. Poonam Tandon, Dean (student' welfare) and former HoD, Department of Physics, Lucknow University, India, for providing software facilities, including the Gaussian 09 program. I would like to extend my heartfelt gratitude to Prof. Alejandro Pedro Ayala, UFC, Brazil, Dr. Maria Silmara Alves de Santana and Prof. Dr. Sudha Jain, University of Lucknow, for their essential assistance.

My sincere thank goes to Dr. Manoj Kumar Chaudhary, Dr. Karthick Thangavel, Dr. Dinesh Chaudhary, Dr. Suresh Basnet, Dr. Amba Datt Pant, Dr. Saran Lamichhane, Mr. Prakash M. Shrestha, Mrs. Usha Joshi, Mr. Bhim Singh Thagunna, Mrs. Nepal Ramadevi, Mr. Tirth Paneru, Mr. Devendra Raj Upadhyay and well-wishers for their invaluable assistance and my friends for their valuable cooperation.

Ultimately, I would like to thank my family members for their support and encouragements. Special thanks to my parents, wife Sharmila Kumari Tharu and son Sriyan Tharu for their supports and patience during whole period.

Tarun Chaudhary
JULY, 2023

ABSTRACT

The spectroscopic characteristics, conformational stability, electronic and biological activity of cefalexin and methyldopa have been investigated using quantum mechanical techniques. The density functional theory (DFT) at the B3LYP/ 6-311++G(d,p) level was utilized to optimize the molecules and explore their vibrational properties. The intramolecular and intermolecular hydrogen bonding in cefalexin has been discussed in terms of IR and Raman spectra. Additionally, the quantum theory of atoms in molecules (QTAIM) was used to predict the nature of hydrogen bonds. Similarly, determining vibrational properties, the presence of hydrogen bond interactions in methyldopa has been scrutinized more precisely, using QTAIM and the reduced density gradient (RDG) in monomer and dimer form. On the basis of electron localization function (ELF), the electron localized region and the delocalized region have been depicted. The Molecular electrostatic potential (MEP) has been used to describe the charge distribution around the molecules. From the MEP map, the electrophilic and nucleophilic sites were anticipated. The energy of the lowest unoccupied molecular orbital, E_{LUMO} the highest occupied molecular orbital energy, E_{HOMO}, and their energy gap ($\triangle E$) have been used to examine the chemical stability of the molecules. Furthermore, the nature of chemical reactivity, the energy gap, global, and local reactivity characteristics were established. Natural bond orbital (NBO) analysis was carried out to determine the stabilization energy due to charge delocalization between the bonding and antibonding. The relation of standard thermodynamic parameters like heat capacity, enthalpy and entropy with temperature has been studied. Ultimately, a molecular docking simulation has been performed to study the biological activities of the molecules. The binding activity of cefalexin with the protein matrix carbonic anhydrase II and leukotriene A-4 hydrolase was predicted from molecular docking approach. Similarly, the binding activity of ligand methyldopa with protein Lysine-specific demethylase 4D-like was performed.

सार

सेफेलेक्सिन र मेथाइलडोपाका स्पेक्ट्रोस्कोपिक स्वरुपहरु, संरचनात्मक स्थिरता, इलेक्ट्रोनिक र जैविक गतिविधि, क्वान्टम मेकानिकल विधि प्रयोग गरेर अनुसन्धान गरिएको छ। अणुहरूलाई अप्टिमाइज गर्न र तिनीहरूको भाइब्रेशनल गुणहरु अन्वेषण गर्न B3LYP/6-311++G(d,p)/Density Functional Theory (DFT) प्रयोग गरिएको थियो। सेफेलेक्सिनको IR र Raman स्पेक्ट्राका आधारमा इन्ट्रामोलिक्युलर र इन्टरमोलिक्युलर हाइड्रोजन बन्डको व्याख्या गरिएकोछ। । साथै, क्वान्टम थ्योरि अफ एटम्स इन मोलिकुल्स (QTAIM) विधि प्रयोग गरि हाइड्रोजन बन्डको प्रकृतिको बारे प्रस्तुत गरिएकोछ। त्यसै गरी, मेथाइलडोपाको मोनोमर र डाइमर संरचनाका भाइब्रेशनल गुणहरु निर्धारण गरि, हाइड्रोजन बन्डलाई QTAIM र रिडिउस्ड डेनसिटी ग्राफ (RDG) को प्रयोग गरेर थप सटीक रूपमा अध्ययन गरिएको थियो। इलेक्ट्रोन लोकलाइजेसन फंक्सन (ELF) को आधारमा, इलेक्ट्रोन लोकलाइज्ड क्षेत्र र डीलोकलाइज्ड क्षेत्रलाई चित्रण गरिएको छ। मोलिकुलर इलेक्ट्रोस्टेटिक पोटेन्सिअल (MEP) मार्फत अणुहरू वरपर रहेको चार्ज वितरणको अवस्थालाई ब्याख्या गरिएको छ । MEP को सहयोगले, इलेक्ट्रोफिलिक र न्यूक्लियोफिलिक साइटहरू पत्ता लगाइएको छ। लोयस्ट अनअकुपाइड मोलिकुलर अर्बिटल इनर्जी (E_{LUMO}), हाइयस्ट अकुपाइड मोलिकुलर अर्बिटल इनर्जी (E_{HOMO}) र तिनीहरूको इनर्जी ग्याप प्रयोग गरि अणुहरूको रासायनिक स्थिरता जाँच गरिएको छ। यसबाहेक, रासायनिक प्रतिक्रियाशीलताको प्रकृति, इनर्जी ग्याप (ΔE), ग्लोबल र लोकल रियाक्तिभिटीका विशेषताहरू स्थापित गरियो। बन्डिङ र एन्टिबन्डिङ बीचको चार्ज डीलोकलाइजेशनको कारणले हुने इस्त्याविलाइजेसन इनर्जी को निर्धारण गर्न नेचुरल बन्ड अर्बिटल (NBO) को विश्लेषण गरिएको थियो। ताप क्षमता, एन्थाल्पी र एन्ट्रोपी जस्ता मानक थर्मोडायनामिक प्यारामिटरहरूको तापक्रमसँगको सम्बन्धको अध्ययन गरिएको छ । अन्ततः अणुहरूको जैविक गतिविधिहरु अध्ययन गर्न मोलिकुलर डकिङ्ग सिमुलेशनको प्रयोग गरिएको थियो। सेफेलेक्सिनको प्रोटिन म्याट्रिक्स कार्बोनिक एनहाइड्रेस-II र ल्युकोट्रिन A-4 हाइड्रोलेजसँगको बाइन्डिंग गतिविधि, मोलिकुलर डकिङ्ग विधि बाट अनुसन्धान गरिएको थियो। त्यस्तै, मेथाइलडोपाको जैविक गतिविधिहरु प्रोटीन लाइसिन-स्पेशिफिक डेमेथाइलेज 4D-लाइकसँग प्रस्तुत गरिएको छ ।

LIST OF ACRONYMS AND ABBREVIATIONS

AIM	Atoms in molecule
BCP	Bond critical point
BLYP	Becke-Lee-Yang-Parr
BOA	Born-Oppenheimer approximation
BSSE	Basis-set-superimposition error
CC	Crystalline cephalexin
CGTO	Contracted Gaussian Type Orbitals
DALY	Disability-adjusted life years
DFT	Density functional theory
DOS	Density of states
DMSO	Dimethylsulphide
CT	Charge transfer
ELF	Electron localization function
FF	Fukai function
FMO	Frontier molecular orbital
FT-IR	Fourier transform infra-red
FT-Raman	Fourier transform Raman
GGA	Generalized gradient approximation
GTO	Gaussian-type orbital
H-F	Hartree-Fock
HOMO	Highest occupied molecular orbital
HSA	Human serum albumin
IR	Infra-red
K-S	Kohan–Sham
K. E.	Kinetic energy
LCAO	Linear combination of atomic orbitals
LDA	Local density approximation
LGA	Lamarckian Genetic Algorithm
LP	Lone pair
LOL	Lcalized orbital locator
LUMO	Lowest unoccupied molecular orbital
MEP	Molecular electrostatic potential
MOs	Molecular orbitals
MP	Molar-Plesset
NACP	Nuclear atomic critical point
NBO	Natural bond orbital

NC	Non-crystalline cefalexin
NCI	Non-covalent interation
NIR	Near-infrared
NLO	Non-linear optical
NMR	Nuclear magnetic resonance
OPDS	Overlap population density of states
PDB	Protein data bank
PDOS	Partial density of states
PED	Potential energy distribution
PES	Potential energy surface
QMC	Quantum Monte-Carlo
QTAIM	Quantum theory of atoms in molecule
RMSD	Root mean square deviation
RCP	Ring critical point
RDG	Reduced density graph
SCF	Self consistent field
STO	Slater-type orbital
TD-DFT	Time dependent density functional theory
TDOS	Total density of states
TFD	Thomas-Fermi-Dirac
TU	Tribhuvan University
USA	United States of America
UV	Ultraviolet
WLS	Wavenumber linear scaling
XC	Exchange correlation

LIST OF TABLES

LIST OF FIGURES

TABLE OF CONTENTS

CHAPTER 1

1. INTRODUCTION

The development of a new drug is a lengthy and slow process. It requires several clinical trials, which is the most expensive and difficult process (Low et al., 2020). Thus, fall in the rate of new drug discovery, increasing the resistance of bacteria towards existing drugs and the significant side effects of drug, have led once to think about the study on the structural and chemical properties of bioactive molecules. The information about natural products as well as existing drugs would be helpful for exploring their novel therapeutic indications. Thus, we have conducted the study on some of the bioactive compounds to explore their possible conformations, optimized energy, electronic, thermal, chemical, and biological properties employing various experimental, and theoretical techniques. The vibrational properties of the compounds were analyzed using FT-IR and FT-Raman spectroscopy and quantum mechanical methods. The bioactive compounds are the secondary metabolites of plants that have biological effects like pharmacological and toxicological effects in humans as well as in animals (Bernhoft, 2010). Initially, the plants were used for sustenance, but as their medicinal properties were discovered, many different human societies began to exploit this natural flora for treating several diseases and health problems (Azmir et al., 2013). The most of the natural products are known for their antibacterial and antitumor properties and hence, they are the sources of modern drug development (Veeresham, 2012). Additionally, organic compounds show remarkable non-linear optical characteristics (Kariper, 2017). Thus, the non-linear properties like polarizability, first hyperpolarizability and second hyperpolarizability have also been examined. Furthermore, the cross reactivity of compounds with human proteins were analyzed using molecular docking approaches. In our work, we have mainly focused our study on the drugs: cefalexin and methyldopa.

1.1 Cefalexin

Cefalexin ($C_{16}H_{17}N_3O_4S$) is a first-generation antibacterial cephalosporin antibiotic, introduced in 1967 (Hey, 2007). Chemically, it has been named as [(6R,7R)-7-[(2R)-aminoph enylacetyl]-3-methyl-8-oxo-5-thia-1-azo-bicyclo[4.2.0]oct-2-ene-2-carboxylic

acid]. The chemial structure of cefalexin consists of amine, carbonyl, and carboxyl groups. It is often used to treat infections brought on by infectious agents in the genital and urinary system, upper and lower respiratory tract, skin, soft tissue, bones, and joints, as well as numerous other infections (Speight et al., 1972). It is effective against most gram-positive cocci, penicillinase-producing Staphylococci and a number of gram-negative bacteria, including *Neisseria gonorrhoeae*, *Escherichia coli*, *Proteus mirabilis*, *Shigella*, *Salmonellae* etc. (Bailey et al., 1970). The cefalexin is found to be stable below mild acidic conditions and it is found in a variety of colors, ranging from white to cream-colored crystalline powder (Manelli, 1975). The reported melting point of cefalexin is 326.8°C) (Shinde et al., 2010). Cefalexin does not have any adverse effects on kidney, so it is usable for patients with renal failure (Speight et al., 1972). Cephalosporins are also a useful alternative to those with mild allergic to penicillin (Pichichero, 2006). The chemical structure of cefalexin is depicted in Figure 1.

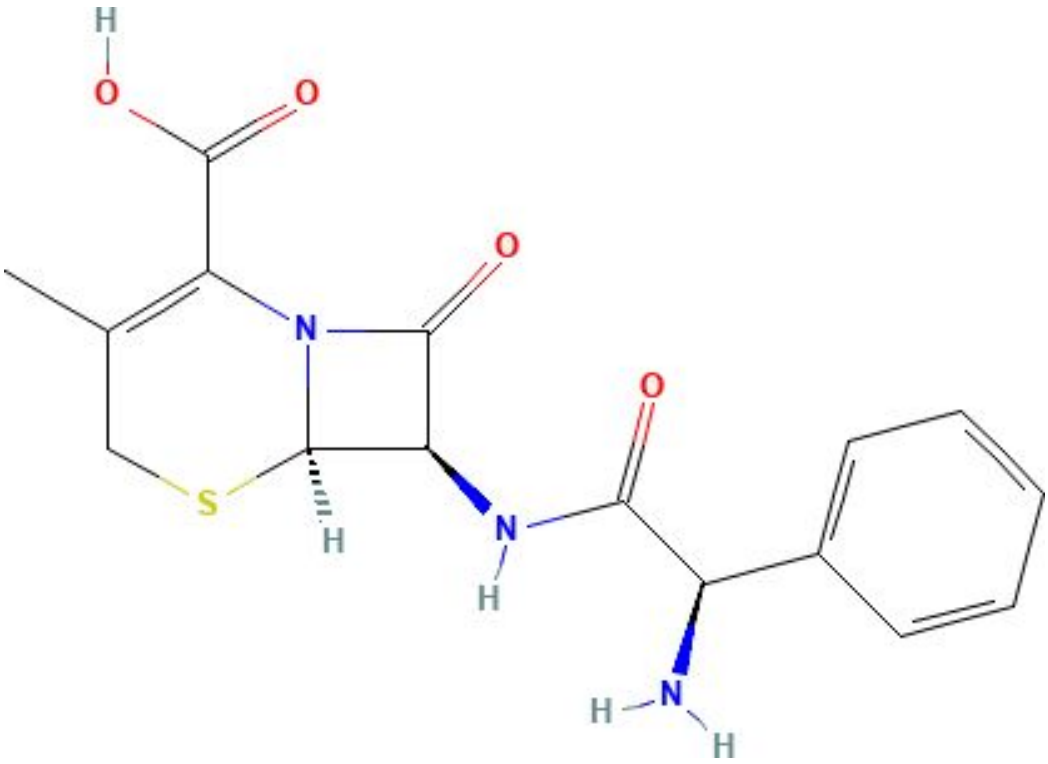

Figure 1: Chemical structure of Cefalexin
(PubChem Compound Database, 2020a)

1.2 Methyldopa

Methyldopa is an antihypertensive drug that has been in practice since 1960s (Mah et al., 2009). It is most often used medication to treat preeclampsia and gestational hypertension (Wiciński et al., 2020). Methyldopa, a catecholamine derivative is a good inhibitor of the enzyme DOPA decarboxylase (Suhuan et al., 2016). It reduces blood pressure by operating through a central mechanism that involves the biotransformation of methyl

norepinephrine (Noei et al., 2017). This medication was initially synthesized from a 3,4-dihydroxyphenylalanine analog, but it can also be synthesized from dimethoxyphenyl-acetonitrile (Prabakaran & Muthu, 2012). The molecular formula of methyldopa is $C_{10}H_{13}NO_4$ and its IUPAC name is (S)-2-amino-3-(3,4-dihydroxyphenyl)-2-methyl-propanoic acid. It contains a variety of functional groups, like as hydroxyl, amine, and carboxylic acids. Methyldopa is highly soluble in dimethyl sulfoxide (DMSO) and acetonitrile (ACN), almost in water and very slightly in solvents like benzene (Sharma et al., 2012). Moreover, methyldopa is seen as a safer medication for a breast-feeding woman to use because it has less adverse effects on infants (Amro et al., 2016). This medication is usually prescribed to patients suffering from heart failure, renal failure, or diabetes (Noei et al., 2017). The chemical structure in two-dimensional of methyldopa is shown in Figure 2.

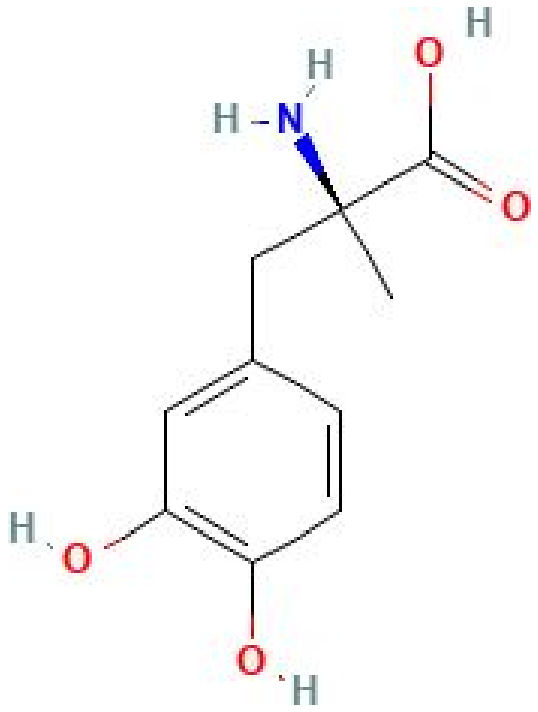

Figure 2: Chemical structure of Methyldopa
(PubChem Compound Database, 2020b)

1.3 Rationale

The majority of nations on earth are developing nations; hence, they have satisfactory health services. Nepal is also a developing country; it lacks trained health workers, public awareness, health facilities, sanitation, etc. Due to this, most people are compelled to live an unhealthy life. Drugs are frequently used in an inappropriate manner and inefficiently at various healthcare centers. Also, the drugs are not used properly by the patients. Consequently, people are facing minor to serious adverse effects of the drugs. Due to the misuse of antibiotics, antibacterial resistance is increasing vig-

orously. Hence, in the present context, we hope our work will assist in enhancing the efficacy of the drugs with the minimum negative impact on people's health. The present work focuses on exploring the detailed structural, chemical, and biological properties of compounds necessary for improving their quality. In addition, molecular docking simulations have been conducted. Using these techniques, the cross-reactivity of molecules with the selected target protein has been determined. This will make studying the toxicity and side effects of drugs easier. Furthermore, clinical research can also be conducted to confirm the novel potentiality of drugs toward the secondary target.

Cefalexin is an essential antibiotic used to treat several bacterial infections (Speight et al., 1972). Despite its important usefulness, it also exhibits side effects (Bailey et al., 1970). The major problem is the increasing resistance of bacteria. Thus, to investigate its biological properties more precisely, the possible stable conformations and electronic properties, reactive sites and the number of hydrogen bonds associated with the molecule were determined. The predicted global and local active and molecular docking studies will further help in developing efficient drugs and a novel inhibitor for the secondary target.

Furthermore, methyldopa is one of the important medications used to treat high blood pressure (Noei et al., 2017). The study has been conducted to explore its essential structural properties (T. Chaudhary et al., 2023). Its biological interaction has been conducted with its most probable targets (T. Chaudhary et al., 2023). This may be helpful in discovering its new therapeutic activity against the secondary target. Moreover, during the interaction of the drug with the receptor protein, the protein may dimerize. In this case, the dimeric drug works better than the monomeric drug. Thus, to obtain the most efficient drug, we have examined the dimeric properties of methyldopa. The dimeric methyldopa was found to be comparatively more active than the monomeric one. Hence, further clinical testing can be used to justify it, so that it will assist in developing a new drug with more enhanced properties. Further, the docking study with the most likely target can also help in exploring the new targets.

In addition to this, certain NLO properties for these organic molecules have been predicted, which are significantly greater than those of the standard molecule, urea. Therefore, these molecules may also be suitable for NLO devices.

1.4 Objective

1.4.1 General Objective

To study structural, spectroscopic, chemical and thermal properties, non-linear properties and biological activities of cefalexin and methyldopa.

1.4.2 Specific Objectives

1. To study structural parameters of the stable conformer.
2. To determine different modes of vibration and NBO analysis.
3. To predict molecular electrostatic potential, electronic transition, hardness of molecule, nucleophilic and electrophilic region, biologically active sites.
4. To study variation of specific heat capacity, enthalpy and entropy with temperature.
5. To study polarizability and hyperpolarizability of molecule.

1.5 Structure of the thesis

The structure of the thesis is as follows:

Chapter 1: Introduction

This chapter includes the introduction of two bioactive active molecules: cefalexin and methyldopa. It also consists of the rationale and the research objectives of the research work.

Chapter 2: Literature Review

This chapter includes the previous works conducted on the molecules, recent trends in the related fields and the research gap.

Chapter 3: Materials and Methods

This chapter includes the details of the experimental and theoretical methods used. It gives a brief introduction to IR and Raman spectroscopy, along with density functional theory. In addition, it includes all quantum mechanical methods and computational tools employed. It explains the methodology that has used to conduct this work.

Chapter 4: Results and Discussion

The result of research work have been included in this chapter. It contains all the estimated important properties of molecules. These findings have been presented in tables, graphs and figures.

Chapter 5: Conclusions and Recommendations

This chapter contains the conclusion as well as a recommendation. It comprises the work's findings and their relevance, as well as its needs and future prsopects.

Chapter 6: Summary

This chapter includes a concise summary of the complete body of research.

CHAPTER 2

2. LITERATURE REVIEW

Delivering safer and more efficient medications is a constant struggle for the pharmaceutical business (Di et al., 2009). Drug discovery initiatives have always prioritized potency over all other factors. The properties of drugs like solubility, metabolic stability, permeability, etc. affect their oral bioavailability, metabolism, toxicity, etc (Di et al., 2009). The drug's action in the body is due to its physico-chemical interactions with proteins, enzymes, DNA, etc., where weak interactions like H-bonding, charge-transfer, hydrophobic interactions, and van der Waals forces are responsible for the formation of the drug-receptor complex (Sharma et al., 2012). Several research has been conducted over the last few decades to improve the structural, thermodynamic, chemical, and biological properties of biologically active molecules to enhance drug potential and reposition of drugs. Additionally, organic materials are more feasible for numerous design features like ultrafast responsiveness, high damage threshold, strong nonlinear behavior, and ease of producing large-sized crystals (R. Kumar et al., 2018). Over the last few decades, fundamental and applied research have been continuously used to identify novel materials with improved nonlinear optical properties (Christodoulides et al., 2010). Renjith et al. (2013) calculated the first hyperpolarizabiity, observed IR and Raman spectra, and hardness of Pyrrole. A. Srivastava et al. (2017) studied the structural and spectroscopic behavior of an alkaloid, piplartine like as molecular conformation and vibrational spectroscopy of the molecule using DFT and analyzed its anti-cancer activity. Shweta et al. (2017) performed a detailed study on the natural product cearine, which is widely used as a local anti-inflammatory, antibiotic, and antiallergic substance. Also, over the years, lots of research work has been conducted in the study of dimeric molecules. Karabacak et al. (2012) investigated the structural and vibrational properties of monomeric and dimeric form of 2-aminonicotinic acid. The thermal properties, charge distribution, and hyperpolarizability of 2-[(2-hydroxyphenyl) carbonyloxy] benzoic acid have been reported (S. Muthu & Paulraj, 2013a). The ground-state optimized structure, and vibrational spectra of 3-thiophenecarboxylic acid were determined using DFT/B3LYP/6-311G(d,p) (Issaoui et al., 2015). Issaoui et al. (2017) used experimental

and theoretical methods to explore the inhibitory activity of 3-(2-thienyl) acrylic acid. The dimeric arylsulfonamides were investigated for their potential to inhibit the metalloproteinase ADAM8 (Cuffaro et al., 2021). Bioactive compounds' dimers frequently exhibit more activity than the monomeric unit (Bérubé, 2006). It was found that when medicine interacts with a biological target; many of the targets dimerize (Paquin et al., 2021). Thus, it was thought that a dimer that could interact with such targets could elicit a more potent biological response than the parent medication (Paquin et al., 2021). A dimeric drug could fit two separate binding sites on a receptor molecule, resulting in a stronger thermodynamic connection than that attained by attaching two monomeric medicines (Paquin et al., 2021).

During the past 30 years, several laboratory and clinical study of antibiotics, mainly the β-lactam- containing group (penicillins and cephalosporins) have been pursued vigorously (Hou & Poole, 1971). Anacona & Rodriguez (2004) tested the effectiveness of cefalexin alone and its complexes with transition d^{10} metal ions. It was found that the bacterial enzyme metallo-β lactamase (MβLs) catalyses the hydrolic cleavage of the four-membered β-lactam ring of antibiotics, which makes the antibiotic inactive (Ghiasi et al., 2017). Thus, increasing antibacterial resistance has been a threat to the public health of the whole world. So, the recent work is focused on antibiotics. Similarly, the electronic and spectroscopic properties of antibiotics like amoxicillin, ampicillin, cefradoxil and cefradine were investigated (Kariper, 2017; K. Muthu et al., 2015; M. K. Chaudhary et al., 2021). Shahabadi et al. (2018) investigated the binding activity of a platinum(II)-cefalexin complex with human serum albumin (HSA), discovering that hydrogen bonds, Van der Waals forces, and electrostatic interactions were mostly responsible for the complex's stability.

Furthermore, by Otsuka & Kaneniwa (1983a) investigated degree of crystallinity of cefalexin powder during grinding was investigated using X-ray diffraction. The research work shows that the solubility of non-crystalline cefalexin (NC) is six times more soluble than the crystalline cefalexin (CC) solid at 10 degrees Celsius in distilled water. The solubility of NC at 10,15 and 20° C were determined to be 59.9 mg/ml, 54.4mg/ml and 49.2mg/ml respectively and solubility of CC at 10,15, 20, 25 and 35 was almost the same (Otsuka & Kaneniwa, 1983b). The elastic properties of cefalexin were studied by N. Kaneniwa, including two more authers and it was found that the elastic behavior appears on high–pressure compression of cefalexin powder (Kaneniwa et al., 1984). Aguiar (2011) identified cefalexin monohydrate as the most common polymorph. They investigated different crystalline properties in different medicines by analyzing X-ray powder diffraction, FTIR and solid state NMR studies. On the basis of NIR spectroscopy study of cefalexin during grinding shows that the intermolecular hydrogen bonds between the amino and carboxyl groups are destroyed and the crystals are changed to amorphous

(Aguiar et al., 2011). This proves that compression destroys the crystalline structure of cefalexin. In the literature, however several physicochemical properties of cefalexin have been computed, but very few works on its structural properties, conformational stability and biological properties have been performed.

According to the report of world health of 2002, hypertension is a major risk factor for heart disease and stroke, which are the leading causes of mortality worldwide (Chockalingam et al., 2006). Hypertension is the third biggest factor for the disability-adjusted life years (DALY) (Chockalingam et al., 2006; Rodgers et al., 2004). Methyldopa is one of the popular medications that has been used since 1960s to control hypertension (Mah et al., 2009). Methyldopa, however, can treat hypertension effectively, it has some minor to severe adverse effects like impairment of renal function, depression, sedation, and bad dreams (Adler, 1974; Rodman et al., 1976; Toghill et al., 1974).

In the literature, a wide range of theoretical and experimental investigations have been done on the biologically active molecule, methyldopa. Methyldopa is a bioactive substance that can bind with MHC class II antigens, which makes it useful in treating autoimmune diabetes (Ostrov et al., 2018). In addition to this, an NMR study was performed and its structural properties were studied using quantum mechanics (Noei et al., 2017). The charge-transfer characteristics of methyldopa with acceptors such as o-chloranil (o-ClN), chloranilic acid (Ostrov et al., 2018). The comparative study of monomer and dimer on the basis of molecular, electronic and biological properties, the occurrence of intermolecular hydrogen bonds between monomers and their implications for chemical and biological processes, however, have not been studied. Consequently, research into the methyldopa dimer is still interesting.

Research Gap

The literature review reveals a number of studies on pharmaceutical properties and a few on structure-based chemical properties of cefalexin and methyldopa. However, there are several important properties that remain undiscussed. Like the structural properties, they need to be evaluated in detail so that they can be useful in determining the therapeutic behaviour and designing effective drugs. At present, detailed research has been conducted on the structural, chemical, and biological properties of the molecules. Also, to obtain a more actual and reliable result, the higher basis set, consisting of both the diffuse and polarisation functions, was used for the computation of molecular properties. The possible conformations and their stability at normal temperatures were investigated using a one-dimensional potential scan surface. The hydrogen bond interactions in the molecular system have been predicted using various techniques. In addition to this, molecular and chemical stability, vibrational spectra, local and global reactivity, and thermal properties have been discussed. The stabilisation of the molecular system due to the interactions between donor and acceptor groups has been examined in NBO

analysis. The charge concentration in the molecule has been visualised using ELF plots. The values of polarizabilty and hyperpolarizabilty of the molecules were estimated. The interaction of molecules with target proteins has been examined. Ultimately, the bilogically reactive sites were discovered. This study will serve as a fundamental prerequisite for the design of new drugs or the development of drugs with enhanced pharmaceutical properties.

CHAPTER 3

3. MATERIALS AND METHODS

3.1 Introduction

In the field of medicine, knowledge of an active pharmaceutical ingredient's structural, chemical, and biological properties is crucial. Thus, in order to investigate the various properties like optimized energy, stable conformation, different modes of vibration, intramolecular hydrogen bonding, chemically active sites, etc., experimental and quantum mechanical methods have been employed. The functional groups and intramolecular hydrogen bonding were identified using the infrared (IR) and Raman spectra. For an insightful study of molecules at a microscopic level, quantum chemical calculations have been performed using a popular approach, density functional theory (DFT/B3LYP). Also, molecular docking approaches were used to explore the cross-reactivity of the drugs (cefalexin and methyldopa) with the secondary targets.

3.2 Experimental technique

The vibrational spectroscopy, infrared and Raman, which were employed to obtain information associated with the chemical structure of active pharmaceutical ingredient have been discussed in details. Both of the vibrational techniques are useful in identifying the functional groups and also, generates distinct fingerprint spectra for each particular chemical compound (Vankeirsbilck et al., 2002). Although X-ray diffraction is a popular technique for determining the structural characterization of pharmaceutical compounds, IR and Raman spectroscopy are better suited for short-range structure molecular solids (Stuart, 2004; Joshi et al., 2011). Vibrational spectroscopy is beneficial analytical tool for drawing information about composition, structure, conformation and intra-molecular interactions of complex molecules (Joshi et al., 2011). Thus, the instruments Fourier-transform infrared (FT-IR) and the Fourier-transform Raman (FT-Raman) were used to fully understand the molecules' vibrational modes.

3.2.1 Infrared spectroscopy

Infrared (IR) spectroscopy is a frequently used technique to obtain quantitative and qualitative information about the basic structure as well as the chemical contents of biological samples (Beć et al., 2020). It is based on the atomic vibrations of a molecule. The atoms in a molecule above the absolute temperature are in continuous vibration and when infrared radiation passes through it, some portion of the incident radiation which is equal to the vibrational frequency of atoms gets absorbed and the infrared spectrum is obtained (Hsu, 1997). Among the several modes of normal vibration of a molecule, those that result in a net change in the dipole moment cause IR activity (Hsu, 1997). The IR region is generally divided into near-IR (13000–4000 cm^{-1}), mid-IR (4000–400 cm^{-1}) and Far-IR (400-100 cm^{-1}). The absorption bands in the mid-IR region are of great importance since it is found that stretching of X-H in region between 4000 and 2500 cm^{-1}, the triple-bond in region between 2500 and 2000cm^{-1}, the double-bond region in between 2000 and 1500 cm^{-1}, and the fingerprint in region between 1500 and 600 cm^{-1} (Stuart, 2004).

The sample of cefalexin was bought from the multinational pharmaceutical company in the USA, Merck and Co. The infrared spectrum of a compound, cefalexin was recorded in the region of 400 to 4000 cm^{-1}, usinng the Bruker Vertex 70 FT-IR spectrometer. The spectral resolution of the spectrometer was 4 cm^{-1}. The purity level of cefalexin in its solid form was above 98 percent. The 200:1 mixture of KBr and cefalexin was used to make the sample pellet (T. Chaudhary et al., 2021).

3.2.2 Raman spectroscopy

Raman spectroscopy is the main scattering technique to identify the molecular structure (Smith & Dent, 2019). It provides information on the biological constituents of drug molecules and is helpful to analyze the atomic location, electron distribution and intermolecular interactions in the molecular system (Willard et al., 1989). Scattering determines the particle size and distribution to sizes smaller than 1μm (Smith & Dent, 2019). Raman scattering uses a single frequency of irradiation to irradiate the sample, where the frequency of incident radiation is different from the vibrational frequency. The vibration is Raman active only if the polarizabilty of a molecule changes (Smith & Dent, 2019). In this case, the radiation distorts the cloud of electrons surrounding the nucleus, which causes the molecule to become polarized. At room temperature, the majority of molecules are in the ground state, so stokes scattering is more probable than the anti-stokes scattering. However, with the increase in temperature,the molecules excite to higher vibrational state, so the anti-stokes scattering may be dominant at higher temperature (Smith & Dent, 2019).

Raman spectra of cefalexin were recorded in the range of 50 to 4000 cm^{-1}. The spectra were recorded using the RAM II module, which employs a diode-pumped Nd:YAG laser. The laser has a maximum power of 100 mW and a maximum excitation wavelength of 1064 nm.

3.3 Theoretical background

For a complete and precise description of the electronic system, the quantum mechanical method is the only one that can be applied (Jensen, 2007). According to quantum mechanics, the wave function can be used to determine a system's observable properties. That is the wave function contains very useful information about molecule like as: dipole moments, polarizzability etc (Sherrill, 2000). Thus, in principle, the molecular structure and its chemical reactivity can be quantitatively predicted at a precise level by implementing the Schrodinger equation. However, in fact, this objective is challenging to achieve due to mathematical and computational complexity, necessitating the use of approximate approaches (J. Pople & Beveridge, 1970).

In order to comprehend chemical issues, methods either based on wave functional theory (WFT) or density functional theory (DFT) can be utilized. The *ab initio* is a non-emperical computational method that is used to estimate the structural and electronic properties of molecules. Basically, the Schrodinger equation serves as the starting point for all quantum mechanical methods (Hehre, 2003). It is used to obtain the properties of non-relativistic quantum system from the given equation (Schrödinger, 1926):

$$\hat{H}\Psi(\mathbf{R},\mathbf{r}) = E\Psi(\mathbf{R},\mathbf{r}) \tag{3.1}$$

For a multi-electron and multi-nuclear molecular system of N-electrons and M-nuclei, The Hamiltonian can be written as

$$\hat{H} = -\frac{\hbar^2}{2m_{\mathrm{e}}}\sum_{i=1}^{N}\nabla_i^2 - \sum_{U=1}^{M}\frac{\hbar^2\nabla_U^2}{2M_U} + \frac{1}{2}\sum_{i\neq j}\frac{e^2}{|\mathbf{r}_i-\mathbf{r}_j|} - \frac{1}{2}\sum_{i,U}\frac{Z_U e^2}{|\mathbf{r}_i-\mathbf{R}_U|} + \frac{1}{2}\sum_{U\neq V}\frac{Z_U Z_V e^2}{|\mathbf{R}_U-\mathbf{R}_V|} \tag{3.2}$$

Where,

$M_{\mathrm{U}} = U^{th}$ nucleus mass

$e =$ electron charge

$m_{\mathrm{e}} =$ electron mass

The summation with U, V stands for nuclei and i, j stands for electrons. Here, the first two terms in the equation 3.2 describe respective kinetic energies of the electrons and nuclei, and among the other three terms, the first indicates attractive electrostatic potential between the electrons and the nuclei and the last two are repulsive potential due to electron-electron and nuclei-nuclei interaction, respectively.

The complete solution of the Schrodinger equation is only possible for a single particle solution, but for a two-electron or many electron system it cannot be solved exactly, so an approximation is needed to be introduced. The non-experimental, the *ab initio* (or first principles) approach is used to solve the many body problem accurately. These calculations uses the correct Hamiltonian that depends on only the fundamental physical parameters. The frequently used approache is Hartree-Fock Self Consistent Field (SCF), *ab initio* calculation that uses an anti-symmetrized wave function.

3.3.1 Born-Oppenheimer approximation (BOA)

The Born-Oppenheimer approximation is the first attempt required to simplify the schrodinger equation. In the many body system, the, interactions between the electrons also increase as the number of electrons increases. Hence, to reduce the complexity the electronic and nuclear part are separated. The masses of the nuclei are multiple times greater than the masses of the electrons. Thus, according to Born & Oppenheimer (1927), the kinetic energy of nuclei are neglible in comparision to the kinetic energy of electrons and nuclear-nuclear coulmb repulsion is constant. Now, the wave function can be interpreted as

$$\Psi(\mathbf{R},\mathbf{r}) = \phi(\mathbf{R}) \cdot \chi(\mathbf{R},\mathbf{r}) \tag{3.3}$$

where, $\phi(\mathbf{R})$ is the wave function associated with nucleus and $\chi(\mathbf{R},\mathbf{r})$ is the wave function associated with electron. The schrodinger equation for electronic part, is as follows:

$$\hat{H}_{el}\chi(\mathbf{R},\mathbf{r}) = E_{el}\chi(\mathbf{R},\mathbf{r}) \tag{3.4}$$

where, the electronic Hamiltonian is,

$$\hat{H}_{\mathrm{el}} = -\frac{\hbar^2}{2m_{\mathrm{e}}}\sum_{i=1}^{N}\nabla_i^2 - \frac{1}{2}\sum_{i,U}\frac{Z_U e^2}{|\mathbf{r}_i - \mathbf{R}_U|} + \frac{1}{2}\sum_{i\neq j}\frac{e^2}{|\mathbf{r}_i - \mathbf{r}_j|} \tag{3.5}$$

The total energy of the system is obtained only after adding the constant repulsion term

(V_{NN}):

$$E_{tot} = E_{el} + V_{NN} \tag{3.6}$$

where, $V_{NN} = \frac{1}{2}\sum_{U\neq J}\frac{Z_U Z_V e^2}{|\mathbf{R}_U - \mathbf{R}_V|}$

Nuclear motion in the average electron field

$$H_N \phi(\mathbf{R}) = E\phi(\mathbf{R}) \tag{3.7}$$

The solution of these two equations gives the information of total energy of the system.

3.3.2 Hatree-Fock approximation

The BOA approximation simplifies the schrodinger equation, seperating Hamiltonian into two parts, electronic and nuclear parts. However, the schrodinger equation is still unsolvable due to inter-electronic repulsion term, $\frac{1}{2}\sum_{i\neq j}\frac{e^2}{|\mathbf{r}_i - \mathbf{r}_j|}$. The distance between electrons are difficult to measure, since their motions are correlated (Jensen, 2007). Hartree and Fock solved the problem by considering electrons with no correlation. According to independent particle approximation introduced by Hartree (1928), an electron, a one-electron molecular orbital (wave function) is assumed to be influenced by average effective field created by nuclei and all other the remaining electrons. This is assumed for each and every electron and the total wave-function of electrons in a many-body system is approximately provided a product of N one-electron wave-functions as follows:

$$\Psi(r_1, r_2, \ldots, r_n) = \chi_1(r_1)\,\chi_2(r_2)\ldots\chi_n(r_n) \tag{3.8}$$

It is referred to as a Hartree product. Now, the energy of system is estimated using this wave function as follows:

$$H\Psi(r_1, r_2, \cdots, r_n) = E\Psi(r_1, r_2, \cdots, r_n) \tag{3.9}$$

Since, the wave function,$\Psi(r_1, r_2, \cdots, r_n)$ obtained from the Hartree product does not satisfy the anti-symmetry property, it fails to describe fermions. Moreover, to incorporate the exchange and correlation terms, Hartree's method was further improved using the anti-symmetric nature of electrons by Fock (1930). As a result, the approach is known as Hatree-Fock (H-F) approximation (Hartree, 1928; Fock, 1930).The wave functions in the H-F approximation are properly arranged in a single Slater determinant

for N spin-orbitals (Slater, 1937).

$$\Psi = \frac{1}{\sqrt{N!}} \begin{vmatrix} \chi_1(r_1,s_1) & \chi_2(r_1,s_2) & \cdots & \chi_n(r_1,s_n) \\ \chi_1(r_2,s_1) & \chi_2(r_2,s_2) & \cdots & \chi_n(r_2,s_n) \\ \vdots & \vdots & & \vdots \\ \chi_1(r_n,s_1) & \chi_2(r_n,s_2) & \cdots & \chi_n(r_n,s_n) \end{vmatrix} \tag{3.10}$$

This is the anti-symmetrized wave function which is used to describe electrons. Now the energy expression is given by

$$E_{el} = \langle \Psi | H_{el} | \Psi \rangle \tag{3.11}$$

The suitable approximate wave function corresponding to the minimum energy can be estimated employing variational theorem in it. Now, the Hartree-Fock energy expression is

$$E^{HF} = \sum_u \langle \Psi | h | \Psi \rangle + \frac{1}{2} \sum_{uv} [uu|vv] - [uv|vu] \tag{3.12}$$

where, for one electron integral

$\sum_u \langle \Psi | h | \Psi \rangle = \int dx_1 \Psi_u^*(x_1) h(r_1) \Psi_v(x_1)$

and for two electron integral

$[uv|wx] = \int dx_1 dx_2 \Psi_u^*(x_1) \Psi_v(x_1) \frac{1}{r_{12}} \Psi_w^*(x_2) \Psi_x(x_2)$

Now, after minimizing and simplifing the Hartree-Fock energy expression, we get

$$h(x_1)\Psi_u(x_1) + \sum_{v \neq u} \left[\int dx_2 |\Psi_v(x_2)|^2 \frac{1}{r_{12}} \right] \Psi_u(x_1) - \sum_{v \neq u} \left[\int dx_2 \Psi_v^*(x_2) \Psi_u(x_2) \frac{1}{r_{12}} \right] \Psi_u(x_1) = \varepsilon_u \Psi_u(x_1) \tag{3.13}$$

where, ε_u is the energy related to Ψ_u, the initial term in the equation above that is $\sum_{v \neq u} \left[\int dx_2 |\Psi_v(x_2)|^2 \frac{1}{r_{12}} \right] \Psi_u(x_1)$ is the coulomb interaction of elctrons and the term $\sum_{v \neq u} \left[\int dx_2 \Psi_v^*(x_2) \Psi_u(x_2) \frac{1}{r_{12}} \right] \Psi_u(x_1)$ is the exchange term (Sherrill, 2000).

Moreover, The H-F approximation could not account for the correlation effect of electrons. It overestimates the total energy. Correlation is the coupling of electron motions that decrease the electron-electron repulsion energy. Thus, correlation is equal to the difference of Hartree-Fock energy and the actual energy of the system (Hehre, 2003). Further, many methods such as MP2, MP3, MP4, etc. were developed to account the

correlated molecular system (Harrison, 2003). However, these methods are based on the wave function and the wave function consists of 4N cooridinates sytem: 3N space coordinates and N spin coordinate. Thus, it requires a large computational cost for a huge system. On the other hand, density functional theory (DFT) method is based on the electron density. Since the electon density depends on only 3N space coordinates, it requires less computaional cost (Harrison, 2003; Baseden & Tye, 2014). Hence, it has become more popular to solve the many body problems.

3.4 Density functional theory (DFT)

DFT is the most commonly used quantum theory for calculating the electronic structure of molecules, which is based on the electron density ρ(r) rather than the many electron wave functions $\Psi(r_1,r_2,.....)$. It is used to compute the electronic ground state energy in terms of electron density. It has become the method of choice for theoretical physicists and chemists for determining the structures, surface, defects, and electrical properties of solids over the last three decades (Kohn et al., 1996). The foundation of DFT is based upon the two theorems presented by Hohenberg and Kohn (Hohenberg & Kohn, 1964) and on Kohn-Sham approximation (Kohn & Sham, 1965). Theses can be stated as follows:

3.4.1 Hohenberg-Kohn Theorem

Hohenberg-Kohn has been stated in two theorems.

Theorem first: It states that "*the ground state density, determines the external potential uniquely*".

$$i.e.\ \rho(r) \rightarrow V(r) \tag{3.14}$$

If for N-electron system, the different external potential V(r) and V'(r) are associated with the same ground state density $\rho(r)$, then, H and H' be the respective Hamiltonian associated with them. Thus,

$$H = T + U + V_{ee}\,, \quad H' = T + U + V'_{ee}$$

where,

$$T = -\frac{1}{2}\sum_{i}^{N} \nabla_i^2$$

$$U = \frac{1}{2}\sum_{i \neq j} \frac{1}{|\mathbf{r}_i - \mathbf{r}_j|}$$

$$V_{ee} = \sum_i V(r_i)$$
$$V'_{ee} = \sum_i V'(r_i)$$

If the energy associated with Ψ and Ψ' are E and E' ,respectively. Then, utilizing the variational principle,

$$E = \langle \Psi | H | \Psi \rangle \leq \langle \Psi' | H | \Psi' \rangle \tag{3.15}$$
$$\leq \langle \Psi' | H' | \Psi' \rangle + \langle \Psi' | H - H' | \Psi' \rangle \tag{3.16}$$
$$\leq \mathrm{E}' + \int \mathrm{d}r\, \rho(r) \left[V(\mathbf{r}) - V'(\mathbf{r}) \right] \tag{3.17}$$

and

$$E' = \langle \Psi' | H' | \Psi' \rangle \leq \langle \Psi | H' | \Psi \rangle \tag{3.18}$$
$$\leq \langle \Psi | H | \Psi \rangle + \langle \Psi | H' - H | \Psi \rangle \tag{3.19}$$
$$\leq \mathrm{E} + \int \mathrm{d}r\, \rho(r) \left[V'(\mathbf{r}) - V(\mathbf{r}) \right] \tag{3.20}$$
$$E' \leq E + \int \mathrm{d}r\, \rho(r) \left[V'(\mathbf{r}) - V(\mathbf{r}) \right] \tag{3.21}$$

summing the equations 3.17 and 3.21, we get

$$E + E' \leq E' + E \tag{3.22}$$

Which is a contradiction. Hence, the theorem is verified by reductio ad absurdum.

Theorem second: It states that."*the universal fuctional $F[\rho_0(\boldsymbol{r})]$, gives the ground state energy of the system with the minimum energy only if the initial density is the true ground state density*". For a given external potential $V_{\mathrm{ex}}(\mathbf{r})$, energy can be defined as

$$E^{(HK)}[\rho(\mathbf{r}), V_{\mathrm{ex}}] = \mathrm{T}[\rho(\mathbf{r})] + V_{ee}[\rho(\mathbf{r})] + \int V_{\mathrm{ex}}(r)\rho(\mathbf{r})\, \mathrm{d}r \tag{3.23}$$

Where, the first, second and third term in the right hand side respectively represents the kinetic energy (K.E.), Coulomb potential energy of interacting electrons and external potential i.e. due to electron-nuclei interactions. The universal functional, $F[n(\mathbf{r})]$, is given as

$$F[\rho(\mathbf{r})] = T[\rho(\mathbf{r})] + V_{ee}[\rho(\mathbf{r})] \tag{3.24}$$

E(ρ), is assumed to be the minimum energy for exact density Where

$$N = \int \rho(\mathbf{r}) d\mathbf{r} \tag{3.25}$$

Now, the above equation can be written as F$[\rho(\mathbf{r})]$ can be expressed as

$$E^{(HK)}[\rho(\mathbf{r}), V_{\text{ex}}] = F[\rho(\mathbf{r})] + \int V_{\text{ex}}(r)\rho(\mathbf{r})\ \mathrm{d}r \tag{3.26}$$

From the principle of minimal

$$E[\rho(r), V_{ex}] \geq E[\rho_0(r), Vex] = E \tag{3.27}$$

The exact ground parameters are obtained by minimizing above with respect to electron density. Nevertheless, obtaining exact energy functional is challenging since it is concerned with the K.E. of the electrons. The $F[\rho(\mathbf{r})]$, is further solve by employing Kohn-Sham approach (Kohn & Sham, 1965).

3.4.2 Kohn-Sham approach

The kinetic energy relating to density is still difficult to determine with sufficient accuracy. However, it is easy to calculate interms of wavefuntion. Thus, Kohn & Sham (1965) considered an interatcing electronic system to a non-interacting such that it gives the exact density as that of the real interacting-sytem. The K-S stated the universal functional as follows (Kohn et al., 1996):

$$F[\rho(\mathbf{r})] = T_{\text{s}}[\rho(\mathbf{r})] + J^H[\rho(\mathbf{r})] + E_{\text{XC}}[\rho(\mathbf{r})] \tag{3.28}$$

In the above equation, where

$T_{\text{s}}[\rho(\mathbf{r})] =$ K.E. for non interacting-particle

$J^H[\rho(\mathbf{r})] = \dfrac{1}{2}\iint \dfrac{\rho(r_i)\rho'(r_j)}{|r_i - r_j|} dr_i dr_j$

$=$ energy resulting from the electrons' coulomb electrostatic interaction

$E_{\text{XC}}[\rho(\mathbf{r})] =$ exchange-correlation energy

And, E_{XC} is defined as,

$$E_{XC} = \triangle T[\rho] + \triangle V[\rho]$$

where,

$$\triangle T[\rho] = T[\rho] - T_s[\rho]$$
$$\triangle V[\rho] = V_{ee} - J^H[\rho(\mathbf{r})]$$

Now, the energy functional can be written as

$$E[\rho] = T_s[\rho] + \int V_{ex}(r)\rho(r)dr + J^H[\rho(r)] + Exc[\rho(r)] \tag{3.29}$$

where, $T_s[\rho(r)] = \sum_i^N \int \psi_i^*(-\frac{1}{2}\nabla_i^2)\psi(i)dr$

The minimum energy is obtained by differentiating the total energy with respect to electron density, $\rho(r)$ i.e. $\delta[E(\rho)]= 0$. Now, the Kohn-sham equation is derived using lagrange undetermined multipliers method employing constrain as follows:

$$\delta[E(\rho) - \lambda N] = 0 \tag{3.30}$$

$$\int \frac{\delta}{\delta\rho(r)}[E(\rho) - \lambda N]\delta\rho(r)dr = 0 \tag{3.31}$$

where, λ = lagrange multiplier and constrain is $\int \rho(r)dr = N$

$$\int \frac{\delta T_s[\rho(r)]}{\delta\rho(r)}\delta\rho(r)dr + \int \frac{\delta V_{ex}(r)\rho(r)}{\delta\rho(r)}\delta\rho(r)dr + \iint \frac{\delta}{\delta\rho(r)}\left[\frac{\rho(r)\rho(r')}{|r-r'|}\right]\delta\rho(r) dr'dr + \int \frac{\delta E_{XC}[\rho(r)]}{\delta\rho(r)}\delta\rho(r)dr - \lambda\int \frac{\delta\rho(r)}{\delta\rho(r)}\delta\rho(r)dr = 0 \tag{3.32}$$

$$\int \left[\frac{\delta}{\delta\rho(r)}[T_s[\rho(r)]] + V_{ex}(r) + \int \frac{\rho(r')}{|r-r'|}dr' + \frac{\delta E_{XC}[\rho(r)]}{\delta\rho(r)} - \lambda\right]\delta\rho(r)dr = 0 \tag{3.33}$$

Now, according to Kohn and Sham' theory, the terms in the bracket in the above equation can be described by one dimensional schrodinger for non-interacting reference system as follows:

$$\left[\left(-\frac{1}{2}\nabla_i^2\right) + V_{KS}\right]\Psi_i = \varepsilon_i\Psi_i \tag{3.34}$$

where, $V_{KS} = J^H(r) + V_{ex}(r) + V_{XC}(r)$

And,

$$\frac{\delta}{\delta\rho(r)}\left[T_s[\rho(r)]\right] = -\frac{1}{2}\nabla_i^2$$

$$Here, J^H(r) = \int \frac{\rho(r')}{|r-r'|}dr',$$

$$V_{XC}(r) = \frac{\delta}{\delta\rho(r)}\left[Exc[\rho(r)]\right]$$

$$\lambda = \varepsilon_i$$

$$\rho(\mathbf{r}) = \sum_{i=1}^{N} |\psi_i|^2$$

Finally, the arbitrary density is taken and V_{KS} is determined. This V_{kS} is used to find out the wavefunction and ulimately, the electron density. The process is repeated unless, the V_{KS} and $\rho(r)$ is converged (Bretonnet, 2017).

Now to determine the exchange-correlaiton energy term E_{XC}, the approximation is required. The most popular approxiamtions for exchange-correlational functinal are local density approximation (LDA), generalized gradient approximation (GGA) and hubrid functionals.

3.4.3 Local density approximation (LDA)

LDA is the simplest approximation proposed by Kohn & Sham (1965). It is suitable for which the density of a system remains almost uniform (Hohenberg & Kohn, 1964). According to this approximation, the exchange-correlation term, is stated as:

$$E_{\mathrm{XC}}^{\mathrm{LDA}}[\rho(\mathbf{r})] = \int \rho(\mathbf{r})\varepsilon_{\mathrm{XC}}[\rho(\mathbf{r})]\ \mathrm{d}\mathbf{r} \tag{3.35}$$

where $\varepsilon_{\mathrm{XC}}[\rho(\mathbf{r})]$ denotes the exchange-correlation energy of each the electron of interacting system and $\rho(\mathbf{r})$ is the density of electron in that homogeneous system. In this approximation, the exchange energy functional is calculated uing Dirac (1930) approach and correlation energy employing quantum Monte-Carlo (QMC) simulations (Ceperley & Alder, 1980)

3.4.4 Generalized gradient approximation (GGA)

LDA can account good for only a homogeneous system. However it is not applicable for inhomogeneous and thermochemisrty system where as GGA can account good for thermochemistry (Kohn et al., 1996; Bretonnet, 2017). GGA has been developed for the real system, where the distribution of electrons may not be uniform. Thus, for inhomogeneous system of electron gas, generalized gradient approximation (GGA) is

stated by:

$$E_{\mathrm{XC}}^{\mathrm{GGA}}[\rho(\mathbf{r})] = \int f[\rho(\mathbf{r}), \nabla\rho(\mathbf{r})]\mathrm{d}\mathbf{r} \tag{3.36}$$

where, $\nabla\rho(\mathbf{r})$ represent, the gradient of $\rho(r)$. Moreover, exchange funcitonal is calculated using the method provided by Becke (1988) and the methods of calculation of correlation functional are Perdew (1986), etc.

3.4.5 Hybrid functionals

The hybrid functional is the combination of both LDA and GGA approxiamtions. The frequently used hybrid functional is the B3LYP functional (Becke, 1988; Lee et al., 1988). B3LYP is means Becke 3-parameter Lee, Yang and parr which is composed of both exchange and correlation functional. The hybrid exchange- correlational term is defined as follows:

$$E_{\mathrm{XC}}^{\mathrm{B3LYP}} = AE_{\mathrm{X}}^{\mathrm{HF}} + (1-A)E_{\mathrm{X}}^{\mathrm{HF}} + B\Delta E_{\mathrm{X}}^{\mathrm{B}} + E_{\mathrm{C}}^{\mathrm{local}} + C\Delta E_{\mathrm{C}}^{\mathrm{LYP}} \tag{3.37}$$

where, A, B, and C are the parameters that provide the computed energy with the best fit to molecule atomization energies. The other terms in the right hand side like; the first two terms indicate the H-F exchange energy function based on KS orbitals, third, fourth and fifth term represent the Becke 88 exchange functional, the homogenous electron gas's exact correlation component in LDA and the LYP correlation functional, respectively.

3.5 Basis set

The wave function of a system is constructed using molecular orbitals. A mathematical representation of molecular orbitals (MOs) is a basis set which is a linear combinations of basis functions.The atomic orbitals often represents the basis function (Hehre, 2003).The molecular orbital ψ_i, is expressed interms basis function,(ϕ_j) as given below:

$$\psi_i = \sum_{j=1}^{N} c_{ij}\phi_j \tag{3.38}$$

where, c_{ji} are the coefficients of the MO expansion. Slater-type and Gaussian-type orbitals are the two most prevalent orbitals.

3.5.1 Slater and Gaussian-type orbitals

The solutioin of Hartree-Fock equations is the atomic orbital known as wave function for a single electron in an atom. The wave functions is subsequently means the basis function. Currently, Slater Type Orbitals (STO) and Gaussian Type Orbitals (GTO) are the two most widely employed basis functions.

Slater-type orbitals have been defined as:

In spherical polar coordianates

$$\psi_{\mathrm{nlm}}^{\mathrm{STO}}(r,\theta,\phi) = Nr^{n-1}e^{-\beta r}Y_{lm}(\theta,\phi) \tag{3.39}$$

where, N represent the normalization constant; n is principal quantum, l is angular momentum and m is a magnetic quantum number; β is orbital exponent that controls the width of orbitals.

In cartesian cordinate,

$$\psi_{\mathrm{nlm}}^{\mathrm{STO}}(r,\theta,\phi) = Nx^{m}y^{l}z^{n}e^{-\beta r}Y_{lm}(\theta,\phi) \tag{3.40}$$

The exponential term has a more significant role in STO. With an expanding number of functions, the exponential dependence assures a surprisingly quick convergence. STOs are mostly employed in semi-empirical approaches and for atomic and diatomic systems. Gaussian-type orbitals have been defined as:

In polar coordinate,

$$\psi_{\mathrm{nlm}}^{\mathrm{GTO}}(r,\theta,\phi) = Nr^{n-1}e^{-\beta r^{2}}(r)Y_{lm}(\theta,\phi) \tag{3.41}$$

where, N denotes the noramlization constant, $r^2 = x^2 + y^2 + z^2$ and l,m,n are the integral exponentials.

In cartesian coordiante,

$$\psi_{\mathrm{lmn}}^{\mathrm{GTO}}(x,y,z) = Nx^{l}y^{m}z^{n}e^{-\beta r^{2}} \tag{3.42}$$

The GTOs functions exhibit no cusp behavior at the nucleus, that is, slope is zero when r tends to zero, whereas STOs exhibit the proper cusp behavior, and when r tends to infinity, that is, in the tail regions, GTOs fall off rapidly while STOs decay exponentially (J. A. Pople et al., 1989; Ditchfield et al., 1971)

3.5.1.1 Minimal and split valence basis set

The minimal basis set is that which includes the minimum number of functions to represent an atomic orbital of an atom (Szabo & Ostlund, 2012). The STO-3G minimal Basis set is the simplest basis set that consists of a single function, 1s. The one basis function, 1s, is used to represent the hydrogen and helium atoms; five basis functions, i.e., 1s, 2s, $2p_x$, $2p_y$, and $2p_z$, to represent atoms from Lithium to neon; and nine basis functions, i.e., 1s, 2s, $2p_x$, $2p_y$, $2p_z$, 3s, $3p_x$, $3p_y$, $3p_z$, for atoms from sodium to argon. Further, the minimum basis set can be improved by adding extra basis functions, i.e., double-zeta or triple-zeta basis sets or so on.The double-zeta basis is obtained by adding one extra basis function to the existing one, so it has twice as many functions as the previous ones. Similarly, the triple-xeta basis is obtained by adding two to the previous set, so it has three times as many functions as the previous ones(Hehre, 2003; J. A. Pople & Hehre, 1978).

In the split valence basis set, the core and valence electrons are described individually. Popel and his colleagues created the n-ijG and n-ijkG Gaussian basis sets. Each valence orbital in this basis set has two or more basis functions of various sizes (Binkley et al., 1980). The double-zeta split valence basis set, n-ijG is referred to as a double-zeta split valence basis set, in which the core orbitas is described by linear combination of n gaussian type orbitals and the valence orbitals are described by two orbitals, one made of linear combination of i-Gaussian and the other made of of j-Gaussian. Similarly, in tripal- zeta split valence basis set, n-ijkG. Some examples of the split valence basis set are 3-21G, 6-31G, 6-311G, etc. The linear combination of primitive gaussian type orbitals is known as the contracted gaussian type orbital (CGTOs). CGTOs can be used to describe the core elctrons, which reduces the computaional cost (Hehre et al., 1972; J. A. Pople & Hehre, 1978).

$$\psi_{\mathrm{lmn}}^{\mathrm{CGTO}}(x,y,z) = N\sum_{i=1}^{n} c_i x^l y^m z^n e^{-\beta r^2} \tag{3.43}$$

3.5.2 Polarization and diffuse function

For anisotropic charge distribution, only increasing the basis set to double or triple or higher-zeta basis set may not improve the result. However, the result can be improved by adding the orbital of higher momentum than the occupied one, known as the polarized basis. For example, basis function p can be added to s occupied orbital and d can be added to p orbital, so that the occupied orbitals are polarized. The examples of polarized basis sets are 6-311G*/6-311G(d), 6-311**/6-311G(d,p) etc. Here, 6-311G* represents that polarized function, has been added to the heavy atoms and 6-311** represents that polarized function has been added to both hydrogen as well as heavy atoms.

Moreover, for the sytem which may characterize with either of the properties like as, lone pair, anions, a lot of negative charge or low ionization potentials, the result can be improved using diffuse functions. The diffuse function is the addional s and p-type orbitals to the atoms. The examples of diffuse functions are 6-31+, 6-31++ etc. Here, 6-31+ represents the addition of addition diffuse function to heavy atoms. Similarly, 6-31++ represents the addion of diffise function to hydrogen and heavy atoms (R. Krishnan et al., 1980).

3.5.3 Thermodynamic properties

The Boltzmann distribution and the partition function q(V, T) determine a system's thermodynamic properties. Translational, rotational, electronic, and vibrational motion all contribute to entropy, enthalpy, and heat capacity. The partition functions utilized for various motions are as follows (Ochterski, 2000).

Rotational partition function,

$$Q_t = \left(\frac{2\pi m k_B T}{h^2}\right)^{3/2} V \tag{3.44}$$

Translational partition function,

$$Q_r = \frac{1}{\sigma_r}\left(\frac{T}{\theta_r}\right) \tag{3.45}$$

Electronic partition function

$$Q_e = \omega_0 e^{-\varepsilon_0/k_B T} + \omega_1 e^{-\varepsilon_1/k_B T} + \omega_2 e^{-\varepsilon_2/k_B T} + \ldots \tag{3.46}$$

Vibrational partition function

$$Q_k = \Pi_k \frac{1}{1 - e^{\Theta_{v,k/T}}} \tag{3.47}$$

where, k_B,ω and ε_n represent Boltzmann constant, degeneracy of the energy level and n-th level energy, respectively; Θ=$h^2/8\pi^2 I k_B$.

3.6 Atoms in molecule, NCI and electron localization function

Quantum theory of atoms in molecules (QTAIM) and the NCI method are both used to analyze the intermolecular and intramolecular hydrogen bonding in the monomer and dimer states of a molecule, initially introduced by Bader and his coworkers (R. F. Bader & Matta, 2004). In QTAIM analysis, parameters like as electron density (ρ) and its Laplacian ($\nabla^2\rho$) along with electron K.E density (G_{BCP}), electron potential energy den-

sity (V_{BCP}) and total electron energy density (H_{BCP}) were determined to characterize the nature of the hydrogen bond. Koch and Popelier stated that hydrogen bonds can exist only if the electron density, (ρ) and Laplacian of electron density at BCP, ($\nabla^2\rho_{\mathrm{BCP}}$) are between 0.002-0.040 a.u. and 0.024-0.139 a.u., respectively (Koch & Popelier, 1995). The nature of strength of hydrogen bond is defined as: for $\nabla^2\rho_{\mathrm{BCP}} > 0$ and $H_{\mathrm{BCP}} < 0$, bond is partially covalent; for $\nabla^2\rho_{\mathrm{BCP}} < 0$ and $H_{\mathrm{BCP}} < 0$, bond is strong and covalent and for $\nabla^2\rho_{\mathrm{BCP}} > 0$ and $(H_{\mathrm{BCP}}) > 0$, bond is weak and ionic in nature (Rozas et al., 2000).

Moreover, the nature of all possible non-covalent interaction (NCI) can be investigated using a reduced density gradient (RDG) analysis. The characteristics of NCI might range from repulsive to attractive. RDG is a dimensionless quantity that is defined in the following ways (Johnson et al., 2010):

$$RDG = \frac{1}{2(3\pi^2)^{1/3}} \frac{\bigtriangledown\rho(r)}{\rho(r)^{4/3}} \tag{3.48}$$

$\Lambda(r)$ is defined as

$$\Lambda(r) = sign(\lambda_2)\rho(r) \tag{3.49}$$

where, λ_2 is the second-largest Hessian matrix. Using analysis, the hydrogen bonds, van der Waals interactions and steric effects have been predicted. Further, the localized and delocalized electron zones in a molecule have been estimated using Electron localization function (ELF). The ELF (η) is defined as (Y. Yang, 2010)

$$\eta = \frac{1}{(1 + \frac{D}{D_h})^2} \tag{3.50}$$

where,

D=$\frac{1}{2}\sum_i |\bigtriangledown \varphi_i|^2 - \frac{1}{8}\frac{|\bigtriangledown\rho|^2}{\rho}$ and $D_h = \frac{3}{10}(3\pi^2)^{2/3}\rho^{5/3}$

Here, in the equation, D and D_h denotes excess of the kinetic energy and its value for a uniform electron gas.

3.7 Electron-hole analysis

From the electron-hole analysis, the charge tansfer (CT) property of a molecular system due to excitation can be predicted. In the situation in which the excitation is equivalent to the HOMO-LUMO transition (Z. Liu et al., 2020), the hole and electron correspond to HOMO and LUMO. For, the molecular system, the overalapping of hole with the electron and the shortest distance between the centroid of hole and the centroid of the

electron, known as the charge transfer length, are obtained utilizing the given relations (Z. Liu et al., 2020):

The overlapping of electron and hole denoted by S_r is obtained as

$$S_r = \int \sqrt{\rho^h(r)\rho^e(r)} \tag{3.51}$$

The Charge Transfer length (S)

$$S = \sqrt{D_X^2 + D_y^2 + D_z^2} \tag{3.52}$$

where, $D_x = X_e$- X_h, $D_y = Y_e$- Y_h and $D_Z = Z_e$- Z_h

Here, X_e, Y_e and Z_e are X, Y and Z coordinates of centroid of electron and X_h, Y_h and Z_h are X, Y and Z coordinates of centroid of hole.

3.8 Non-linear optical (NLO) properties analysis

In general, NLO optics deals with how light interacts nonlinearly with objects, changing their optical properties (Shen, 2002). The NLO materials have a diverse range of uses in optoelectronics and telecommunications such as optical switching, data storage, optical signal processing etc.(Günter, 2012). In presence of electric field (E), the induced polarization (P) changes linearly for medium electric field strength and nonlinearly for strong electric field. For the strong field, the relation between E and P is provided by power series expansion.

For the determination of non-linear optical properties, consider a molecule exposed to a static electric field (E), then it experiences weak polarization and hence the energy (E) is stated in terms of the Taylor series expansion as follows.

$$E = E^0 - \mu_a F^a - \frac{1}{2}\alpha_{ab}F^aF^b - \frac{1}{6}\beta_{abc}F^aF^bF^c - \frac{1}{24}\gamma_{abcd}F^aF^bF^cF^d - \cdots \tag{3.53}$$

where

$$\begin{aligned} E^0 &= \text{molecular energy without an electric field} \\ \mu_a &= \text{dipole moment} \\ \alpha_{ab} &= \text{polarizability} \\ \beta_{abc} &= \text{first-order hyperpolarizability} \\ \gamma_{abcd} &= \text{second-order hyperpolarizability} \end{aligned}$$

where, cartesian coordinates are indicated by the subscripts a, b, c, and d.
The total static dipole moment μ_0, the mean poalarizabiltiy ($|\alpha_0|$) which is the average

of diagonal components, anisotropy of polarizability $\Delta\alpha$, first-order hyperpolarizabiltiy (β) and second-order hyperpolarizabiltiy (γ_0) can be calculated using the given equations (Jiang et al., 2012):

$$\mu_0 = \left(\mu_x^2 + \mu_y^2 + \mu_z^2\right)^{1/2} \tag{3.54}$$

$$|\alpha_0| = \frac{1}{3}(\alpha_{xx} + \alpha_{yy} + \alpha_{zz}) \tag{3.55}$$

$$\Delta\alpha = 2^{-1/2}\left[(\alpha_{xx} - \alpha_{yy})^2 + (\alpha_{yy} - \alpha_{zz})^2 + (\alpha_{zz} - \alpha_{xx})^2 + 6\alpha_{xx}^2\right]^{1/2} \tag{3.56}$$

$$\beta_0 = \left[(\beta_{xxx} + \beta_{xyy} + \beta_{xzz})^2 + (\beta_{yyy} + \beta_{xxy} + \beta_{yzz})^2 + (\beta_{zzz} + \beta_{xxz} + \beta_{yyz})^2\right]^{1/2} \tag{3.57}$$

$$\gamma_0 = \frac{1}{5}[\gamma_{xxxx} + \gamma_{yyyy} + \gamma_{zzzz} + 2(\gamma_{xxyy} + \gamma_{yyzz} + \gamma_{zzxx})] \tag{3.58}$$

The dipole momoent belongs to the first, polarizability belongs to the second and first-order hyperpolarizability (β) belongs to the third-ranked tensor. (β) has total 27 components. However, due to Kleinman symmetry its component is reduced to only 10 components (Wortmann et al., 1993).

3.9 Frontier molecular orbital analysis and global reactivity descriptors

The frontier molecular orbitals, HOMO and LUMO are used to anticipate the chemical activity of a molecular system. The HOMO and LUMO corresponds to the ionization potential (I) and electron affinity (A), respectively. (Manne & Åberg, 1970; Heinrich et al., 1986). The chemical stability of a molecule is treated on the basis of energy difference of HOMO and lumo orbitals. That is the molecule with a smaller energy difference is more active than the molecule with the larger one.
On the basis of HOMO energy (E_{H}) and LUMO energy (E_{L}), the global reactivity descriptor parameters are calculated as follows (Chattaraj et al., 2003):

$$\text{Electronegativity}(\chi) = -\frac{1}{2}(E_{\mathrm{HOMO}} + E_{\mathrm{LUMO}}) \tag{3.59}$$

$$\text{Chemical potential}(\mu) = -\chi = \frac{1}{2}(E_{\mathrm{HOMO}} + E_{\mathrm{LUMO}}) \tag{3.60}$$

$$\text{hardness}(\eta) = \frac{1}{2}(E_{\mathrm{LUMO}} - E_{\mathrm{HOMO}}) \tag{3.61}$$

$$\text{softness}(S) = \frac{1}{2\eta} \tag{3.62}$$

$$\text{electrophilicity index}(\omega) = \frac{\mu^2}{2\eta} \tag{3.63}$$

Here, the chemical potential depicts the chances of escaping of electrons from a molecular system. Also, it states that the flow of electron occurs from higher to lower value of chemical potential. At constant external potential $V(r)$, chemical potential is obtained as follows:

$$\mu = \left(\frac{\partial E}{\partial N}\right)_{V(r)} = -\chi \tag{3.64}$$

where, E and N represents the energy, number of electrons in a molecular system
Similarly, the global hardness explains the resistance of accepting or giving electrons which is obtained as follows:

$$\eta = \frac{1}{2}\left(\frac{\partial^2 E}{\partial N^2}\right)_{V(r)} = \frac{1}{2}\left(\frac{\partial \mu}{\partial N}\right)_{V(r)} \tag{3.65}$$

The reactivity descriptor, electrophilicity index (ω) is used to analyse the chemical reactivity. It is a measure of a system's stabilization energy after an electrophile gains an extra charge (ΔN) from neighbors.

The maximum electron gained by an electrophile from the environment represented by $(\Delta N_{\max})$ is obtained as follows:

$$\Delta N_{\max} = -\frac{\mu}{\eta} \tag{3.66}$$

For any two molecules p and Q, the amount of charge transfer between them is calculated as:

$$\text{ECT} = (\Delta N_{\max})_A - (\Delta N_{\max})_B \tag{3.67}$$

3.10 Local reactivity descriptor

Moreover, the global reactivity are specially used to determine the global chemical activity where as the Fukui functions (FF) is used to predict the local chemical reactivity of a specific sites of a molecular system. It predicts the sites for nucleophilic, electrophilic and radial attack. The FF is defined as follows (Parr & Yang, 1984):

$$f^{+}(r) = \left(\frac{\partial \rho(r)}{\partial N}\right)^{+}_{v} \qquad \text{for nucleophilic attack} \tag{3.68}$$

$$f^{-}(r) = \left(\frac{\partial \rho(r)}{\partial N}\right)^{-}_{v} \qquad \text{for electrophilic attack} \tag{3.69}$$

$$f^{0}(r) = \left(\frac{\partial \rho(r)}{\partial N}\right)^{0}_{v} \qquad \text{for neutral attack} \tag{3.70}$$

where, $\rho(r)$ represents electron density, V(r) represents the potential on an electron caused by all nuclei and N represents the total number of electrons in a molecular systems. Furthermore, in a molecule, for an atom k, the condensed Fukui function may take the values f_k^+, f_k^- or f_k^0 based on the kind of electron transfer in the atom (r). The nucleophilic, electrophilic or radial attacks are predicted on the basis of the Fukui functions f_k^+, f_k^- or f_k^0, respectively. The reactivity associated with a particular site increases if the values fukui functions increases (Parr & Yang, 1984). For conviniene, the values of Fukui functions can be estimated using the given equations W. Yang & Mortier (1986).

$$f_k^+ = q_k(N+1) - q_k(N) \tag{3.71}$$

$$f_k^- = \frac{1}{2}\left[q_k(N) - q_k(N-1)\right] \tag{3.72}$$

$$f_k^0 = \frac{1}{2}\left[q_k(N+1) - q_k(N-1)\right] \tag{3.73}$$

$$\tag{3.74}$$

where, q_k represents the charge at k^{th} atomic sites of neutral (N), anionic (N+1), or cationic (N-1) chemical species.

Moreover, the local softness: s_k^+, s_k^-, s_k^0 and local electrophilicity indices: $\omega_k^+, \omega_k^-, \omega_k^0$ are are estimated from given equation:

$$s_k^+ = Sf_k^+, \quad s_k^- = Sf_k^-, \quad s_k^0 = Sf_k^0$$

and

$$\omega_k^+ = \omega f_k^+, \quad \omega_k^- = \omega f_k^-, \quad \omega_k^0 = \omega f_k^0$$

3.11 Molecular electrostatic potential (MEP) surface

Molecular electrostatic potential (MEP) is a widely used technique to predict the nucleophilic and the electrophilic reactive sites in the molecular system (Sjoberg et al., 1990). In the molecular system, the molecular electrostatic potential V(r) is calculated from the equation: (Sen & Murray, 1996)

$$V(r) = \sum_A \frac{Z_A}{|\vec{R}_A - \vec{r}|} - \int \frac{\rho(\vec{r'})}{|\vec{r'} - \vec{r}|} \tag{3.75}$$

where Z_A represent the charge on nucleus A at position R_A and $\rho(\vec{r'})$ represent the electronic density. The final potential $V(r)$ is the combined effect of the potential due to nuclei (represented by first term) and the potential due to electrons (represented by second term).

3.12 Natural bond orbital (NBO) analysis

The transfer of charge from occupied orbital to unoccupied orbital which has great impact on the molecular stability has been studied on the basis of natural bond orbital (NBO) analysis. Strong or weak interaction between filled and unfilled orbitals is indicated high or low value of interaction energy . The interaction energy $E^{(2)}$ between these filled and unfilled orbitals is calculated using second order perturbation theory (Weinhold & Landis, 2001, 2005).

$$E^{(2)} = E(i,j) = -q_i \frac{\left(F_{ij}\right)^2}{E_j - E_i} \tag{3.76}$$

where q_i represent occupancy of filled (donor) orbital, F_{ij}, the off-diagonal Fock matrix element, Kohn–Sham matrix element).is the diagonal element of Fock-matrix, E_i is the real energy and E_j is the virtual orbitals.

3.13 Vibrational analysis

The assighnment of potential energy distribution (PED) contribution to each of the vibratinal modes has been investigated using The internal coordinates applied to normal mode of vibration were according to Pulay's recommendation (Pulay et al., 1979). The Raman intensities are proportional to the Raman scattering cross-section $\frac{\partial \sigma_j}{\partial \Omega}$ and hence, it is calculated on the basis of Raman scattering cross-section (Polavarapu, 1990; Guirgis et al., 2003) by the equation:

$$\frac{\partial \sigma_j}{\partial \Omega} = \left(\frac{2^4 \pi^4}{45}\right) \frac{\left(v_0 - v_j\right)^4}{1 - \exp\left[(-hcv_j)/(kT)\right]} \left(\frac{h}{8\pi^2 c v_j}\right) S_j \tag{3.77}$$

where,
S_j = scattering activities
ν_j = estimated wavenumbers for j^{th} normal mode
ν_0 =Wave number for the Raman-excited state
h, c, and k represent the universal constants.

Generally, the wave numbers computed by this formula gives the greater value than the actual ones because of suppositions of simple harmonic vibrational motions; as a result their values are corrected using the WLS factor, $\nu_{observed}$=$(1.008700 - 0.0000163 \times \nu_{calculated})\ \nu_{calculated}$ (Yoshida et al., 2002). Finally, from each of the Raman and IR intensities were convoluted using, a Lorentzian line shape (FWHM = 8 cm^{-1} to generate artificial spectra.

3.14 Molecular docking

Molecular docking is a well-known computer-based technique that has been rigorously implemented at present to predict the best binding mode and find out the binding affinity of drugs with the recepter (Morris & Lim-Wilby, 2008; Fan et al., 2019). For performing docking, there are three types of software available. They are rigid docking (the conformation of both ligand and receptor doesn't change), flexible-rigid docking (the conformation of both ligand and receptor doesn't change), and flexible docking (the conformation of both ligand and receptor changes) software (Fan et al., 2019). During the actual docking process, both the ligand and receptor undergo conformational changes. Hence, the most appropriate docking software is flexible docking to obtain the most accurate result. However, due to its heavy computational work, flexible-rigid docking has become more friendly in recent days (Morris & Lim-Wilby, 2008; Fan et al., 2019).

In our work, the biological activity of different molecules have been studied performing flexible-rigid docking in which the ligand is considered to be flexible where as the receptor protein is considered to be rigid. For docking analysis, the stable conformation of ligand molecule corresponding to its lowest ground state energy has been choosen. The partial charges were estimated employing Geisteiger method (Gasteiger & Marsili, 1980). The target protein has been predicted using an online web server, SwissTarget-Prediction (Gfeller et al., 2014). The PDB code corresponding to the target protein were obtained from the protein data bank (Rose et al., 2010). The receptor protein is prepared by removing water and the co-crystalized ligands present in it and then, the polar hydrogen were added to it. Finally, the Kollman charges were added to the protein, receptor and the docking was performed.

3.15 Computational details

The computational investigation on the structural and spectroscopic properties of biologically active molecules with DFT (Hohenberg & Kohn, 1964; Kohn & Sham, 1965) using B3LYP functional (Becke, 1988; Lee et al., 1988) was carried out using the Gaussian 09 program (M. Frisch et al., 2009). The DFT uses a hybrid functional B3LYP, which is consist of a hybrid exchange functional, Becke's three parameters (local, non-local, and Hartree-Fock) and correlation functional, Lee-Yang-Parr. The geometry optimization and computation of vibrational modes were performed at 6-311++G(d,p) level of theory (Dunning Jr, 1989). Using the GAR2PED software tool, the potential energy distribution (PED) was attributed to the derived wavenumbers (Martin & Van Alsenoy, 1995). The distribution of charges in the MEP map, the energy of HOMO abd LUMO were all investigated using GaussView 05 (A. Frisch et al., 2000) . Additionally, by using the NBO 3.1 tool (Glendening & Weinhold, 1998), the hyper-conjugative interaction in the molecule and NBO analysis were carried out.The QTAIM approach was used to assess the electron density function using the AIMALL and AIM 2000 software (Keith, 2009; R. Bader et al., 1979). Furthermore,the analysis of non-covalent interactions, ELF and LOL, DOS, PDOS, and electron-hole distribution were carried out using Multiwfn (Lu & Chen, 2012) and (visual molecular dynamics) VMD (Humphrey et al., 1996). The moledcular docking of ligand and protein have been utilizing AutoDock Vina (Trott & Olson, 2010) and analysis of non-covalent interacitons were conducted using Discovery studio Visualizer software (Studio, 2009).

CHAPTER 4

4. RESULTS AND DISCUSSION

4.1 Introduction

This chapter analyzes and discusses the important research findings. FT-IR and FT-IR, as well as quantum mechanical techniques, were used to gain insight into the structural and spectroscopic properties of bioactive molecules such as cefalexin and methyldopa. The DFT method was used to investigate electronic structures, conformational stability, chemical and biological activity. The main discoveries concerning the molecule of interest are cefalexin and methyldopa.

i. The stable conformers of cefalexin were investigated using a one dimensional potential surface scan. The optimized parameters, like bond lengths, bond angles and dihedral angles, were calculated for stable conformers. The electron localization and delocalization zones were visualized with the help of a two-dimensional plot of electron localization functions (ELF). The charge concentrations in space around the molecule were analyzed on the basis of electrostatic potential. The presence of intramolecular and intermolecular hydrogen bonding has been explained in terms of IR, and Raman spectra. The highest occupied molecular orbital energy (E_{HOMO}) and the lowest unoccupied molecular orbital energy (E_{LUMO}) were obtained to explain the chemical stability of the molecule. Utilizing these frontier molecular orbitals (FMOs) and their energy gap ($\triangle E_{\mathrm{L\text{-}H}}$), global reactivity parameters were calculated. The active sites of the interactions have been predicted using the molecular electrostatic potential (MEP). Both the global and the local reactivity of molecules were predicted. The interactions between filled and unfilled orbitals along with their contributions to the stabilization energy of molecules were used to explain the charge transfer characteristics. Furthermore, utilizing the quantum theory of atoms in molecules (QTAIM) the strength of hydrogen bonds was determined. The Mulliken atomic charge associated with each of the atoms in a molecule was calculated. The first and second hyperpolarizability of a molecule were calculated, which indicates that molecule

could be a suitable candidate for NLO materials. The thermodynamic behavior at different temperatures was studied. Finally, the biological activity of cefalexin with the selected target proteins was determined following the molecular docking simulation.

ii. The structural and chemical stability of methyldopa were studied using quantum chemical methods. The Quantum theory of atoms in mlecules (QTAIM) along with the reduced density gradient (RDG) were analyzed to explore the non-covalent interactions. The ELF was used to depict the electronic environment of each atom in a molecule. The chemical stability of a monomer and its dimer state have been examined. The intramolecular hydrogen bonding present in monomer and dimers has been analyzed using QTAIM and non-covalent interaction (NCI) methods. The hydrogen bonds, along with their contribution to the stabilization energy, were further confirmed using natural bond orbital (NBO) analysis as well. The chemical reactivity was analyzed on the basis of the FMOs, energy gap, and global and local reactivity descriptor parameters. In addition, the density of states (DOS) was used to depict FMOs. The MEP predicted the active sites of hydrogen bonding. The electron-hole analysis was performed to confirm the charge-transfer in the molecule. The thermodynamic properties were studied. The first hyperpolarizability and second hyperpolarizability were computed for methyldopa. The biological interactions of the molecule with the target protein have been studied.

4.2 Cefalexin

Cefalexin, is an antibiotic which is used to treat the bacterial infections. To gain more insight into its electronic and biological properties, the study was conducted in its different possible conformers.

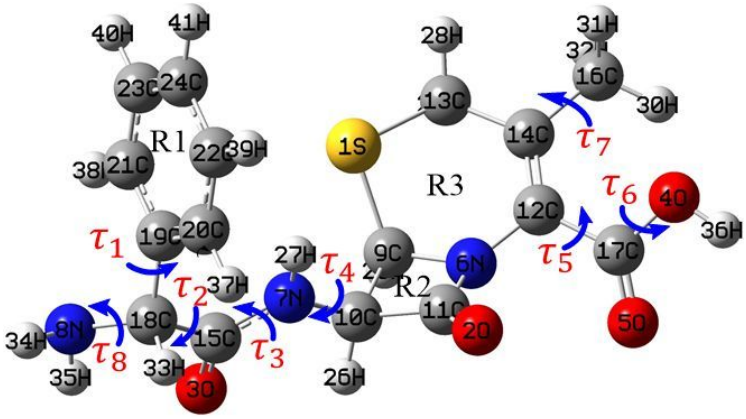

Figure 3: Eight flexible dihedral angles of cefalexin molecule.

4.2.1 Conformational analysis and estimation of optimized parameter

At a room temperature, the same molecule may be present in various configuration (K. Srivastava et al., 2016). Thus, the main objective of conformational analysis of the drug cefalexin has been to predict the change in its characteristics due to a change in the conformation. The three dimensional structure of cefalexin was downloaded from the online tool PubChem Compound Database. The molecule was optimized first, using the B3LYP/6-311++G(d,p) level of basis sets and then, the one-dimensional potential energy surface (PES) scan was performed across the eight rotatable bonds: C19-C18, C18-C15, C15-C7, C7-C10, C12-C17, C17-C4, C14-C16, C18-C8, denoted by τ_1, τ_2, τ_3, τ_4, τ_5, τ_6, τ_7 and τ_8 as shown in Figure 3. The graph in Figure 4, shows the relative energy variation across each of these rotatable bonds. From, the PES scan, the eight conformers either corresponding to global or local minimum energy, were explored. The structure at each and every minima, were again optimized using the same level of theory. The optimized geometry of all possible conformers are shown in Figure 5.

Table 1 shows the ground state and relative energy of the conformers A, B, C, D, E, F, G and H. The conformers that are only expected to exist at room temperature are those with relative energies smaller than 0.56 kcal/mol (or kT) (M. K. Chaudhary et al., 2020). Since the conformers A and B have a relative energy below 0.56 kcal/mol, their existence is possible at room temperature. The conformer A exhibits the lowest minimum energy state, so it is the most stable one. The ground state optimized energy was found to be -930983.638 kcal/mol for conformer A and -930983.102 kcal/mol for conformer B. (T. Chaudhary et al., 2021).

Table 1: Estimated ground state energy of conformers at B3LYP/6-311++G(d,p) level and their respective relative energy.

Dihedral Angles	Conformers	Energy (Hartree)	Energy (kcal/mol)	Relative Energy (kcal/mol)
τ_5(N6-C12-C17-O4)	A	-1483.6156	-930983.638	0.000
τ_2(N7-C15-C18-C19)	B	-1483.6148	-930983.102	0.536
τ_1(N8-C18-C19-C20)	C	-1483.6135	-930982.299	1.339
τ_7(C13-C14-C16-H32)	D	-1483.6130	-930982.015	1.624
τ_8(C19-C18-N8-H34)	E	-1483.6109	-930980.660	2.979
τ_6(C12-C17-O4-H36)	F	-1483.6057	-930977.381	6.257
τ_3(C10-N7-C15-O3)	G	-1483.6039	-930976.277	7.359
τ_4(C11-C10-N7-C15)	H	-1483.6038	-930976.245	7.393

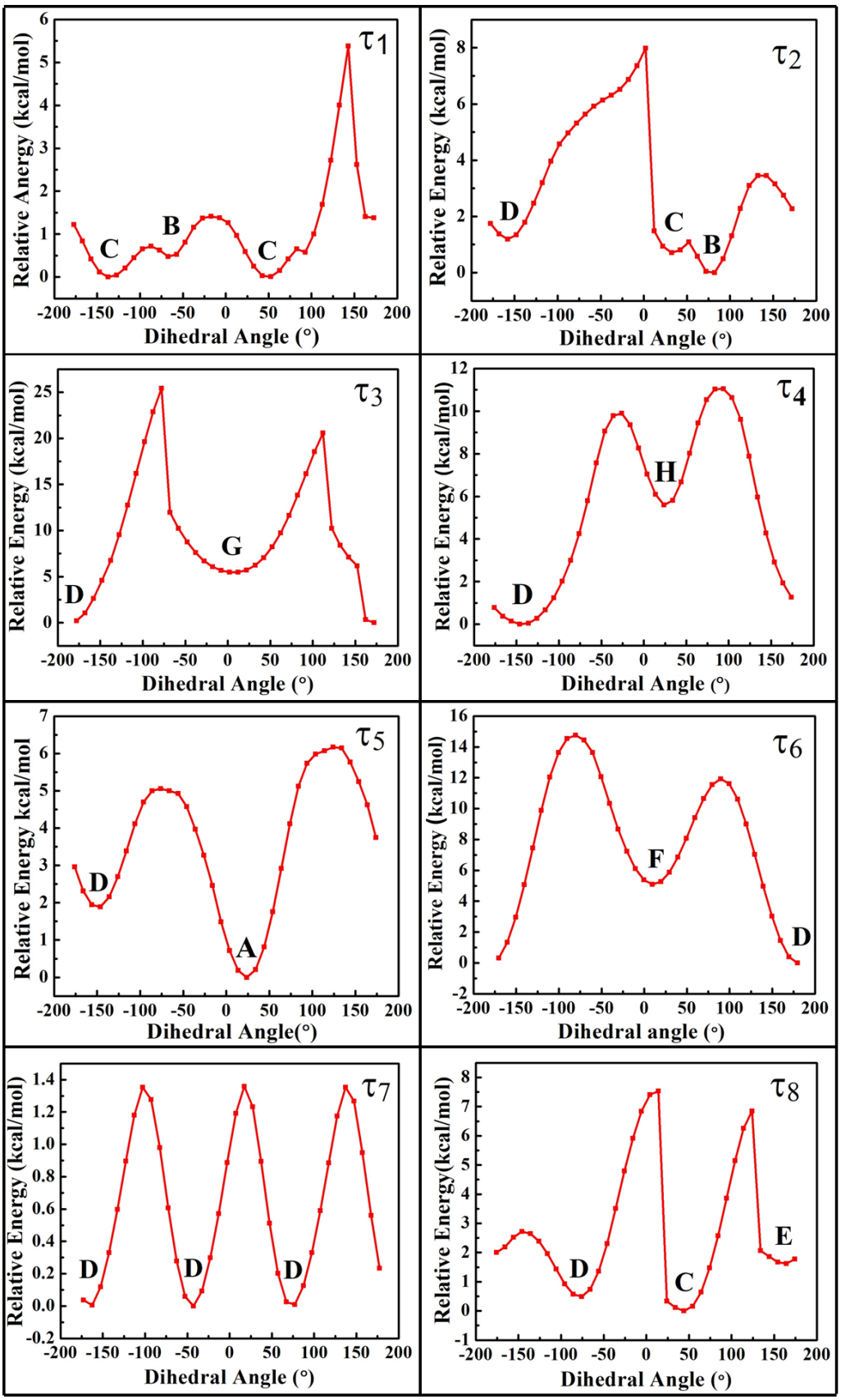

Figure 4: A, B, C, D, E, F, G are the different minima obtained from potential energy surface scans across torsional angles $\tau_1, \tau_2, \tau_3, \tau_4, \tau_5, \tau_6, \tau_7, \tau_8$

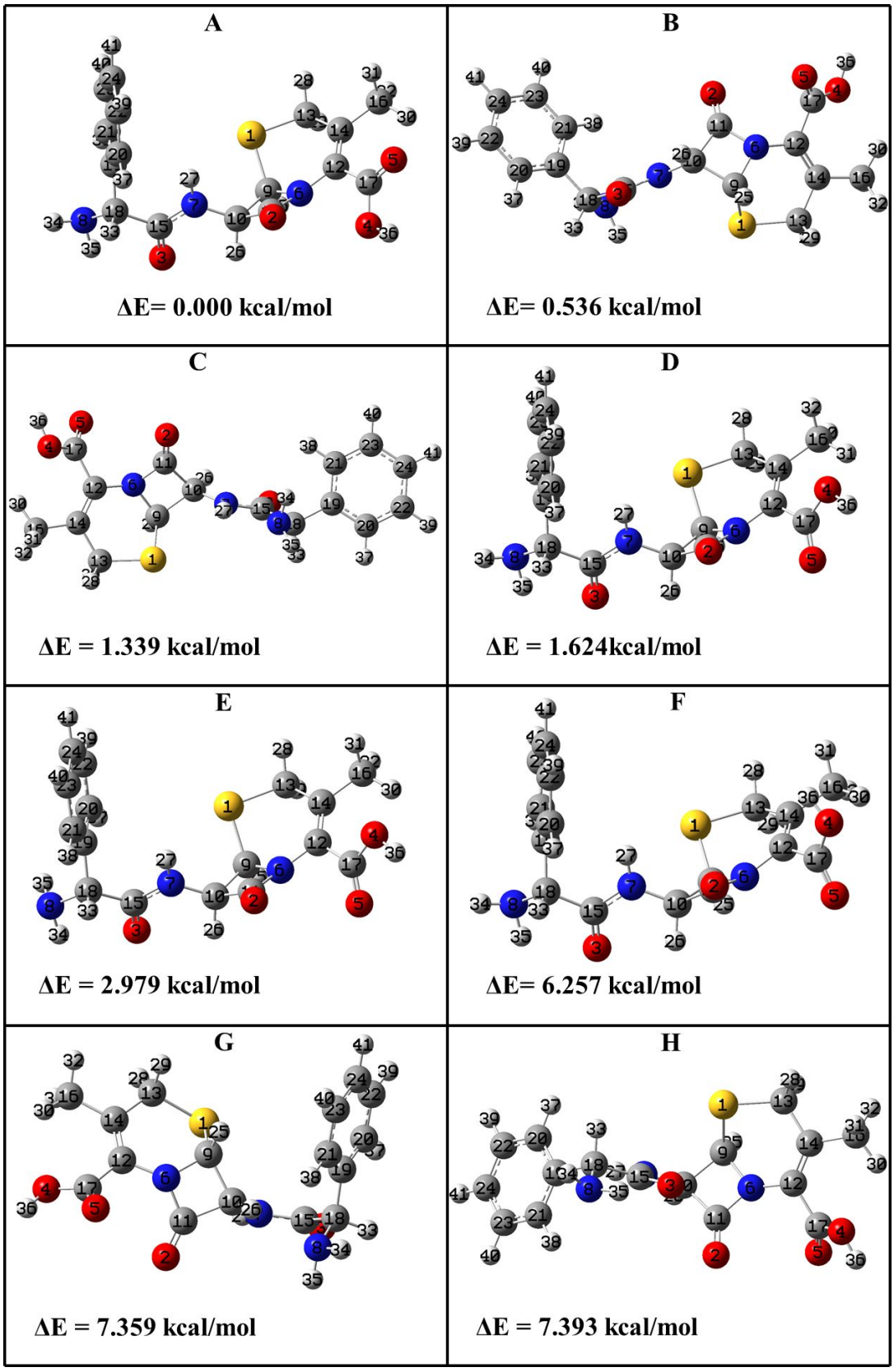

Figure 5: Optimized structure of eight conformers: A, B, C, D, E, F, G, H.

The optimized structures of A and B conformers have been overlapped with the related crystal structure using a least-square algorithm as shown in Figure 6. Thus, the mean

square deviation (RMSD) value of superimposed structure of A and B with the crystal, were obtained as 0.80 Å and 2.16 Å. Since, the A has the lower RMSD than the B conformer, A is closer to the crystal structure. The optimized parameters of conformer A and B i.e. bond length, bond angle and dihedral angle have been presented in Table 2. Both conformers exhibit similar parameters, except some of them vary by a small amount. For instance, the bond length N8-C18 is 0.01 Å longer in conformer B than in conformer A. The angles A(C10-N7-H27), A(C15-N7-H27), A(C18-N8-H35), and A(H34-N8-H35) also differ by respective values of 1.96°, 2.39°, 1.86°, and 1.85°. This indicates the hydrogen bonding in B conformer i.e. H27...N8. Moreover, the bond length X-H contracts rather than lengthens as a result of the blueshift in X-H...Y due to weak hydrogen bonding (Barnes, 2004). Hence, the actual bond length between N7 and H27 in the crystal is 0.13 Å shorter than the calculated bond length 1.10 Å. This is also supported by a noticeable peak in the infrared spectrum that is described in section 4.2.3. The bonds connected to the hydrogen atom often experience a low scattering effect since the X-ray diffraction depends on the atomic mass of an element (K. Srivastava et al., 2016). As a result, it is discovered that the experimental bond lengths C-H (0.94–1.00) Å are shorter than the calculated bond length C–H (1.08–1.10) Å . Moreover, a mirror image or a structural isomer causes the sign of the estimated and measured torsional angles to differ (Swamy & Ravikumar, 2021). Since the study involved optimizing the molecule in an isolated gaseous state, there are still a few minor differences between the optimized crystal parameters and the optimized structure. These differences are caused by interactions between molecules' hydrogen bonds and crystal packing in the crystal structure (T. Chaudhary et al., 2021).

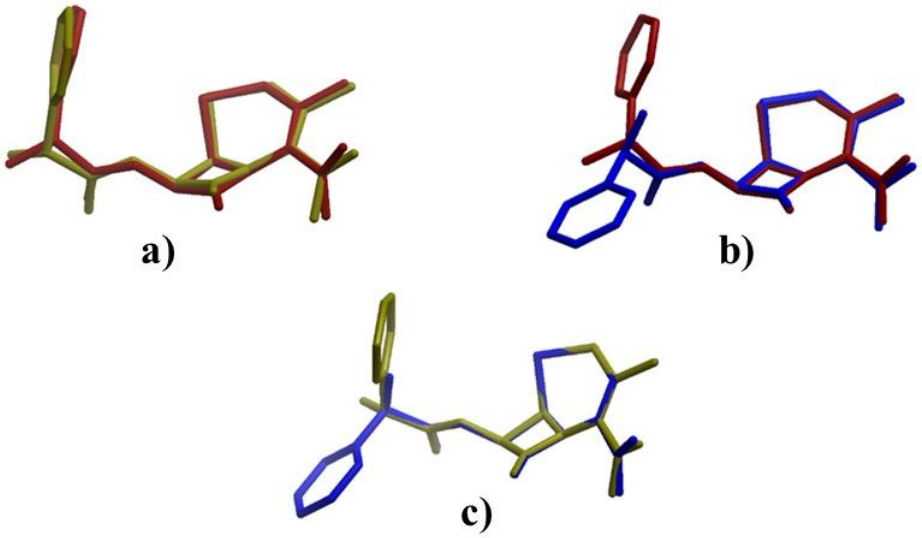

Figure 6: Superimposition of a) crystal (red) with conformer A (green), b) crystal (red) with conformer B (blue), and c) conformer A (green) with conformer B (blue).

Table 2: Optimized parameters of conformers A and B of cefalexin computed at B3LYP/6-311++G(d,p).

Bond	crystal (Å)	Conformer A (Å)	Conformer B (Å)
S1-C9	1.809	1.83	1.83
S1-C13	1.806	1.84	1.84
O2-C11	1.208	1.20	1.20
O3-C15	1.218	1.22	1.22
O4-C17	1.246	1.35	1.35
O4-H36	-	0.97	0.97
O5-C17	1.246	1.21	1.20
N6-C9	1.466	1.46	1.46
N6-C11	1.367	1.40	1.40
N6-C12	1.402	1.41	1.41
N7-C10	1.430	1.43	1.43
N7-C15	1.218	1.37	1.37
N7-H27	0.880	1.01	1.01
N8-C18	1.482	1.46	1.47
N8-H34	-	1.01	1.01
N8-H35	-	1.02	1.02
C9-C10	1.544	1.57	1.57
C9-H25	0.999	1.09	1.09
C10-C11	1.534	1.55	1.55
C10-H26	1.000	1.09	1.09
C12-C14	1.340	1.35	1.35
C12-C17	1.523	1.49	1.50
C13-C14	1.502	1.52	1.52
C13-H28	0.990	1.09	1.09
C13-H29	0.990	1.10	1.10
C14-C16	1.511	1.51	1.51
C15-C18	1.526	1.55	1.55
C16-H30	0.979	1.09	1.09
C16-H31	0.981	1.09	1.09
C16-H32	0.979	1.10	1.10
C18-C19	1.526	1.52	1.52
C18-H33	1.001	1.10	1.10
C19-C20	1.379	1.39	1.39
C19-C21	1.387	1.40	1.40
C20-C22	1.389	1.39	1.39
C20-H37	0.949	1.09	1.09
C21-C23	1.384	1.39	1.39
C21-H38	0.950	1.08	1.08
C22-C24	1.376	1.39	1.39

C22-H39	0.951	1.08	1.08
C23-C24	1.389	1.39	1.39
C23-H40	0.950	1.09	1.08
C24-H41	0.951	1.08	1.08
Bond Angles (°)	Crystal	A	B
C9-S1-C13	93.56	94.18	93.97
C17-O4-H36	-	107.00	106.50
C9-N6-C11	94.06	94.86	94.88
C9-N6-C12	127.17	126.09	126.39
C11-N6-C12	132.25	131.92	131.55
C10-N7-C15	120.41	121.80	122.09
C10-N7-H27	119.80	119.42	121.38
C15-N7-H27	119.79	118.77	116.37
C18-N8-H34	-	110.90	110.59
C18-N8-H35	-	109.28	111.15
H34-N8-H35	-	109.06	107.76
S1-C9-N6	110.24	110.75	110.61
S1-C9-C10	115.36	115.52	115.77
S1-C9-H25	113.50	110.45	110.26
N6-C9-C10	88.25	87.92	87.97
N6-C9-H25	113.53	113.75	113.81
C10-C9-H25	113.50	116.67	116.68
N7-C10-C9	119.16	121.00	121.00
N7-C10-C11	114.80	116.99	116.80
N7-C10-H26	111.86	108.38	108.74
C9-C10-C11	84.73	84.87	84.82
C9-C10-H26	111.78	111.06	110.76
C11-C10-H26	111.87	113.05	113.12
O2-C11-N6	132.33	133.01	132.76
O2-C11-C10	135.27	136.02	136.22
N6-C11-C10	92.39	90.89	90.89
N6-C12-C14	118.22	120.98	121.02
N6-C12-C17	114.81	115.67	112.49
C14-C12-C17	126.94	123.30	126.25
S1-C13-C14	116.41	118.00	117.77
S1-C13-H28	108.18	104.87	104.92
S1-C13-H29	108.24	109.13	109.01
C14-C13-H28	108.12	108.67	108.75
C14-C13-H29	108.19	109.14	109.32
H28-C13-H29	107.37	106.38	106.45
C12-C14-C13	124.85	122.79	122.62

C12-C14-C16	121.29	124.58	124.98
C13-C14-C16	113.13	112.58	112.33
O3-C15-N7	123.78	122.79	123.94
O3-C15-C18	121.50	120.70	121.55
N7-C15-C18	114.53	116.41	114.50
C14-C16-H30	109.56	113.18	113.40
C14-C16-H31	109.45	109.81	110.08
C14-C16-H32	109.49	109.81	109.79
H30-C16-H31	109.42	107.32	107.76
H30-C16-H32	109.38	109.44	108.67
H31-C16-H32	109.53	107.07	106.93
O4-C17-O5	126.52	122.81	122.82
O4-C17-C12	117.10	111.62	113.55
O5-C17-C12	116.37	125.56	123.63
N8-C18-C15	106.39	107.14	110.95
N8-C18-C19	111.98	111.85	110.84
N8-C18-H33	110.14	112.78	113.08
C15-C18-C19	107.46	114.72	109.25
C15-C18-H33	110.15	102.92	104.68
C19-C18-H33	110.12	107.20	107.80
C18-C19-C20	118.55	120.42	119.98
C18-C19-C21	120.86	120.69	121.04
C20-C19-C21	120.49	118.90	118.98
C19-C20-C22	119.85	120.72	120.61
C19-C20-H37	120.08	119.66	119.54
C22-C20-H37	120.47	119.62	119.84
C19-C21-C23	119.85	120.39	120.39
C19-C21-H38	120.00	118.83	119.96
C23-C21-H38	120.15	120.77	119.65
C20-C22-C24	119.49	119.96	120.11
C20-C22-H39	120.31	119.81	119.73
C24-C22-H39	120.20	120.23	120.16
C21-C23-C24	119.27	120.36	120.26
C21-C23-H40	120.40	119.70	119.63
C24-C23-H40	120.33	119.94	120.11
C22-C24-C23	120.99	119.67	119.64
C22-C24-H41	119.65	120.14	120.19
C23-C24-H41	119.37	120.19	120.16
Dihedral Angles (°)	crystal	A	B
C13-S1-C9-N6	54.94	53.36	53.63
C13-S1-C9-C10	152.91	151.28	151.65

C13-S1-C9-H25	−73.68	−73.58	−73.13
C9-S1-C13-C14	−48.89	−44.79	−45.70
C9-S1-C13-H28	−170.80	−165.88	−166.77
C9-S1-C13-H29	73.16	80.49	79.54
H36-O4-C17-O5	-	5.03	−0.02
H36-O4-C17-C12	-	−175.73	179.43
C11-N6-C9-S1	110.48	107.05	107.43
C11-N6-C9-C10	−5.96	−9.52	−9.41
C11-N6-C9-H25	−120.90	−127.85	−127.80
C12-N6-C9-S1	−43.65	−46.04	−45.42
C12-N6-C9-C10	−160.10	−162.60	−162.26
C12-N6-C9-H25	84.96	79.06	79.35
C9-N6-C11-O2	−172.80	−167.37	−166.83
C9-N6-C11-C10	6.00	9.62	9.52
C12-N6-C11-O2	−20.81	−16.81	−16.22
C12-N6-C11-C10	157.99	160.18	160.13
C9-N6-C12-C14	8.28	12.28	11.20
C9-N6-C12-C17	−169.78	−165.02	−163.53
C11-N6-C12-C14	−135.71	−130.39	−131.39
C11-N6-C12-C17	46.24	52.29	53.88
C15-N7-C10-C9	102.79	114.19	111.76
C15-N7-C10-C11	−159.55	−144.92	−147.55
C15-N7-C10-H26	−30.69	−15.71	−18.07
H27-N7-C10-C9	−77.58	−67.36	−73.06
H27-N7-C10-C11	20.59	33.54	27.63
H27-N7-C10-H26	149.45	162.75	157.11
C10-N7-C15-O3	2.48	−4.37	−5.48
C10-N7-C15-C18	−172.68	172.13	173.60
H27-N7-C15-O3	−177.66	177.17	179.11
H27-N7-C15-C18	−7.18	−6.34	−1.81
H34-N8-C18-C15	-	157.75	−160.69
H34-N8-C18-C19	-	−75.73	−39.13
H34-N8-C18-H33	-	45.21	82.05
H35-N8-C18-C15	-	37.49	79.67
H35-N8-C18-C19	-	164.01	−158.78
H35-N8-C18-H33	-	−75.05	−37.60
S1-C9-C10-N7	9.22	15.04	14.79
S1-C9-C10-C11	−106.30	−103.49	−103.48
S1-C9-C10-H26	142.23	143.80	143.74
N6-C9-C10-N7	120.84	127.10	126.75
N6-C9-C10-C11	5.32	8.57	8.48

N6-C9-C10-H26	−106.15	−104.18	−104.30
H25-C9-C10-N7	−124.19	−117.26	−117.51
H25-C9-C10-C11	120.29	124.21	124.22
H25-C9-C10-H26	8.82	11.46	11.44
N7-C10-C11-O2	53.26	45.56	45.04
N7-C10-C11-N6	−125.48	−131.27	−131.09
C9-C10-C11-O2	−172.80	167.88	167.29
C9-C10-C11-N6	−5.71	−8.95	−8.84
H26-C10-C11-O2	−75.60	−81.40	−82.33
H26-C10-C11-N6	105.66	101.78	101.54
N6-C12-C14-C13	2.88	2.06	2.47
N6-C12-C14-C16	−173.41	−175.28	−174.00
C17-C12-C14-C13	−179.33	179.17	176.43
C17-C12-C14-C16	4.39	1.82	−0.05
N6-C12-C17-O4	−138.03	26.68	−145.50
N6-C12-C17-O5	41.62	−154.10	33.95
C14-C12-C17-O4	44.11	−150.57	40.11
C14-C12-C17-O5	−136.23	28.65	−140.44
S1-C13-C14-C12	24.71	21.37	22.03
S1-C13-C14-C16	−158.72	−161.00	−161.09
H28-C13-C14-C12	146.66	140.48	141.11
H28-C13-C14-C16	−36.77	−41.89	−42.02
H29-C13-C14-C12	−97.36	−103.91	−103.04
H29-C13-C14-C16	79.21	73.73	73.83
C12-C14-C16-H30	4.94	15.87	12.03
C12-C14-C16-H31	−119.04	−104.03	−108.77
C12-C14-C16-H32	120.90	138.50	133.78
C13-C14-C16-H30	−175.74	−161.71	−164.76
C13-C14-C16-H31	64.28	78.39	74.45
C13-C14-C16-H32	−57.79	−39.09	−43.01
O3-C15-C18-N8	27.36	−33.11	−161.03
O3-C15-C18-C19	−93	−157.91	76.48
O3-C15-C18-H33	147.02	86.00	−38.74
N7-C15-C18-N8	−157.36	150.32	19.86
N7-C15-C18-C19	82.26	25.51	−102.63
N7-C15-C18-H33	−37.83	−90.57	142.15
N8-C18-C19-C20	131.74	141.41	136.01
N8-C18-C19-C21	−51.90	−39.23	−44.82
C15-C18-C19-C20	−111.80	−96.30	−101.44
C15-C18-C19-C21	65.17	83.06	77.74
H33-C18-C19-C20	8.90	17.29	11.76

H33-C18-C19-C21	−174.75	−163.35	−169.06
C18-C19-C20-C22	174.47	178.65	179.41
C18-C19-C20-H37	−5.49	−1.74	−0.18
C21-C19-C20-C22	−1.90	−0.72	0.22
C21-C19-C20-H37	178.14	178.90	−179.37
C18-C19-C21-C23	−175.21	−178.80	−179.56
C18-C19-C21-H38	4.63	2.26	0.15
C20-C19-C21-C23	−179.07	0.57	−0.38
C20-C19-C21-H38	−179.08	−178.37	179.33
C19-C20-C22-C24	2.65	0.40	0.04
C19-C20-C22-H39	−177.45	179.82	−179.96
H37-C20-C22-C24	−177.39	−179.21	179.63
H37-C20-C22-H39	2.51	0.21	−0.37
C19-C21-C23-C24	1.00	−0.10	0.27
C19-C21-C23-H40	179.09	−179.91	179.83
H38-C21-C23-C24	179.16	178.82	−179.44
H38-C21-C23-H40	−0.74	−0.99	0.12
C20-C22-C24-C23	−2.61	0.08	−0.15
C20-C22-C24-H41	177.55	179.65	−179.98
H39-C22-C24-C23	177.48	−179.35	179.85
H39-C22-C24-H41	−2.35	0.23	0.01
C21-C23-C24-C22	1.80	−0.22	−0.01
C21-C23-C24-H41	−178.36	−179.80	179.83
H40-C23-C24-C22	−178.30	179.58	−179.56
H40-C23-C24-H41	1.54	0.00	0.28
C17-C12-C14-C13	−179.33	179.17	176.43
C17-C12-C14-C16	4.39	1.82	−0.05

4.3 NCI analysis from QTAIM approach

Quantum theory of atoms in molecules (QTAIM) (R. Bader, 1990) has also been examined in order to examine structural differences resulting from intra-molecular interactions. Many physical, chemical, and biological processes are explained using QTAIM, which correctly characterizes an atom as an open system (Koch & Popelier, 1995; Grabowski, 2011). On the basis of ρ_{BCP}, $\bigtriangledown^2\rho_{\mathrm{BCP}}$ and H_{BCP} at BCP, it analyzes the nature of intra- and intermolecular hydrogen bonding. Moreover, Van der Waals interaction is used to describe interactions when the total of the participating atoms' Van der Waals radii $(r_{\mathrm{H}} + r_{\mathrm{A}})$ is larger than the distance between the engaging atoms, where r_{H} and r_{A} are, respectively, the Van der Waals radii of hydrogen and aceptor atoms. Using the AIM2000 program at the B3LYP/6-311++G(d,p) level, the title molecule's conformers A and B's molecular graph has been calculated and is shown in Figure 7.

Both conformers' topological and geometrical parameters are shown in Tables 3 and 4, respectively. We identified just one hydrogen bonding C16-H30...O5 in conformer A and two hydrogen bonding C16-H30...O4 and N7-H27...N8 in conformer B from the molecular graph. All of the observed interactions between a proton and an acceptor atom meet all requirements to be classified as hydrogen bonds (T. Chaudhary et al., 2021). Furthermore, $\bigtriangledown^2\rho_{BCP} > 0$ and $H_{BCP} < 0$ are true for each hydrogen bond in both conformers. Thus, all hydrogen bonds are of the medium type, which are somewhat covalent in nature, in accordance with the criteria of Rozas et al. (2000).

Table 3: Topological parameters for existing intramolecular interactions in conformers A nd B.

Interactions	Bond length (Å)	ρ_{BCP} (a.u.)	$\nabla^2\rho_{BCP}$ (a.u.)	G_{BCP} (a.u.)	V_{BCP} (a.u.)	H_{BCP} (a.u.)	E_{int} (kcal/mol)
Conformer A							
H30...O5	2.30	0.015	0.055	−0.002	−0.100	−0.012	−3.075
Conformer B							
H30...04	2.33	0.022	0.083	−0.003	−0.015	−0.018	−4.709
H27...N8	2.18	0.022	0.053	−0.002	−0.009	−0.011	−2.953

Table 4: The physical parameters of intramolecular interactions in conformer A and B: bond length (D-H and H...A) (Å), bond angle (D-H...A) (°) and the sum of van der Waal radii ($r_H + r_A$) Å of atoms taking part in intramolecular interaction.

D-H...A	D-H (Å)	H...A (Å)	D-H...A (°)	($r_H + r_A$)) (Å)
Conformer A				
C16-H30...O5	1.09	2.30	115.92	2.72
N7-H27...N8	1.01	2.17	108.95	2.75
Conformer B				
C16-H30...O4	1.09	2.33	113.40	2.72
N7-H27...N8	1.014	2.18	108.85	2.75

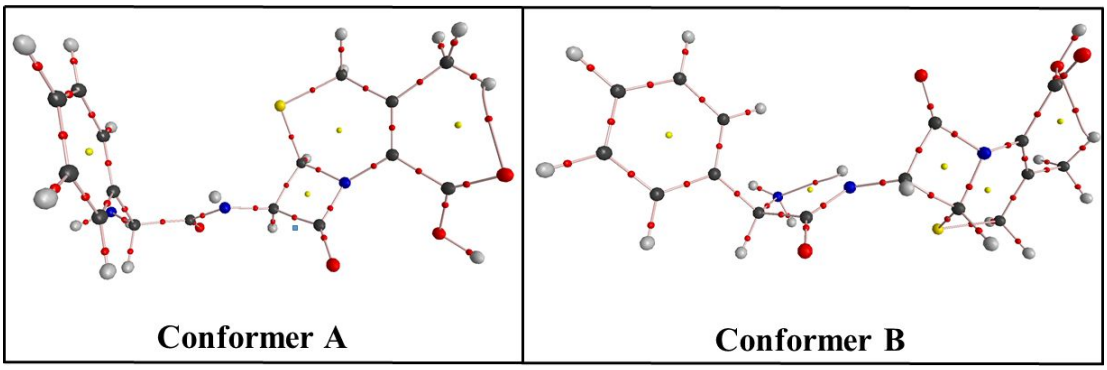

Figure 7: Molecular graph, representing bond critical points and intramolecular hydrogen bonds in cefalexin.

4.3.1 Analysis of vibrational modes

The FTIR and FT-Raman analysis of cefalexin has been analyzed. Also, for each and every vibrational modes with percentage of PED, is illustrated in Table 28 (APPENDIX A1), have been calculated using GAR2PED software employing 6-311++G(d,p) basis sets. Vibrational modes with a very low PED contribution that is below 5% are not taken into consideration. The molecule being a non-linear, it exhibits total 117 (3N-6) modes of vibration. The computed wavenumbers typically have a higher value than the observed one because vibrational analysis assumes simple harmonic vibrations. Thus, the calculated wavenumbers were rescaled using the WLS factor (Yoshida et al., 2002). The observed and calculated FT-IR and Raman spectrafor A and B conformers are shown in Figure 8 and 9, respectively. The conformer A, being the most stable and closer to the crystal structure, it is has received the most attention in the subsequent vibrational study.

4.3.1.1 O-H vibration

The stretching vibration of the hydroxyl group with 100 % PED contribution was calculated at 3570 cm^{-1}. Moreover, stretching bands for an unbonded O-H group often occur in the range 3530–3645 cm^{-1} in various compounds, whereas stretching bands for an H-bonded O-H group typically occur in the C–H characteristic range 3300–2500 cm^{-1} in carboxylic acid (Coates, 2006). A large peak that confirms O-H stretching has been seen in the range of 2800-3300 cm^{-1} in the FT-IR spectra. Strong hydrogen bonding is prevalent in the crystal form, as seen by the lowering of stretching bands with a large peak. In the IR/Raman, deformation of CHO with a low PED contribution was found at 1152 cm^{-1} and assigned to 1157/1156 cm^{-1} (T. Chaudhary et al., 2021).

4.3.1.2 N-H vibration

Stretching vibrations of the primary and secondary amine often occur in the ranges of 3460–3325 cm^{-1} and 3490–3310 cm^{-1}, respectively (Coates, 2006). The symmetric stretching of NH_2 was obtained at 3412 cm^{-1} and seen at 3356 cm^{-1} in the infrared spectra. Similar to this, the calculated asymmetric stretching at 3333 cm^{-1} was seen in the IR spectra at 3331 cm^{-1}. The inter-molecular hydrogen bonding of the amine group in the crystal form is indicated by the redshift in the symmetric vibration. Moreover, the scissoring vibration described in the Raman spectra at 1601 cm^{-1} and 1600 cm^{-1} is within the range of 1638–1575 cm^{-1} in the literature (Lin-Vien et al., 1991; Karabacak et al., 2010). Once more, the Raman spectra showed that NH_2 was waging at 817 cm^{-1} and 819 cm^{-1}. Secondary amine's stretching band was estimated at 3421 cm^{-1} and found in FT-IR spectra at 3480 cm^{-1}. Barnes claims that in hydrogen bonding, weakly interacting bases cause the blueshift to become less intense, whereas highly

interacting bases cause the redshift to become more intense (Barnes, 2004). Hence, hydrogen bonding between weakly interacting bases is the cause of the constriction of the bond N7-H27 and the blue shift in the vibration. Moreover, the Raman spectra revealed a rocking of the secondary amine N7H27 at the absorption band 1227 cm^{-1}, observable at 1229 cm^{-1} (T. Chaudhary et al., 2021).

4.3.1.3 C-H vibration

In aromatic structure, the region for C-H stretching bands lies in the range 3100-3000 cm^{-1} (S. Muthu & Maheswari, 2012; Sevvanthi et al., 2017). In the ring R1, five CH moieties were vibrating in five different stretching modes between 3018 and 3058 cm^{-1}. In the Raman spectrum for R1[ν(CH)], calculated bands at 3054, 3048, and 3041 cm^{-1} were found at 3057, 3049, and 3047 cm^{-1}. Both IR and Raman were able to detect the stretching of R2[ν(CH)] at 2977 cm^{-1} at frequencies of 2983 cm^{-1} and 2967 cm^{-1}, respectively. The aromatic CH was found to exhibit in-plane bending vibrations in the ranges of 1350-950 cm^{-1} and out-of-plane bending vibrations in the range of 1100-600 cm^{-1} (S. Muthu & Maheswari, 2012; Karrouchi et al., 2021). In the IR and Raman spectra, the methine moieties of ring R2 were seen to rock at frequencies of 1245 cm^{-1} and 1246/1245 cm^{-1}. In the range of 713-1001 cm^{-1}, the out of plane bending of CH in the ring R1 was seen. The regions 3000-2905 cm^{-1} and 2870-2860 cm^{-1} are predicted to contain the methyl group's (CH_3) asymmetric and symmetric stretching bands, respectively (C. Liu et al., 1991; Alpert et al., 1970). In the IR/Raman spectra, the asymmetric stretching calculated at 2935 cm^{-1} was seen at 2934/2933 cm^{-1} while the symmetric stretching at 2895 cm^{-1} was seen at 2897/2884 cm^{-1}. In the provided range of asymmetric (1465-1440 cm^{-1}) and symmetric deformation (1390-1370 cm^{-1}) the asymmetric deformation was assigned at 1454 cm^{-1} in the IR and the symmetric deformation at 1398/1397 cm^{-1} in the IR/Raman spectrum (Joshi et al., 2014). The measured results and the rocking of CH_3 predicted at 1041cm^{-1} agreed nicely (T. Chaudhary et al., 2021).

The typical ranges for the asymmetric and symmetric stretching of CH_2 are 3000-2900 cm^{-1} and 2900-2800 cm^{-1}, respectively (S. Muthu & Maheswari, 2012). In the IR/Raman Spectra, the asymmetric stretching band of CH_2 connected to ring R3 was calculated at 2949 cm^{-1} and observed at 2947/2942 cm^{-1}, while symmetric stretching at 2900 cm^{-1} was seen at 2910/2912 cm^{-1}. The twisting vibration at 1193 cm^{-1} was seen at 1194/1994 cm^{-1} in the IR/Raman spectrum, while the scissoring vibration estimated at 1429 cm^{-1} was observed at the same frequency in Raman spectra. Moreover, low-intensity waging of CH_2 was found at 1286 cm^{-1} in the Raman spectrum and 863 cm^{-1} in the IR spectrum, respectively (T. Chaudhary et al., 2021).

4.3.1.4 C=O, C-C vibration

In the range of 1870–1550 cm^{-1}, the carbonyl group (C=O) typically displays prominent stretching bands (Socrates, 2004). In the experimental IR spectra with a strong peak, the stretching bands of the carbonyl groups (C11=O, C17=O, and C15=O) calculated at 1817, 1751, and 1709 cm^{-1} were detected at 1756, 1743, and 1681 cm^{-1}. In carboxylic acid, the typical zone for C=O stretching falls between 1750 and 1600 cm^{-1} (Joshi et al., 2014). Due to the intramolecular hydrogen bonding, C15-O5...H30 as depicted in FT-IR spectra, the observed frequency of C15=O is lower than the expected frequency. Moreover, the intense red zone over oxygen around the carbonyl groups, as shown in ESP, indicates oxygen as a highly electronegative region. Hence, hydrogen bonding is responsible for the decrease in the wavenumbers of C11=O and C15=O. In addition, the deformation of C17=O was visible at 788 /766 cm^{-1} and the rocking at 694 /693 cm^{-1} in the IR and Raman spectra (T. Chaudhary et al., 2021).

Typically, the range of 1650 to 1100 cm^{-1} is where the stretching vibration of C-C occurs (A. Srivastava et al., 2017). The stretching bands of C-C estimated at 1056, 1076, and 1593 were observed in the IR/Raman spectra at 1063/1058 cm^{-1}, 1077/1077 cm^{-1} and 1593/1583 cm^{-1}, respectively. The stretching of C12=C14 estimated at 1648 cm^{-1} was found to be 1645 cm^{-1} in FT-IR and 1643 cm^{-1} in Raman spectra (T. Chaudhary et al., 2021).

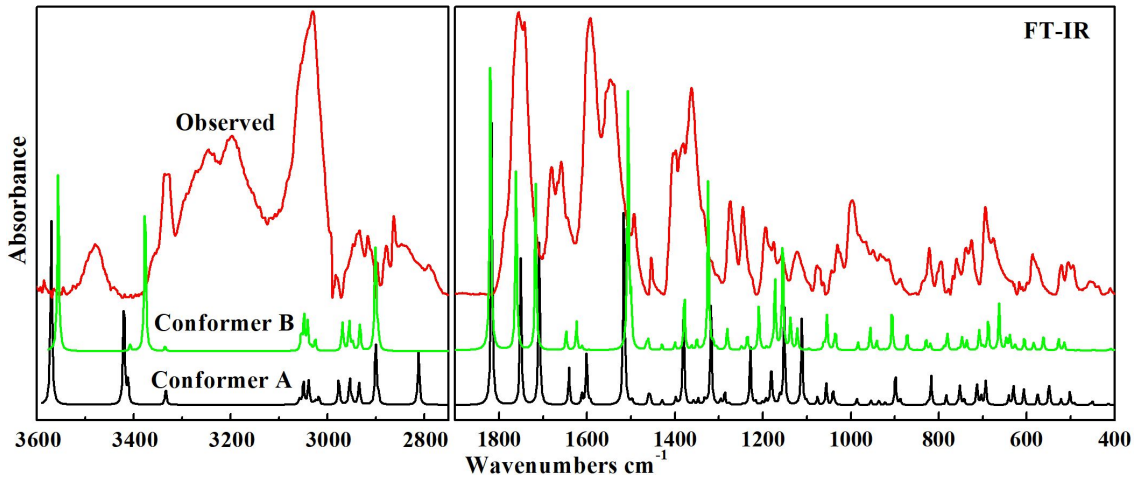

Figure 8: Obsereved and calculated IR spectra for cefalexin.

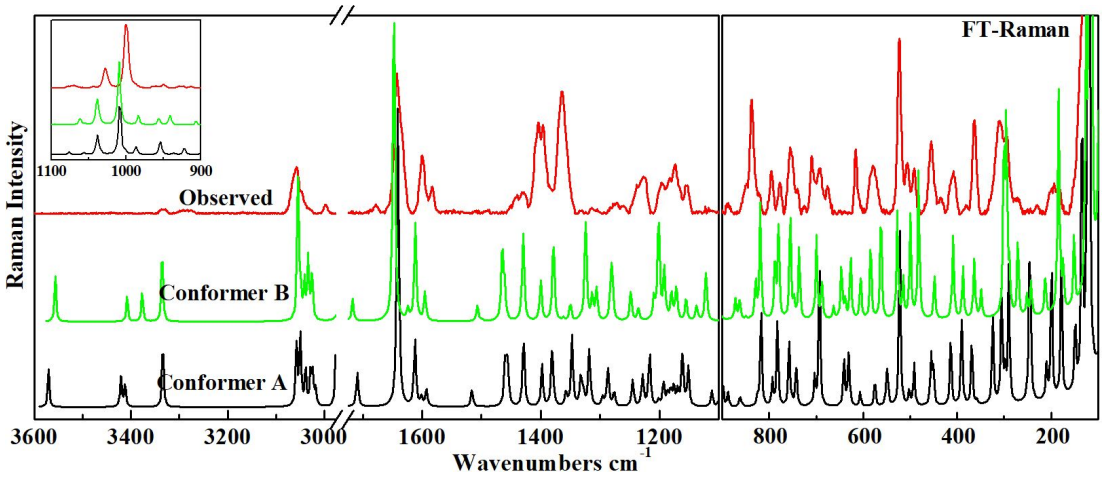

Figure 9: Obsereved and calculated Raman spectra for cefalexin.

4.3.2 Natural bond orbital (NBO) analysis

The NBO analysis was carried out for the most stable conformer A to investigate the interactions between orbitals with filled (donor) and empty (acceptor) Lewis-type NBOs at the B3LYP/6311++G(d,p) level of theory. The analysis was performed using Fock matrix second-order perturbation theory as shown in Table 5. It was explored that the delocalization of electrons from LP(1)N7 to π*(O3-C15) , from LP(1)N6 to π*(O2-C11) and from LP(2)O4 to π*(O5-C17) have the maximum calculated stabilization energies, 46.73, 45.86, and 43.68 kcal/mol, respectively. The greatest charge delocalization energy was 21.47 kcal/mol and was caused by the occupancy of π bonds and π* bonds. The π bonds and π* bonds have respective occupancy ranges of 1.656-1.871 and 0.247-0.361. The maximal delocalization energy, on the other hand, was 7.21 kcal/mol due to the interactions between bonds σ and σ* having occupancy in the range of 1.964-1.977 and 0.018-0.046 (T. Chaudhary et al., 2021).

Table 5: Second-order perturbation theory analysis of Fock matrix in NBO basis for cefalexin.

Donor (i) (i)	ED(i)/e	Acceptor (j)	ED(j)/e	$E^{(2)x}$ kcal/mol	$E(j)-E(i)^y$ (a.u)	$F(i,j)^z$ (a.u.)
σ (N6-C9)	1.977	σ*(O2-C11)	0.018	6.33	1.38	0.084
σ(C9-C10)	1.964	σ*(O2-C11)	0.018	6.39	1.25	0.080
σ (C9-C10)	1.964	σ*(N6-C12)	0.046	6.12	1.01	0.070
σ(C10-C11)	1.965	σ*(N6-C12)	0.046	7.25	1.01	0.077
π (C12-C14)	1.871	π*(O5-C17)	0.247	15.47	0.30	0.062
π (C19-C20)	1.676	π*(C21-C23)	0.306	19.20	0.29	0.067
π (C19-C20)	1.676	π*(C22-C24)	0.306	19.81	0.29	0.067
π (C21-C23)	1.656	π*(C19-C20)	0.361	21.47	0.28	0.069
π (C21-C23)	1.656	π*(C22-C24)	0.306	20.58	0.28	0.068
π (C22-C24)	1.665	π*(C19-C20)	0.361	20.21	0.28	0.068

π (C22-C24)	1.665	π*(C21-C23)	0.306	19.45	0.29	0.067
LP(2)O2	1.818	σ*(N6-C11)	0.103	30.40	0.66	0.129
LP(2)O2	1.818	σ*(C10-C11)	0.095	24.21	0.59	0.109
LP(2)O3	1.856	σ*(N7-C15)	0.073	23.92	0.72	0.119
LP(2)O3	1.856	σ*(C15-C18)	0.079	20.02	0.61	0.101
LP(1)O4	1.977	σ*(O5-C17)	0.019	6.64	1.24	0.081
LP(2)O4	1.817	π*(O5-C17)	0.246	43.68	0.34	0.111
LP(2)O5	1.848	σ*(O4-C17)	0.095	32.46	0.61	0.128
LP(2)O5	1.848	σ*(C12-C17)	0.072	18.34	0.67	0.101
LP(1)N6	1.659	σ*(S1-C9)	0.055	9.14	0.42	0.060
LP(1)N6	1.659	π*(O2-C11)	0.238	45.86	0.30	0.107
LP(1)N6	1.659	π*(C12-C14)	0.159	18.45	0.32	0.072
LP(1)N7	1.699	π*(O3-C15)	0.252	46.73	0.33	0.112
LP(1)N7	1.699	σ*(C9-C10)	0.042	9.86	0.57	0.072
LP(1)N8	1.951	σ*(C18-H33)	1.958	7.48	0.68	0.064
σ (N6-C9)	1.977	σ∗ (O2-C11)	0.018	6.22	1.38	0.083
σ (C9-C10)	1.963	σ*(O2-C11)	0.018	6.38	1.25	0.080
σ (C9-C10)	1.963	σ*(N6-C12)	0.044	6.18	1.01	0.071
σ (C10-C11)	1.965	σ*(N6-C12)	0.044	7.21	1.01	0.076
π (C12-C14)	1.882	π*(O5-C17)	0.225	12.80	0.31	0.058
σ (C16-H31)	1.972	π*(C12-C14)	0.161	5.35	0.55	0.050
π (C19-C20)	1.659	π*(C21-C23)	0.321	20.09	0.28	0.068
π (C19-C20)	1.659	π*(C22-C24)	0.328	20.16	0.28	0.068
π (C21-C23)	1.662	π*(C19-C20)	0.352	21.05	0.28	0.069
π (C21-C23)	1.662	π*(C22-C24)	0.328	20.26	0.28	0.068
π (C22-C24)	1.661	π*(C19-C20)	0.352	20.56	0.28	0.068
π (C22-C24)	1.661	π*(C21-C23)	0.321	20.22	0.28	0.068
LP(2) O2	1.817	σ*(N6-C11)	0.103	30.51	0.66	0.129
LP(2) O2	1.817	σ*(C10-C11)	0.094	24.12	0.59	0.109
LP(2) O3	1.858	σ*(N7-C15)	0.078	24.91	0.72	0.121
LP(2) O3	1.858	σ*(C15-C18)	0.083	20.40	0.60	0.101
LP(1) O4	1.977	σ*(O5-C17)	0.021	6.49	1.24	0.080
LP(2) O4	1.825	π*(O5-C17)	0.225	40.80	0.36	0.110
LP(2) O5	1.840	σ*(O4-C17)	0.099	33.28	0.60	0.129
LP(2) O5	1.840	σ*(C12-C17)	0.075	18.93	0.66	0.102
LP(1) N6	1.658	σ*(S1-C9)	0.056	9.24	0.42	0.060
LP(1) N6	1.656	π*(O2-C11)	0.234	45.21	0.30	0.107
LP(1) N6	1.658	π*(C12-C14)	0.161	18.78	0.32	0.072
LP(1) N7	1.695	π*(O3-C15)	0.275	62.53	0.28	0.120
LP(1) N7	1.695	σ*(C9-C10)	0.043	10.28	0.56	0.073
LP(1) N8	1.946	σ*(C18-H33)	0.030	6.07	0.72	0.060

$^{x}E^{(2)}$ represents the stabilization energy due to hyperconjugative interaction.

^{y} represents the difference of energy between donor (i) and acceptor (j) NBO's orbitals.

$^{z}F(i,j)$ epresents the Fock matrix element between donor and acceptor NBO orbitals.

4.3.3 Chemical reactivity

4.3.3.1 HOMO-LUMO analysis

The frontier molecular orbitals (FMOs) have been utilized to predict the reactivity. Figure 10 shows the HOMO and LUMO plots for both conformers. The HOMO and LUMO orbitals corresponding to ionization potential and electron affinity, respectively, illustrates the molecular properties of electron donation and acceptance (Borah & Devi, 2020). The calculated LUMO energy for conformer A was -1.878 eV and that of conformer B was -1.761 eV. This confirms that conformer A has a higher electron affinity than the B. Similarly, the lower energy gap (4.806 eV) corresponds to conformer A and the higher energy gap (4.961 eV) to conformer B, indicating that conformer A is more reactive. Furthermore, for conformer A, the additional occupied and unoccupied MOs with their respective energy gaps are presented in Figure 11 (T. Chaudhary et al., 2021).

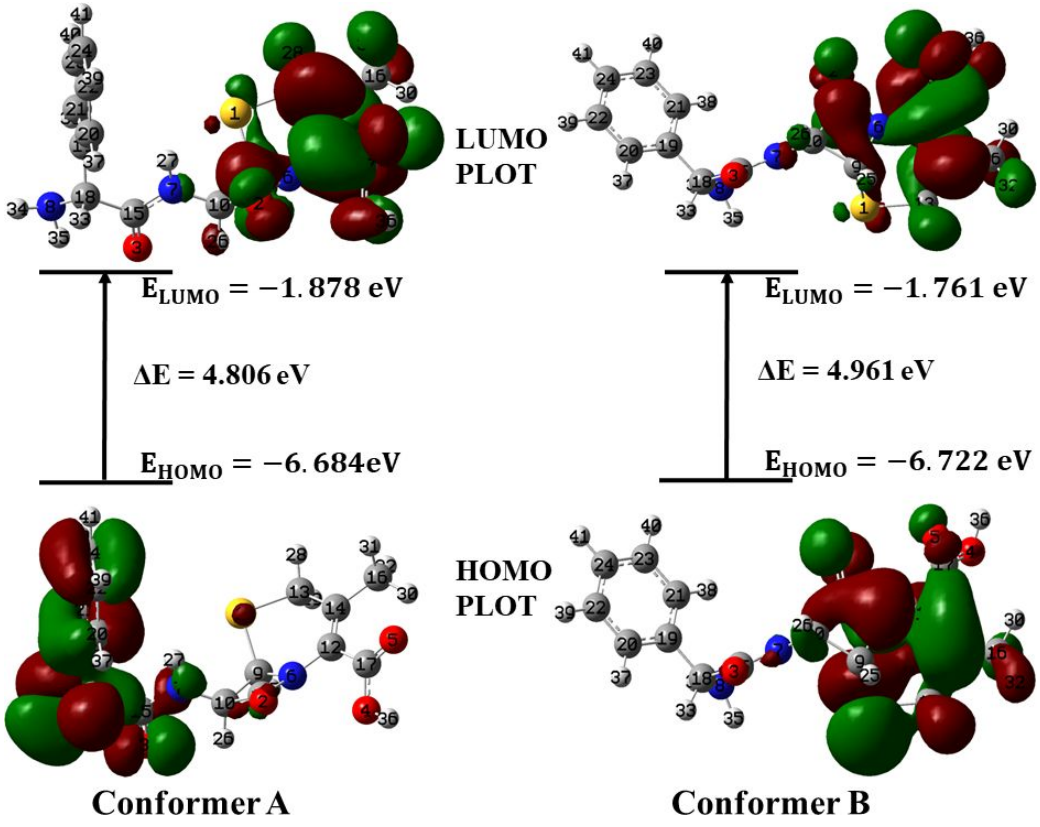

Figure 10: HOMO and LUMO orbitals of cefalexin in gaseous phase.

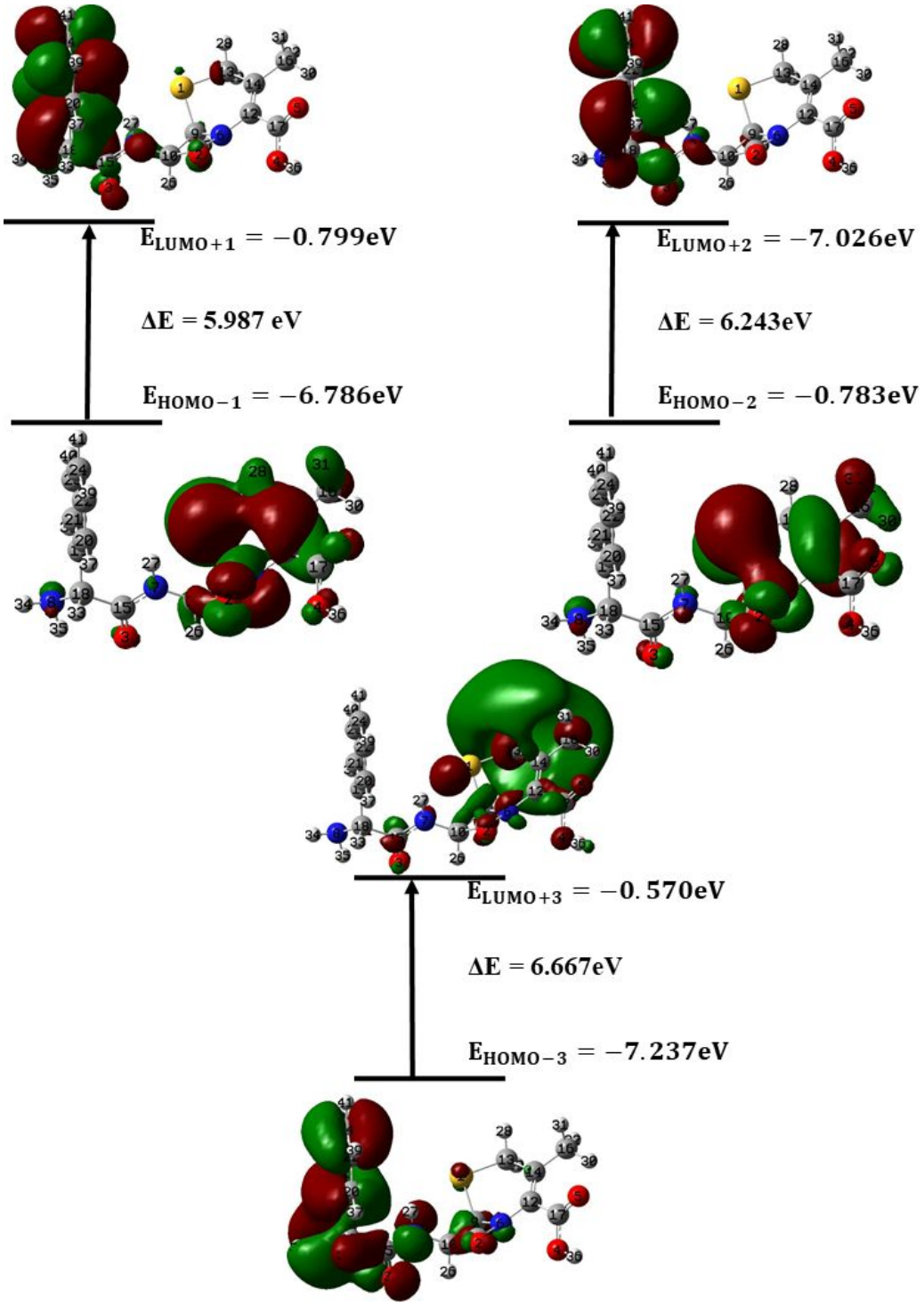

Figure 11: HOMO−1, HOMO−2, HOMO−3, LUMO+1, LUMO+2 and LUMO+3 orbitals of conformer A.

4.3.4 Mulliken charge

The B3LYP/6-311++G(d,p) level of theory has been used to determine the Mulliken charge of cefalexin atoms. Table 6 and Figure 12 both shows the calculated Mulliken charges of the compound's constituent atoms in terms of simple bar diagrams. The bar diagram shows that the atoms C9 and C14 possess the maximum atomic charges. Other

N6, N7, C9, C12, C14, C19, C21 and all hydrogen atoms also have positive atomic charges. Since C13 is attached to the less electronegative atom S1, it has the greatest magnitude of negative atomic charge (-0.925 |e|). Other atoms with atomic charges ranging from -0.170 |e| to -0.315 |e| include O2, O3, O4, O5, and N8. As discussed in the section 4.2.10, oxygen atoms with negative charges and hydrogen atoms play an important role in intermolecular hydrogen bonding (T. Chaudhary & Joshi, 2022).

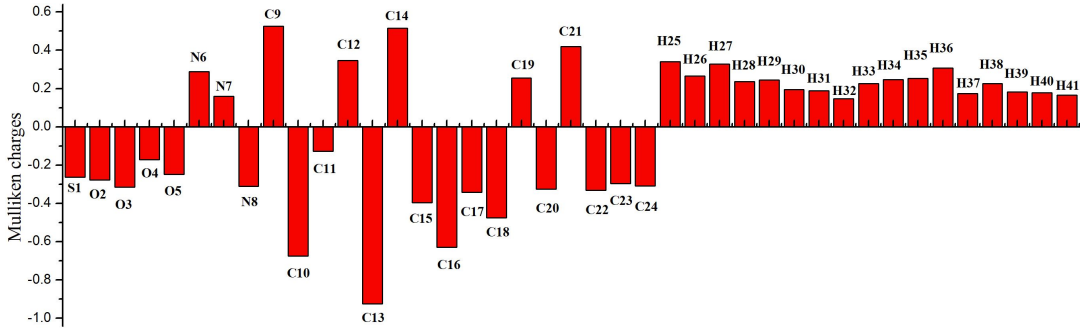

Figure 12: Mulliken charges across each atoms of cefalexin.

Table 6: Value of mulliken charges associated with each atom, calculated at B3LYP/6-311++G(d,p) level of theory.

Atom	Charges |e|	Atom	Charges |e|	Atom	Charges |e|	Atom	Charges |e|
S1	−0.2627	C 12	0.3474	C 23	−0.2968	H 34	0.2467
O2	−0.2766	C 13	−0.9247	C 24	−0.3093	H 35	0.2539
O3	−0.3149	C 14	0.5152	H 25	0.3406	H 36	0.3076
O4	−0.1704	C 15	−0.3956	H 26	0.2647	H 35	0.2539
O5	−0.2480	C 16	−0.6283	H 27	0.3280	H 36	0.3076
N6	0.2893	C 17	−0.3411	H 28	0.2361	H 37	0.1741
N7	0.1596	C 18	−0.4754	H 29	0.2440	H 38	0.2266
N8	−0.3104	C 19	0.2556	H 30	0.1944	H39	0.1815
C9	0.5247	C 20	−0.3248	H 31	0.1888	H40	0.1780
C10	−0.6755	C 21	0.4194	H 32	0.1468	H41	0.1664
C11	−0.1275	C 22	−0.3326	H 33	0.2252	-	-

4.3.4.1 Molecular electrostatic potential surface

The molecular electrostatic potential (MEP) for conformer A and B has been analyzed. The electrostatic potential increases as the colour code: red < yellow < green < blue. That is the most lowest potential is represented by the red colour and the highest potential is represented by the blue colour. The Figure 13 shows the nucleophilic and electrophilic sites for both conformers. The region over the atoms O2, O3, and O5 is designated as having a low electrostatic potential (red region), whereas the region over the atoms H36, H34, and H35 is designated as having a high electrostatic potential (blue region). This may be because the oxygen atom in the carbonyl group contains

lone pairs, which enhances the electron density across oxygen and, as a result, increases the nucleophilic character of oxygen. Yet, because oxygen in carboxylic acid has a high electronegativity, electrons are drawn to H36, increasing the electrophilicity across H36. Also, due to the nitrogen atom's electronegative nature, it is discovered that the region between H34 and H35 has an electrophilic tendency. Also, the molecule's anticipated nucleophilic and electrophilic sites served as proton acceptors and donors, respectively, in the protein-ligand interaction described in sec 4.2.10. (T. Chaudhary et al., 2021).

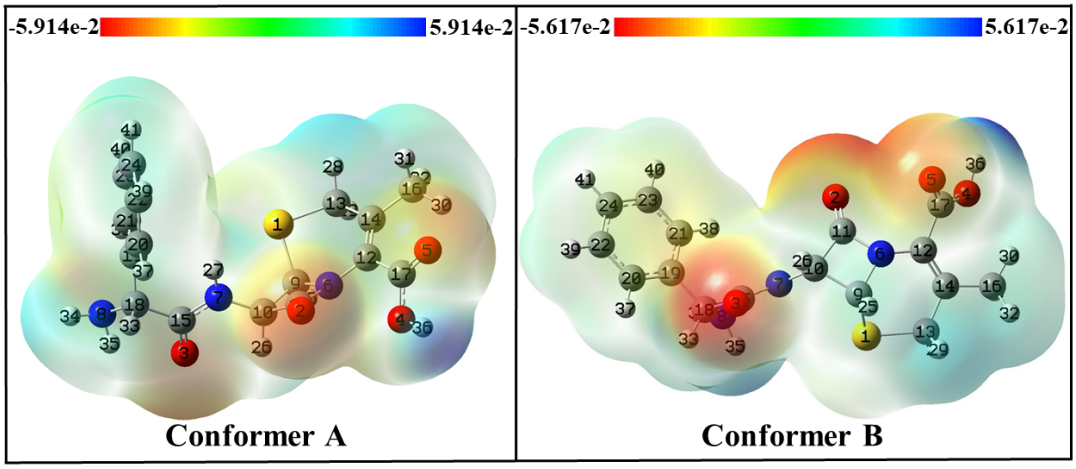

Figure 13: Nucleophilc and electrophilic regions depicted by MEP map of cefalexin.

4.3.4.2 Global reactivity descriptor

The global reactivity descriptors like: hardness (η), softness (S), electronegativity (χ), chemical potential (μ), and electrophilicity index (ω) have been calculated and analyzed for the molecule. In Table 7, the global reactivity descriptors for conformers A and B are displayed. As conformer A has a larger value of ω than conformer B, it has a stronger propensity to draw electrons than conformer B. Moreover, conformer A's global hardness is a little bit lower than conformer B's. This demonstrates that conformer A is, in general, more reactive. Furthermore, the stability of both conformers is specified by the negative chemical potential values for both conformers (T. Chaudhary et al., 2021).

Table 7: Global reactivity descriptors for conformer A and B of cefalexin.

Conformer	E_H	E_L	$\Delta E_{L\text{-}H}$	χ	μ	η	S	ω	ΔN_{max}
A	−6.684	−1.878	4.806	4.281	−4.281	2.403	0.208	3.814	1.782
B	−6.722	−1.761	4.961	4.242	−4.242	2.481	0.202	3.626	1.710

4.3.4.3 Local reactivity descriptors

In order to quantitatively analyze charge in terms of local reactivity factors that describe the chemical activity and specific sites in a molecular system, the Fukui function (FF) is

frequently utilized. A molecule's reactive sites for nucleophilic, electrophilic, and radial attack were predicted by the Fukui function (Fukui, 1982). Table 8 and 9 provides the FF values, local softness, and local electrophilicity of conformers A and B, respectively. For both conformers, it is found that N8 is the most likely site for nucleophilic attack and C17 is the most likely site for electrophilic attack (T. Chaudhary et al., 2021).

Table 8: Calculated local reactivity descriptor parameters of cefalexin: conformer A at B3LYP/6-311++G(d,p) level.

Site	f_k^+	f_k^-	f_0^+	s_k^+	s_k^-	s_k^0	ω_k^+	ω_k^-	ω_k^0
					Conformer A				
S1	0.0184	0.1242	0.1496	0.0038	0.0258	0.0311	0.0701	0.4737	0.5707
O2	0.3487	−0.2675	−0.2459	0.0726	−0.0557	−0.0512	1.3298	−1.0202	−0.9380
O3	0.3857	−0.3070	−0.2884	0.0803	−0.0639	−0.0600	1.4710	−1.1709	−1.0999
O4	0.3380	−0.3261	−0.3376	0.0703	−0.0679	−0.0702	1.2892	−1.2438	−1.2875
O5	0.3212	−0.2875	−0.2883	0.0668	−0.0598	−0.0600	1.2251	−1.0966	−1.0995
N6	0.3459	−0.2558	−0.2067	0.0720	−0.0532	−0.0430	1.3191	−0.9755	−0.7883
N7	0.3300	−0.3304	−0.3120	0.0687	−0.0688	−0.0649	1.2588	−1.2602	−1.1901
N8	0.5768	−0.4226	−0.3447	0.1200	−0.0879	−0.0717	2.1998	−1.6117	−1.3149
C9	0.0494	−0.0633	−0.0629	0.0103	−0.0132	−0.0131	0.1885	−0.2413	−0.2399
C10	0.0613	−0.0488	−0.0495	0.0128	−0.0102	−0.0103	0.2338	−0.1862	−0.1889
C11	−0.3665	0.3403	0.3576	−0.0763	0.0708	0.0744	−1.3977	1.2978	1.3638
C12	0.0209	0.0182	0.0343	0.0043	0.0038	0.0071	0.0795	0.0696	0.1307
C13	0.2525	−0.2712	−0.2669	0.0526	−0.0564	−0.0555	0.9631	−1.0344	−1.0180
C14	0.0631	−0.0536	0.0993	0.0131	−0.0112	0.0207	0.2405	−0.2046	0.3788
C15	−0.3539	0.3549	0.3522	−0.0737	0.0739	0.0733	−1.3499	1.3537	1.3434
C16	0.2938	−0.3027	−0.3021	0.0611	−0.0630	−0.0629	1.1207	−1.1544	−1.1523
C17	−0.4000	0.3647	0.4035	−0.0832	0.0759	0.0840	−1.5254	1.3910	1.5388
C18	0.0473	−0.0529	−0.0546	0.0098	−0.0110	−0.0114	0.1803	−0.2017	−0.2083
C19	0.0920	−0.0452	0.0000	0.0191	−0.0094	0.0000	0.3509	−0.1724	0.0001
C20	0.1130	−0.1052	−0.1043	0.0235	−0.0219	−0.0217	0.4311	−0.4010	−0.3977
C21	0.1257	−0.1010	−0.0751	0.0262	−0.0210	−0.0156	0.4794	−0.3854	−0.2866
C22	0.1201	−0.1011	−0.0864	0.0250	−0.0210	−0.0180	0.4581	−0.3855	−0.3295
C23	0.0907	−0.0926	−0.1012	0.0189	−0.0193	−0.0211	0.3460	−0.3533	−0.3859
C24	0.1820	−0.1051	−0.0572	0.0379	−0.0219	−0.0119	0.6941	−0.4008	−0.2180
H25	−0.0937	0.1089	0.1038	−0.0195	0.0227	0.0216	−0.3574	0.4155	0.3958
H26	−0.1220	0.1375	0.1292	−0.0254	0.0286	0.0269	−0.4653	0.5246	0.4928
H27	−0.2092	0.2119	0.2095	−0.0435	0.0441	0.0436	−0.7977	0.8081	0.7992
H28	−0.1060	0.1254	0.1192	−0.0220	0.0261	0.0248	−0.4041	0.4781	0.4545
H29	−0.0842	0.1173	0.1219	−0.0175	0.0244	0.0254	−0.3213	0.4473	0.4647
H30	−0.1135	0.1240	0.1217	−0.0236	0.0258	0.0253	−0.4327	0.4728	0.4643
H31	−0.0974	0.1202	0.1156	−0.0203	0.0250	0.0241	−0.3715	0.4583	0.4410
H32	−0.0883	0.1120	0.1042	−0.0184	0.0233	0.0217	−0.3369	0.4270	0.3975
H33	−0.0603	0.1025	0.1137	−0.0125	0.0213	0.0237	−0.2298	0.3909	0.4337
H34	−0.1678	0.1819	0.1806	−0.0349	0.0378	0.0376	−0.6401	0.6936	0.6889
H35	−0.1853	0.1922	0.1923	−0.0386	0.0400	0.0400	−0.7065	0.7329	0.7335
H36	−0.2367	0.2568	0.2408	−0.0493	0.0534	0.0501	−0.9028	0.9792	0.9182
H37	−0.0973	0.1060	0.1057	−0.0203	0.0221	0.0220	−0.3711	0.4044	0.4032
H38	−0.1115	0.1167	0.1139	−0.0232	0.0243	0.0237	−0.4253	0.4450	0.4344
H39	−0.0947	0.1086	0.1059	−0.0197	0.0226	0.0220	−0.3611	0.4141	0.4038
H40	−0.0930	0.1072	0.1055	−0.0193	0.0223	0.0219	−0.3545	0.4088	0.4022
H41	−0.0953	0.1085	0.1039	−0.0198	0.0226	0.0216	−0.3636	0.4139	0.3962

Table 9: Calculated local reactivity descriptor parameters of cefalexin: conformer B at B3LYP/6-311++G(d,p) level.

Site	f_k^+	f_k^-	f_0^+	s_k^+	s_k^-	s_k^0	ω_k^+	ω_k^-	ω_k^0
					Conformer B				
S1	0.0332	0.1162	0.1529	0.0067	0.0234	0.0308	0.1202	0.4212	0.5546
O2	0.3580	−0.2674	−0.2382	0.0721	−0.0539	−0.0480	1.2981	−0.9695	−0.8638
O3	0.3894	−0.3038	−0.2796	0.0785	−0.0612	−0.0564	1.4119	−1.1016	−1.0140
O4	0.3466	−0.3329	−0.3424	0.0699	−0.0671	−0.0690	1.2568	−1.2070	−1.2416
O5	0.3109	−0.2763	−0.2719	0.0627	−0.0557	−0.0548	1.1273	−1.0019	−0.9860
N6	0.3555	−0.2546	−0.2003	0.0716	−0.0513	−0.0404	1.2890	−0.9233	−0.7265
N7	0.3371	−0.3361	−0.3184	0.0679	−0.0677	−0.0642	1.2224	−1.2188	−1.1544
N8	0.4647	−0.4333	−0.4147	0.0937	−0.0873	−0.0836	1.6850	−1.5711	−1.5036
C9	0.0465	−0.0612	−0.0631	0.0094	−0.0123	−0.0127	0.1686	−0.2219	−0.2289
C10	0.0617	−0.0484	−0.0467	0.0124	−0.0098	−0.0094	0.2239	−0.1755	−0.1692
C11	−0.3710	0.3420	0.3567	−0.0748	0.0689	0.0719	−1.3452	1.2403	1.2934
C12	0.0161	0.0195	0.0426	0.0032	0.0039	0.0086	0.0585	0.0707	0.1545
C13	0.2485	−0.2684	−0.2676	0.0501	−0.0541	−0.0539	0.9010	−0.9731	−0.9702
C14	0.0931	−0.0501	0.0905	0.0188	−0.0101	0.0182	0.3375	−0.1815	0.3282
C15	−0.3437	0.3493	0.3483	−0.0693	0.0704	0.0702	−1.2462	1.2665	1.2630
C16	0.2903	−0.3011	−0.3008	0.0585	−0.0607	−0.0606	1.0528	−1.0919	−1.0908
C17	−0.3991	0.3657	0.4010	−0.0804	0.0737	0.0808	−1.4472	1.3262	1.4542
C18	0.0546	−0.0517	−0.0499	0.0110	−0.0104	−0.0100	0.1981	−0.1874	−0.1808
C19	0.1042	−0.0317	0.0239	0.0210	−0.0064	0.0048	0.3778	−0.1149	0.0866
C20	0.0942	−0.0920	−0.0936	0.0190	−0.0185	−0.0189	0.3416	−0.3336	−0.3394
C21	0.1411	−0.1075	−0.0779	0.0284	−0.0217	−0.0157	0.5118	−0.3897	−0.2823
C22	0.1338	−0.0938	−0.0813	0.0270	−0.0189	−0.0164	0.4851	−0.3400	−0.2947
C23	0.0895	−0.0914	−0.1024	0.0180	−0.0184	−0.0206	0.3245	−0.3315	−0.3711
C24	0.2024	−0.1005	−0.0483	0.0408	−0.0203	−0.0097	0.7339	−0.3644	−0.1751
H25	−0.0934	0.1087	0.1042	−0.0188	0.0219	0.0210	−0.3387	0.3943	0.3778
H26	−0.1188	0.1343	0.1288	−0.0240	0.0271	0.0259	−0.4309	0.4871	0.4669
H27	−0.2124	0.2163	0.2150	−0.0428	0.0436	0.0433	−0.7700	0.7843	0.7796
H28	−0.1032	0.1241	0.1187	−0.0208	0.0250	0.0239	−0.3742	0.4500	0.4304
H29	−0.0806	0.1158	0.1228	−0.0162	0.0233	0.0247	−0.2922	0.4200	0.4452
H30	−0.1075	0.1192	0.1163	−0.0217	0.0240	0.0234	−0.3898	0.4323	0.4216
H31	−0.0931	0.1180	0.1142	−0.0188	0.0238	0.0230	−0.3377	0.4278	0.4140
H32	−0.0887	0.1120	0.1071	−0.0179	0.0226	0.0216	−0.3216	0.4061	0.3884
H33	−0.0841	0.1042	0.1065	−0.0169	0.0210	0.0215	−0.3048	0.3779	0.3862
H34	−0.1783	0.1884	0.1871	−0.0359	0.0380	0.0377	−0.6467	0.6831	0.6783
H35	−0.1755	0.1808	0.1858	−0.0354	0.0364	0.0375	−0.6362	0.6557	0.6738
H36	−0.2366	0.2541	0.2417	−0.0477	0.0512	0.0487	−0.8580	0.9214	0.8766
H37	−0.0966	0.1060	0.1068	−0.0195	0.0214	0.0215	−0.3501	0.3844	0.3871
H38	−0.1056	0.1063	0.1103	−0.0213	0.0214	0.0222	−0.3828	0.3854	0.4001
H39	−0.0936	0.1073	0.1053	−0.0189	0.0216	0.0212	−0.3392	0.3892	0.3819
H40	−0.0941	0.1061	0.1066	−0.0190	0.0214	0.0215	−0.3413	0.3846	0.3865
H41	−0.0955	0.1076	0.1039	−0.0193	0.0217	0.0209	−0.3464	0.3902	0.3767

4.3.4.4 ELF and LOL

The ELF and LOL of the optimized structure of cefalexin have been analyzed using Multiwfn software. Although both the ELF and LOL maps reveal regions associated with high electron-pair density (Y. Yang, 2010), LOL gives a clearer picture than the ELF (Cremer & Kraka, 1984). Figures 14 and 15 show the ELF and LOL plots of the title molecule. The red region in the ELF and LOL represents localized electrons, while the blue region represents delocalized electrons. The bond critical point is represented

by the red zone between each of the two atoms. The lone pair associated with nitrogen and oxygen is represented by the additional red spot around them. Similarly, the high electron localization is depicted across bond critical points of hydrogen atoms. This justifies the strong covalent interaction between hydrogen and other heavy atoms. On the other hand, the region between core and valence electrons in the atomic shells is represented by a blue ring-like spot. This indicates the higher delocalization of electrons in this region (T. Chaudhary & Joshi, 2022).

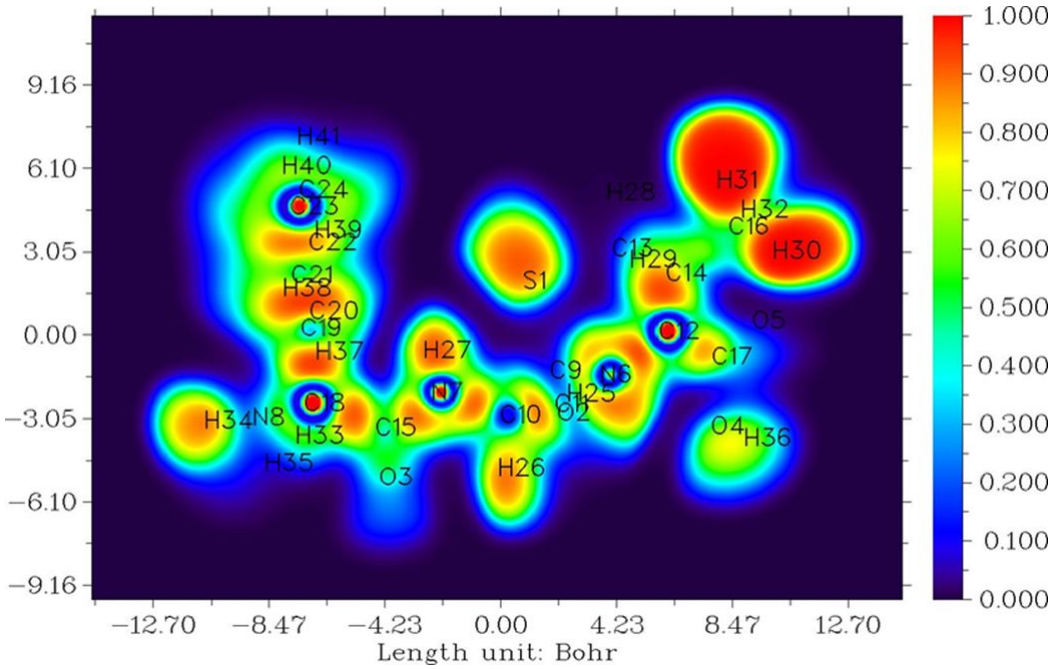

Figure 14: Two dimensional plot of ELF of cefalexin.

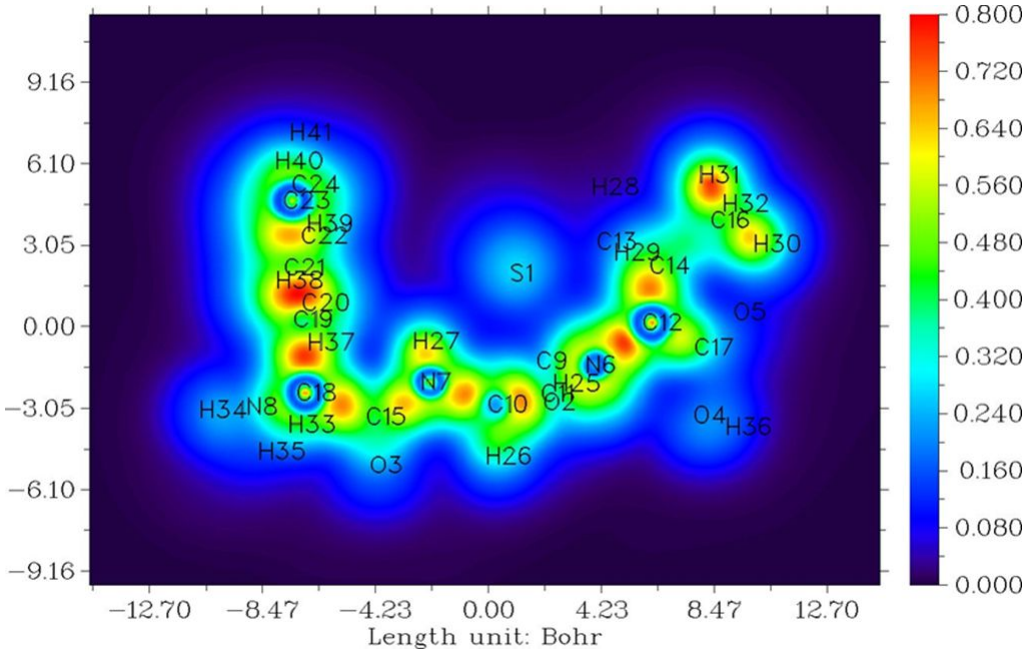

Figure 15: Two dimensional plot of LOL of cefalexin.

4.3.5 Thermodynamic properties

On the basis of the Boltzmann distribution and partition function, the thermodynamic parameters have been calculated (Singh et al., 2016). Table 10 provides estimated values of thermodynamic properties and graph in Figure 16 shows the thermodynamic variations with respect to the temperature in the range of 50K to 600K. The quantities like enthalpy (H^0_{m}), heat capacity $(C^0_{\mathrm{p,m}})$, entropy (S^0_{m}) were found to be positively correlated with the temperature. Due to the increase in vibrational motion that occurs when temperature rises, the quantitative value of the thermodynamic parameters also rises. It has been determined that the title compound has a specific heat capacity of 1022.07 J/kg-K at room temperature (298.15 K). (T. Chaudhary & Joshi, 2022). This value is closer to the value (960.36 J/kg-K) of the specific heat capacity of a biologically active molecule, the alkaloid aristolochic acid, as reported by Joshi et al. (2013) .

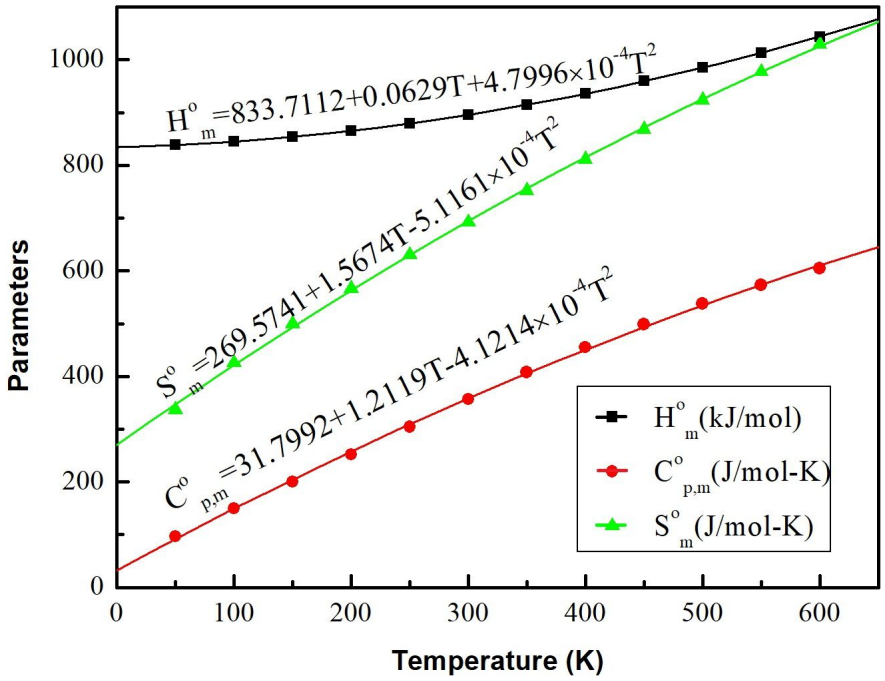

Figure 16: Variation of thermodynamic parameters of cefalexin with increasing temperature.

$$H^0_{\mathrm{m}} = 833.7112 + 0.0629T + 4.7996 \times 10^{-4}T^2 \quad (R^2 = 1,\ SD = 0.649) \tag{4.1}$$

$$C^0_{\mathrm{p,m}} = 31.7992 + 1.2119T - 4.1214 \times 10^{-4}T^2 \quad (R^2 = 0.9996,\ SD = 4.763) \tag{4.2}$$

$$S^o_{\mathrm{m}} = 269.5741 + 1.5674T - 5.1161 \times 10^{-4}T^2 \quad (R^2 = 0.9994,\ SD = 5.184) \tag{4.3}$$

These equations can also be used to investigate the interaction of the title compound with another compound. They assist in predicting the Gibbs free energy and subsequently the

Table 10: Thermodynamic parameters of cefalexin calculated at the B3LYP/6-311++G(d, p) level.

Temperature (K)	Enthalpy (kJ/Mol)	Specific Heat (J/Mol-K)	Entropy (J/Mol-K)
50	838.6870	97.0019	336.7200
100	844.8877	149.9211	426.3036
150	853.6448	200.4513	500.0298
200	864.9458	251.7471	567.0743
250	878.8450	304.2981	630.7296
300	895.3760	356.8952	692.3934
350	914.5011	407.7141	752.5635
400	936.0947	455.2778	811.2483
450	959.9644	498.8081	868.4059
500	985.9052	538.0959	923.7895
550	1013.7037	573.3293	977.6627
600	1043.1758	604.8725	1029.6410

reaction's spontaneity. Also, these provide helpful information that may be applied to the analysis of thermodynamic energies and utilized to predict the direction of chemical reactions in the thermochemical sector by applying the second law of thermodynamics (Joshi et al., 2013).

4.3.6 NLO properties

The properties which are associated with non-linear activities of cefalexin have been calculated at B3LYP/6-311++ G(d,p) level of theory. The calculated NLO properties have been illustrated in Table 11. The dipole moment (μ_0) have been found to have the

Table 11: The estimated dipole moment (μ_0), mean polarizability $|\alpha_0|$, anisotropy of polarizability ($\Delta\alpha$), first hyperpolarizability (β_0) and second hyperpolarizability (γ_0) of cefalexin.

Dipole moment (debye)		Polarizability ($\times10^{-24}$ e.s.u)		First Hyperpolarizability ($\times10^{-30}$ e.s.u)		Second Hyperpolarizability ($\times10^{-35}$ e.s.u)	
μ_x	0.5882	α_{xx}	−140.4955	β_{xxx}	14.7286	γ_{xxxx}	−9060.7026
μ_y	2.9643	α_{xy}	−2.4790	β_{xxy}	−40.9736	γ_{yyyy}	−2271.7508
μ_z	−0.8380	α_{yy}	−143.0230	β_{xyy}	22.0851	γ_{zzzz}	−2271.7508
μ_0	3.1362	α_{xz}	−17.9694	β_{yyy}	32.0184	γ_{xxyy}	−1683.9580
μ_0 (urea)	1.3732	α_{yz}	−5.6946	β_{xxz}	−7.2215	γ_{xxzz}	− 1756.0085
-	-	α_{zz}	−151.5867	β_{xyz}	− 17.3457	γ_{yyzz}	−611.3782
-	-	$\lvert\alpha_0\rvert$	21.4940	β_{yyz}	12.7285	γ_0	−0.1285
-	-	$\Delta\alpha$	36.0946	β_{xzz}	12.0654	-	-
-	-	$\Delta\alpha$(urea)	9.7710	β_{yzz}	6.9303	-	-
-	-	-	-	β_{zzz}	10.2229	-	-
-	-	-	-	β_0	0.4440	-	-
-	-	-	-	β_0(urea)	0.3728	-	-

value of 3.1362 Debye and mean polarizability ($|\alpha_0|$) and anisotropy of polarizability

($\triangle\alpha$) were found to be 21.4940×10^{-24} esu and 36.0946×10^{-24} esu, respectively. Furthermore, the calculated value of first hyperpolarizability (β_0), 0.4440×10^{-30} esu was found to be closer to the standard value that is the value of urea 0.3728×10^{-30} esu. of different molecules (Abraham et al., 2017). In addition to this, second hyperpolarizability (γ_0) has a negative value i.e. -0.1285×10^{-35} esu (T. Chaudhary & Joshi, 2022). The negative value of γ_0 is crucial since it has the effect of defocusing an incident beam and, thus such molecular systems can be a promising candidate for systems of controllable non-linear features (Nakano et al., 1996; A. Kumar et al., 2017).

4.3.7 Drug likeness properties

A drug molecule's biological activity and nontoxicity can be predicted on the basis of molecular weight, AlogP, polar surface area, molar refractivity, number of rotatable bonds, number of H-bond acceptors and H-bond donors of the molecule where, in protein-ligand complexes, AlogP is used to assess local hydrophobicity and hydrophobic interactions (Rizwana et al., 2020; Ghose et al., 1998). The drug likeness properties for cefalexin is illustrated in Table 12 (T. Chaudhary et al., 2021). As, the molecule satisfies Lipinki's five rule as shown in table 12, it is justified as a biologically active and a non-toxic (Lipinski, 2004; Prasana et al., 2020) .

Table 12: Estimated drug likeness properties for cefalexin.

Drug likeness parameters	Value	Range expected
Molecular weight	347.39 g/mol	<500
Molar refractivity	92.05	40-130
AlogP	0.67	<5
Number of rotatable bonds	5	<10
Polar surface area (PSA)	138.03 $Å^2$	< 140
H-bond donors	3	<5
H-bond acceptors	5	<10

4.3.8 Molecular Docking

The molecular docking simulation of cefalexin with human proteins Leukotriene A-4 hydrolase (PDB code; 3B7R, 3CHP) and matrix carbonic anhydrase II (PDB code; 3K7K and 5LNE) have been carried out. The Ramachandran plots of target proteins demonstrated in Figure 17, contains the maximum residues inside the blue line (the permitted region) hence, they are stable. The target protein Leukotirence A-4 hydralase is a zinc-dependent bifunctional metalloenzyme that belongs to a class of metallohydroses. It is a precursor to Leukotrine B4 (LTB4), which is a pro-inflammatory activator for a number of inflammatory diseases, including psoriasis, arthritis, obstructive pulmonary diseases, bowl diseases, and asthma (Kirkland et al., 2008). The next taret, matrix carbonic anhydrase II, is a second isoform ususally present in the most of the tissues and

which catalyzes the reversible conversion of carbon dioxide to carbonic acid (D. Krishnan et al., 2018).

For the docking analysis, the most stable structure of ligand molecule, conformer A, was obtained from its one dimensional conformational analysis. The molecular docking of cefalexin has been performed with in the grid box of size 60 Å× 60 Å× 60 Å, having spacing of 0.375 Å. The interactions of cefalexin with the target proteins are demonstrated in Figure 18. The calculated important docking parameters like binding affinity, binding residues and inhibition constants of docked-complexes are presented in Table 13 (T. Chaudhary et al., 2021).

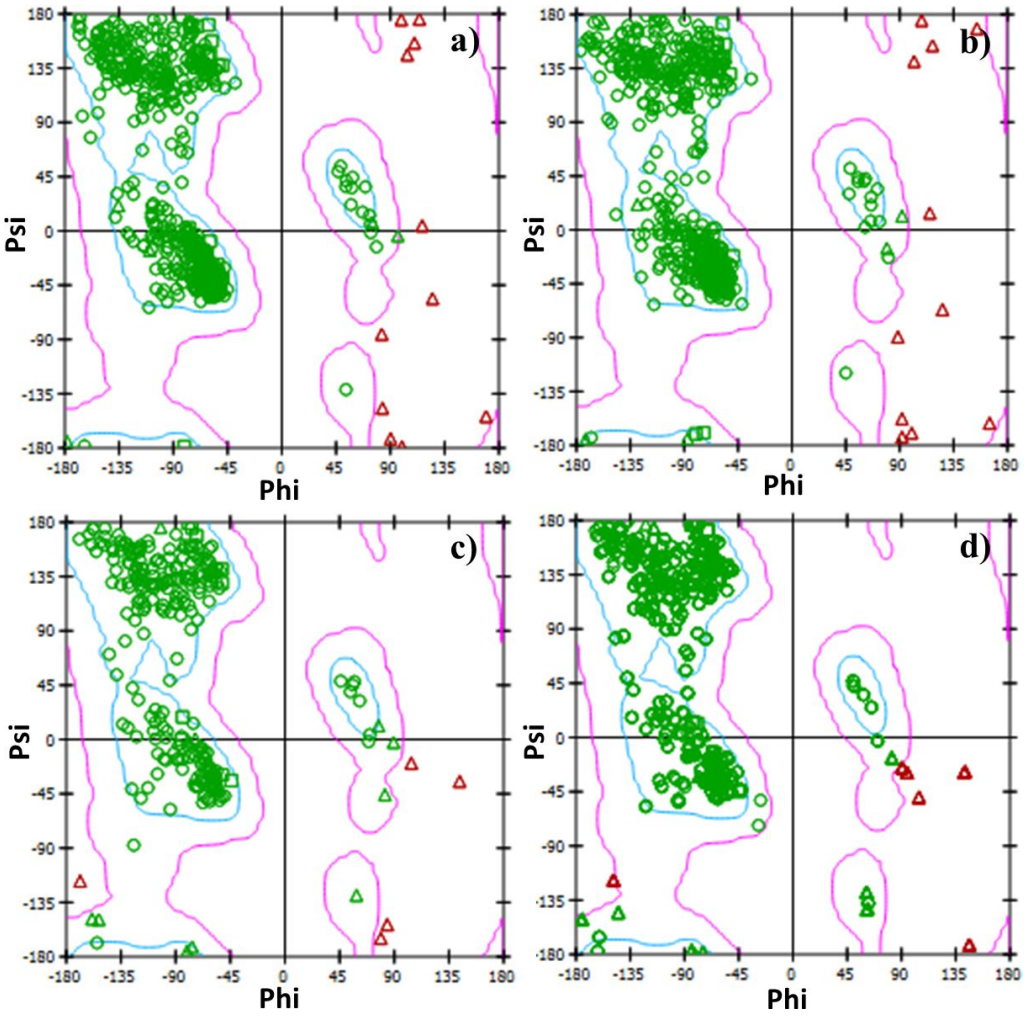

Figure 17: Ramachandran's plot of cefalexin proteins: (a) 3B7R, (b) 3CHP, (c) 3K7K and (d) 5L9E.

The cefalexin complex formed with Leukotriene A-4 hydrolase, that is with 3B7R and 3CHP, has extremely low binding affinities of −8.3 kcal/mol and −8.6 kcal/mol, respectively. In the 3B7R complex, atoms O2, O3, O4, and H36 formed six hydrogen bonds with residues SER352, SER380, and THR355. For the 3CHP complex, five strong hydrogen bonds were formed by atoms O2, O3, O4, O5, and H35 with the residues

ASN291, ARG326, ASN341, and GLU325. Moreover, Cefalexin has a very low inhibition constant value when bound to 3B7R and 3CHP, i.e., 0.82 μM and μM, respectively. Similarly, cefalexin binds with matrix carbonic anhydrase II that is, with 3K7K and 5LNE, with binding affinities of -7.3 and -8.0 kcal/mol and respective inhibition coefficients of 4.42μM and 1.37μM. In the 3K7K complex, the atoms O2, O3, and O5 interacted with the residues GLN92, THR200, and HIS64 via two conventional hydrogen bonds and one carbon hydrogen bond. In the 5LNE, the residues GLN92, HIS94, HIS96, and HIS199 were discovered to be bonded with three strong hydrogen bonds and two Pi-sulphur bonds. Finally, it is explored that cefalexin binds with proteins with at least two conventional hydrogen bonds and maximum six hydrogen bonds. The length of hydrogen bond lies in the range of 2.11 to 3.04 Å (T. Chaudhary et al., 2021).

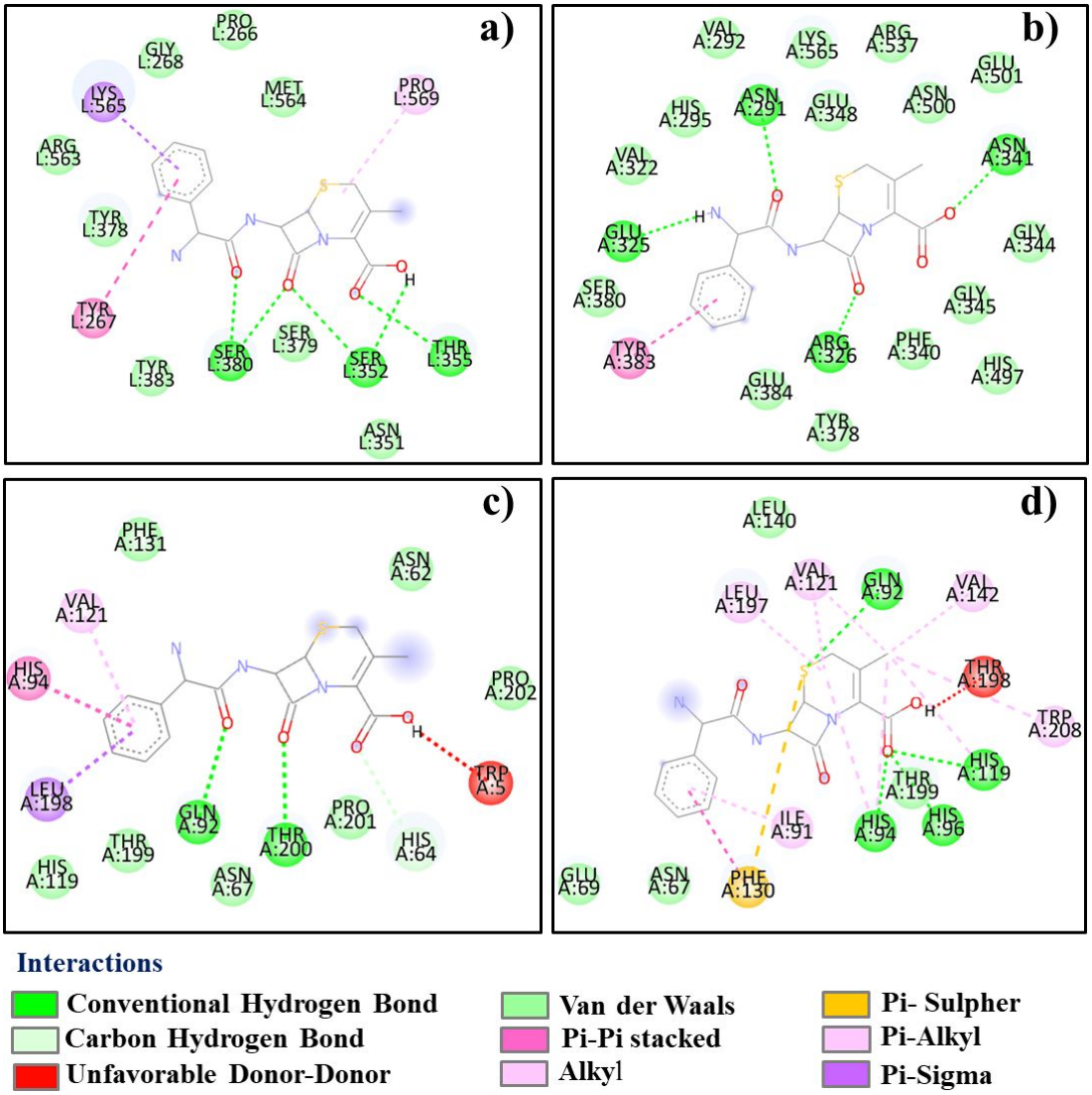

Figure 18: Non-covalent ineractions of cefalexin with proteins a) 3B7R, b)3CHP, c) 3K7K and d) 5L9E

Table 13: Docking parameters of cefalexin with the target protein targets.

Target Proteins	PDB structure of proteins	H-Bonding residues	H-bond lengths (Å)	Inhibition constant (μM)	Binding affinity (kcal/mol)	RMSD (Å)
Leukotriene A-4 hydrolase	3B7R (1.81 Å)	SER352 THR355 SER380 SER380 SER380 SER352	3.04 2.98 3.00 2.85 3.04 2.52	0.82	−8.3	1.14
	3CHP (2.10 Å)	ASN291 ARG326 ARG326 ASN341 GLU325	2.41 2.81 2.O6 2.58 2.09	0.84	−8.6	0.49
Carbonic anhydraseII	3K7K (1.90 Å)	GLN92 THR200 HIS64	3.05 2.85 3.43	4.42	−7.3	2.18
	5l9E (2.90 Å)	GLN92 GLN92 HIS94 HIS96	3.08 3.07 2.11 2.21	1.37	−8.0	0.65

4.4 Methyldopa

Methyldopa is an antihypertensive medicine. To examine its biological and chemical activities, the optimized parameters: bond lengths, angles and dihedral angles were calculated, further the conformational analysis was performed and the non-covalent interactions were studied using various quantum mechanical methods.

4.4.1 Conformational analysis and geometrical parameters

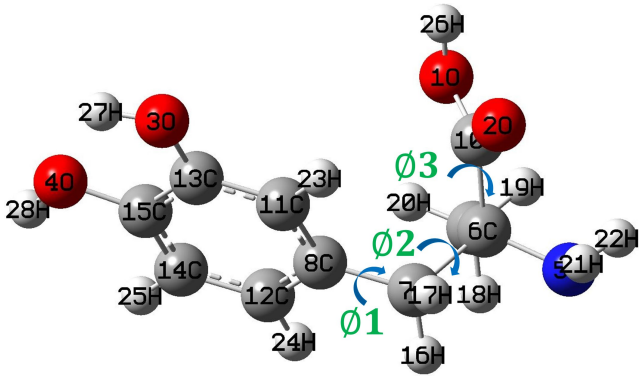

Figure 19: The torsional angles, across which the potential energy surface scan has been carried out.

The one-dimensional PES scan has been carried out across three flexible rotational bonds: C7-C8, C6-C7, and C6-C10, as shown in figure 19. The potential energy was calculated at every 10° variation of the dihedral angle. figure 20 demonstrates the global and local minimum energy of a molecule. As a result, four conformers: C1, C2, C3, and C4, as shown in figure 21 were discovered. The relative energies of the conformers are presented in Table 14. The conformer C1 exhibits the lowest relative energy and its ground state energy, −467356.724 kcal/mol.

Table 14: Ground state energy relative energy of conformers of methyldopa calculated at B3LYP/6-311++G(d,p) level.

Dihedral angles	Conformers	Energy Hartree	Energy kcal/mol	Relative Energy (△E) kcal/mol
C10-C6-C7-C8	C1	−744.782	−467357.754	0.000
C6-C7-C8-C12	C2	−744.780	−467356.724	1.030
O2-C10-C6-C7	C3	−744.780	−467356.657	1.097
C10-C6-C7-C8	C4	−744.780	−467356.634	1.121

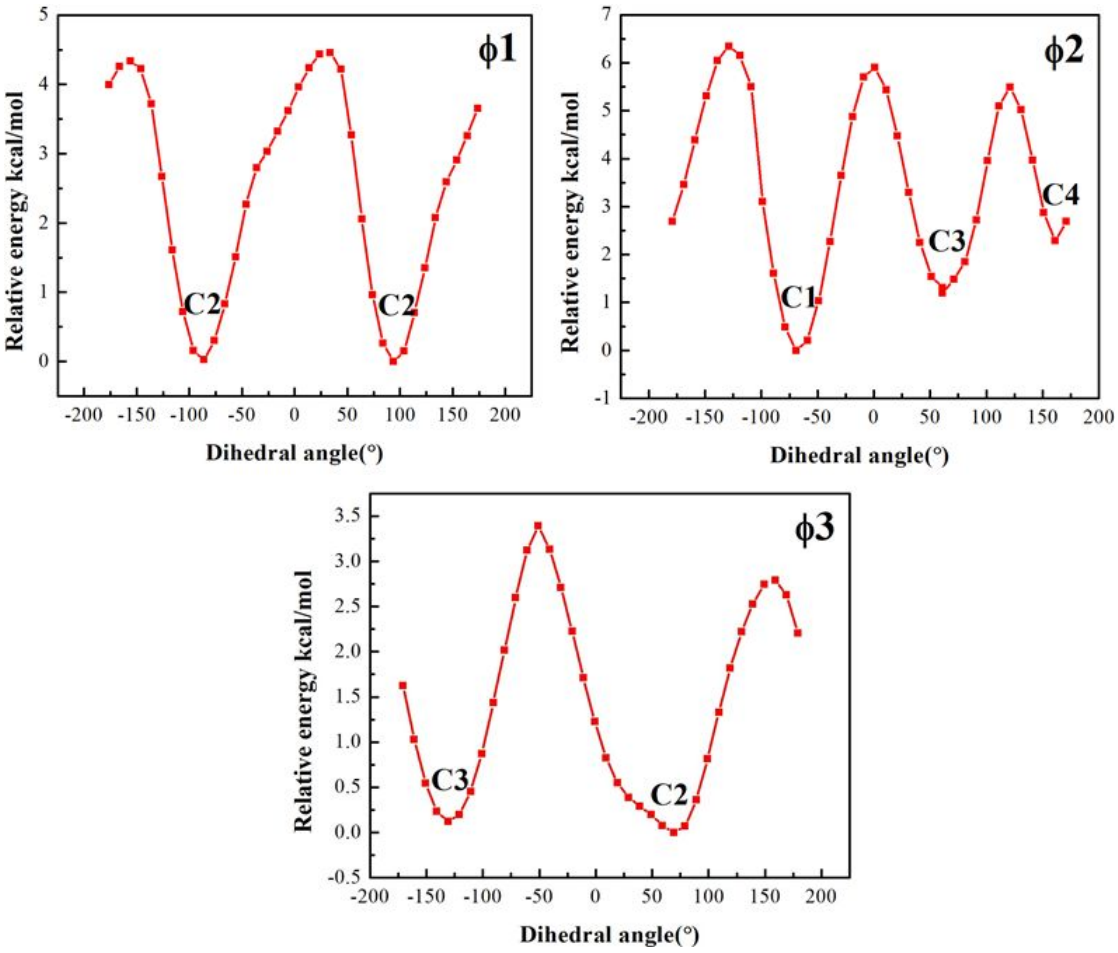

Figure 20: Variation of energy of methyldopa across rotational bonds,C6-C7, C10-C6 and C7-C8.

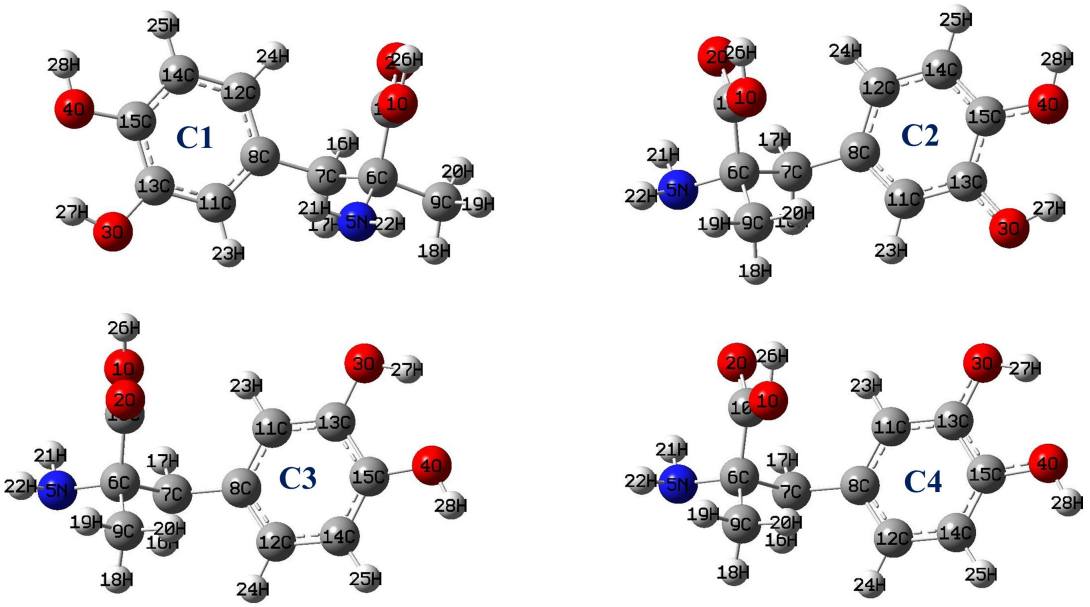

Figure 21: Optimized structure of conformers: C1, C2, C3, C4, C5 of methyldopa.

Next, the stability of dimeric form of the molecule have been examined. The most likely component for the creation of a cyclic dimer structure in the methyldopa molecule is its carboxylic group (Prabakaran & Muthu, 2012; Malaganvi et al., 2019; Sagaama et al., 2020). Hence, the carboxylic group acid has been used to create the dimer structure. These four monomer structures allowed for the creation of the dimer structures: C1C1, C3C3, C4C4, C1C3, C1C4, C2C2, C1C2, C2C3, and C3C4 as shown in Figure 22. At the B3LYP/6-31G(d,p) level, the ground state and relative energy of each of the dimers were determined. Table 15 displays the relative energies of different dimers. On the basis of relative energy, C1C1 is the most stable dimer. To obtain a more precise result, C1C1 was further optimized using B3LYP/6-311++G(d,p) basis sets. Table 16 displays the basis-set-superimposition error (BSSE), interction energy before and after correction, relative energy and ground state energy C1C1. The interaction energy ($\triangle$E) that results from dimerization is determined using the relation, $\triangle$E = Energy of dimer-2 $\times$ Energy of monomer (Issaoui et al., 2015). It was discovered that the ground state energy and BSSE corrections of C1C1 were determined to be -934733.811 kcal/mol and 0.003 kcal/mol, respectively (T. Chaudhary et al., 2023).

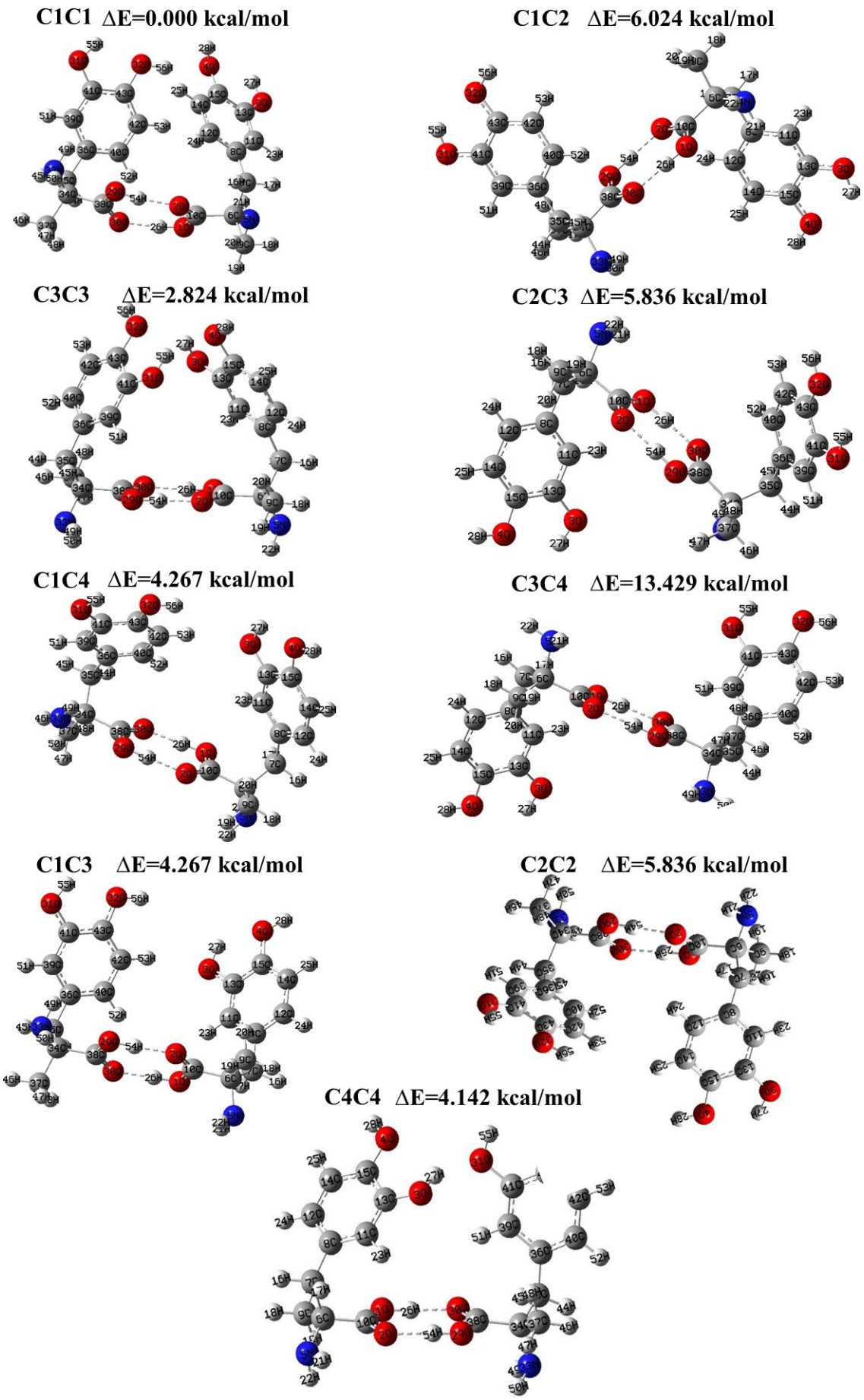

Figure 22: Optimized structure of dimers of methyldopa.

Table 15: Ground state and relative energy of dimers.

Dimers	Energy (Hartree)	Energy (kcal/mol)	Relative Energy (△E) kcal/mol
C1C1	−1489.1841	−934477.331	0.000
C3C3	−1489.1796	−934474.507	2.824
C4C4	−1489.1775	−934473.189	4.142
C1C3	−1489.1773	−934473.064	4.267
C1C4	−1489.1773	−934473.064	4.267
C2C2	−1489.1748	−934471.495	5.836
C1C2	−1489.1745	−934471.307	6.024
C2C3	−1489.1731	−934470.428	6.903
C3C4	−1489.1627	−934463.902	13.429

Table 16: The optimized energies and the interaction energy of dimer (ΔE) calculated at B3LYP /6-311++G(d,p) level of theory.

Methyldopa structure	Energy (Hartree)	Energy (kcal/mol)	Relative energy kcal/mol	BSSE uncorrected ΔE(kcal/mol)	BSSE corrected ΔE(kcal/mol)	BSSE (kcal/mol)
Monomer C1	−744.782	−467357.754	-	-	-	-
Dimer C1C1	−1489.593	−934733.811	0	−18.303	−16.497	0.003

The optimized parameters of the stable monomer conformer have been illustrated in Table 17. The bond lengths of O-C, O-H, C-C and N-H, respectively, lie in the range of 1.32-1.38 Å, 0.96-1.00 Å, 1.51 Å and 1.02 Å. The minimum bond angle was calculated for (N5,C6,C7) and the maximum for (O4, C15, C14). The minimum and maximum bond angles were 105.87° and 123.93 ° (T. Chaudhary et al., 2023).

Table 17: Optimized parameters of methyldopa: bond lengths, bond angles and dihedral angles calculated at B3LYP/6-311++G(d,p).

Bonds	(Å)	Bonds	(Å)
(O1,C10)	1.32	(C7,H16)	1.09
(O1,H26)	1.00	(C7,H17)	1.09
(O2,C10)	1.23	(C8,C11)	1.40
(O3,C13)	1.36	(C8,C12)	1.40
(O3,H27)	0.97	(C9,H18)	1.09
(O4,C15)	1.38	(C9,H19)	1.09
(O4,H28)	0.96	(C9,H20)	1.09
(N5,C6)	1.47	(C11,C13)	1.39
(N5,H21)	1.02	(C11,H23)	1.08
(N5,H22)	1.02	(C12,C14)	1.40
(C6,C7)	1.57	(C12,H24)	1.08
(C6,C9)	1.53	(C13,C15)	1.40

(C6,C10)	1.54	(C14,C15)	1.39
(C7,C8)	1.51	(C14,H25)	1.09
Angles	(°)	Angles	(°)
(C10,O1,H26)	110.49	(C6,C9,H20)	111.54
(C13,O3,H27)	111.16	(H18,C9,H19)	108.37
(C15,O4,H28)	109.79	(H18,C9,H20)	109.36
(C6,N5,H21)	110.01	(H19,C9,H20)	107.72
(C6,N5,H22)	110.60	(O1,C10,O2)	123.30
(H21,N5,H22)	107.20	(O1,C10,C6)	115.65
(N5,C6,C7)	106.52	(O2,C10,C6)	121.05
(N5,C6,C9)	108.65	(C8,C11,C13)	121.75
(N5,C6,C10)	110.67	(C8,C11,H23)	120.75
(C7,C6,C9)	111.60	(C13,C11,H23)	117.47
(C7,C6,C10)	107.27	(C8,C12,C14)	120.53
(C9,C6,C10)	111.99	(C8,C12,H24)	120.17
(C6,C7,C8)	116.04	(C14,C12,H24)	119.30
(C6,C7,H16)	105.87	(O3,C13,C11)	118.79
(C6,C7,H17)	107.04	(O3,C13,C15)	122.07
(C8,C7,H16)	111.00	(C11,C13,C15)	119.13
(C8,C7,H17)	109.42	(C12,C14,C15)	120.48
(H16,C7,H17)	107.03	(C12,C14,H25)	120.04
(C7,C8,C11)	119.82	(C15,C14,H25)	119.47
(C7,C8,C12)	121.83	(O4,C15,C13)	116.32
(C11,C8,C12)	118.31	(O4,C15,C14)	123.93
(C6,C9,H18)	108.82	(C13,C15,C14)	119.75
(C6,C9,H19)	110.97	-	-
Dihedral	(°)	Dihedral	(°)
(H26,O1,C10,O2)	−5.34	(C7,C6,C10,O2)	73.23
(H26,O1,C10,C6)	173.76	(C9,C6,C10,O1)	16.88
(H27,O3,C13,C11)	157.60	(C9,C6,C10,O2)	−163.99
(H27,O3,C13,C15)	−23.22	(C6,C7,C8,C11)	−86.87
(H28,O4,C15,C13)	172.55	(C6,C7,C8,C12)	90.87
(H28,O4,C15,C14)	−7.85	(H16,C7,C8,C11)	152.23
(H21,N5,C6,C7)	−69.41	(H16,C7,C8,C12)	−30.03
H21,N5,C6,C9)	170.23	(H17,C7,C8,C11)	34.33
(H21,N5,C6,C10)	46.87	(H17,C7,C8,C12)	−147.93
(H22,N5,C6,C7)	172.35	(C7,C8,C11,C13)	175.54
(H22,N5,C6,C9)	51.99	(C7,C8,C11,H23)	−2.92
(H22,N5,C6,C10)	−71.36	(C12,C8,C11,C13)	−2.28
(N5,C6,C7,C8)	171.39	(C12,C8,C11,H23)	179.26
(N5,C6,C7,H16)	−65.00	(C7,C8,C12,C14)	−176.79

(N5,C6,C7,H17)	48.93	(C7,C8,C12,H24)	3.40
(C9,C6,C7,C8)	−70.17	(C11,C8,C12,C14)	0.99
(C9,C6,C7,H16)	53.44	(C11,C8,C12,H24)	−178.82
(C9,C6,C7,H17)	167.37	(C8,C11,C13,O3)	−178.75
(C10,C6,C7,C8)	52.85	(C8,C11,C13,C15)	2.04
(C10,C6,C7,H16)	176.46	(H23,C11,C13,O3)	−0.25
(C10,C6,C7,H17)	−69.62	H23,C11,C13,C15)	−179.45
(N5,C6,C9,H18)	56.09	(C8,C12,C14,C15)	0.51
(N5,C6,C9,H19)	−63.07	(C8,C12,C14,H25)	−179.38
(N5,C6,C9,H20)	176.82	(H24,C12,C14,C15)	−179.68
(C7,C6,C9,H18)	−61.07	(H24,C12,C14,H25)	0.43
(C7,C6,C9,H19)	179.77	(O3,C13,C15,O4)	−0.05
(C7,C6,C9,H20)	59.66	(O3,C13,C15,C14)	−179.66
(C10,C6,C9,H18)	178.65	(C11,C13,C15,O4)	179.13
(C10,C6,C9,H19)	59.49	(C11,C13,C15,C14)	−0.48
(C10,C6,C9,H20)	−60.62	(C12,C14,C15,O4)	179.65
(N5,C6,C10,O1)	138.28	(C12,C14,C15,C13)	−0.77
(N5,C6,C10,O2)	−42.59	(H25,C14,C15,O4)	−0.46
(C7,C6,C10,O1)	−105.90	(H25,C14,C15,C13)	179.12

4.4.2 AIM and NCI analysis

A popular method for identifying the covalent and non-covalent interactions present in the molecule is the QTAIM (R. Bader, 1990). Based on a topological examination of the electron density ρ(r), the non-covalent interactions in methyldopa were found in the current work. The topological parameters: BCP, NACP, RCP, electron density (ρ_{BCP}), $\bigtriangledown^2\rho_{BCP}$, electronic energy density H(r), kinetic energy density G(r), potential energy density, V(r), |V|/G and the ellipticity (ε) at BCP of methyldopa are illustrated in the Table 29 and 30 (APPENDIX A1). As shown in Figure 24, there are a total: 28, NACP (3, −3); 29, BCP (3, −1) and 2, RCP (3, +1) in monomer. Similarly, 56, NACP (3, −3); 63, BCP (3, −1) and 8, RCP (3, +1) in dimer. In the monomer structure, the computed values of |V|/G for O2-C10 were found to be 2.0681 and for C-C, C-N, C-H and N-H in the range of 3.6359 to 8.4524. Despite of having shared shell interaction, O2-C10 has very small |V|/G. Thus, it has a very low covalent effect. The H26-O1, on the other hand, has the highest value of |V|/G, 11.4021. Thus, it exhibits the highest covalent effect. In the dimer, |V|/G values for C2-C10 and C38-O30 were calculated to be 2.1086 and 2.1099 respectively. Similarly, for H55-O31, H56-O32, H27-O3, and H28-O4 were calculated to be 11.2402,11.2535, 11.2593, and 11.0483 respectively. This states that H-O bonds have generally very high covalent effect. In comparison to most of the other electron densities with positive values of ellipticity, the electron density (ρ_{BCP}) at O2-C10 (0.4155 a.u) in monomer and O2-C10 (0.3970

a.u), O38-O30 (0.3961 a.u) in dimer were almost twice as high. Furthermore, electron density at O2-C10 (0.4155 a.u) in monomer and O2-C10 (0.3970 a.u), O38-O30 (0.3961 a.u) in dimer were almost twice as high with other electron density with, $\varepsilon > 0$. That is electron density are anisotropic in nature. For non-ring bonds such as C-H have ellipticity in the range of $0.0073 \leq \varepsilon \geq 0.0496$ for monomers, $0.0073 \leq \varepsilon \geq 0.0104$ for dimers, and C-C have $0.0199 \leq \rho_{BCP} \geq 0.0630$ for monomers and $0.0155 \leq \rho_{BCP} \geq 0.0356$ for dimers, respectively, which equivalent to the standard value i.e. ε=0 (Y. Yang, 2010). This justifies the existance of single bond between these bonds. On the other hand $\rho_{BCP} > 0.2$ for C-C indicates the delocalization of charge across the aromatic carbon atoms. (T. Chaudhary et al., 2023).

Using the molecular graph as shown in Figure 23, the hydrogen bond interactions in the molecular systems have been analyzed. The monomer (C1) only displays one hydrogen bond, but the dimer (C1C1) has three such interactions. The topological and geometrical parameters associated with the hydrogen bonds have been presented in Table 18 and 19, respectively. The nature of hydrogen-bonds have been determined utilizing the criteria proposed by Rozas et al. (2000). That is, in monomer, H-bond C12-H24...O2 is considered as a weak hydrogen bond since $\bigtriangledown^2\rho_{BCP} > 0$ and $H_{BCP} > 0$. Similarly, H-Bond O29-H54...O2 and O1-H26...O30 in the dimer are considered as a medium hydrogen bond since $\bigtriangledown^2\rho_{BCP} > 0$ and $H_{BCP} < 0$ whereas O32-H56...O4 is characterized by $\bigtriangledown^2\rho_{BCP} > 0$ and $H_{BCP} > 0$, thus it is a weak hydrogen bond (T. Chaudhary et al., 2023).

Table 18: Topological parameters of non-covalent interactions in methyldopa.

Interactions	Bond length (Å)	ρ_{BCP} (a.u.)	$\nabla^2\rho_{BCP}$ (a.u.)	G_{BCP} (a.u.)	V_{BCP} (a.u.)	H_{BCP} (a.u.)	E_{int} (kcal/mol)
Monomer							
H24...O2	2.70	0.007	0.023	0.005	−0.004	0.001	−1.255
Dimer							
H54...O2	1.70	0.045	0.132	0.037	−0.041	−0.004	−12.801
H26...030	1.653	0.050	0.140	0.041	−0.047	−0.006	−14.872
H56...O4	1.99	0.023	0.082	0.019	−0.017	0.002	−5.271
H52...O30	2.74	0.007	0.023	0.005	−0.004	0.001	−0.002
H24...O2	2.77	0.007	0.023	0.005	−0.004	0.001	−0.002
H21...C11	2.65	0.009	0.032	0.006	−0.005	0.002	−0.002
H53...C15	3.31	0.003	0.008	0.002	−0.001	0.000	−0.001

Table 19: Geometrical parameters of intramolecular and and interamolecular interactions and van der Waal's radius of interacting atoms in monomer and diner of methyldopa.

D-H...A	D-H (Å)	H...A (Å)	D-H...A (°)	$(r_H + r_A))$ (Å)
Monomer				
C12-H24...O2	1.08	2.70	118.09	2.72
Dimer				
O29-H54...O2	1.00	1.70	173.39	2.72
O1-H26...O30	1.00	1.65	173.74	2.72
O32-H56...O4	0.97	1.98	158.18	2.72
C40-H52...O30	1.08	2.74	114.80	2.72
C12-H24...O2	1.08	2.77	108.52	2.72
C5-H21...C11	1.02	2.65	115.13	2.9
C42-H53...C15	1.08	3.31	113.91	2.9

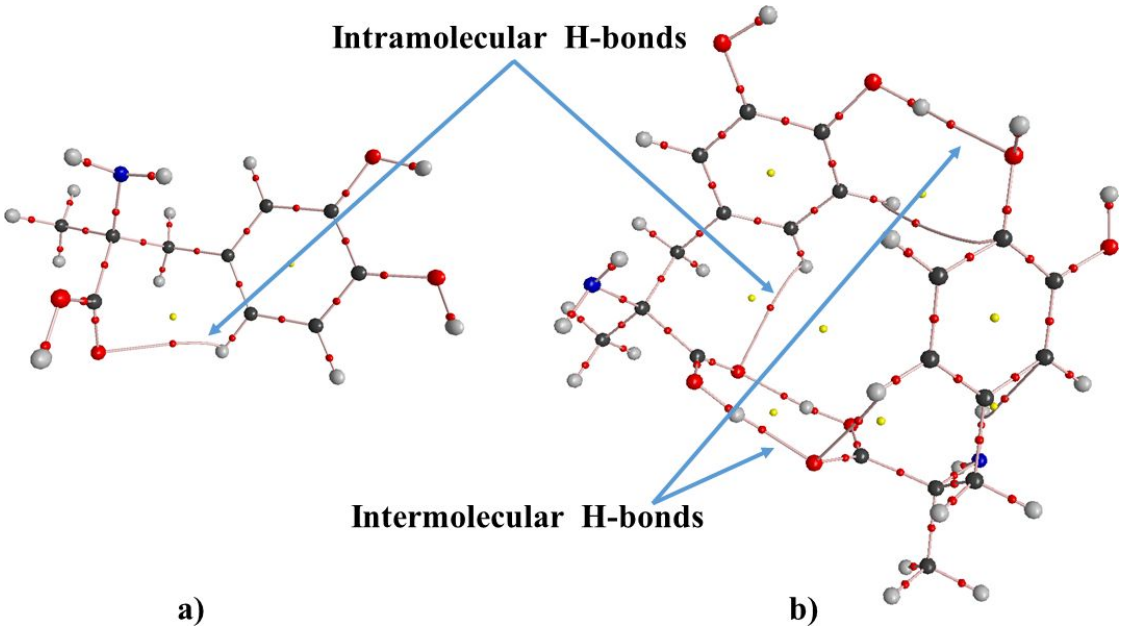

Figure 23: Molecular graph of methyldopa a) monomer and b) dimer (C1C1).

In addition to this, NCI analysis has been carried out to obtain possible non covalent interactions like steric effects, Van der Waals interaction including hydrogen bond interaction. The scattered graph of sign (λ_2) and RDG in Figure 24(a,b) represents the different types of non-covalent interactions. The red, blue and green coloured inverted spikes, respectively indicate the steric effects, hydrogen bonds and van der Waals interaction (Johnson et al., 2010). The isosurface of RDG in Figure 24(c,d). Depicts the strength of hydrogen bonds. That is in the dimer, the two strong bonds, H54$\cdots$02 and H26$\cdots$030 were shown by the intense blue colour and the weak bonds H56$\cdots$O4 was shown by a less intense blue colour. (T. Chaudhary et al., 2023).

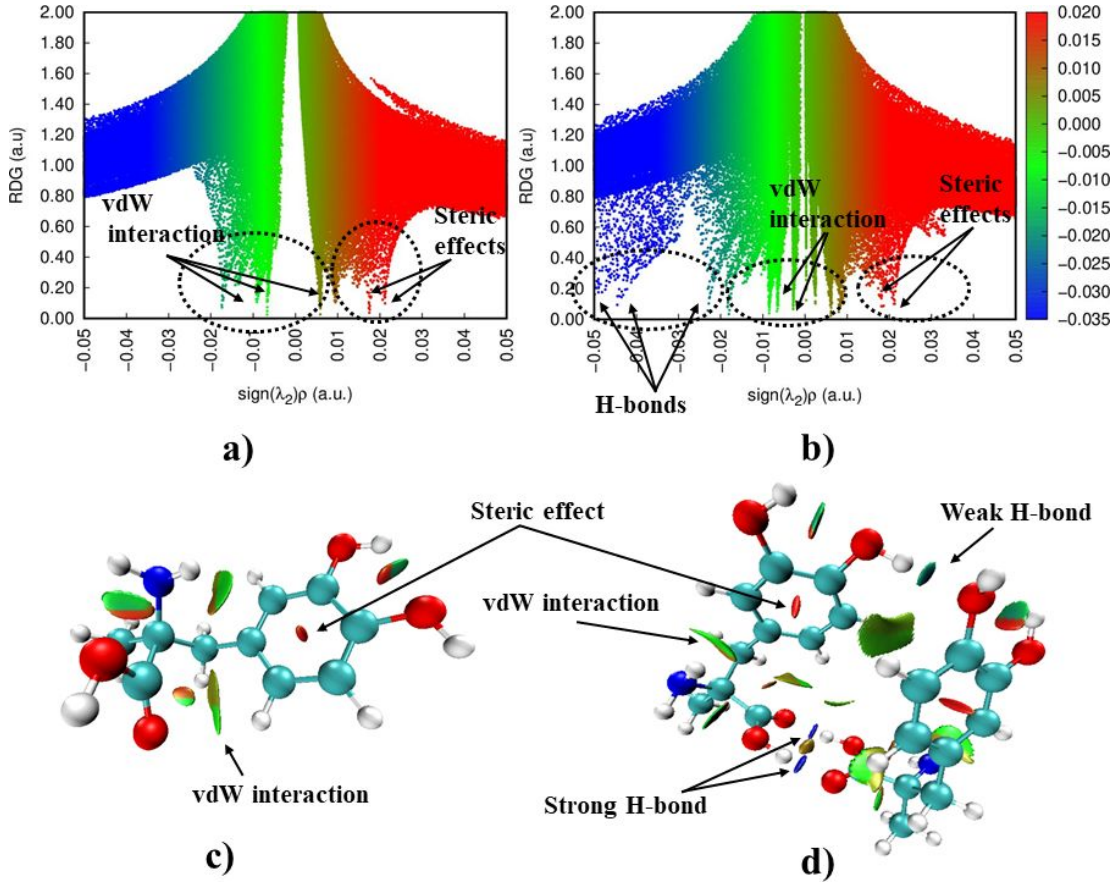

Figure 24: NCI graph (a,b) and its isosurface (c,d) for methyldopa (monomer, dimer(C1C1)).

4.4.3 Electron localization function analysis

The ELF plots have been used to visualize the charge localized and delocalized regions in the methyldopa compound. Figure 25(a,b) depicts the graphical representation of ELF. The red areas in the ELF colour-filled map show electron localized zones like as bond critical points or loan pairs. The covalent character of the connection is supported by the red colored spot between the atoms, which represent the bond critical point. The localization of the lone pair was represented by two extra red zones connected to O4, and O32 in dimer. The electron depletion zone between the valence and inner shells was depicted by the blue ring-like structure that surrounds the nuclei of C6, C10, C11, C13, C14, and C15 in monomers as well as the nuclei of several carbon and oxygen atoms in dimers. These blue ring illustrates the electrons depleted area between the valence and inner shells. Moreover, dark blue area inside the ring, is due to the π electrons delocalization as a result of aromaticity. The chemically active region linked to charge transfer are thus predicted by the ELF plots. The elevated regions of the 3D projection map, as seen in Figure 25(c,d), depict the electronic environment in the compound (T. Chaudhary et al., 2023).

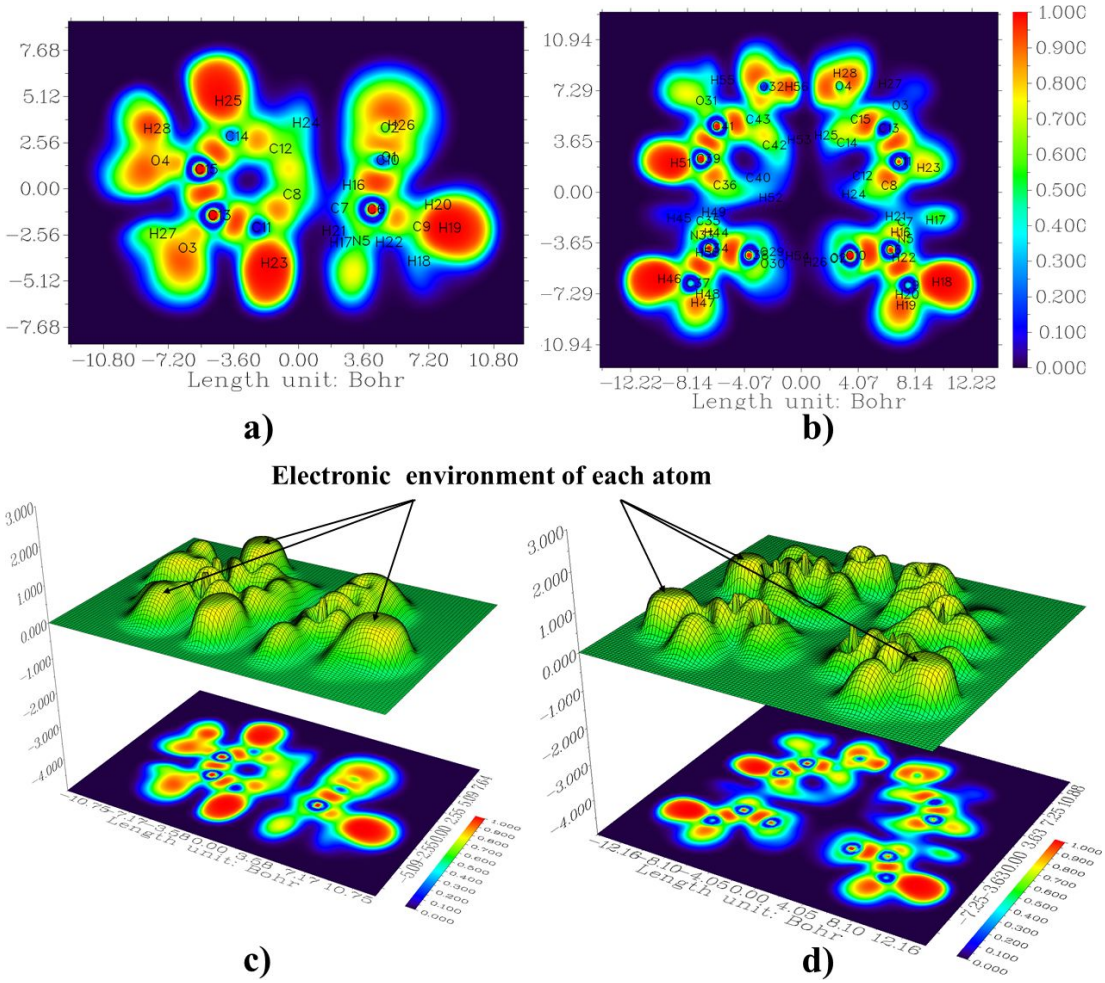

Figure 25: 2-Dimensional ELF (a,b) and 3-Dimensionla ELF (c,d) for methyldopa (monomer, dimer (C1C1)).

4.4.4 Natural bond orbital analysis

Table 20 shows the stabilization energy of methyldopa during interactions between donor and acceptor orbitals. The interactions involving lone pairs and antibonding π orbitals have a major role in the stability of dimers. The dimer form of methyldopa is stabilized by the delocalization of charge from the lone pair LP(2)O1 to π^*(O2-C10), LP(2)O3 to π^*(C11-C15), LP(2)O2 to σ^*(O1-C10) in C1 unit with their energies of 46.33, 28.96, 21.14 kcal/mol, respectively and LP(2)O29 to π^*(O30-C38), LP(2)O31 to π^*(C39-C41), LP(2)O30 to $\sigma*$(C29-C38) in C2 unit with their energies 47.63, 27.04, 20.06 kcal/mol, respectively. The greatest stabilization energy, 23.55 kcal/mol is attained due to the interactions π(C8-C11)$\rightarrow$ π^*(C13-C15). Moreover, the hydrogen bond interactions O29-H54$\cdots$O2 and O1-H26$\cdots$O30 are confirmed by the charge transfer from lone pairs LP(1)O2/LP(2)O2 to antibonding sigma orbitals, σ^*(O29-H54) with 7.75/18.04 stabilization energy and LP(1)O3/LP(2)O3 to σ^*(O1-H26) with 8.83/21.36 kcal/mol respectively. Similar to this, the interaction LP(2) O4$\rightarrow$ σ^*(O32-H56) results in the formation of a weak hydrogen bond, O32-H56$\cdots$O4 with 6.39 kcal/mol stabiliza-

tion energy (T. Chaudhary et al., 2023).

Table 20: Second-order perturbation theory analysis of Fock matrix in NBO basis for in dimer form.

Donor (i) (i)	ED(i)/e	Acceptor (j)	ED(j)/e	$E^{(2)x}$ kcal/mol	E(j) - $E(i)^y$ (a.u)	$F(i,j)^z$ (a.u.)
Unit 1						
π (C8-C11)	1.681	π*(C12-C14)	0.355	18.50	0.28	0.065
π (C8-C11)	1.681	π*(C13-C15)	0.431	23.55	0.26	0.072
σ (C12-C14)	1.972	σ*(O4-C15)	0.027	5.18	0.99	0.064
π (C12-C14)	1.685	π*(C8-C11)	0.363	21.09	0.29	0.070
π (C13-C15)	1.646	π*(C13-C15)	0.431	19.83	0.27	0.067
π (C13-C15)	1.646	π*(C8-C11)	0.363	16.57	0.31	0.064
π (C13-C15)	1.646	π*(C12-C14)	0.355	21.14	0.30	0.073
LP(1) O1	1.968	σ*(O2-C10)	0.037	8.98	1.13	0.092
LP(2) O1	1.761	π*(O2-C10)	0.254	46.33	0.35	0.123
LP(2) O2	1.854	σ*(O1-C10)	0.074	21.14	0.71	0.109
LP(2) O2	1.854	σ*(C6-C10)	0.085	17.89	0.67	0.097
LP(1) O3	1.975	σ*(C13-C15)	0.039	5.34	1.12	0.074
LP(2) O3	1.872	π*(C13-C15)	0.431	28.96	0.43	0.062
LP(1) O4	1.978	σ*(C14-C15)	0.024	5.72	1.17	0.073
LP(2) O3	1.872	π*(C13-C15)	0.039	9.17	0.43	0.062
LP(1) N5	1.946	σ*(C6- C10)	0.431	10.06	0.66	0.073
Unit 2						
σ(O32-C43)	1.678	π*(C42-C43)	0.371	9.14	2.71	0.157
π (C36-C40)	1.678	π*(C39-C41)	0.402	18.98	0.27	0.065
π (C39-C41)	1.669	π*(C36-C40)	0.366	20.36	0.30	0.071
π (C42-C43)	1.701	π*(C36-C40)	0.366	18.23	0.30	0.068
π (C42-C43)	1.701	π*(C39-C41)	0.371	19.32	0.29	0.068
LP(1) O29	1.968	σ*(O30-C38)	0.028	8.92	1.11	0.089
LP(2) O29	1.769	π*(O30-C38)	0.269	47.63	0.37	0.119
LP(2) O30	1.856	σ*(C29-C38)	0.072	20.06	0.71	0.109
LP(2) O30	1.856	σ*(C34-C38)	0.082	17.45	0.67	0.098
LP(2) O31	1.885	σ*(C41-C43)	1.977	5.07	1.17	0.069
LP(2) O31	1.885	π*(C39- C41)	0.371	27.04	0.35	0.093
LP(2) O32	1.899	σ*(C42-H53)	0.024	12.53	2.36	0.157
LP(1) N33	1.946	σ*(C34-C38)	0.082	10.48	0.65	0.075
From unit 1 to 2						
LP(1) O2	1.957	σ*(O29-H54)	0.069	7.75	1.08	0.082
LP(2) O2	1.854	σ*(O29-H54)	0.069	18.04	0.70	0.102
LP(2) O4	1.929	σ*(O32-H56)	1.987	6.39	0.84	0.066
From unit 2 to 1						
LP(1) O30	1.957	σ*(O1-H26)	0.069	8.83	1.07	0.087
LP(2) O30	1.856	σ*(O1-H26)	0.069	21.36	0.70	0.108

$^x E^{(2)}$ represents the stabilization energy due to hyperconjugative interaction.
^{y} represents the difference of energy between donor (i) and acceptor (j) NBO's orbitals.
$^z F(i,j)$ epresents the Fock matrix element between donor and acceptor NBO orbitals.

4.4.5 Analysis of monomeric and dimeric vibrational modes

The monomeric form of compound consists of 28 molecules, so it has total 78 vibrational modes. The PED contributions has been assigned to each of the fundamental vibrational modes of monomer. The calculated wavenumbers were rescaled using the WLS factor (Yoshida et al., 2002). Calculated IR and Raman frequencies for monomer and dimer (C1C1) are demonstrated in Figure 26 and 27 respectively. The PED assigned to different vibrational modes of methyldopa molecule is illustrated in Table 31 (APPENDIX A1). The shift in vibrational frequency of hydroxyl group in dimer has been explained. The different modes of vibration are stated below:

4.4.5.1 O-H vibration

Generally, the stretching vibration of O-H group occurs in between 3530–3645 cm^{-1} (Coates, 2006). The stretching vibrations of non-bonded O-H group in monomer were calculated at 3636.18 cm^{-1} for O4H28, 3583.47 cm^{-1} for O3H27 and 3549.67 cm^{-1} for O1H26. The first two hydroxyl group has almost the same frequency i.e. 3599.46 cm^{-1}, 3567.59 cm^{-1} in dimer. However, the stretching bands of third hydroxyl group was significantly shifted to the lower band 2814.64 cm^{-1}. This red shift in the frequency falls in the range of 3300–2500 cm^{-1} which is the frequency range of hydrogen bonded O-H group of carboxylic group (Coates, 2006). This justifies the strong hydrogen-bond interaction between two carboxylic groups in dimer.

4.4.5.2 N-H_2 vibration

Stretching vibrational bands of amine occur in the ranges of 3490–3310 cm^{-1} (Coates, 2006). In the monomer, the asymmetric stretching of amine group was calculated at 3403.87 cm^{-1} and symmetric stretching at 3330.73 cm^{-1}. Similarly, asymmetric and symmetric stretching for dimer were obtained at 3399.56 cm^{-1} and 3327.20 cm^{-1}, respectively. All estimated frequencies fall within the specified range. The locations of the monomer's and dimer's intense in plane bending vibration of NH_2 were determined at 1642.94 cm^{-1} and 1620.34 cm^{-1}, respectively. The waging with the highest contribution for monomer was found across 874.42 cm^{-1}. It was discovered that the frequency bands of monomer and dimer were comparable, with the exception of those involved in hydrogen bonding.

4.4.5.3 C-H vibration

The C-H stretching band in the ring were calculated at 3071.16, 3065.59, 3030.41 cm^{-1} for monomer and at 3068.16, 3019.16, 2994.82 cm^{-1} for dimer, which lies very close to the specified C-H stretching range 3100-3000 cm^{-1} (S. Muthu & Maheswari, 2012;

Sevvanthi et al., 2017). In plane bending vibration of C-H occurs in the wide range of 1486.04 - 1127.89 cm^{-1} and out-of-plane bending in 918.49, 810.00 cm^{-1} (S. Muthu & Maheswari, 2012; Karrouchi et al., 2021).

Furthermore, the symmetric stretching of CH_2 was calculated at 2992.55 cm^{-1} in monomer and the symmetric stretching at 2942.90 cm^{-1} (monomer), 2945.81 cm^{-1}(dimer). This is equivalent to its typical frequency band 3000-2900 cm^{-1} (for asymmetric) and 2900-2800 cm^{-1} (for symmetric) (S. Muthu & Maheswari, 2012). Similarly, different kinds of other vibrations like as: deformation, rocking, waging and scissoring occurred intensely at 1464.65, 863.90, 1351.18 cm^{-1} and 1259.53 cm^{-1} respectively.

The asymmetric and symmetric stretching of CH_3 were estimated at 2990.61 (monomer), 2994.82 cm^{-1} (dimer) and 2924.10 (monomer), 2921.27 (dimer), respectively. Also, vibrational frequency from 3000 to 2905 cm^{-1} and from 2870-2860 cm^{-1} are for asymmetric and symmetric vibrations, respectively (C. Liu et al., 1991; Alpert et al., 1970). In addition to this, with 87 percent PED contribution, the deformation occurred at 1393.39. The rocking occurred below 1127.89 cm^{-1}.

4.4.5.4 C=O, C-C vibration

The carbonyl group (C=O) often exhibits strong stretching bands in the region of 1870-1550 cm^{-1} Socrates (2004). The stretching frequency band of C=O in monomer, was determined at 1782.40 cm^{-1}. However, it was found to be slightly less in dimer i.e. 1723.86 cm^{-1}. This fall in frequency is due to the intermolecular hydrogen bonding between oxygen of carbonyl group and hydrogen of hydroxyl group.

The C-C stretching in monomer and dimer were found almost the same. In monomer, prominent stretching was discovered in between 1644.87 cm^{-1} and 1040.80 cm^{-1}. The typical, range for C-C stretching is between 1650 and 1100 cm^{-1} (A. Srivastava et al., 2017).

4.4.6 Ring vibration

The ring suffered different kinds of vibraiton, like torsional vibration, trigonal deformtion and puckering. The puckering of a rimg R was detected with a high intensity at 698.03 cm^{-1} and the prominant aasymatric tosional vibrational was obtained at a very low frequency, 156.03 cm^{1}.

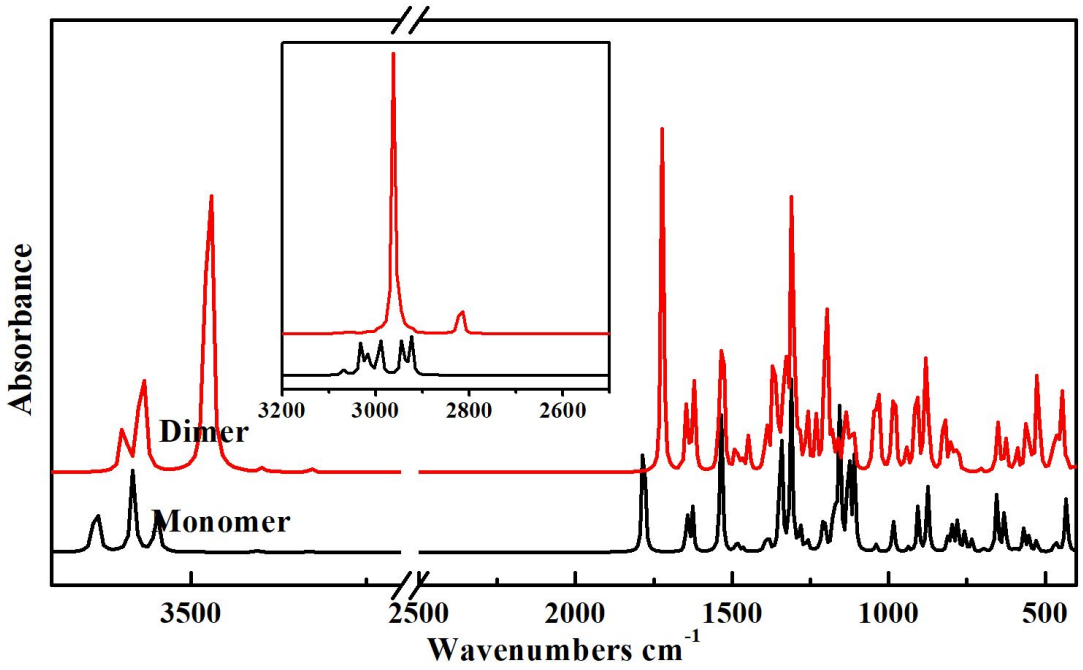

Figure 26: Estimated IR spectra of methyldopa.

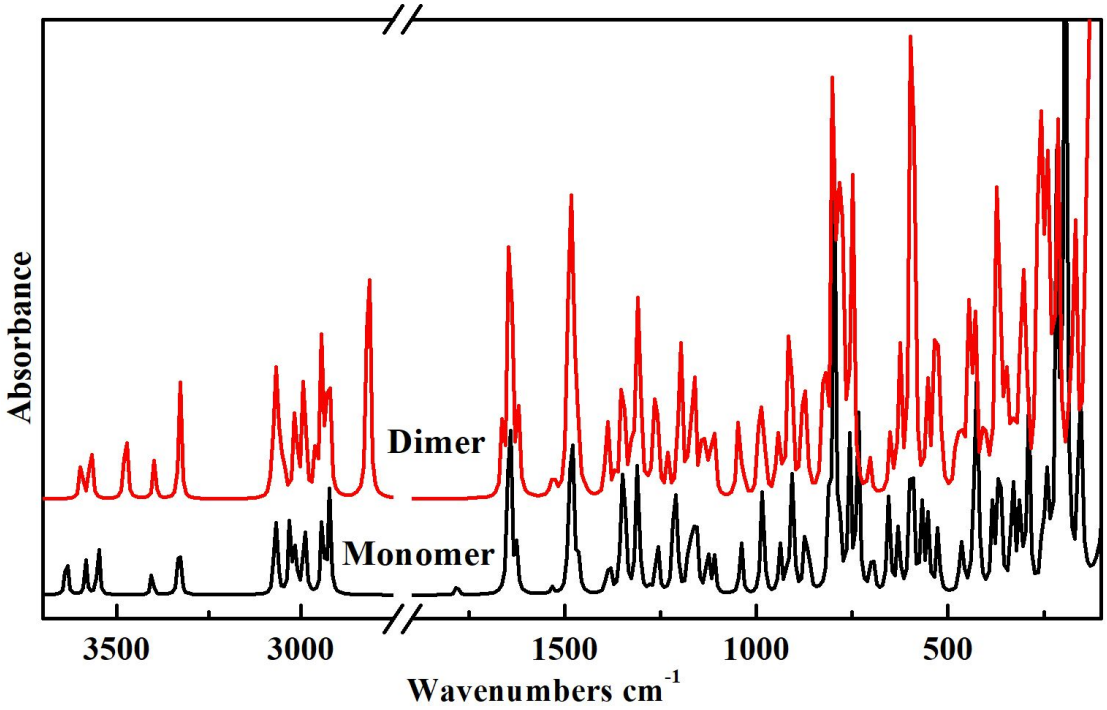

Figure 27: Estimated Raman spectra of methyldopa.

4.4.7 HOMO-LUMO analysis

The chemical activities of methyldopa have been investigated in the current work in both gaseous and aqueous conditions. Figure 28 displays the HOMO and LUMO plots along with the corresponding energy gaps in the gaseous state. The HOMO-LUMO energy gaps ($\triangle E_{\text{L-H}}$)in gas were determined to be 5.536 eV for monomer and 5.052 eV

for dimer. Similarly, the values of $\triangle E_{\text{L-H}}$ in water, methanol and ethanol were 5.446 eV, 5.448 eV and 5.450 eV for monomer and 5.052 eV, 5.414 eV, 5.406 eV and 5.401 eV for dimer. Finally, the dimer was justified with a smaller energy gap than that of the monomer (T. Chaudhary et al., 2023).

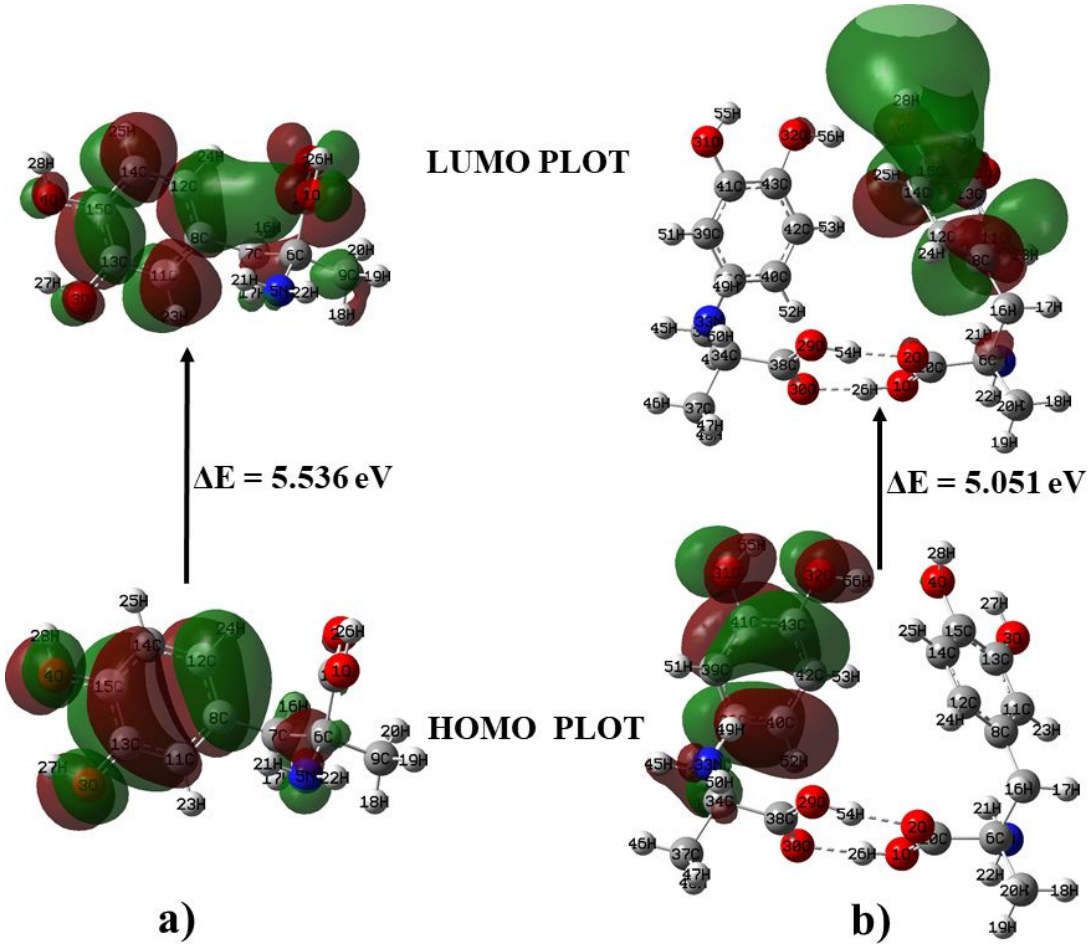

Figure 28: HOMO and LUMO plots for methyldopa a) monomer b) dimer.

4.4.8 Composition analysis of molecular orbitals (MO)

Generally, adjacent orbitals in the boundary area could have quasi-degenerate energy levels (S. Muthu & Paulraj, 2013b). Thus, the graphs of total density of states (TDOS), partial density of states (PDOS) and overlap population density of states (OPDOS) shown in figure 29 were drawn using Multiwfn to provide a more useful explanation HOMO and LUMO orbitals. According to whether two atoms, orbitals, or groups interact in a bonding, non-bonding, or anti-bonding manner, respectively, the values of OPDS may be positive, zero, or negative (S. Muthu & Paulraj, 2013b). The HOMO energy levels, which are at -5.638 eV for the monomer and -5.475 eV for the dimer, are represented by the vertical dashed lines. Furthermore, the study aims to find out the contributions of hydrogen, carbons and electronegative negative atoms to molecular

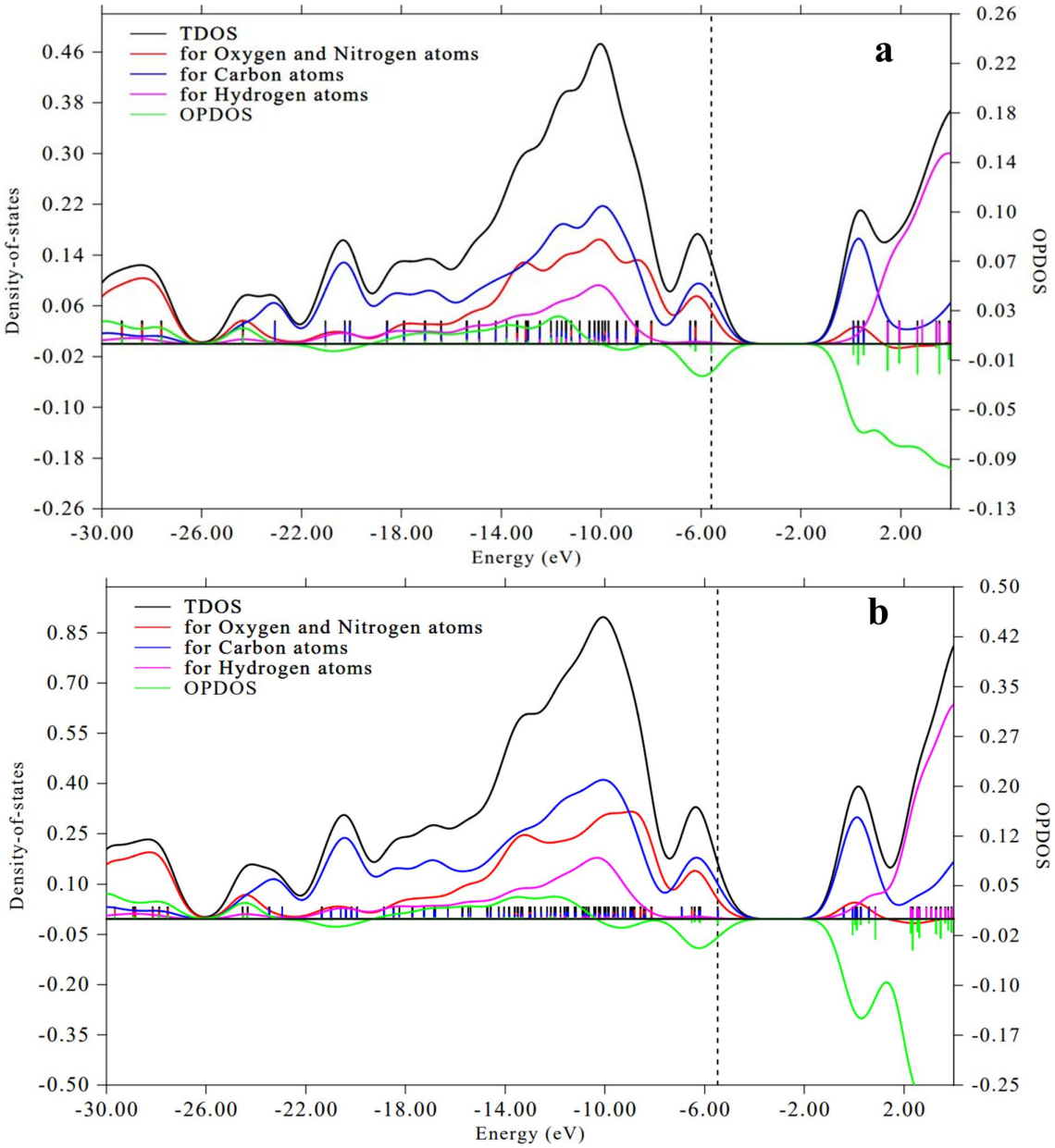

Figure 29: Molecular orbitals composition anlaysis of methyldopa a) monomer b) dimer.

orbitals. Since nitrogen and oxygen are both electronegative atoms, the same colour has been used to represent the PDOS of both atoms in the graph. It shows that the contributions of the electronegative atoms and carbon to HOMO are about identical. Nonetheless, carbon atoms contribute significantly more than other elements to LUMO. It has been discovered that HOMO and LUMO are both influenced by the antibonding properties of oxygen and nitrogen with carbon atoms. The hydrogen atoms contribute very little to HOMO but significantly around -11.00 eV and they make up the majority of the virtual molecular orbital LUMO+3. It is observed that the anti-bonding behaviour of oxygen as well as nitrogen atoms with carbon atoms at this level (T. Chaudhary et al., 2023).

4.4.9 Global reactivity

The values of global reactivity parameters:S, η and ω which were calculated using HOMO and LUMO energy, are shown in Table 21. The ionization potential and electron affinity, softness and hardness of the molecule were estimated in different medium. The value of softness was found to be 0.181 eV^{-1} and 0.198 eV^{-1} for monomer and dimer in the gaseous state, respectively. This suggests that the molecule is less hazardous (Prasana et al., 2020). Similarly, the chemical hardness in gaseous state was found to be 2.768 eV for monomer and 2.526 eV for dimer. The values of the electrophilicity index of monomer and dimer have been discovered to be 1.488 eV and 1.722 eV, respectively (T. Chaudhary et al., 2023). It is one of the basic descriptors used to measure the biological activity of the compound. The molecule acts as an electrophile for its greater value of electrophilicity index and acts as a nucleophile for its lower value of electrophilicity index. (Shafi et al., 2020). Thus, toxicity and stability of the molecule have been examined.

Table 21: Global reactivity descriptors for methyldopa monomer and dimer in different medium.

Molecule	E_{H}	E_{L}	$\Delta E_{\mathrm{L\text{-}H}}$	χ	μ	η	S	ω	$\Delta N_{\max}$
Monomer									
Gas	−5.638	−0.102	5.536	4.242	−2.870	2.768	0.18	1.488	1.037
Water	−5.704	−0.259	5.446	2.870	−2.982	2.723	0.184	1.633	1.095
Methanol	−5.700	−0.252	5.448	2.982	−2.976	2.724	0.184	1.626	1.093
Ethanol	−5.698	−0.248	5.450	2.976	−2.973	2.725	0.184	1.622	1.091
Dimer									
Gas	−5.475	−0.424	5.051	2.973	−2.949	2.526	0.198	1.722	1.168
Water	−5.688	−0.275	5.414	2.949	−2.981	2.707	0.185	1.642	1.101
Methanol	−5.681	−0.276	5.406	2.981	−2.979	2.703	0.185	1.641	1.102
Ethanol	−5.678	−0.277	5.401	2.979	−2.977	2.701	0.185	1.641	1.103

4.4.10 Molecular electrostatic potential

The MEP of methyldopa has been depicted in Figure 30. It was noted that in the monomer, the regions over oxygen in hydroxyl and carboxylic acid, were demonstrated by red colour and regions over hydrogen in hydroxyl and carbonyl groups were demonstrated by blue colour in the MEP map. In the map, red and blue colour, respectively, indicate the lower electrostatic and higher electrostatic potential region. In the dimer, it was found that the effects of the electro-negativity of oxygen in carboxylic acid and the positivity of hydrogen have greatly diminished. In the monomer, the electrostatic potential over the atoms rises in the following order: O1<N5<O3<O2 and in the dimer, N5<O3<N33<O31. The most probable nucleophilic sites are therefore O2 and O31 respectively, in monomer and dimer, whereas H28 is the most electrophilic site in both monomer and dimer. These anticipated nucleophilic and electrophilic sites are the main

locations for hydrogen bond interaction during the protein-ligand interaction, as shown in Section 4.3.15. Hence, these sites play a key role in both hydrogen bonding in crystal packing and the biological activities of the molecule (T. Chaudhary et al., 2023).

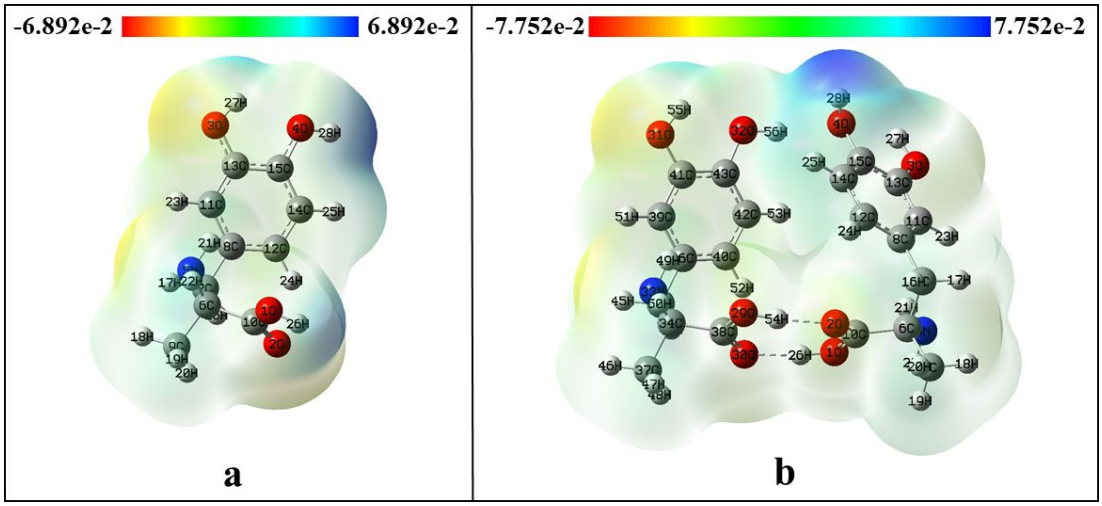

Figure 30: MEP map for methyldopa a)monomer b) dimer.

4.4.11 Electron-hole distribution analysis

Electron-hole distribution has been analyzed using Multiwfn software. The charge transfer (CT) owing to excitation in the molecule due to excitation was examined. Figure 31 displays the plots of the electron-hole distribution for various excited states along with their corresponding electron-hole overlap integrals (S). In these plots, the green and blue regions respectively, represent electron and hole distributions. The different estimated parameters with are associated with CT are electron-hole overlap integral (S), charge transfer length (D), and △r are illustrated in Table 22. D is the distance between the centroids of electrons and holes and △r is the excitation mode of electron (Guido et al., 2013). The S and D values for first, second and third excited states, are 0.27 and 2.73 Å, 0.58 and 1.83 AA and are 0.45, 1.63 Å, respectively. That is the first and third excited states, both of them have △r index greater than 2 Å. Due to the higher value of D and the lower value of S, the first excited is more probable to charge transfer due to excitation (T. Chaudhary et al., 2022).

Table 22: Electron-hole overlap integral, charge transfer length (D), △r and excitation energy in methyldopa.

Excitation States	Overlap integral of electron-hole (S)	Charge transfer length(D)(Å)	△r (Å)	Excitation energy (E) eV
First	0.2706	2.73	2.76	4.612
Second	0.5825	1.83	1.85	4.705
Third	0.4500	1.63	2.99	4.995

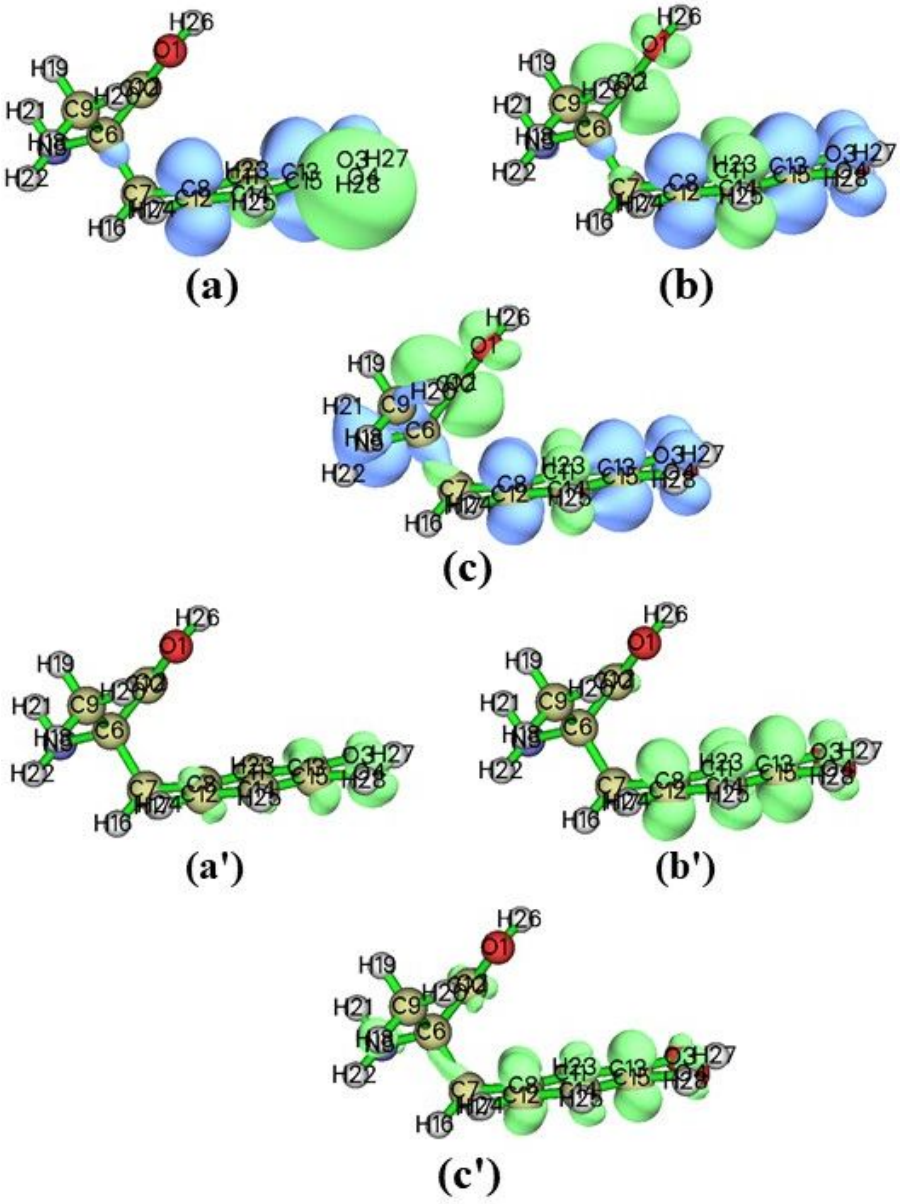

Figure 31: Electron-hole distribution (a,b,c) and overlap (a',b',c') for excited states (first, second, third) of methyldoopa.

4.4.12 Local reactivity

In contrast to the global reactivity, the local reactivity descriptors were utilized to explore the local reactive sites in the molecular system. Along with the FF, the dual descriptor ($\triangle f_k$), was calculated at B3LYP/6-311++G(d,p) level of theory to view the nucleophilic and electrophilic sites. Table 23 and 24 show the values of f_k^+ or $f_k^-(r)$and $\triangle f_k$, for the monomer and dimer molecule. For the positive value of $\triangle f_k$, the reactive site is more prone to nucleophilic attack and for its negative value it is more prone to electrophilic attack (Morell et al., 2005). Hence, it has been predicted that C9 is the most favorable sites for nucleophilic attack in monomer and N5 in dimer. On the other hand, C10 has the most extreme negative values in monomer and in dimer as well. So it is a very favourable site for electrophilic attack (T. Chaudhary et al., 2023). Hence, using

the local reactivity descriptors, the biological activity can be more precisely determined.

Table 23: Calculated local reactivity descriptor parameters and dual descripter of methyldopa monomer using Hirshfeld charges at B3LYP/6-311++G(d,p) level.

Site	N+1	N-1	N	f_k^+	f_k^-	f_k^0	Δf_k
O1	−0.3331	−0.3382	−0.6804	0.3473	−0.3422	−0.3356	0.6895
O2	−0.2867	−0.3146	−0.6191	0.3324	−0.3045	−0.3007	0.6369
O3	−0.2167	−0.3412	−0.6735	0.4568	−0.3323	−0.2790	0.7890
O4	−0.2540	−0.3564	−0.7080	0.4540	−0.3516	−0.3052	0.8056
N5	−0.3142	−0.4194	−0.8337	0.5195	−0.4143	−0.3668	0.9338
C6	0.0369	0.0200	0.0460	−0.0091	0.0260	0.0285	−0.0351
C7	−0.2053	−0.1929	−0.3918	0.1865	−0.1989	−0.1991	0.3854
C8	0.0935	−0.0298	−0.0460	0.1396	−0.0162	0.0319	0.1557
C9	0.0935	−0.2918	−0.5850	0.6786	−0.2933	−0.0991	0.9719
C10	0.4003	0.4064	0.8021	−0.4018	0.3957	0.4033	−0.7975
C11	−0.1425	−0.1235	−0.2390	0.0964	−0.1155	−0.1330	0.2119
C12	0.0658	−0.1048	−0.2390	0.3048	−0.1341	−0.0195	0.4389
C13	0.2591	0.1405	0.2821	−0.0230	0.1416	0.1998	−0.1646
C14	−0.1669	−0.1243	−0.2601	0.0932	−0.1358	−0.1456	0.2290
C15	0.2855	0.1291	0.2460	0.0395	0.1169	0.2073	−0.0774
H16	0.1254	0.1079	0.2215	−0.0961	0.1136	0.1166	−0.2097
H17	0.1246	0.1057	0.2188	−0.0942	0.1131	0.1151	−0.2073
H18	0.1112	0.1023	0.2188	−0.1076	0.1165	0.1067	−0.2241
H19	0.1144	0.1026	0.2050	−0.0906	0.1024	0.1085	−0.1929
H20	0.1078	0.1138	0.2237	−0.1160	0.1099	0.11077	−0.2259
H21	0.1876	0.1812	0.3670	−0.1791	0.1855	0.1844	−0.3646
H22	0.1875	0.1772	0.3526	−0.1652	0.1755	0.1823	−0.3406
H23	0.1286	0.1078	0.2235	−0.0950	0.1158	0.11818	−0.2107
H24	0.1142	0.0990	0.2043	−0.0900	0.1053	0.1066	−0.1954
H25	0.1205	0.1074	0.2017	−0.0813	0.0943	0.1140	−0.1756
H26	0.2489	0.2406	0.4790	−0.2302	0.2385	0.2448	−0.4686
H27	0.2504	0.2443	0.4852	−0.2349	0.2410	0.2473	−0.4758
H28	0.2520	0.2513	0.4791	−0.2272	0.2278	0.2516	−0.4550

Table 24: Calculated local reactivity descriptor parameters for methyldopa in dimer form using Hirshfeld charges at B3LYP/6-311++G(d,p) level.

Site	N+1	N-1	N	f_k^+	f_k^-	f_k^0	Δf_k
O1	−0.3395	−0.3481	−0.6881	0.3486	−0.3400	−0.3438	0.6886
O2	−0.3293	−0.3413	−0.6818	0.3526	−0.3405	−0.3353	0.6930
O3	−0.2923	−0.3419	−0.6686	0.3763	−0.3267	−0.3171	0.7030
O4	−0.3643	−0.3842	−0.7531	0.3888	−0.3689	−0.3742	0.7576

N5	−0.3734	−0.4224	−0.8416	0.4683	−0.4193	−0.3979	0.8875
C6	0.0256	0.0209	0.0451	−0.0194	0.0241	0.0233	−0.0435
C7	−0.2014	−0.1941	−0.3958	0.1944	−0.2017	−0.1978	0.3961
C8	0.0121	−0.0240	−0.0284	0.0405	−0.0045	−0.0059	0.0450
C9	−0.2849	−0.281	−0.5667	0.2818	−0.2857	−0.2830	0.5674
C10	0.4188	0.4274	0.8306	−0.4118	0.4032	0.4231	−0.8151
C11	−0.1219	−0.1224	−0.2496	0.1277	−0.1273	−0.1221	0.2550
C12	−0.0448	−0.1080	−0.2093	0.1645	−0.1013	−0.0764	0.2658
C13	0.1752	0.1436	0.2861	−0.1109	0.1425	0.1594	−0.2534
C14	−0.1338	−0.1087	−0.2295	0.0958	−0.1208	−0.1213	0.2165
C15	0.1552	0.1236	0.2114	−0.0563	0.0878	0.1394	−0.1441
H16	0.1177	0.1091	0.2240	−0.1063	0.1149	0.1134	−0.2211
H17	0.1199	0.1068	0.2224	−0.1024	0.1155	0.1134	−0.2180
H18	0.1127	0.1047	0.2157	−0.1030	0.1110	0.1087	−0.2139
H19	0.1072	0.0984	0.2053	−0.0980	0.1069	0.1028	−0.2049
H20	0.1105	0.1056	0.2146	−0.1041	0.1090	0.1080	−0.2134
H21	0.1785	0.1841	0.3622	−0.1837	0.1782	0.1813	−0.3619
H22	0.1860	0.1769	0.3623	−0.1763	0.1854	0.1814	−0.3617
H23	0.1205	0.1063	0.2262	−0.1058	0.1200	0.1134	−0.2257
H24	0.1129	0.1029	0.2176	−0.1048	0.1148	0.1079	−0.2195
H25	0.1099	0.1086	0.2147	−0.1047	0.1061	0.1093	−0.2108
H26	0.2540	0.2532	0.5097	−0.2557	0.2565	0.2536	−0.5122
H27	0.2442	0.2462	0.4835	−0.2393	0.2373	0.2452	−0.4766
H28	0.2509	0.2638	0.4887	−0.2378	0.2248	0.2573	−0.4626
O29	−0.3374	−0.3438	−0.6845	0.3471	−0.3406	−0.3406	0.6877
O30	−0.3303	−0.3441	−0.6845	0.3542	−0.3404	−0.3372	0.6946
O31	−0.2522	−0.3415	−0.6760	0.4239	−0.3345	−0.2968	0.7584
O32	−0.2893	−0.3641	−0.7336	0.4443	−0.3695	−0.3267	0.8138
N33	−0.3748	−0.4235	−0.84182	0.4670	−0.4183	−0.3991	0.8854
C34	0.0306	0.0196	0.0440	−0.0134	0.0245	0.0251	−0.0379
C35	−0.2047	−0.1933	−0.3912	0.1865	−0.1979	−0.1990	0.3844
C36	0.0667	−0.0320	−0.0526	0.1193	−0.0207	0.0174	0.1399
C37	−0.2856	−0.2821	−0.5668	0.2812	−0.2847	−0.2839	0.5659
C38	0.4175	0.4282	0.8364	−0.4189	0.4082	0.4228	−0.8272
C39	−0.1419	−0.1284	−0.2493	0.1074	−0.1209	−0.1352	0.2283
C40	0.0026	−0.1091	−0.2173	0.2198	−0.1082	−0.0532	0.3281
C41	0.2253	0.1397	0.2798	−0.0545	0.1401	0.1825	−0.1946
C42	−0.1486	−0.1213	−0.2485	0.0998	−0.1271	−0.1350	0.2270
C43	0.2392	0.1279	0.2432	−0.0041	0.1154	0.1835	−0.1194
H44	0.1228	0.1095	0.2232	−0.1005	0.1137	0.1161	−0.2142
H45	0.1227	0.1058	0.2197	−0.0969	0.1139	0.1143	−0.2108

H46	0.1124	0.1041	0.2151	−0.1026	0.1109	0.1083	−0.2135
H47	0.1088	0.0988	0.2021	−0.0933	0.1033	0.1038	−0.1965
H48	0.1122	0.1067	0.2159	−0.1037	0.1092	0.1094	−0.2129
H49	0.1787	0.1854	0.3659	−0.1872	0.1804	0.1821	−0.3676
H50	0.1874	0.1775	0.3588	−0.1714	0.1813	0.1825	−0.3528
H51	0.1239	0.1065	0.2213	−0.0974	0.1148	0.1152	−0.2122
H52	0.1142	0.1038	0.2115	−0.0972	0.1077	0.1090	−0.2049
H53	0.1146	0.1070	0.2066	−0.0920	0.0996	0.1108	−0.1916
H54	0.2560	0.2549	0.5096	−0.2537	0.2547	0.2554	−0.5084
H55	0.2474	0.2457	0.4847	−0.2373	0.2390	0.2466	−0.4763
H56	0.2557	0.2562	0.5009	−0.2452	0.2447	0.2560	−0.4899

4.4.13 NLO properties

Methyldopa, an organic compound, has been found to have significant NLO features. This is due to the interactions between donor and acceptor groups in the π-conjugated system (Venkatesan et al., 2016; Kalinowska et al., 2014). In the present, we have examined the NLO properties of methyldopa. Table 25 illustrates the estimated value . The value of β_0 was found to be 0.9017×10^{-30} esu which is approximately three times

Table 25: The dipole moment (μ_0), mean polarizability $|\alpha_0|$, anisotropy of polarizability ($\Delta\alpha$), first hyperpolarizability (β_0) and second hyperpolarizability (γ_0) of methyldopa.

Dipole moment (debye)		Polarizability ($\times 10^{-24}$ e.s.u)		First Hyperpolarizability ($\times 10^{-30}$ e.s.u)		Second Hyperpolarizability ($\times 10^{-35}$ e.s.u)	
μ_x	1.6148	α_{xx}	−76.8156	β_{xxx}	54.7143	γ_{xxxx}	−2741.6992
μ_y	−1.8569	α_{xy}	−6.6647	β_{xxy}	−12.4652	γ_{yyyy}	−911.8254
μ_z	2.5238	α_{yy}	−89.8383	β_{xyy}	24.8604	γ_{zzzz}	−432.5846
μ_0	3.5250	α_{xz}	0.1714	β_{yyy}	4.2333	γ_{xxyy}	−676.5233
μ_0 (urea)	1.3732	α_{yz}	−1.3593	β_{xxz}	−37.0746	γ_{xxzz}	− 605.0103
-	-	α_{zz}	−90.3878	β_{xyz}	− 6.741	γ_{yyzz}	−211.7205
-	-	$\|\alpha_0\|$	12.6980	β_{yyz}	25.0753	γ_0	−0.0412
-	-	$\Delta\alpha$	19.8162	β_{xzz}	−3.1589		-
-	-	$\Delta\alpha$(urea)	9.7710	β_{yzz}	16.1659	-	-
-	-	-	-	β_{zzz}	8.5069	-	-
-	-	-	-	β_0	0.9017	-	-
-	-	-	-	β_0(urea)	0.3728	-	-

of that urea (0.372810×10^{-30} esu. Nevertheless, Prabakaran and Muthu's calculation of the initial hyperpolarizability using the 6-31G(d,p) basis set yielded a value of 3.78210×10^{-30} esu (Prabakaran & Muthu, 2012). This value discrepancy was due to the use of different basis sets. Both μ_0 and $|\alpha_0|$ are greater than the value of urea. It is discovered that γ_0 has a negative value of $-0.041210 \times 10^{-35}$ esu. Thus, methyldopa has suitable properties necessary for NLO devices (T. Chaudhary et al., 2022).

4.4.14 Thermodynamic Properties

The standard thermodynamic parameters of methyldopa have been computed using DFT/B3LYP using the basis set, 6-311++G(d,p). Methyldopa's thermodynamic quantities have been examined at a interval of 50 K which is even smaller then the previously conducted research (Prabakaran & Muthu, 2012). The variation of thermal parameters have been between recorded between the temperature, 50 K and 600 K. Table 26 lists the estimated values of the thermodynamic parameters. Figure 32 shows that the quantities like heat capacity, enthalpy, and entropy increase with the increase in temperature. This is due to rise in molecules' vibrational energies with rise in temperature (Abraham et al., 2018). Enthalpy (H_m^0), heat capacity ($C_{p,m}^0$), entropy (S_m^0) and temperature are correlated according to the given equations (T. Chaudhary et al., 2022).

$$H_m^0 = 590.7424 + 0.0328T + 3.1488 \times 10^{-4}T^2 \quad (R^2 = 1,\ SD = 0.554) \tag{4.4}$$

$$C_{p,m}^0 = 1.2755 + 0.2019T - 8.2253 \times 10^{-4}T^2 \quad (R^2 = 0.9995,\ SD = 2.515) \tag{4.5}$$

$$S_m^o = 229.4271 + 0.9572T - 2.6464 \times 10^{-4}T^2 \quad (R^2 = 0.9999,\ SD = 1.567) \tag{4.6}$$

The Gibbs free energy can also be calculated using the aforementioned formulae, which further aids in assessing the spontaneity of the reactions. The study of thermodynamic energy and determining the reaction's direction in accordance with the second law of thermodynamics are two further uses for these thermodynamic relations (Joshi et al., 2013).The thermodynamic properties are useful to predict the stability and chemical reactivity of the drug (Buvaneswari et al., 2021; M. Chaudhary et al., 2020).

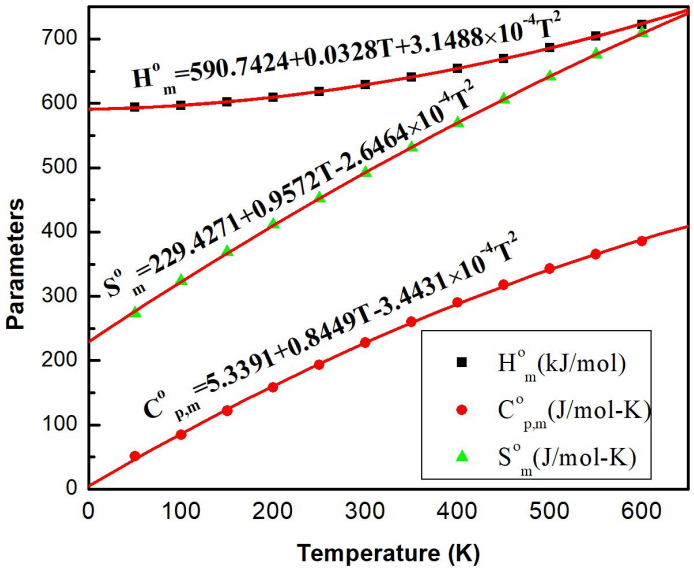

Figure 32: Variation of thermodynamic parameters of methyldopa with respect to temperature.

Table 26: Calculated thermodynamic parameters of methyldopa at different temperatures.

Temperature (K)	Enthalpy (kJ/Mol)	Specific Heat (J/Mol-K)	Entropy (J/Mol-K)
50	593.8385	51.1655	273.5509
100	597.1789	84.4442	324.3062
150	602.3403	121.9382	369.0336
200	609.3518	158.2057	411.5005
250	618.1466	193.4351	452.4606
300	628.6786	227.5886	492.2862
350	640.8776	260.1013	531.1155
400	654.6485	290.3786	568.9611
450	669.8730	318.0690	605.7686
500	686.4119	343.1013	641.4752
550	704.1396	365.6011	676.0432
600	722.9348	385.8111	709.4600

4.4.15 Molecular docking

Molecular docking is a frequently used computational technique that is often used to explain how receptor proteins and ligand molecules will interact (Morris & Lim-Wilby, 2008; Shoichet et al., 1992; R. Srivastava et al., 2020). Thus, a docking analysis was conducted in the current work to look at how methyldopa interacts with the predicted target protein. The most probable target for a ligand molecule methyldopa is Lysine-specific demethylase 4D-like (PDB code: 5PNO and 5PNQ. The stability of proteins was confirmed from Ramachandran plots, shown in Figure 33. The plots show most of the residues are within the permissible zone (region under the blue line) Figure 34 shows the docked protein structure's optimal binding mode and interactions. Table 27 lists the binding affinity, traditional hydrogen bond lengths, inhibition constants, and RMSD between the docked and starting ligand structure. The binding conformation with the lowest binding affinity and the lowest lower bound RMSD has been chosen from the several binding modes of the ligand (T. Chaudhary et al., 2023).

The docked-complex of methyldopa with 5PNO and 5PNQ reveal binding affinity of -7.6 kcal/mol and -7.4 kcal/mol, respectively. Both complexes have inhibition coefficient below 4 μM . Also, RMSD of ligand with initial structure lie below 2 $\mathring{A}$. The complex 5PNQ possesses five strong hydrogen bonds with bond lengths between 2.22 $\mathring{A}$ and 2.79 $\mathring{A}$. The residues GLU194, TYR136, and ASN202 take part in hydrogen bonding with the ligand's atoms H2, H22, H26, O3, and O4. Similarly, the 5PNQ complex possesses seven hydrogen bonds, with the bonds ranging from 1.89 to 2.60 Å. The atoms H21, H22, H28, O1, O2, and O3 of ligand, interact with the residues GLU194, TYR136, ASN202, LYS245, HIS280, and SER200 of 5PNQ to form hydrogen bonds. Thus, methyldopa strongly reacts with the selected protein (T. Chaudhary et al., 2023).

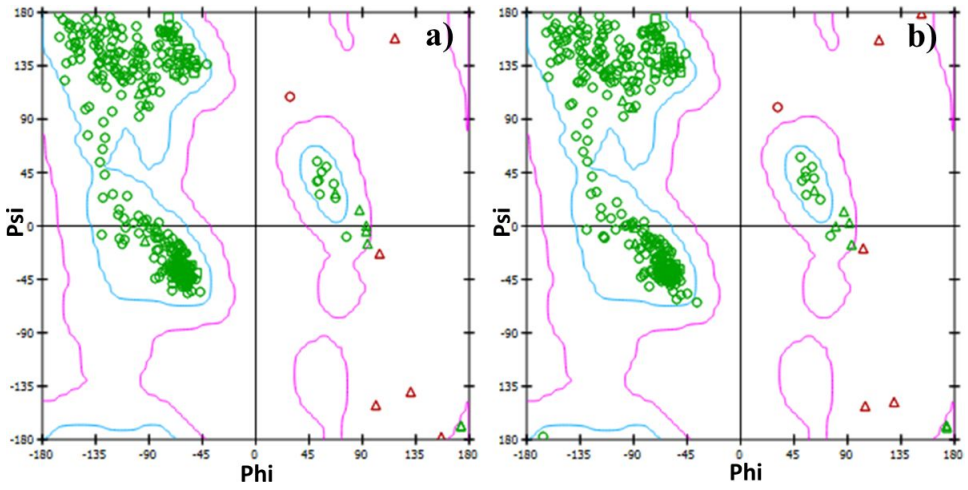

Figure 33: Ramachandran's plot of methyldopa proteins: a)5PNO and b)5PNQ).

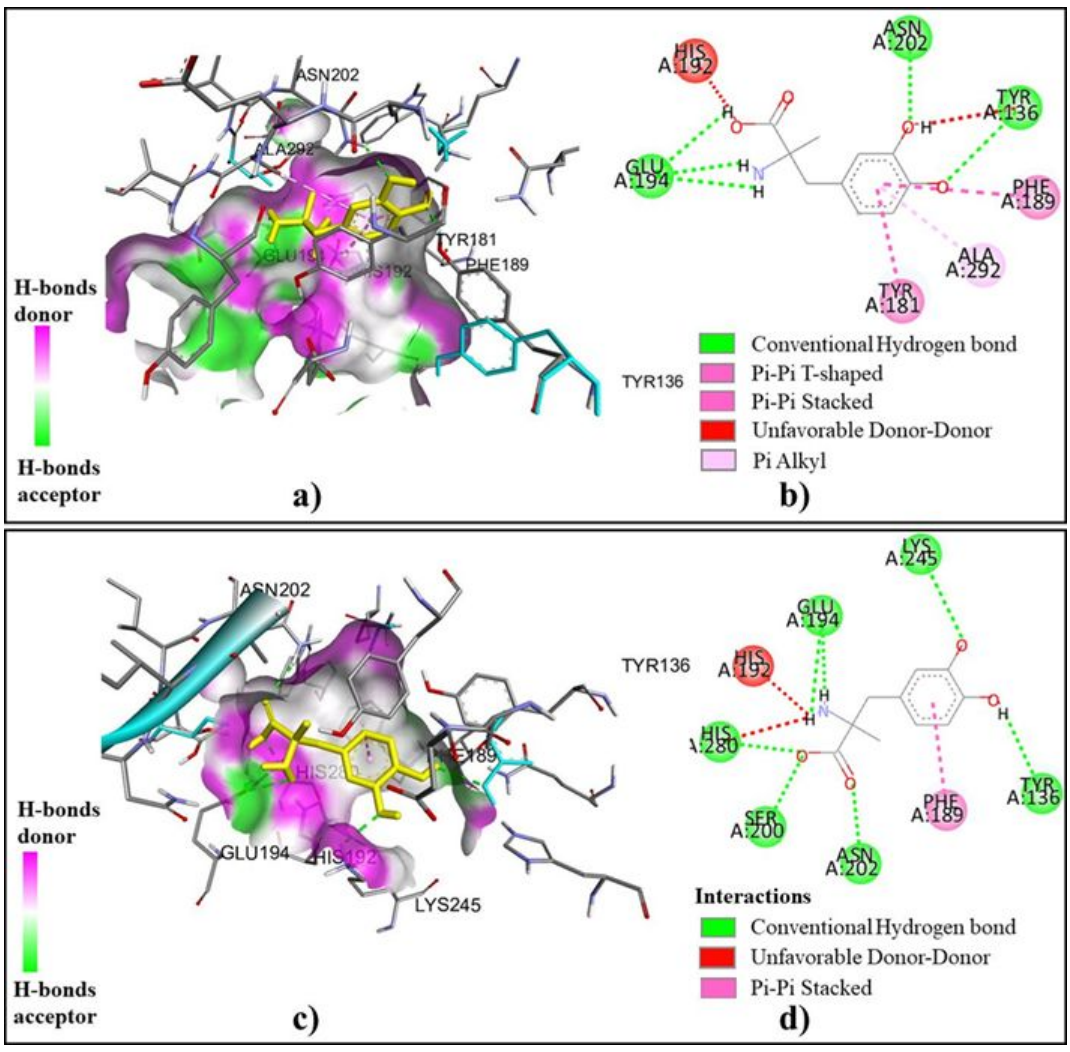

Figure 34: Docked pose (a,c) and non-covalent interactions (b,d) of methyldopa with (5PNO,5PNQ).

Table 27: Docking parameters of methyldopa complex with probable target proteins.

Target Proteins	PDB structure of proteins	H-Bonding residues	H-bond lengths ($\mathring{A}$)	Inhibition constant (μM)	Binding affinity (kcal/mol)	RMSD ($\mathring{A}$)
Lysine-specific demethylase 4D-like	5PNO (1.55Å)	GLU194	2.79	2.67	−7.6	1.18
		GLU194	2.63			
		GLU194	2.48			
		TYR136	2.35			
		ASN202	2.22			
	5PNQ (1.47Å)	SER200	1.89	3.74	−7.4	1.25
		ASN202	2.34			
		LYS245	2.53			
		HIS280	2.09			
		GLU194	2.36			
		GLU194	2.45			
		TYR136	2.60			

CHAPTER 5

5. CONCLUSIONS AND RECOMMENDATIONS

5.1 Conclsuions

Finally, using quantum approaches, spectroscopic techniques, and a molecular docking approach, the molecular stability, chemical reactivity, NLO characteristics, thermodynamic properties, and biological activity of cefalexin and methyldopa have been examined.

The title molecule cefalexin has just two stable conformers, A and B. The optimized parameters have been calculated and FT-IR and Raman spectra were analyzed. The redshift in FT-IR spectra was obtained at the frequencies of C=O, NH_2, and O-H, as well as the blueshift in N7H27. This signifies the molecule has intramolecular or intermolecular hydrogen bonding. QTAIM analysis reveals one partial covalent hydrogen bond interaction in conformer A and two in conformer B. The ELF and LOL maps reveal that majority of electrons are localized across oxygen, nitrogen, hydrogen, and carbon atoms. Furthermore, interactions involving lone pairs and antibonding π, such as LP(1)N7 $\rightarrow$ π*(O3-C15) and LP(1)N6 $\rightarrow$ π*(O2-C11), contribute the most to stabilize the molecular system. Conformer A is confirmed to be more reactive than conformer B based on HOMO and LUMO energy gaps as well as global metrics such as hardness, softness, and electrophilic index. Based on the MEP map, the atoms O2, O3, O5, and H34, H35, and H36 have been identified as suitable locations for nucleophilic and electrophilic attack in nature, respectively. Furthermore, the Fukui function analysis shows that the N8 atom is the most favorable local site for nucleophilic attack while the C17 atom is the most favorable local site for electrophilic attack. As the temperature rises, thermodynamic parameters such as specific heat, capacity, and entropy rise as well. The first hyperpolarizability (0.4440×10^{-30} esu) of the molecule was found to be comparable to that of urea. Thus, it is also important for constructing NLO devices. Furthermore, the molecule has negative second hyperpolarizability (-0.12849×10^{-35} esu) which is crucial for building controllable NLO devices. The molecular docking studies suggest that cefalexin binding sites are predominantly asso-

ciated with carboxyl group, carbonyl group, primary amine, and hydroxyl group. Cefalexin binds to the proteins leukotriene A-4 hydrolase and carbonic anhydrase II with binding affinity ranging from -7.3 to -8.3 kcal/mol. Hence, it has a high inhibitory potential against both proteins. The chemical and biological properties of methyldopa compound have been studied. The covalency of each bond was examined. It was revealed that methyldopa forms a dimer with three intramolecular hydrogen bonds. On the basis of NBO analysis, two strong hydrogen bonds were confirmed by the interactions: LP(1)O2/LP(2)O2$\rightarrow\sigma$*(O29-H54) and LP(1)O3/LP(2)O3$\rightarrow\sigma$*(O1-H26) with their respective stabilization energies of 7.75/18.04 kcal/mol and 8.83/21.36 kcal/mol, respectively. The high degree of electron localization was investigated across C-H bonds, oxygen, and nitrogen, with electron delocalization at the RCP. The energy gap of the dimer is shown to be smaller than that of the monomer. The hardness of the dimeric form was found to be smaller and the softness was found to be greater than the monomeric form. Oxygen in carbonyl groups in monomers and nitrogen amine groups in dimers were predicted to be nucleophilic sites. Similarly, electrophilic sites have been discovered in the hydrogen atom of the hydroxyl group in both. The most suitable sites for nucleophilic attack were discovered as; C9 in monomers and N5 in dimers, while for electrophilic attack C10 in both.The thermodynamic properties of molecules have a strong positive correlation with temperature. The polarizabilty and hyperpolarizabilty of the molecule are significantly greater than the value of urea. The calculated value of mean polarizability, first hyperpolarizability and second hyperpolarizability are, resoectively (12.6980×10^{-10} esu), (0.9017×10^{-30} esu) and (-0.0412×10^{-35}esu). As a result, methyldopa has considerable NLO capabilities that is required for NLO devices. The protein Lysine-specific demethylase 4D-like strongly binds with methyldopa. Each of the docked-complexes exhibit five strong hydrogen bonds and their binding affinity ranges from -7.6 to -7.4 kcal/mol.

As a result, the active sites for biological activity have been predicted for cefalexin and methyldopa. It is also justified that the dimeric form of the molecule is more reactive than the monomeric form. Additionally, both molecules are suitable for NLO devices as well. The computer modeling tools predict that the molecules have very strong inhibitory characteristics against their target proteins. However, additional in vitro and preclinical trials are required to validate the predicted outcomes.

5.2 Recommendations

The structural and conformational stability, electronic and thermal properties, and chemical and biological activities of drugs have been computationally determined using the quantum mechanical method. Hence, the findings of the work may need experimental verification as well. Further, the work contains the basic essential properties of drugs.

Thus, these can be helpful in improving the quality of the drugs. The recommendations for further work are stated below:

1. Cefalexin's FT-IR and FT-Raman spectra, as well as quantum mechanical computations, reveal intramolecular and intermolecular hydrogen bonding. Thus, research on the dimeric and trimeric forms of cephalexin can be carried out to predict the molecular properties more precisely.
2. The biological active sites of dimeric methyldopa have been generated. Thus, molecular docking of dimeric ligand with target proteins can be examined.
3. The molecular docking demonstrated that cephalexin and methyldopa were effective inhibitors of certain target proteins. In addition, MD simulations can be carried out to explore the stability of the binding of these biological molecules to their proteins.

CHAPTER 6

6. SUMMARY

The structural and spectroscopic properties of an antibiotic, cefalexin, and an antihypertensive medicine, methyldopa, have been determined using the DFT approach at the 6-311++G(d,p) level of theory. The Gaussian 09 package was used solely in the computation of different properties. The conformational stability, vibrational spectra, chemical stability, global and local reactivity parameters, MEP, hydrogen bond interactions, NLO properties, and ligand-protein interactions have been discussed.

Using B3LYP/6-311++G(d,p), the title molecule was optimized, and a one - dimensional potential energy surface (PES) scan was carried out. Among the eight predicted conformers, only the conformers A and B were found to be stable. The optimized parameters of the two conformers were nearly identical. However, some of the parameters diverge by a small value. It was discovered from QTAIM analysis that all hydrogen bonds in both conformers were medium-type in nature. Utilizing experimental IR and Raman spectra as well as theoretical methods, the vibrational analysis of cefalexin was carried out. The vibrational frequencies were computed for O-H, CHO, N-H, C-H, C=O, C-O, and C=C. The calculated frequencies were well matched with the experimental IR and Raman frequency. However, for carbonyl amine groups the frequencies were slightly diverged from the experimental frequencies due to hydrogen bonding. The NBO analysis of cefalexin cephalexin depicts that the interactions: LP(1)N7$\rightarrow \pi$*(O3-C15) , LP(1)N6$\rightarrow \pi$*(O2-C11) and LP(2)O4$\rightarrow \pi$*(O5-C17), respectively exhibits the maximum stabilization energies of 46.73, 45.86, and 43.68 kcal/mol. The HOMO and LUMO energies of the conformers were examined. The conformer A has a smaller HOMO-LUMO energy gap than the conformer B. Analysis of the MEP for conformers A and B shows that the region covering the atoms O2, O3, and O5 has a low electrostatic potential, whereas the region covering the atoms H36, H34, and H35 has a high electrostatic potential. The ELF and LOL of cefalexin have been investigated using Multiwfn software. The additional red zone around nitrogen and oxygen was due to the presence of lone pairs. Similarly, strong electron localization was depicted across hydrogen atoms due to maximum Pauli repulsion. Cefalexin's nonlinear properties, like

the value of first hyperpolarizability and second hyperpolarizability, were determined to be 0.4440×10^{-30} esu and 0.12849×10^{-35} esu, respectively. In relation to temperature, the thermodynamic parameters have been established. The biological activity of cefalexin with molecular docking simulation was employed. Hydrogen bond lengths between cefalexin and leukotriene A-4 hydrolase range from 2.52 to 3.04 Å and binding affinity from -8.3 to -8.6 kcal/mol.

The molecular and chemical stability of methyldopa were discussed in detail. A PES scan of the molecule revealed four conformers: C1, C2, C3, and C4. Using these conformers, different possible dimers were created. Among these dimers, dimer C1C1 was determined to be the most stable one. The QTAIM method was used to identify covalent and non-covalent interactions in dimers. Topological parameters such as BCP, NACP, RCP, electron density, electronic energy density, kinetic energy density, potential energy density, the ratio of the local potential and kinetic energy density, and the ellipticity at BCP were examined. In monomer, the value of |V|/G for O2-C10 was 2.0681 and 2.1086 in dimer. Non-ring C-H bonds have ellipticity in the range of 0.0073 to 0.0496 for monomers and 0.0073 to 0.0104 for dimers. The molecular graph along with NCI technique, the non-covalent interactions , such as steric effects, van der Waals interactions, and hydrogen bond interactions, were explored. Furthermore, utilizing NBO analysis, two strong hydrogen bonds interactons corrsponding to the charge delocalization from LP(2) O2 to σ*(O29-H54) and LP(2)O3 to σ*(O1-H26) were examined. ELF plots have been used to visualize charge localized and delocalized regions in the molecules. The HOMO and LUMO of methyldopa have been studied in both gaseous and aqueous conditions. In gas, the predicted HOMO-LUMO energy gaps were 5.536 eV for a monomer and 5.052 eV for a dimer. Furthermore, the density of states (DOS) was used to depict the frontier molecular orbitals (FMOs). Also, the charge transfer activity was explored through electron-hole analysis. Similarly, the chemical hardness in the gaseous state was found to be 2.768 eV for monomer and 2.526 eV for dimer. The values of the electrophilicity index for monomer and dimer have been discovered to be 1.488 eV and 1.722 eV, respectively. The dual descriptor ($\triangle f_k$) was calculated to view the nucleophilic and electrophilic sites of a molecular system. It has been predicted that C9 is the most favorable site for nucleophilic attack in monomers and N5 in dimers, while C10 is the most favorable site for electrophilic attack. The thermodynamics between 50 and 600 K were studied for monomers, and the equations relating enthalpy, heat capacity, and entropy to temperature were determined. The NLO properties, like first hyperpolarizability and second hyperpolarizability, were determined. Its first hyperpolarizability was found to be 0.9017×10^{-30} esu, and its second hyperpolarizability was found to be -0.0412×10^{-35} esu. The docking of 5PNO with methyldopa revealed a binding affinity of -7.6 kcal/mol and an inhibition constant of 2.67 μM. 5PNQ has

a binding affinity of -7.4 kcal/mol and an inhibition constant of 3.74 μM, with seven hydrogen bonds and good binding activity with 5*PNQ*.

Finally, the optimized parameters; NBO analysis; PED associated with vibrational frequency; HOMO and LUMO energies, MEP, AIM analysis, global and local reactivity parameters; NLO properties; standard thermodynamic parameters and mollecular docking have been addressed.

REFERENCES

Abraham, C. S., Muthu, S., Prasana, J. C., Armaković, S. J., Armaković, S., AS, B. G., et al. (2018). Spectroscopic profiling (ft-ir, ft-raman, nmr and uv-vis), autoxidation mechanism (h-bde) and molecular docking investigation of 3-(4-chlorophenyl)-n, n-dimethyl-3-pyridin-2-ylpropan-1-amine by dft/td-dft and molecular dynamics: A potential ssri drug. *Computational biology and chemistry*, *77*, 131–145. doi: 10.1016/j.compbiolchem.2018.08.010

Abraham, C. S., Prasana, J. C., & Muthu, S. (2017). Quantum mechanical, spectroscopic and docking studies of 2-amino-3-bromo-5-nitropyridine by density functional method. *Spectrochimica Acta Part A: Molecular and Biomolecular Spectroscopy*, *181*, 153–163. doi: 10.1016/j.saa.2017.03.045

Adler, S. (1974). Methyldopa-induced decrease in mental activity. *JAMA*, *230*(10), 1428–1429. doi: 10.1001/jama.1974.03240100046027

Aguiar, D., SAN GIL, R. A., BORRE, L. B., MARQUES, M. R., & GEMAL, A. L. (2011). Evaluation of polymorphs in cephalexin medicines by 13c solid state nmr. *Int. J. Pharm. Pharm. Sci*, *3*(3), 293–298. Retrieved from `https://innovareacademics.in/journal/ijpps/Vol3Issue3/2369.pdf`

Alpert, N. L., Keiser, W. E., Szymanski, H. A., Alpert, N. L., Keiser, W. E., & Szymanski, H. A. (1970). Instruments. *IR: Theory and Practice of Infrared Spectroscopy*, 9–64. doi: 10.1007/978-1-4684-8160-0_2

Amro, F. H., Moussa, H. N., Ashimi, O. A., & Sibai, B. M. (2016). Treatment options for hypertension in pregnancy and puerperium. *Expert Opinion on Drug Safety*, *15*(12), 1635–1642. doi: 10.1080/14740338.2016.1237500

Anacona, J. R., & Rodriguez, I. (2004). Synthesis and antibacterial activity of cephalexin metal complexes. *Journal of Coordination Chemistry*, *57*(15), 1263–1269. doi: 10.1080/00958970410001721411

Azmir, J., Zaidul, I. S. M., Rahman, M. M., Sharif, K., Mohamed, A., Sahena, F., ... Omar, A. (2013). Techniques for extraction of bioactive compounds from

plant materials: A review. *Journal of food engineering*, *117*(4), 426–436. doi: 10.1016/j.jfoodeng.2013.01.014

Bader, R. (1990). Atoms in molecules: a quantum theory: Oxford univ. *Press.: Oxford*. Retrieved from `http://surl.li/lkgfe`

Bader, R., Anderson, S., & Duke, A. (1979). Quantum topology of molecular charge distributions. 1. *Journal of the American Chemical Society*, *101*(6), 1389–1395. doi: 10.1021/ja00500a006

Bader, R. F., & Matta, C. F. (2004). Atomic charges are measurable quantum expectation values: a rebuttal of criticisms of QTAIM charges. *The Journal of Physical Chemistry A*, *108*(40), 8385–8394. doi: 10.1021/jp0482666

Bailey, A., Hadley, A., Walker, A., & James, D. G. (1970). Cephalexin—a new oral antibiotic. *Postgraduate Medical Journal*, *46*(533), 157. doi: 10.1136%2Fpgmj.46.533.157

Barnes, A. (2004). Blue-shifting hydrogen bonds—are they improper or proper? *Journal of molecular structure*, *704*(1-3), 3–9. doi: 10.1016/j.molstruc.2004.02.040

Baseden, K. A., & Tye, J. W. (2014). Introduction to density functional theory: Calculations by hand on the helium atom. *Journal of chemical education*, *91*(12), 2116–2123. doi: 10.1021/ed5004788

Beć, K. B., Grabska, J., & Huck, C. W. (2020). Biomolecular and bioanalytical applications of infrared spectroscopy–a review. *Analytica chimica acta*, *1133*, 150–177. doi: 10.1016/j.aca.2020.04.015

Becke, A. D. (1988). Density-functional exchange-energy approximation with correct asymptotic behavior. *Physical Review A*, *38*(6), 3098. doi: 10.1103/PhysRevA.38.3098

Bernhoft, A. (2010). A brief review on bioactive compounds in plants. *Bioactive compounds in plants-benefits and risks for man and animals*, *50*, 11–17.

Bérubé, G. (2006). Natural and synthetic biologically active dimeric molecules: anticancer agents, anti-hiv agents, steroid derivatives and opioid antagonists. *Current medicinal chemistry*, *13*(2), 131–154. doi: 10.2174/092986706775197908

Binkley, J. S., Pople, J. A., & Hehre, W. J. (1980). Self-consistent molecular orbital methods. 21. Small split-valence basis sets for first-row elements. *Journal of the American Chemical Society*, *102*(3), 939–947. doi: 10.1021/ja00523a008

Borah, B., & Devi, T. G. (2020). Characterization of zn (l-proline) 2 complex using spectroscopic techniques and dft analysis. *Journal of Molecular structure*, *1210*, 128022. doi: 10.1016/j.molstruc.2020.128022

Born, M., & Oppenheimer, R. (1927). Zur quantentheorie der molekeln. *Annalen der Physik*, *389*(20), 457–484. doi: 10.1002/andp.19273892002

Bretonnet, J.-L. (2017). Basics of the density functional theory. *AIMS Materials Science*, *4*(6), 1372–1405. doi: 10.3934/matersci.2017.6.1372

Buvaneswari, M., Santhakumari, R., Usha, C., Jayasree, R., & Sagadevan, S. (2021). Synthesis, growth, structural, spectroscopic, optical, thermal, dft, homo–lumo, mep, nbo analysis and thermodynamic properties of vanillin isonicotinic hydrazide single crystal. *Journal of Molecular Structure*, *1243*, 130856. doi: 10.1016/j.molstruc.2021.130856

Ceperley, D. M., & Alder, B. J. (1980). Ground state of the electron gas by a stochastic method. *Physical Review Letters*, *45*(7), 566. doi: 10.1103/PhysRevLett.45.566

Chattaraj, P., Nath, S., & Maiti, B. (2003). *Reactivity descriptors*. Marcel Dekker: New York. Retrieved from `http://surl.li/lkfrg`

Chaudhary, M., Prajapati, P., & Joshi, B. (2020). Quantum chemical calculation and dft study of sitagliptin: Insight from computational evaluation and docking approach. *Journal of Nepal Physical Society*, *6*(1), 73–83. doi: 10.3126/jnphyssoc.v6i1.30553

Chaudhary, M. K., Karthick, T., Joshi, B. D., Prajapati, P., de Santana, M. S. A., Ayala, A. P., ... Tandon, P. (2021). Molecular structure and quantum descriptors of cefradine by using vibrational spectroscopy (ir and raman), nbo, aim, chemical reactivity and molecular docking. *Spectrochimica Acta Part A: Molecular and Biomolecular Spectroscopy*, *246*, 118976. doi: 10.1016/j.saa.2020.118976

Chaudhary, M. K., Srivastava, A., Singh, K. K., Tandon, P., & Joshi, B. D. (2020). Computational evaluation on molecular stability, reactivity, and drug potential of frovatriptan from dft and molecular docking approach. *Computational and Theoretical Chemistry*, *1191*, 113031. doi: 10.1016/j.comptc.2020.113031

Chaudhary, T., Chaudhary, M. K., & Joshi, B. D. (2022). A theoretical study on charge transfer and hyperpolarizability of (s)-2-amino-3-(3, 4-dihydroxyphenyl)-2-methyl-propanoic acid. *Journal of Nepal Physical Society*, *8*(1), 16–21. doi: 10.3126/jnphyssoc.v8i1.48280

Chaudhary, T., Chaudhary, M. K., Joshi, B. D., de Santana, M. S. A., & Ayala, A. P. (2021). Spectroscopic (ft-ir, raman) analysis and computational study on conformational geometry, aim and biological activity of cephalexin from dft and molecular docking approach. *Journal of Molecular Structure*, *1240*, 130594. doi: 10.1016/j.molstruc.2021.130594

Chaudhary, T., & Joshi, B. D. (2022). Electronic, thermodynamic properties, nonlinear optical responses, and molecular docking studies on cephalexin. *Journal of Institute of Science and Technology*, *27*(1), 83–92. doi: 10.3126/jist.v27i1.46361

Chaudhary, T., Karthick, T., Chaudhary, M. K., Tandon, P., & Joshi, B. D. (2023). Computational evaluation on molecular stability and binding affinity of methyldopa against lysine-specific demethylase 4d enzyme through quantum chemical computations and molecular docking analysis. *Journal of Molecular Structure*, *1286*, 135518. doi: 10.1016/j.molstruc.2023.135518

Chockalingam, A., Campbell, N. R., & Fodor, J. G. (2006). Worldwide epidemic of hypertension. *Canadian journal of cardiology*, *22*(7), 553–555. doi: 10.1016/S0828-282X(06)70275-6

Christodoulides, D. N., Khoo, I. C., Salamo, G. J., Stegeman, G. I., & Van Stryland, E. W. (2010). Nonlinear refraction and absorption: mechanisms and magnitudes. *Advances in Optics and Photonics*, *2*(1), 60–200. doi: 10.1364/AOP.2.000060

Coates, J. (2006). Interpretation of infrared spectra, a practical approach. encycl. *Anal. Chem*, *12*(10), 815–10. doi: 10.1002/9780470027318.a5606

Cremer, D., & Kraka, E. (1984). A description of the chemical bond in terms of local properties of electron density and energy. *Croatica Chemica Acta*, *57*(6), 1259–1281. Retrieved from `https://hrcak.srce.hr/file/286247`

Cuffaro, D., Camodeca, C., Tuccinardi, T., Ciccone, L., Bartsch, J. W., Kellermann, T., ... Rossello, A. (2021). Discovery of dimeric arylsulfonamides as potent adam8 inhibitors. *ACS Medicinal Chemistry Letters*, *12*(11), 1787–1793. doi: 10.1021/acsmedchemlett.1c00411

Di, L., Kerns, E. H., & Carter, G. T. (2009). Drug-like property concepts in pharmaceutical design. *Current pharmaceutical design*, *15*(19), 2184–2194. doi: 10.2174/138161209788682479

Dirac, P. A. (1930). Note on exchange phenomena in the Thomas atom. In *Mathematical proceedings of the Cambridge philosophical society* (Vol. 26, pp. 376–385). doi: 10.1017/S0305004100016108

Ditchfield, R., Hehre, W. J., & Pople, J. A. (1971). Self-consistent molecular-orbital methods. IX. An extended Gaussian-type basis for molecular-orbital studies of organic molecules. *The Journal of Chemical Physics*, *54*(2), 724–728. doi: 10.1063/1.1674902

Dunning Jr, T. H. (1989). Gaussian basis sets for use in correlated molecular calculations. i. the atoms boron through neon and hydrogen. *The Journal of chemical physics*, *90*(2), 1007–1023. doi: 10.1063/1.456153

Fan, J., Fu, A., & Zhang, L. (2019). Progress in molecular docking. *Quantitative Biology*, *7*, 83–89. doi: 10.1007/s40484-019-0172-y

Fock, V. (1930). Bemerkung zum virialsatz. *Zeitschrift für Physik*, *63*(11-12), 855–858. doi: 10.1007/BF01339281

Frisch, A., Nielson, A., Holder, A., et al. (2000). Gaussview user manual. *Gaussian Inc., Pittsburgh, PA*, *556*.

Frisch, M., Trucks, G., Schlegel, H., Scuseria, G., Robb, M., Cheeseman, J., ... others (2009). 09, revision d. 01, gaussian. *Inc., Wallingford, CT*.

Fukui, K. (1982). Role of frontier orbitals in chemical reactions. *science*, *218*(4574), 747–754. doi: 10.1126/science.218.4574.747

Gasteiger, J., & Marsili, M. (1980). Iterative partial equalization of orbital electronegativity—a rapid access to atomic charges. *Tetrahedron*, *36*(22), 3219–3228. doi: 10.1016/0040-4020(80)80168-2

Gfeller, D., Grosdidier, A., Wirth, M., Daina, A., Michielin, O., & Zoete, V. (2014). Swisstargetprediction: a web server for target prediction of bioactive small molecules. *Nucleic acids research*, *42*(W1), W32–W38. doi: 10.1093/nar/gku293

Ghiasi, M., Noohi, B., & Zahedi, M. (2017). Quantum mechanical approach for the catalytic mechanism of dinuclear zinc metallo-β-lactamase by penicillin and cephalexin: Kinetic and thermodynamic points of view.
doi: 10.22036/pcr.2017.82104.1368

Ghose, A. K., Viswanadhan, V. N., & Wendoloski, J. J. (1998). Prediction of hydrophobic (lipophilic) properties of small organic molecules using fragmental methods: an analysis of alogp and clogp methods. *The Journal of Physical Chemistry A*, *102*(21), 3762–3772. doi: 10.1021/jp980230o

Glendening, E. D., & Weinhold, F. (1998). Natural resonance theory: I. general for-

malism. *Journal of computational chemistry*, *19*(6), 593–609. doi: 10.1002/(SICI)1096-987X(19980430)19:6%3C593::AID-JCC3%3E3.0.CO;2-M

Grabowski, S. J. (2011). Red-and blue-shifted hydrogen bonds: the bent rule from quantum theory of atoms in molecules perspective. *The Journal of Physical Chemistry A*, *115*(45), 12789–12799. doi: 10.1021/jp203908n

Guido, C. A., Cortona, P., Mennucci, B., & Adamo, C. (2013). On the metric of charge transfer molecular excitations: a simple chemical descriptor. *Journal of chemical theory and computation*, *9*(7), 3118–3126. doi: 10.1021/ct400337e

Guirgis, G. A., Klaboe, P., Shen, S., Powell, D. L., Gruodis, A., Aleksa, V., ... Durig, J. R. (2003). Spectra and structure of silicon-containing compounds. xxxvi—raman and infrared spectra, conformational stability, ab initio calculations and vibrational assignment of ethyldibromosilane. *Journal of Raman Spectroscopy*, *34*(4), 322–336. doi: 10.1002/jrs.989

Günter, P. (2012). *Nonlinear optical effects and materials* (Vol. 72). Springer. doi: 10.1007/978-3-540-49713-4

Harrison, N. (2003). An introduction to density functional theory. *Nato Science Series Sub Series III Computer and Systems Sciences*, *187*, 45–70. Retrieved from `https://www.ch.ic.ac.uk/harrison/Teaching/DFT_NATO.pdf`

Hartree, D. R. (1928). The wave mechanics of an atom with a non-Coulomb central field. Part I. Theory and methods. In *Mathematical Proceedings of the Cambridge Philosophical Society* (Vol. 24, pp. 89–110). doi: 10.1017/S0305004100011919

Hehre, W. J. (2003). *A guide to molecular mechanics and quantum chemical calculations* (Vol. 2). Wavefunction Irvine, CA. Retrieved from `http://surl.li/lkfuo`

Hehre, W. J., Ditchfield, R., & Pople, J. A. (1972). Self—consistent molecular orbital methods. XII. Further extensions of Gaussian—type basis sets for use in molecular orbital studies of organic molecules. *The Journal of Chemical Physics*, *56*(5), 2257–2261. doi: 10.1063/1.1677527

Heinrich, N., Koch, W., & Frenking, G. (1986). On the use of Koopmans' theorem to estimate negative electron affinities. *Chemical Physics Letters*, *124*(1), 20–25. doi: 10.1016/0009-2614(86)85005-9

Hey, E. (2007). *Neonatal formulary 5: Drug use in pregnancy and the first year of life*. Blackwell Pub.

Hohenberg, P., & Kohn, W. (1964). Inhomogeneous electron gas. *Physical Review*, *136*(3B), B864. doi: 10.1103/PhysRev.136.B864

Hou, J., & Poole, J. (1971). β-lactam antibiotics: their physicochemical properties and biological activities in relation to structure. *Journal of Pharmaceutical Sciences*, *60*(4), 503–532. doi: 10.1002/jps.2600600402

Hsu, C.-P. S. (1997). Infrared spectroscopy. *Handbook of instrumental techniques for analytical chemistry*, *249*. Retrieved from `https://mmrc.caltech.edu/FTIR/Literature/General/IR%20spectroscopy%20Hsu.pdf`

Humphrey, W., Dalke, A., & Schulten, K. (1996). Vmd: visual molecular dynamics. *Journal of molecular graphics*, *14*(1), 33–38. doi: 10.1016/0263-7855(96)00018-5

Issaoui, N., Ghalla, H., Bardak, F., Karabacak, M., Dlala, N. A., Flakus, H., & Oujia, B. (2017). Combined experimental and theoretical studies on the molecular structures, spectroscopy, and inhibitor activity of 3-(2-thienyl) acrylic acid through aim, nbo, ft-ir, ft-raman, uv and homo-lumo analyses, and molecular docking. *Journal of Molecular Structure*, *1130*, 659–668. doi: 10.1016/j.molstruc.2016.11.019

Issaoui, N., Ghalla, H., Muthu, S., Flakus, H., & Oujia, B. (2015). Molecular structure, vibrational spectra, aim, homo–lumo, nbo, uv, first order hyperpolarizability, analysis of 3-thiophenecarboxylic acid monomer and dimer by hartree–fock and density functional theory. *Spectrochimica acta part a: molecular and biomolecular spectroscopy*, *136*, 1227–1242. doi: 10.1016/j.saa.2014.10.008

Jensen, F. (2007). Electronic structure methods: Independent-particle models. *Introduction to computational chemistry*, *80*. Retrieved from `http://surl.li/lkfvf`

Jiang, Y., Liu, Z., Liu, H., Cui, W., Wang, N., Liu, D., & Ge, X. (2012). DFT study on nonlinear optical properties of lithium-doped corannulene. *Chinese Science Bulletin*, *57*(34), 4448–4452. doi: 10.1007/s11434-012-5437-z

Johnson, E. R., Keinan, S., Mori-Sánchez, P., Contreras-García, J., Cohen, A. J., & Yang, W. (2010). Revealing noncovalent interactions. *Journal of the American Chemical Society*, *132*(18), 6498–6506. doi: 10.1021/ja100936w

Joshi, B. D., Mishra, R., Tandon, P., Oliveira, A. C., & Ayala, A. P. (2014). Quantum chemical studies of structural, vibrational, nbo and hyperpolarizability of ondansetron hydrochloride. *Journal of Molecular Structure*, *1058*, 31–40. doi: 10.1016/j.molstruc.2013.10.062

Joshi, B. D., Srivastava, A., Gupta, V., Tandon, P., & Jain, S. (2013). Spectroscopic and quantum chemical study of an alkaloid aristolochic acid i. *Spectrochimica Acta Part A: Molecular and Biomolecular Spectroscopy*, *116*, 258–269. doi: 10.1016/j.saa.2013.07.036

Joshi, B. D., Srivastava, A., Tandon, P., & Jain, S. (2011). Molecular structure, vibrational spectra and homo, lumo analysis of yohimbine hydrochloride by density functional theory and ab initio hartree–fock calculations. *Spectrochimica Acta Part A: Molecular and Biomolecular Spectroscopy*, *82*(1), 270–278. doi: 10.1016/j.saa.2011.07.047

Kalinowska, M., Piekut, J., Bruss, A., Follet, C., Sienkiewicz-Gromiuk, J., Świsłocka, R., ... Lewandowski, W. (2014). Spectroscopic (ft-ir, ft-raman, 1h, 13c nmr, uv/vis), thermogravimetric and antimicrobial studies of ca (ii), mn (ii), cu (ii), zn (ii) and cd (ii) complexes of ferulic acid. *Spectrochimica Acta Part A: Molecular and Biomolecular Spectroscopy*, *122*, 631–638. doi: 10.1016/j.saa.2013.11.089

Kaneniwa, N., Imagawa, K., & Otsuka, M. (1984). Compression properties of cephalexin powder and physical properties of the tablet. *Chemical and pharmaceutical bulletin*, *32*(12), 4986–4993. doi: 10.1248/cpb.32.4986

Karabacak, M., Cinar, M., Unal, Z., & Kurt, M. (2010). Ft-ir, uv spectroscopic and dft quantum chemical study on the molecular conformation, vibrational and electronic transitions of 2-aminoterephthalic acid. *Journal of Molecular Structure*, *982*(1-3), 22–27. doi: 10.1016/j.molstruc.2010.07.033

Karabacak, M., Kose, E., & Atac, A. (2012). Molecular structure (monomeric and dimeric structure) and homo–lumo analysis of 2-aminonicotinic acid: A comparison of calculated spectroscopic properties with ft-ir and uv–vis. *Spectrochimica Acta Part A: Molecular and Biomolecular Spectroscopy*, *91*, 83–96. doi: 10.1016/j.saa.2012.01.072

Kariper, S. E. (2017). Spectroscopic and quantum chemical studies on some β-lactam inhibitors. *Turkish Computational and Theoretical Chemistry*, *1*(2), 13–26. Retrieved from `https://dergipark.org.tr/en/pub/tcandtc/issue/32792/314979`

Karrouchi, K., Brandán, S. A., Sert, Y., El Karbane, M., Radi, S., Ferbinteanu, M., ... others (2021). Synthesis, structural, molecular docking and spectroscopic studies of (e)-n'-(4-methoxybenzylidene)-5-methyl-1h-pyrazole-3-carbohydrazide. *Journal of Molecular Structure*, *1225*, 129072. doi: 10.1016/j.molstruc.2020.129072

Keith, T. (2009). Aimall version 090201 tk gristmill software overland park, ks. In *Usa.*

Kirkland, T. A., Adler, M., Bauman, J. G., Chen, M., Haeggström, J. Z., King, B., ... others (2008). Synthesis of glutamic acid analogs as potent inhibitors of leukotriene a4 hydrolase. *Bioorganic & medicinal chemistry*, *16*(9), 4963–4983. doi: 10.1016/j.bmc.2008.03.042

Koch, U., & Popelier, P. L. (1995). Characterization of CHO hydrogen bonds on the basis of the charge density. *The Journal of Physical Chemistry*, *99*(24), 9747–9754. doi: 10.1021/j100024a016

Kohn, W., Becke, A. D., & Parr, R. G. (1996). Density functional theory of electronic structure. *The Journal of Physical Chemistry*, *100*(31), 12974–12980. doi: 10.1021/jp960669l

Kohn, W., & Sham, L. J. (1965). Self-consistent equations including exchange and correlation effects. *Physical Review*, *140*(4A), A1133. doi: 10.1103/PhysRev.140.A1133

Krishnan, D., Pan, W., Beggs, M. R., Trepiccione, F., Chambrey, R., Eladari, D., ... Alexander, R. T. (2018). Deficiency of carbonic anhydrase ii results in a urinary concentrating defect. *Frontiers in Physiology*, *8*, 1108. doi: 10.3389/fphys.2017.01108

Krishnan, R., Binkley, J. S., Seeger, R., & Pople, J. A. (1980). Self-consistent molecular orbital methods. XX. A basis set for correlated wave functions. *The Journal of Chemical Physics*, *72*(1), 650–654. doi: 10.1063/1.438955

Kumar, A., Kumar, R., Gupta, A., Tandon, P., & D'silva, E. D. (2017). Molecular structure, nonlinear optical studies and spectroscopic analysis of chalcone derivative (2e)-3-[4-(methylsulfanyl) phenyl]-1-(3-bromophenyl) prop-2-en-1-one by dft calculations. *Journal of Molecular Structure*, *1150*, 166–178. doi: 10.1016/j.molstruc.2017.08.072

Kumar, R., Karthick, T., Tandon, P., Agarwal, P., Menezes, A. P., & Jayarama, A. (2018). Structural and vibrational characteristics of a non-linear optical material 3-(4-nitrophenyl)-1-(pyridine-3-yl) prop-2-en-1-one probed by quantum chemical computation and spectroscopic techniques. *Journal of Molecular Structure*, *1164*, 180–190. doi: 10.1016/j.molstruc.2018.03.060

Lee, C., Yang, W., & Parr, R. G. (1988). Development of the colle-salvetti correlation-energy formula into a functional of the electron density. *Physical review B*, *37*(2), 785. doi: 10.1103/PhysRevB.37.785

Lin-Vien, D., Colthup, N. B., Fateley, W. G., & Grasselli, J. G. (1991). *The handbook of infrared and raman characteristic frequencies of organic molecules*. Elsevier. Retrieved from http://surl.li/lkfzx

Lipinski, C. A. (2004). Lead-and drug-like compounds: the rule-of-five revolution. *Drug discovery today: Technologies*, *1*(4), 337–341. doi: 10.1016/j.ddtec.2004.11.007

Liu, C., Alfano, R., Sha, W., Zhu, H., Akins, D., Cleary, J., ... Cellmer, E. (1991). Human breast tissues studied by ir fourier-transform raman spectroscopy. In *Conference on lasers and electro-optics* (p. CWF51). Retrieved from https://opg.optica.org/abstract.cfm?uri=cleo-1991-CWF51

Liu, Z., Lu, T., & Chen, Q. (2020). An sp-hybridized all-carboatomic ring, cyclo [18] carbon: Electronic structure, electronic spectrum, and optical nonlinearity. *Carbon*, *165*, 461–467. doi: 10.1016/j.carbon.2020.05.023

Low, Z. Y., Farouk, I. A., & Lal, S. K. (2020). Drug repositioning: New approaches and future prospects for life-debilitating diseases and the covid-19 pandemic outbreak. *Viruses*, *12*(9), 1058. doi: 10.3390/v12091058

Lu, T., & Chen, F. (2012). Multiwfn: A multifunctional wavefunction analyzer. *Journal of computational chemistry*, *33*(5), 580–592. doi: 10.1002/jcc.22885

Mah, G. T., Tejani, A. M., & Musini, V. M. (2009). Methyldopa for primary hypertension. *Cochrane Database of Systematic Reviews*(4). doi: 10.1002%2F14651858.CD003893.pub3

Malaganvi, S. S., Tonannavar, J., & Tonannavar, J. (2019). Experimental, dft dimeric modeling and aim study of h-bond-mediated composite vibrational structure of chelidonic acid. *Heliyon*, *5*(5), e01586. doi: 10.1016/j.heliyon.2019.e01586

Manelli, L. P. (1975). Cephalexin. In *Analytical profiles of drug substances* (Vol. 4, pp. 21–46). Elsevier.

Manne, R., & Åberg, T. (1970). Koopmans' theorem for inner-shell ionization. *Chemical Physics Letters*, *7*(2), 282–284. doi: 10.1016/0009-2614(70)80309-8

Martin, J., & Van Alsenoy, C. (1995). Gar2ped. *University of Antwerp*.

Morell, C., Grand, A., & Toro-Labbé, A. (2005). New dual descriptor for chemical reactivity. *The Journal of Physical Chemistry A*, *109*(1), 205–212. doi: 0.1021/jp046577a

Morris, G. M., & Lim-Wilby, M. (2008). Molecular docking. *Molecular modeling of proteins*, 365–382. doi: 10.1007/978-1-59745-177-2_19

Muthu, K., Gunasekaran, K., Kala, A., Govindasamy, P., Rajesh, P., & Moorthi, P. (2015). Spectroscopic (ft-ir, ft-raman & uv-vis) and density functional theory studies of cefadroxil. *Int. J. Curr. Microbiol. App. Sci.*, *11*, 211–222. Retrieved from https://www.ijcmas.com/vol-4-11/Kesavan%20Muthu,%20et%20al.pdf

Muthu, S., & Maheswari, J. U. (2012). Quantum mechanical study and spectroscopic (ft-ir, ft-raman, 13c, 1h, uv) study, first order hyperpolarizability, nbo analysis, homo and lumo analysis of 4-[(4-aminobenzene) sulfonyl] aniline by ab initio hf and density functional method. *Spectrochimica Acta Part A: Molecular and Biomolecular Spectroscopy*, *92*, 154–163. doi: 10.1016/j.saa.2012.02.056

Muthu, S., & Paulraj, E. I. (2013a). Spectroscopic and molecular structure (monomeric and dimeric structure) investigation of 2-[(2-hydroxyphenyl) carbonyloxy] benzoic acid by dft method: A combined experimental and theoretical study. *Journal of Molecular Structure*, *1038*, 145–162. doi: 10.1016/j.molstruc.2013.01.043

Muthu, S., & Paulraj, E. I. (2013b). Spectroscopic and molecular structure (monomeric and dimeric structure) investigation of 2-[(2-hydroxyphenyl) carbonyloxy] benzoic acid by dft method: A combined experimental and theoretical study. *Journal of Molecular Structure*, *1038*, 145–162. doi: 10.1016/j.molstruc.2013.01.043

Nakano, M., Kiribayashi, S., Yamada, S., Shigemoto, I., & Yamaguchi, K. (1996). Theoretical study of the second hyperpolarizabilities of three charged states of pentalene. a consideration of the structure-property correlation for the sensitive second hyperpolarizability. *Chemical physics letters*, *262*(1-2), 66–73. doi: 10.1016/0009-2614(96)01051-2

Noei, M., Holoosadi, M., & Anaraki-Ardakani, H. (2017). Design of methyldopa structure and calculation of its properties by quantum mechanics. *Arabian Journal of Chemistry*, *10*, S1923–S1937. doi: 10.1016/j.arabjc.2013.07.021

Ochterski, J. W. (2000). Thermochemistry in gaussian. *Gaussian Inc*, *1*, 1–19. Retrieved from https://gaussian.com/thermo/

Ostrov, D. A., Alkanani, A., McDaniel, K. A., Case, S., Baschal, E. E., Pyle, L., ... others (2018). Methyldopa blocks mhc class ii binding to disease-specific antigens in autoimmune diabetes. *The Journal of clinical investigation*, *128*(5), 1888–1902. doi: 10.1172/jci97739

Otsuka, M., & Kaneniwa, N. (1983a). Effect of grinding on the degree of crystallinity of

cephalexin powder. *Chemical and pharmaceutical bulletin*, *31*(12), 4489–4495. doi: 10.1248/cpb.31.4489

Otsuka, M., & Kaneniwa, N. (1983b). Hygroscopicity and solubility of noncrystalline cephalexin. *Chemical and Pharmaceutical Bulletin*, *31*(1), 230–236. doi: 10 .1248/cpb.31.230

Paquin, A., Reyes-Moreno, C., & Bérubé, G. (2021). Recent advances in the use of the dimerization strategy as a means to increase the biological potential of natural or synthetic molecules. *Molecules*, *26*(8), 2340. doi: 10.3390/molecules26082340

Parr, R. G., & Yang, W. (1984). Density functional approach to the frontier-electron theory of chemical reactivity. *Journal of the American Chemical Society*, *106*(14), 4049–4050. doi: 10.1021/ja00326a036

Perdew, J. P. (1986). Density-functional approximation for the correlation energy of the inhomogeneous electron gas. *Physical Review B*, *33*(12), 8822. doi: 10.1103/ PhysRevB.33.8822

Pichichero, M. E. (2006). Cephalosporins can be prescribed safely for penicillin-allergic patients. *Journal of family practice*, *55*(2), 106.

Polavarapu, P. L. (1990). Ab initio vibrational Raman and Raman optical activity spectra. *Journal of Physical Chemistry*, *94*, 8106–8112. doi: 10.1021/j100384a024

Pople, J., & Beveridge, D. (1970). Approximate molecular orbital theory', mcgraw-hill, new york. Retrieved from `https://www.scribd.com/document/495242088/Approximate-Molecular-Orbital-Theory`

Pople, J. A., Head-Gordon, M., Fox, D. J., Raghavachari, K., & Curtiss, L. A. (1989). Gaussian-1 theory: A general procedure for prediction of molecular energies. *The Journal of Chemical Physics*, *90*(10), 5622–5629. doi: 10.1063/1.456415

Pople, J. A., & Hehre, W. J. (1978). Computation of electron repulsion integrals involving contracted Gaussian basis functions. *Journal of Computational Physics*, *27*(2), 161–168. doi: 10.1016/0021-9991(78)90001-3

Prabakaran, A., & Muthu, S. (2012). Normal coordinate analysis and vibrational spectroscopy (ft-ir and ft-raman) studies of (2s)-2-amino-3-(3, 4-dihydroxyphenyl)-2-methylpropanoic acid using ab initio hf and dft method. *Spectrochimica Acta Part A: Molecular and Biomolecular Spectroscopy*, *99*, 90–96. doi: 10.1016/j.saa.2012.09.014

Prasana, J. C., Muthu, S., Abraham, C. S., et al. (2020). Wavefunction analysis, charge transfer and molecular docking studies on famciclovir and entecavir: Potential

anti-viral drugs. *Chemical Data Collections*, *26*, 100353. doi: 10.1016/j.cdc .2020.100353

PubChem Compound Database. (2020a). *Cephalexin.* U.S. National Library of Medicine, USA.

PubChem Compound Database. (2020b). *Methyldopa.* U.S. National Library of Medicine, USA.

Pulay, P., Fogarasi, G., Pang, F., & Boggs, J. E. (1979). Systematic ab initio gradient calculation of molecular geometries, force constants, and dipole moment derivatives. *Journal of the American Chemical Society*, *101*(10), 2550–2560.

Renjith, R., Bhagysree, J., Ulahannan, R. T., Varghese, H. T., & Panicker, C. Y. (2013). Ft-ir, ft-raman and quantum chemical calculations of 1-phenylpyrrole. *Oriental Journal of Chemistry*, *29*(1), 321. doi: 10.13005/ojc/290152

Rizwana, B. F., Prasana, J. C., Muthu, S., & Abraham, C. S. (2020). Vibrational spectroscopy, reactive site analysis and molecular docking studies on 2-[(2-amino-6-oxo-6, 9-dihydro-3h-purin-9-yl) methoxy]-3-hydroxypropyl (2s)-2-amino-3-methylbutanoate. *Journal of Molecular Structure*, *1202*, 127274. doi: 10.1016/ j.molstruc.2019.127274

Rodgers, A., Ezzati, M., Vander Hoorn, S., Lopez, A. D., Lin, R.-B., Murray, C. J. L., & Collaborating, G. C. R. A. (2004). Distribution of major health risks: findings from the global burden of disease study. *PLoS medicine*, *1*(1), e27. doi: 10 .1371%2Fjournal.pmed.0010027

Rodman, J. S., Deutsch, D. J., & Gutman, S. I. (1976). Methyldopa hepatitis: A report of six cases and review of the literature. *The American Journal of Medicine*, *60*(7), 941–948. doi: 10.1016/0002-9343(76)90564-7

Rose, P. W., Beran, B., Bi, C., Bluhm, W. F., Dimitropoulos, D., Goodsell, D. S., ... others (2010). The rcsb protein data bank: redesigned web site and web services. *Nucleic acids research*, *39*(suppl_1), D392–D401. doi: 10.1093/nar/gkq1021

Rozas, I., Alkorta, I., & Elguero, J. (2000). Behavior of ylides containing N, O, and C atoms as hydrogen bond acceptors. *Journal of the American Chemical Society*, *122*(45), 11154–11161. doi: 10.1021/ja0017864

Sagaama, A., Noureddine, O., Brandán, S. A., Jarczyk-Jędryka, A., Flakus, H. T., Ghalla, H., & Issaoui, N. (2020). Molecular docking studies, structural and spectroscopic properties of monomeric and dimeric species of benzofuran-carboxylic acids derivatives: Dft calculations and biological activities. *Com-*

putational Biology and Chemistry, *87*, 107311. doi: 10.1016/j.compbiolchem .2020.107311

Schrödinger, E. (1926). Quantisierung als eigenwertproblem. *Annalen der physik*, *385*(13), 437–490. doi: http://surl.li/lkfsn

Sen, K. D., & Murray, J. (1996). *Molecular electrostatic potentials: Concepts and applications (theoretical and computational chemistry; 3)*. Elsevier Science Limited. Retrieved from https://shop.elsevier.com/books/molecular-electrostatic-potentials/murray/978-0-444-82353-3

Sevvanthi, S., Muthu, S., & Raja, M. (2017). Quantum mechanical, spectroscopic studies and molecular docking analysis on 5, 5-diphenylimidazolidine-2, 4-dione. *Journal of Molecular Structure*, *1149*, 487–498. doi: 10.1016/j.molstruc.2017 .08.015

Shafi, A., Sathyamurthy, R. D. T., Seetharaman, J., Sambanthan, M., Murugesan, R., Sundaram, S., & Ramarathinam, R. B. (2020). Molecular docking, quantum chemical computational and vibrational studies on bicyclic heterocycle "6-nitro-2, 3-dihydro-1, 4-benzodioxine": Anti-cancer agent. *Computational Biology and Chemistry*, *86*, 107226. doi: 10.1016/j.compbiolchem.2020.107226

Shahabadi, N., Hashempour, S., Taherpour, A., & Mohsenzadeh, F. (2018). Synthesis, characterization, hsa interaction, and antibacterial activity of a new water-soluble pt (ii) complex containing the drug cephalexin. *Journal of Coordination Chemistry*, *71*(22), 3708–3730. doi: 10.1080/00958972.2018.1525488

Sharma, K., Sharma, S., & Lahiri, S. (2012). Spectrophotometric, fourier transform infrared spectroscopic and theoretical studies of the charge–transfer complexes between methyldopa [(s)-2 amino-3-(3, 4-dihydroxyphenyl)-2-methyl propanoic acid] and the acceptors (chloranilic acid, o-chloranil and dichlorodicyanobenzoquinone) in acetonitrile and their thermodynamic properties. *Spectrochimica Acta Part A: Molecular and Biomolecular Spectroscopy*, *92*, 212–224. doi: 10.1016/j.saa.2012.02.072

Shen, Y.-R. (2002). *The principles of nonlinear optics. 3rd edn, 576.* Wiley-Interscience, New York. Retrieved from https://www.wiley.com/en-sg/The+Principles+of+Nonlinear+Optics-p-9780471430803

Sherrill, C. D. (2000). An introduction to hartree-fock molecular orbital theory. *School of Chemistry and Biochemistry Georgia Institute of Tech-*

nology. Retrieved from http://vergil.chemistry.gatech.edu/notes/hf-intro/hf-intro.pdf

Shinde, A. J., Patil, M. S., & More, H. N. (2010). Formulation and evaluation of an oral floating tablet of cephalexin. *Indian J Pharm Educ Res*, *44*(3), 243–252. Retrieved from https://www.ijper.org/article/276

Shoichet, B. K., Kuntz, I. D., & Bodian, D. L. (1992). Molecular docking using shape descriptors. *Journal of computational chemistry*, *13*(3), 380–397. doi: 10.1002/jcc.540130311

Shweta, Khan, E., Tandon, P., Bharti, P., Kumar, P., & Maurya, R. (2017). Experimental and quantum chemical studies on the structure and vibrational spectra of cearoin (a neoflavonoid). *Canadian Journal of Physics*, *95*(10), 905–915. doi: 10.1139/cjp-2016-0847

Singh, S., Singh, H., Karthick, T., Agarwal, P., Erande, R. D., Dethe, D. H., & Tandon, P. (2016). Combine experimental and theoretical investigation on an alkaloid–dimethylisoborreverine. *Journal of Molecular Structure*, *1103*, 187–201. doi: 10.1016/j.molstruc.2015.09.021

Sjoberg, P., Murray, J. S., Brinck, T., & Politzer, P. (1990). Average local ionization energies on the molecular surfaces of aromatic systems as guides to chemical reactivity. *Canadian Journal of Chemistry*, *68*(8), 1440–1443. doi: 10.1139/v90-220

Slater, J. C. (1937). Wave functions in a periodic potential. *Physical Review*, *51*(10), 846. doi: 10.1103/PhysRev.51.846

Smith, E., & Dent, G. (2019). *Modern raman spectroscopy: a practical approach*. John Wiley & Sons. Retrieved from http://surl.li/lkfvy

Socrates, G. (2004). *Infrared and raman characteristic group frequencies: tables and charts*. John Wiley & Sons. Retrieved from http://surl.li/lkfpl

Speight, T., Brogden, R., & Avery, G. (1972). Cephalexin: a review of its antibacterial, pharmacological and therapeutic properties. *Drugs*, *3*(1-2), 9–78. doi: 10.2165/00003495-197203010-00002

Srivastava, A., Karthick, T., Joshi, B., Mishra, R., Tandon, P., Ayala, A., & Ellena, J. (2017). Spectroscopic (far or terahertz, mid-infrared and raman) investigation, thermal analysis and biological activity of piplartine. *Spectrochimica Acta Part A: Molecular and Biomolecular Spectroscopy*, *184*, 368–381. doi: 10.1016/j.saa.2017.05.007

Srivastava, K., Srivastava, A., Tandon, P., Sinha, K., & Wang, J. (2016). Spectroscopic, quantum chemical calculation and molecular docking of dipfluzine. *Journal of Molecular Structure*, *1125*, 751–762. doi: 10.1016/j.molstruc.2016.07.078

Srivastava, R., Gupta, S. K., Naaz, F., Gupta, P. S. S., Yadav, M., Singh, V. K., ... others (2020). Alkylated benzimidazoles: Design, synthesis, docking, dft analysis, admet property, molecular dynamics and activity against hiv and yfv. *Computational Biology and Chemistry*, *89*, 107400. doi: 10.1016/j.compbiolchem.2020.107400

Stuart, B. H. (2004). *Infrared spectroscopy: fundamentals and applications*. John Wiley & Sons. Retrieved from `http://surl.li/lkfwj`

Studio, D. (2009). *2.5 Guide, Accelrys Inc., San Diego, 2009.* Retrieved from `https://www.3ds.com/products-services/biovia//`

Suhuan, W., Siyue, J., & Xiaodong, D. (2016). 'study on detection methods for methyldopa in biological samples. *Int. J. Curr. Res. Chem. Pharm. Sci*, *3*(7), 8–11. Retrieved from `http://ijcrcps.com/pdfcopy/july2016/ijcrcps2.pdf`

Swamy, R., & Ravikumar, C. (2021). Crystal structure determination, hirshfeld surface analysis and quantum computational studies of (3e, 5e)-1-ethyl-3, 5-bis (naphthalen-1-yl-methylidene) piperidin-4-one: A novel rorc inhibitor. *Journal of Molecular Structure*, *1225*, 129313. doi: 10.1016/j.molstruc.2020.129313

Szabo, A., & Ostlund, N. S. (2012). *Modern quantum chemistry: introduction to advanced electronic structure theory*. Courier Corporation. Retrieved from `http://surl.li/lkfrw`

Toghill, P., Smith, P., Benton, P., Brown, R., & Matthews, H. (1974). Methyldopa liver damage. *Br Med J*, *3*(5930), 545–548. doi: 10.1136/bmj.3.5930.545

Trott, O., & Olson, A. J. (2010). AutoDock Vina: improving the speed and accuracy of docking with a new scoring function, efficient optimization, and multithreading. *Journal of Computational Chemistry*, *31*(2), 455–461. doi: 10.1002/jcc.21334

Vankeirsbilck, T., Vercauteren, A., Baeyens, W., Van der Weken, G., Verpoort, F., Vergote, G., & Remon, J. P. (2002). Applications of raman spectroscopy in pharmaceutical analysis. *TrAC trends in analytical chemistry*, *21*(12), 869–877. doi: 10.1016/S0165-9936(02)01208-6

Veeresham, C. (2012). Natural products derived from plants as a source of drugs. *Journal of Advanced Pharmaceutical Technology and Research*, *3*(4), 200–201. doi: 10.4103%2F2231-4040.104709

Venkatesan, P., Thamotharan, S., Ilangovan, A., Liang, H., & Sundius, T. (2016). Crystal structure, hirshfeld surfaces and dft computation of nlo active (2e)-2-(ethoxycarbonyl)-3-[(1-methoxy-1-oxo-3-phenylpropan-2-yl) amino] prop-2-enoic acid. *Spectrochimica Acta Part A: Molecular and Biomolecular Spectroscopy*, *153*, 625–636. doi: 10.1016/j.saa.2015.09.002

Weinhold, F., & Landis, C. R. (2001). Natural bond orbitals and extensions of localized bonding concepts. *Chemistry Education Research and Practice*, *2*(2), 91–104. doi: 10.1039/B1RP90011K

Weinhold, F., & Landis, C. R. (2005). *Valency and bonding: a natural bond orbital donor-acceptor perspective*. Cambridge University Press. Retrieved from `http://surl.li/lkfqp`

Wiciński, M., Malinowski, B., Puk, O., Socha, M., & Słupski, M. (2020). Methyldopa as an inductor of postpartum depression and maternal blues: A review. *Biomedicine & Pharmacotherapy*, *127*, 110196. doi: 10.1016/j.biopha.2020.110196

Willard, H. H., Merritt, J. L. L., Dean, J. A., & Settle, J. F. A. (1989). *Instrumental methods of analysis*. Wadsworth Publishing Company, USA. Retrieved from `https://www.osti.gov/biblio/5209599`

Wortmann, R., Krämer, P., Glania, C., Lebus, S., & Detzer, N. (1993). Deviations from Kleinman symmetry of the second-order polarizability tensor in molecules with low-lying perpendicular electronic bands. *Chemical Physics*, *173*(1), 99–108. doi: 10.1016/0301-0104(93)80221-T

Yang, W., & Mortier, W. J. (1986). The use of global and local molecular parameters for the analysis of the gas-phase basicity of amines. *Journal of the American Chemical Society*, *108*(19), 5708–5711. doi: 10.1021/ja00279a008

Yang, Y. (2010). Hexacoordinate bonding and aromaticity in silicon phthalocyanine. *The Journal of Physical Chemistry A*, *114*(50), 13257–13267. doi: 10.1021/jp109278v

Yoshida, H., Takeda, K., Okamura, J., Ehara, A., & Matsuura, H. (2002). A new approach to vibrational analysis of large molecules by density functional theory: wavenumber-linear scaling method. *The Journal of Physical Chemistry A*, *106*(14), 3580–3586. doi: 10.1021/jp013084m

APPENDIX

A1. Tables

Table 28: Potential energy distribution contribution assigned to vibrational modes of cefalexin.

Unscaled	Scaled DFT		Experimental		Potential energy Distribution
DFT	A	B	IR	Raman	percent
3769	3570	3556		-	ν(OH)(100)
3601	3421	3408	3480		ν(NH)(99)
3591	3412	3377	3356		$\nu_a(NH_2)$(100)
3504	3333	3335	3331	3329	$\nu_s(NH_2)$(100)
3196	3058	3054	-	3057	R1[ν(CH)](98)
3188	3050	3048	-	3049	R1[ν(CH)](96)
3176	3039	3041	-	3047	R1[ν(CH)](95)
3164	3029	3034	3030		R1[ν(CH)](99)
3159	3024	3027	-		$\nu_a(CH_3)$(97)
3152	3018	3025	-	-	R1[ν(CH)](95)
3107	2977	2969	2983	2977	R2[ν(CH)](97)
3082	2955	2955	2947	2961	R3[ν(CH)](97)
3076	2949	2948	2947	2942	R3[$\nu_a(CH_2)$](99)
3061	2935	2933	2934	2933	$\nu_a(CH_3)$(99)
3023	2900	2902	2910	2912	R3[$\nu_s(CH_2)$](73)+$\nu_s(CH_3)$(25)
3017	2895	2900	2897	2884	$\nu_s(CH_3)$(73)+R3[$\nu_s(CH_2)$](27)
2926	2812	2895	2802		ν(C18H)(99)
1857	1817	1820	1756	-	R2[ν(C=O)(83)+ν(N6C11)(7)+δ_{ring}(5)+ν(CC)(5)]
1787	1751	1761	1743	-	ν(C17=O)(76)+R3[ν(C12C17)(5)]
1743	1709	1717	1681	-	ν(C15=O)(74)+ν(N7C15)(5)+ρ'(C15=O)(5)
1672	1641	1648	1645	1643	R3[ν(C=C)(66)+ν(N6C12)(5)+δ_{in}(CC)(6)]
1642	1612	1624	-		R1[ν(CC)(58)+δ_{in}(CH)(20)+δ(9)]+$\delta_{sci}(NH_2)$(5)
1630	1601	1611	-	1600	$\delta_{sci}(NH_2)$(77)+R1[ν(CC)(6)]
1621	1593	1595	1593	1583	R1[ν(CC)(63)+δ_{in}(CH)(9)+δ'_a(8)]+$\delta_{sci}(NH_2)$(6)
1541	1516	1507	-	1497	ρ(N7H)(52)+ν(N7C15)(23)+R2[ν(N7C10)(9)+oop(C10H)(5)]
1522	1498	1500	1493	1466	R1[δ_{in}(CH)(60)+ν(CC)(37)]
1483	1460	1465	-	1461	[δ_a(74)+δ'_a(13)](CH_3)
1482	1459	1461	-	1452	R1[δ_{in}(CH)(62)+ν(CC)(32)]
1479	1456	1461	1454	-	[δ_a(88)+ρ'(7)](CH_3)
1451	1429	1430	1436	1429	R3[$\delta_{sci}(CH_2)$](93)
1419	1398	1400	1398	1397	$\delta_s(CH_3)$(85)+R3[ν(C14C16)(6)]
1401	1381	1379	1382	1386	R3[ν(N6C12)(24)+ν(C12C17)(15)+δ'_a(5)]+$\delta_s(CH_3)$(7) +R2[oop(C10H)(7)]+δ(CHO)(6)
1377	1358	1362	1363	1363	[ω(23)+δ(13)+γ(11)+ρ(5)](C18NH33)+R1[δ_{in}(CH)(19) +ν(C18C19)(6)]
1366	1348	1350	-	-	R2[oop(C10H)(37)]+δ(CHO)(5)+δ(C18NH33)(6)+ν(C15C18)(5) +$\gamma(NH_2)$(6)
1351	1333	1333	-	-	$\rho(NH_2)$(14)+[δ(8)+ω(12)](C18NH33)+R1[δ_{in}(CH)](14)
1347	1329	1324	1317	-	R1[ν(CC)(48)+δ_{in}(CH)(53)]+δ(C18NH33)(5)
1336	1318	1313	-	1314	R2[oop(C10H)(15)+ν(N6C11)(12)+ρ(C9H)(7)]+R3[ν(N6C12)](12) +δ(CHO)(7)
1313	1296	1306	-	-	R1[ν(CC)(49)+δ_{in}(CH)(10)]+ δ(C18NH33)(20)
1303	1287	1282	-	1286	R3[ω(CH2)(49)+ν(CC)(18)+δ_{trig}(5)]+δ(CHO)(6)
1292	1276	1280	1275	1276	R2[ρ(54)+ρ'(15)](CH)
1260	1245	1249	1246	1245	R2[ρ'(CH)(44)+δ(C11H26)(17)+ν(CC)(9)]+R3[$\omega(CH_2)$(6)]
1243	1229	1236	-	1227	ν(N7C15)(28)+ρ(N7H)(21)+R2[ν(N7C10)](16)+ρ(C15=O)(9) +ν(C15C18)(6)
1231	1217	1210	-	1212	[γ(23)+ ω(22)+ ρ(8)](NH_2)+R1[ν(CC)](23)
1215	1202	1202	-	-	R3[ω(20)+γ(8)(CH2)+ν(C14C16)(11)+δ_{trig}(6)]+R2[+ρ(C9H)(8) +δ(C11H26)(8)]

1207	1193	1192	1194	1196	R3[γ(CH_2)](62)+R2[δ(C11H26)](17)
1199	1186	1191	-	-	R1[δ_{in}(CH)(68)+ν(CC)(15)]+ρ(NH_2)(5)
1194	1181	1179	-	1183	δ(CHO)(18)+ν(CO)(11)+ρ(CH3)(10)+R2[ν(N6C9)(6)
1189	1176	1172	-	1173	R2[ν(N7C10)(20)+ρ(C9H)](6)]+ρ(NH_2)(12)+δ(C18NH33)(6)
1182	1170	1170	1176	1169	R1[δ_{in}(CH)(74)+ν(CC)(7)]
1173	1162	1155	-		ρ(NH_2)(16)+R1[ν(C18C19)(13)+δ_{trig}(6)]+ R2[ν(N7C10)](9)
1164	1152	1138	1157	1156	R2[δ(C11H26)(16)+ρ'(C9H)(11)+ν(C9C10)(7)]+ν(CO)(16) +δ(CHO)(15)
1123	1112	1122	-	1117	R2[ν(N6C9)(30)+δ(C11H26)(13)+ν(CO)(11)+ν(N6C11)(9) +ρ(C9H)](9)]
1111	1101	1095	-	-	ν(N8C18)(30)+R1[ν(CC)(22)+δ_{in}(CH)(23)+δ(C20C18)(5)]
1086	1076	1062	1077	1077	R1[ν(CC)(20)+δ_{in}(CH)(16)]+ν(N8C18)(36)
1066	1056	1055	1063	1058	R3[ν(CC)(20)+ν(N6C12)(8)]+R2[ν(N6C11)(14)+δ(N6O)(12) +ν(CC)(13)]
1050	1041	1038	1043	1045	ρ(CH_3)(35)+ν(CO)(12)+ρ'(CH_3)(5)+ R2[ν(N6C9)](11)
1047	1038	1037	-	1039	R1[ν(CC)(54)+δ_{trig}(14)+δ_{in}(CH)(18)]
1042	1033	1035	1031	1027	[ρ'(57)+δ_a(5)](CH_3)+R3[oop(C14C16)(6)+puck(5)]
1017	1009	1009	-	1013	R1[δ_{trig}(61)+ν(CC)(35)]
1009	1001	996	997	1000	R1[oop(CH)(82)+puck(14)]
994	986	984	-	-	R2[oop(C10H)(15)+oop(N7C10)(15)]+δ(N7H)(11)+ρ(C15=O)(7)
993	985	978	981	983	R1[oop(CH)(87)+(τ'_a)(7)]
961	954	956	950	951	R3[ν(CC)(25)+δ_{trig}(6)+ν(C12C17)(5)]+R2[ν(CC)(8)+ρ(CH_3)(14) +ν(CO)(5)
943	937	941	933	-	R1[oop(CH)(68)+puck(5)+τ(5)]+oop(C18C19)(5)
928	922	925	925	923	R2[ν(CC)(30)+δ(N7C11)(6)+δ_{ring}(5)]+R1[oop(CH)(7)]+R3[ν(SC9)(8) +ν(C15C18)
904	899	906	914		ω(NH_2)(44)+ρ(C18N8H33)(15)+ω(C15=O)(9)+ν(N8C18)(8)
893	888	872	888	888	R2[ν(CC)(10)+δ_{ring}(7)]+ω(NH_2)(6)+R3[ν(C14C16)(7)] +ν(C15C18)(16)
867	863	863	863		R3[ρ(CH_2)(59)+puck(17)+oop(C14C16)(6)]+ρ'(CH_3)(6)
863	858	849	852	859	R1[oop(CH)(98)]
829	825	829	822	823	R2[δ_{ring}(13)+ν(C10C11)(8)]+R1[ν(C18C19)(8)+ν(C19C21)(4)] +ω(NH_2)(8)
821	817	819	-	819	R2[δ_{ring}](11)+R1[ν(C18C19)(6)]+ω(NH_2)(23)+ω(C15=O)(7)
797	793	788	795	795	R1[puck(15)+oop(CH)(10)+oop(C18C19)(9)]+ρ(C15=O)(5) +δ(C17=O)(11)
786	783	780	788	766	ω(C17=O)(31)+R3[oop(C17C12)(13)+puck(10)]
760.5	758	755	760	755	R3[ν(SC13)(38)+ν(C14C16)(6)+δ_{trig}(5)]
755	752	747	-	-	R1[puck(23)+oop(CH)(35)+oop(C18C19)(5)]+ω(C15=O)(11)
745	742	736	739	740	R3[ν(SC13)(15)+ν(SC9)(13)+δ(7)]+R2[δ_{ring}](8)
716	713	708	725	709	R1[oop(CH)(31)+puck(9)+oop(C18C19)(6)]
705	704	700	-		R2[δ(N7C11)(15)+δ(N6O)(12)+oop(C=O)(9)]+R3[δ_{trig}(5) +ν(SC13)(5) +ν(SC9)(5)]
695	693	688	694	693	ρ(C17=O)(37)+δ(CHO)(7)+R3[δ_{trig}(8)+puck(6)+ν(C12C17)6)] +ν(CO)(6)
642	641	663	668	-	R1[δ(38)+δ'_a(12)]+γ(C18NH33)(7)+[ρ(6)+ρ'(5)](C15=O) +ν(C15C18)(6)
632	631	647			R1[δ'_a(71)+δ(6)]
631	630	639	629	-	R3[oop(C12C17)(12)+puck(11)+τ(C6C9)(9)+τ'_a(8)] +R2[oop(C11=O)](5) +τ(O4C17](21)
607	606	626	609	604	R2[oop(C11=O)](11)+R3[ν(SC9)(11)+puck](10)+oop(C12C17)](5)] +τ(CO)(12)
575	575	605	587	577	τ(N7C15)(30)+ω(N7H)(15)+τ(N7C10)(7)
551	551	584	-	-	R1[τ(23)+R1[oop(C18C19)(13)+puck(12)+oop(CH)(7)] +δ(C18NH33)(9)
548	548	562	-	-	R3[puck(13)]+τ(CO)(21)+τ(C6C9)(13)
522	522	527	521	523	R3[ν(SC9)(7)+R2[δ(N7C11)(6)+oop(N7C10)(5)]+ω(N7H)(13)

					+δ(C15=O)(7)
502	502	515	505	506	R3[δ_{trig}(8)+ν(C12C17)(7)]+ρ(C17=O)(18)+δ(C15=O)(9)+ω(N7H)(8)
491	491	499	495	491	R3[δ(9)+puck(9)+oop(C14C16)(13)]+ω(N7H)(5)+τ(N7C15)(5) +δ(C15=O)(8)
455	456	482	456	456	R3[oop(C14C16)(21)+τ'_a(11)+δ_{trig}(7)+puck(6)+ν(SC9)(5)]+R1[τ_a](5)
450	450	448	449	411	R1[τ_a](14)+R3[oop(C14C16)](8)+τ'_a(5)] +τ(C6C9)(12)
416	417	414	-	-	R1[τ'_a(83)+oop(CH)(16)]
413	414	408	410	408	R3[puck(19)+δ(16)+δ'_a(8)]+ρ'(C17=0)(15)+τ(C6C9)(13)
389	390	388		382	R1[δ(9)+ν(C18C19)(9)]+ρ'(C15=O)(8)+R2[oop(N7C10)](7)
368	369	364		-	R3[oop(C14C16)(59)+ν(SC13)(7)+τ(6)]+τ(C6C9)(8)
357	358	349		363	R1[τ_a](10)+[γ(23)+ω(8)](C18NH33)+τ(N8C18)(20)+ρ'(C15=O)(5)
323	325	301			R1[τ_a](13)+R3[τ(7)+oop(C14C16)(6)]+τ(C6C9)(13)+ρ'(C15=O)(7)
304	306	295		309	R3[τ(16)+oop(C14C16)(25)+oop(C12C17)(12)+τ(C6C9)(14)
297	298	288		295	R3[δ'_a(11)+δ(6)]+R1[τ_a](5)+τ(N8C18)(41)
289	290	271			R3[δ'_a(19)+δ(16)+ R2[δ(N6O)](5)+τ(N8C18)(17)
245	246	252			R1[τ_a(22)]+R3[δ'_a(7)+ρ'(C17=O)(6)+δ(C18NH33)(9)
242	243	242			R1[δ(C18C20)](10)+R2[δ(N7C11)(18)
209	210	213		203	R1[δ(C18C20)](36)+R2[δ(N7C11)](6)+ρ(C18NH33)(21)
198	199	184		199	R2[oop(N7C10)(9)+ν(C9C10)(7)+oop(C10H)(6)]+R3[puck](8) +δ(N7H)(19)
177	178	175		175	R3[puck(14)+τ(7)]+R1[τ_a](9)+ρ'(C15=O)(6)+τ(C6C9)(15) +τ(C14C16)(14)
148	149	151			R3[τ(29)+puck(29)]+τ(C14C16)(6)
134	134	126			R3[τ(13)+δ(C14C17)(7)+τ'_a(6)]+R2[oop(N7C10)](7)+τ(C14C16)(30)
122	122	119			R3[puck(14)+δ(C14C17)(11)+τ(9)+τ'_a(8)]+R2[puck(8)]+τ(C14C16)(22)
117	118	115			R3[τ(37)+oop(C12C17)(6)]+R2[puck](12) +τ(C6C9)(30)
80	81	94			R3[τ'_a(22)+δ(C14C17)(5)]+R2[puck](6)+τ(C12C17)(18)+τ(C6C9)(7)
74	75	76		72	R3[τ'_a(23)+τ(10)]+τ(C6C9)(8)+τ(C14C16)(8)+τ(C12C17)(24)
62	62	65			τ(C15C18)(18)+τ(C12C17)(14)+δ(C18NH33)(10)+τ(C18C19)(9) +τ(C6C9)(7)
51	52	51	-		τ(C15C18)(28)+R3[τ_a](17)+τ(C12C17)(10)+τ(C6C9)(9)+τ(N7C10)(6)
42	42	34			τ(C18C19)(23)+R3[τ_a](13)+τ(C15C18)(12)+τ(N7C10)(11)+ω(N7H)(7)
25	26	26	-		τ(C18C19)(24)+R3[τ_a](17) +τ(C6C9)(13) +ω(N7H)(7) +R2[oop(N7C10)](6)
25	25	25			τ(C6C9)(21)+R2[oop(N7C10)(19)+oop(C10H)(9)+puck(6)]+τ_a](6) +ω(N7H)(7)
15	15	15	-		τ(N7C10)(40)+τ(C15C18)(29)

Table 29: Topological parameters of interacting bond and ring elements of methyldopa monomer.

BCP and RCP	ρ_{BCP} (a.u)	$\nabla^2\rho_{BCP}$ (a.u.)	V (a.u.)	G (a.u.)	H (a.u.)	$\lvert V\rvert/G$	ε
C10-C6	0.2461	−0.5730	−0.2566	0.0567	−0.1999	4.5256	0.0630
C6-N5	0.2633	−0.6667	−0.3705	0.1019	−0.2686	3.6359	0.0455
C7-C6	0.2288	−0.4787	−0.2248	0.0526	−0.1722	4.2738	0.0364
C13-C11	0.3130	−0.8859	−0.4304	0.1045	−0.3259	4.1187	0.2547
(C8-C11-C13-C15-C14-C12)	0.0211	0.1545	−0.0237	0.0312	0.0075	0.7596	-
C8-C7	0.2492	−0.5834	−0.2610	0.0576	−0.2034	4.5313	0.0349
C9-C6	0.2438	−0.5558	−0.2505	0.0558	−0.1947	4.4892	0.0199
O1-C10	0.2978	−0.4659	−0.7428	0.3132	−0.4296	2.3716	0.0449

O2-C10	0.4155	−0.1797	−1.3668	0.6609	−0.7059	2.0681	0.0678
C13-C15	0.3118	−0.8802	−0.4130	0.0965	−0.3165	4.2798	0.2925
C11-C8	0.3035	−0.8238	−0.4038	0.0989	−0.3049	4.0829	0.2176
C15-C14	0.3122	−0.8726	−0.4324	0.1071	−0.3253	4.0373	0.2687
C8-C12	0.3065	−0.8397	−0.4106	0.1004	−0.3102	4.0896	0.2243
O3-C11	0.2856	−0.3873	−0.7133	0.3083	−0.405	2.3137	0.0202
C14-C12	0.3049	−0.8356	−0.4092	0.1002	−0.309	4.0838	0.2174
O4-C15	0.2724	−0.3211	−0.6763	0.2980	−0.3783	2.2695	0.0249
C7-H16	0.2772	−0.9276	−0.3145	0.0413	−0.2732	7.6150	0.0096
C7-H17	0.2767	−0.9231	−0.3144	0.0418	−0.2726	7.5215	0.0073
C9-H18	0.2747	−0.9134	−0.3131	0.0424	−0.2707	7.3844	0.0086
C9-H19	0.2732	−0.9024	−0.3125	0.0434	−0.2691	7.2005	0.0090
H20-C9	0.2776	−0.9322	−0.3162	0.0416	−0.2746	7.6010	0.0077
H21-N5	0.3368	−1.5173	−0.4970	0.0588	−0.4382	8.4524	0.0457
N5-H22	0.3363	−1.4753	−0.4907	0.0609	−0.4298	8.0575	0.0496
H23-C11	0.2810	−0.9625	−0.3167	0.0380	−0.2787	8.3342	0.0233
C12-H24	0.2807	−0.9590	−0.3196	0.0399	−0.2797	8.0100	0.0261
C14-H25	0.2774	−0.9387	−0.3159	0.0406	−0.2753	7.7808	0.0245
H26-O1	0.3577	−2.4968	−0.7571	0.0664	−0.6907	11.4021	0.0165
H27-O3	0.3624	−2.5456	−0.7732	0.0684	−0.7048	11.3041	0.0220
O4-H28	0.3651	−2.5395	−0.7760	0.0705	−0.7055	11.0071	0.0228
O2-H24	0.0067	0.0228	−0.0040	0.0049	0.0008	0.0020	0.4160

Table 30: Topological parameters of interacting bond and ring elements of methyldopa dimer.

BCP and RCP	ρ_{BCP} (a.u)	$\nabla^2\rho_{BCP}$ (a.u.)	V (a.u.)	G (a.u.)	H (a.u.)	$\lvert V\rvert/G$	ε
C6 -C10	0.2467	−0.5747	−0.2567	0.0565	−0.2002	4.5413	0.0862
O2-C10	0.0061	0.0245	−0.0038	0.0050	0.0012	0.7659	-
(C6-C7-							
C14-C12-							
C8-C12- H24)							
H20-C9	0.2760	−0.9224	−0.3139	0.0417	−0.2723	7.5347	0.0104
C6-N5	0.2687	−0.6957	−0.3817	0.1039	−0.2778	3.6738	0.0423
(N5-C6-C7-	0.0084	0.0345	−0.0052	0.0069	0.0017	0.7474	-
C8-C11-H21)							
C7-C6	0.2316	−0.4936	−0.2287	0.0527	−0.1761	4.3438	0.0155
(O2-H24-C12-	0.0003	0.0010	−0.0001	0.0002	0.0001	0.3902	-
C14-C15-H53-							
C42-C40-H52-							
O30-C38-C34							
C35-C36-O29-							
H54)							
(C8-C11-C13-	0.0213	0.1545	−0.0239	0.0313	0.0074	0.7647	-
C15-C14- C12)							
C13-C11	0.3105	−0.8743	−0.4233	0.1023	−0.3209	4.1358	0.2440
C8-C7	0.2483	−0.5790	−0.2596	0.0574	−0.2022	4.5217	0.0311
H18-C9	0.2752	−0.9170	−0.3122	0.0415	−0.2707	7.5302	0.0088
C6-C9	0.2371	−0.5232	−0.2401	0.0546	−0.1854	4.3944	0.0259
C10-O1	0.3202	−0.4386	−0.8516	0.3710	−0.4806	2.2956	0.0289
O2-C10	0.3970	−0.2585	−1.2546	0.5950	−0.6596	2.1086	0.0457
C9-H19	0.2733	−0.9043	−0.3118	0.0429	−0.2689	7.2741	0.0103
C13-C15	0.3130	−0.8810	−0.4185	0.0991	−0.3194	4.2220	0.3130
C11-H21	0.0085	0.0315	−0.0049	0.0064	0.0015	0.7620	1.4396
C11-C8	0.3044	−0.8283	−0.4059	0.0994	−0.3065	4.0833	0.2167
H24-O2	0.0065	0.0232	−0.0040	0.0049	0.0009	0.8148	0.7206
C15-C14	0.3132	−0.8802	−0.4329	0.1064	−0.3265	4.0678	0.2665
H17-C7	0.2770	−0.9266	−0.3146	0.0415	−0.2731	7.5872	0.0075
C8-C12	0.3050	−0.8344	−0.4056	0.0985	−0.3071	4.1180	0.2118
O3-C13	0.2873	−0.3933	−0.7191	0.3104	−0.4087	2.3168	0.0095
C15-H53	0.0028	0.0084	−0.0012	0.0017	0.0004	0.7336	2.2702
C14-C12	0.3074	−0.8507	−0.4157	0.1015	−0.3142	4.0945	0.2108
O4-C15	0.2570	−0.3303	−0.6087	0.2631	−0.3457	2.3138	0.0248
H16-C7	0.2792	−0.9408	−0.3179	0.0414	−0.2766	7.6865	0.0076
H21-N5	0.3376	−1.5077	−0.4973	0.0602	−0.4371	8.2627	0.0464

N5-H22	0.3375	−1.5059	−0.4964	0.0600	−0.4365	8.2770	0.0459
H23-C11	0.2813	−0.9643	−0.3168	0.0379	−0.2790	8.3638	0.0246
C12-H24	0.2831	−0.9759	−0.3204	0.0382	−0.2822	8.3872	0.0241
C14-H25	0.2799	−0.9579	−0.3161	0.0383	−0.2778	8.2474	0.0188
O1-H26	0.3170	−2.1900	−0.6739	0.0632	−0.6107	10.6605	0.0122
(O1-C10-O2-H54-O29- C38-O30-H26)	0.0080	0.0323	−0.0061	0.0071	0.0010	0.8619	-
H27-O3	0.3617	−2.5356	−0.7711	0.0686	−0.7025	11.2402	0.0218
H28-O4	0.3617	−2.5163	−0.7681	0.0695	−0.6986	11.0483	0.0237
O2-H54	0.0445	0.1317	−0.0408	0.0369	−0.0040	1.1074	0.0247
H26-O30	0.0495	0.1397	−0.0474	0.0412	−0.0062	1.1517	0.0237
(O4-C15-H53-H56-C42-C43-O32-H56)	0.0025	0.0102	0.0102	0.0019	0.0121	5.2344	–
O4-H56	0.0230	0.0818	−0.0169	0.0187	0.0018	0.9044	0.0878
C38-C34	0.2465	−0.5742	−0.2581	0.0573	−0.2008	4.5048	0.0886
C38-O30	0.3961	−0.2604	−1.2495	0.5922	−0.6573	2.1099	0.0418
O30-C38-C34-(C35-C36-C40-H52)	0.0062	0.0248	−0.0036	0.0049	0.0013	0.7366	-
C37-H48	0.2764	−0.9248	−0.3143	0.0415	−0.2727	7.5663	0.0097
N33-C34	0.2701	−0.7042	−0.3860	0.1050	−0.2810	3.6772	0.0424
C34-C35	0.2299	−0.4854	−0.2268	0.0527	−0.1741	4.3013	0.0148
(C36-C39-C41-C43-C42-C40)	0.0212	0.1541	−0.0238	0.0312	0.0074	0.7641	-
C41-C39	0.3122	−0.8809	−0.4276	0.1037	−0.3239	4.1240	0.2549
C36-C35	0.2483	−0.5779	−0.2594	0.0575	−0.2019	4.5147	0.0356
C37-H46	0.2754	−0.9185	−0.3126	0.0415	−0.2711	7.5324	0.0085
C34-C37	0.2377	−0.5264	−0.2408	0.0546	−0.1862	4.4102	0.0278
O29-C38	0.3190	−0.4341	−0.8476	0.3695	−0.4781	2.2937	0.0334
H47-C37	0.2727	−0.9006	−0.3116	0.0432	−0.2684	7.2109	0.0102
C43-C41	0.3115	−0.8781	−0.4122	0.0964	−0.3159	4.2780	0.2928
C39-C36	0.3029	−0.8205	−0.8205	0.0986	−0.7219	8.3222	0.2191
H52-O30	0.0067	0.0227	−0.0040	0.0048	0.0009	0.8232	0.6904
C43-C42	0.3120	0.3120	−0.4301	0.1060	−0.3241	4.0588	0.2630
C35-H45	0.2771	−0.9274	−0.3148	0.0415	−0.2733	7.5893	0.0075
C40-C36	0.3054	−0.8339	−0.4082	0.0998	−0.3083	4.0880	0.2223
O31-C41	0.2850	−0.3864	−0.7113	0.3074	−0.4040	2.3143	0.0176
C42-C40	0.3056	−0.8399	−0.4106	0.1003	−0.3103	4.0930	0.2136
O32-C43	0.2753	−0.3554	−0.6780	0.2946	−0.3834	2.3017	0.0270

C35-H44	0.2786	−0.9364	−0.3168	0.0414	−0.2755	7.6589	0.0073
H49-N33	0.3375	−1.5169	−0.4985	0.0596	−0.4389	8.3581	0.0467
H50-N33	0.3374	−1.4968	−0.4951	0.0605	−0.4346	8.1895	0.0468
C39-H51	0.2806	−0.9595	−0.3166	0.0384	−0.2782	8.2523	0.3166
C40-H52	0.2820	−0.9673	−0.3204	0.0393	−0.2811	8.1571	0.0255
H53-C42	0.2791	−0.9500	−0.3169	0.0397	−0.2772	7.9843	0.0225
H54-O29	0.3218	−2.2394	−0.6846	0.0624	−0.6222	10.9764	0.0122
H55-O31	0.3617	−2.5382	−0.7716	0.0685	−0.7031	11.2593	0.0220
H56-O32	0.3527	−2.4829	−0.7549	0.0671	−0.6878	11.2535	0.0213

Table 31: Potential energy distributution (PED) associated with vibrational frequency methyldopa

Unscaled	scaled	PED distribution perecent
3843.54	3636.18	ν(O4H28)(100)
3783.94	3583.47	ν(O3H27)(100)
3745.78	3549.67	ν(O1H26)(100)
3581.83	3403.87	ν_a(NH2)(100)
3499.95	3330.73	ν_s(NH2)(100)
3211.32	3071.16	R[ν(CH)](95)
3205.60	3065.99	R[ν(CH)](98)
3166.28	3030.41	R[ν(CH)](96)
3149.67	3015.37	ν(C9H20)(99)
3124.50	2992.55	ν_a(CH_2)(98)
3122.36	2990.61	ν_a(CH_3)(99)
3069.80	2942.90	ν_s(CH_2)(98)
3049.12	2924.10	ν_s(CH_3)(99)
1820.59	1782.40	ν (C=O)(80)+δ_{in}(C10H26)(6)
1676.08	1644.87	R[ν(CC)(45)+δ_a(10)]
1674.06	1642.94	δ_{in}(NH_2)(87)
1656.47	1626.16	R[ν(CC)(65)+δ'_a(9)]
1561.47	1535.31	R[ν(CC)(36)+δ_{in}(CH)(36)+ν(C15O)(9)+ν(C13O)(6)]
1514.41	1490.20	[δ_a(45)+δ'_a(20)+ρ(5)](CH_3)
1510.07	1486.04	[δ_a(18)+δ'_a(6)](CH_3)+R[δ_{in}(C12H)(11)+ν(CC)](30)]+δ(O3H)(11)
1502.99	1479.24	[δ'_a(57)+δ_a(23)+ρ'(6)](CH3)+δ(CH_2)(9)
1487.79	1464.65	δ(CH_2)(85)+δ'_a(CH3)(6)
1413.67	1393.39	δ(CH3)(87)
1403.66	1383.76	R[ν(CC)(60)]+δ(O3H)(9)+ δ(CH_2)(10)
1369.85	1351.18	ω(CH_2)(40)+ρ(NH_2)(10)+ν(C6C9)(6)+δ(C8C6C7)(6)
1365.08	1346.58	δ(C8C6C7)(10)+δ(O4H)(9)+ν(C10O)(8)+R[δ_{in}(CH)(15)]+ν(C6C10)(7)
1359.85	1341.54	δ(O3H)(16)+R[δ_{in}(CH)](19)+δ(O4H)(8)+δ(C8C6C7)(8)+ν(C10O)(6)+ω(CH2)(6)
1328.81	1311.59	R[ν(CC)(33)+ δ_{in}(CH)(7)+ν(C7C8)(6)+ ν(C13O)(21)+ν(C15O)(6)]+ ρ(NH_2)(8)
1322.28	1305.28	ρ(NH_2)(28)+ω(CH_2)(19)+δ(C6C9N)(8)+δ'(CH_3)(6)
1298.31	1282.13	R[ν(C15O)(17)+δ_{trig}(15)+δ_{in}(C12H)(17)+ν(C13O)(12)]+[γ(9)+ω(7)](CH_2)+ δ(O3H)(8)
1274.93	1259.53	γ(CH_2)(24)+ν (N5C6)(15)
1227.59	1213.71	δ(C8C6C7)(10)+ν (N5C6)(10)+ν(C6C7)(9)+ν (C6C9)(8)+ω(CH_2)(7)+ρ(NH_2)(6)
1219.71	1206.07	δ(O3H)(30)+R[ν(CC)(16)+δ_{in}(CH)(14)+ν(C15O)(6)]+δ(O4H)(5)
1187.41	1174.76	δ(O4H)(22)+R[δ_{in}(CH)(22)+ν(C8C12)(8)]+ν(C7C8)(18)
1174.20	1161.94	R[δ_{in}(CH)(36)+ν(CC)(19)]+δ(O4H)(13)+ν(C7C8)(9)
1168.26	1156.18	δ(C8C6C7)(23)+ν(C10O)(22)+γ(CH2)(14)+ν(N5C6)(8)
1139.13	1127.89	δ(O4H)(15)+ν(C10O)(11) -R[δ_{in}(CH)(10)+δ_{trig}(8)+ν(C15O)(7)]+ρ(CH_3)(8)
1120.54	1109.82	ρ(CH_3)(21)+ν(C10O)(11)+γ(CH_2)(9)+δ(O4H)(6)+ν(C8C11)(6)+R[δ_{trig}](6)
1049.63	1040.80	ν(C6C9)(25)+ρ'(CH_3)(22)+δ(NH2)(19)
992.71	985.28	ρ'(CH_3)(15)+ν(C6C7)(12)+ν(C6C9)(11)+R[ν(CC)](7)+ν(C7C8)(6)+ω(NH_2)(6)
988.81	981.48	ρ(CH_2)(26)+ρ'(CH_3)(17)+ρ(CH_3)(11)+R[δ_{trig}](6)
945.22	938.88	ω(NH_2)(17)+ρ(CH_2)(13)+ρ(CH3)(10)+ν(C6C9)(8)+R[ν(C8C12)(7)+δ_{trig}(7)]
924.38	918.49	R[oop(CH)(74)+τ'_a](6)
911.56	905.95	R[oop(CH)](35)+puck(6)]+ω(NH2)(20)+ν(C6C7)(12)
879.37	874.42	R[oop(CH)](36)+ω(NH_2)(26)+ν(N5C6)(14)
868.64	863.90	ν (N5C6)(18)+ρ(CH_2)(16)+R[oop(CH)](14)+ν(C6C7)(12)+ν(C6C10)(9)+ ρ(CH3)(6)
813.71	810.00	R[oop(CH)](67)+R[τ_a](8)
799.84	796.37	R[ν(C15O)(23)+ν(CC)(28)+δ_{trig}(9)+δ_a(7)]
783.91	780.71	oop(C10O)(38)+τ(C10O)(13)+ν(C6C9)(11)+R[oop(C14H)](6)
760.38	757.57	R[δ_{trig}(16)+δ'_a(10)+ν(C7C8)(10)+puck(6)]+oop(C10O)(10)
737.43	734.98	ν(C6C10)(19)+δ_{in}(C10O)(14)+R[puck(13)+oop(C8C7)(7)]+ν(C10O)(9)
699.93	698.03	R[puck(56)+oop(C13O)(14)+oop(C15O)(14)+oop(C8C7)(5)]
656.53	655.22	τ(C10O)(28)+R[oop(C13O)(16)+τ_a(10)+oop(C15O)(10)+oop(C8C7)(6)]
630.29	629.30	τ(C10O)(26)+R[τ_a(18)+oop(C13O)(13)+oop(C8C7)(13)+oop(C15O)(8)]

596.02	595.41	R[$\delta' a$](38)+δ_{in}(C15O)(21)+ν(CC)(9)+δ_{in}(C13O)(6)+ν(C13O)(6)]
568.84	568.51	δ_{in}(C10O)(22)+δ_a(C6C9N)(12)+ν(C6C10)(9)+δ(C6C10O)(9)+R[δ_a](6)+ $\rho'(CH_3)$(6)
552.08	551.91	R[δ_a(12)+puck(9)+δ_{in}(C13O)(8)+τ_a(7)]+ρ(C6C9N)(9)
526.41	526.47	(C6C10O)(17)+δ(C6C9N)(14)+δ_{in}(C10O)(12)+δ'_a(C6C9N)(10)+R[puck(8)]
471.29	471.77	R[τ'_a(14)+δ'_a(13)+δ_a(11)+δ_{in}(C13O)(10)+δ_{in}(C8C7)(8)+δ_{in}(C15O)(7)]
461.79	462.33	R[τ'_a(32)+oop(C15O)(17)+oop(C13O)(17)+τ_a(11)+τ(C13O)(6)]
433.05	433.76	R[τ(C13O)(65)+τ'_a(11)+oop(C15O)(11)+τ_a(7)]
423.15	423.91	[δ_a(27)+δ(13)+ ρ(8)](C6C9N)+R[δ_a](12)
382.40	383.34	ρ(C6C9N)(25)+τ(C6C7)(10)+δ_a(C6C9N)(8) +[δ_{in}(C8C7)(8)]+$\rho(CH_2)$(7)
364.17	365.18	R[oop(C15O)(26)+τ'_a(11)+δ_a(C6C9N)(10)]
330.74	331.83	τ(C6N)(70)+δ(C6C9N)(7)
312.80	313.93	R[δ_{in}(C15O)(40)+δ_{in}(C13O)(23)]
302.27	303.41	R[δ_{in}(C13O)(14)]+δ_{in}(C8C7)(14)+τ(C6N)(12)+δ(C6C9N)(9)+δ(C6C10O)(9)+ δ_{in}(C10O)(8)
289.10	290.25	ρ'(C6C9N)(17)+[δ_a+$\delta' a$](C6C9N)(10)+ν(C7C8)(7)+δ(C6C10O)(6)
254.13	255.29	R[τ'_a(20)+puck(11)+oop(C15O)(6)]+ρ(C6C9N)(9)+τ(C15O)(8)+δ(C8C6C7)(6)
248.71	249.87	τ(C6C9)(66)+ρ'(C6C9N)(7)+δ'_a(C6C9N)(6)
237.94	239.09	δ'_a(C6C9N)(37)+τ(C6C9)(13)+ρ'(CH3)(12)+δ(C6C10O)(9)
214.19	215.31	R[τ(C15O)(62)+τ(C13O)(8)+ρ(C6C9N)(6)
193.70	194.77	R[τ(C15O)(20)+τ_a(13)+ puck(6)+τ'_a(11)]+ρ(C6C9N)(8)+δ_{in}(C8C7)(8)
155.07	156.03	R[τ_a](39)+$\rho'(CH_3)$(15)+δ(C8C6C7)(9)+δ_{in}(C8C7)(6)
75.69	76.26	τ(C6C7)(26)+oop(C8C7)(17)+δ(C8C6C7)(12)+τ(C7C8)(10)+R[τ_a](9)
69.86	70.39	τ(C6C7)(18)+τ(C7C8)(16)+R[τ_a](14)+τ(C6C10)(13)+oop(C8C7)(12)+ δ(C8C6C7)(11)
38.37	38.68	τ(C7C8)(56)+τ(C6C10)(16)+τ(C6C7)(10)
25.67	25.88	τ(C6C10)(51)+τ(C6C7)(14)+δ(C6C9N)(7)+oop(C10O)(6)

A2. Articles published in peer-reviewed international journals

- Chaudhary, T., Chaudhary, M. K., Joshi, B. D., de Santana, M. S. A., and Ayala, A. P. (2021). Spectroscopic (FT-IR, Raman) analysis and computational study on conformational geometry, AIM and biological activity of cephalexin from DFT and molecular docking approach. *Journal of Molecular Structure*, *1240*, 130594.

- Chaudhary, T., Karthick, T., Chaudhary, M. K., Tandon, P., and Joshi, B. D. (2023). Computational evaluation on molecular stability and binding affinity of methyldopa against Lysine-specific demethylase 4D Enzyme through quantum chemical computations and molecular docking analysis. *Journal of Molecular Structure*, *1286*, 135518.

- Chaudhary, T., Chaudhary, M. K., Jain, S., Tandon, P., and Joshi, B. D. (2023). The experimental and theoretical spectroscopic elucidation of molecular structure, electronic properties, thermal analysis, biological evaluation, and molecular docking studies of isococculidine. *Journal of Molecular Liquids*, *391*, 123212.

A3. Articles published in peer-reviewed national journals

- Chaudhary, T., and Joshi, B. D. (2022). Electronic, Thermodynamic Properties, Nonlinear Optical Responses, and Molecular Docking Studies on Cephalexin. *Journal of Institute of Science and Technology*, *27*(1), 83-92.

- Chaudhary, T., Chaudhary, M. K., and Joshi, B. D. (2022). A Theoretical Study on Charge Transfer and Hyperpolarizability of (S)-2-amino-3-(3, 4-dihydroxyphenyl)-2-methyl-propanoic Acid. *Journal of Nepal Physical Society*, *8*(1), 16-21.

- Chaudhary, T., Chaudhary, M. K., and Joshi, B. D. (2021). Topological and reactivity descriptor of carisoprodol from DFT and molecular docking approach. *Journal of Institute of Science and Technology*, *26*(1), 74-82.

- Chaudhary, M. K., Chaudhary, T., and Joshi, B. D. (2021). Simulated spectra (IR and Raman), NLO, AIM and molecular docking of carisoprodol from DFT approach. *BIBECHANA*, *18*(1), 48-57.

A4. Participation in international and national conferences, seminars and workshops

- " Fifth international Conference on Internationl Approaches in Applied Sciences and Technologies, jointly organized by Scientific Educational Research Society, Meerut 250004 (U.P.) and BabasahebBhimrao Ambedkar University (A Central University) (U.P.) India", 03-05 December 2021
  Oral presentation: "Spectroscopic and quantum chemical studies on cephalexin."

- " International Conference on Frontiers of Physics (ICFP)-2022, organized by Nepal Physical Society, January 22-24 2022.
  Oral presentation: Topology (ELF, LOL) analysis, chemical activity and hyperpolarizability study of aldomet: Antihypertensive drug."

- "ANPA conference-2021" organized by ANPA, 16-17 July 2020.
  Oral presentation: "Spectroscopic and quantum chemical studies on cephalexin."

- "International conference on Material Science and Characterisation Technology (ICMSCT)." organized by Department of Physics, St. Xavier's College, Maitighar, Kathmandu, Nepal, September 26-28 2021.
  Oral presentation: "Spectroscopic and computational study of structural, chemical, AIM, and molecular docking analysis on cephalexin."

- "Scientific secession of NPS 37^{th} Annual Convention" organized by Nepal Physical Society, Febuary-6 2021.
  Oral presentation: "Structural, quantum mechanical and molecular dockig studies of carisoprodal."

- "Seminar on Research Methodology, Project selection and Scientific writing organized by: Nepal Physical Society Sudurpaschim Chapter(2076) Mahendranagar, Nepal,Chaitra 27-28, 2077
  Invited lecture: "Spectroscopy and quantum chemical methods."

- "Workshop on Computer Aided Drug Design using BIOVIA Discovery Studio" organized by Department of Physics, Deen Dayal Upadhyaya Gorakhpur University, Gorakhpur, India, 13-14 August 2020.

- "Indo-Brazilian e-Symposium on Solid-State Properties of Pharmaceuticals" or-

ganized by University of Lucknow, India and Federal University of Ceará, Brazil, 29-30 April 2020.

- " Conference on science and technology for prosperous fedaral Nepal," organized by Nepal Academy of science and technology (NAST), Khumaltar Lalitpur, 21-22 May 2018.

Journal of Molecular Structure 1240 (2021) 130594

Contents lists available at ScienceDirect

Journal of Molecular Structure

journal homepage: www.elsevier.com/locate/molstr

Spectroscopic (FT-IR, Raman) analysis and computational study on conformational geometry, AIM and biological activity of cephalexin from DFT and molecular docking approach

Tarun Chaudhary[a], Manoj Kumar Chaudhary[a,b], Bhawani Datt Joshi[c,*], Maria Silmara Alves de Santana[d], Alejandro Pedro Ayala[d]

[a] Central Department of Physics, Tribhuvan University, Kirtipur, Kathmandu, Nepal
[b] Department of Physics, University of Lucknow, Lucknow 226007, India
[c] Department of Physics, Tribhuvan University, Siddhanath Science Campus, Mahendranagar 10406, Nepal
[d] Departamento de Física, Universidade Federal do Ceará CP. 6030, Fortaleza, CE 60.455-900, Brazil

ARTICLE INFO

Article history:
Received 2 January 2021
Revised 26 April 2021
Accepted 28 April 2021
Available online 5 May 2021

Keywords:
Cephalexin
Vibrational spectroscopy
QTAIM
Chemical reactivity
Molecular docking

ABSTRACT

The spectroscopic properties, molecular stability in terms of conformational analysis, and biological activities of cephalexin have been studied by quantum mechanical methods from combined experimental and computational approaches. The entire calculation was performed using density functional theory (DFT) employing Becke's three-parameter hybrid functional B3LYP method with 6-311++G(d,p) basis set. The accumulation of charge in space around the title molecule has been presented in terms of electrostatic potential. The intra-molecular hydrogen bonding has been discussed in terms of IR and Raman spectra. The chemical reactivity has been scrutinized from the highest occupied molecular orbital energy (E_{HOMO}), the lowest unoccupied molecular orbital energy (E_{LUMO}) and their energy gap (ΔE_{L-H}). On the basis of optimized structure, natural bond orbital (NBO) analysis dealing with intra and inter-molecular charge delocalization between the bonding and antibonding of the molecular system was performed. Moreover, the nature and strength of intra-molecular hydrogen bonding were predicted from the quantum theory of atoms in molecule (QTAIM). Further, molecular docking simulation has been performed with Leukotriene A-4 hydrolase and matrix carbonic anhydrase II.

1. Introduction

Cephalexin, $C_{16}H_{17}N_3O_4S$, with IUPAC name [(6R,7R)-7-[(2R)-aminophenylacetyl]-3-methyl-8-oxo-5-thia-1-azo-bicyclo[4.2.0]oct-2-ene-2-carboxylic acid] is a first-generation cephalosporin consisting of a beta-lactam ring. It is generally used for the treatment of infections against the genitourinary system, skin and soft tissue, upper and lower respiratory tract, bones and joints and several other infections due to susceptible organisms [1]. Most of the gram-positive cocci including penicillinase-producing Staphylococci, *Corynebacterium diphtheriae* and also the gram-negative cocci mainly *Neisseria gonorrhoeae* and several gram-negative bacilli including *Escherichia coli, Proteus mirabilis*, Salmonellae, *Klebsiella pneumoniae*, Shigella and some strains of *Haemophilus influenza* are sensitive to cephalexin [2]. Cephalexin does not have any nephrotoxic effect, so it can be used for patients with renal failure [1].

The literature reflect some laboratory, clinical and spectroscopic studies on antibacterial, chemical, thermodynamic and biological activity of cephalexin and its derivatives [3–7]. Anacona and Rodriguez used the physicochemical and spectroscopic methods to characterize cephalexin and its metal complexes, investigated their antibacterial activities, and demonstrated that the metal complexes of Cu (II) and Zn (II) were more active than the cephalexin alone [4]. Shahabadi et al. studied the binding activity of a platinum (II) complex of cephalexin (CEX) with human serum albumin (HSA), in which the result showed that hydrogen bonds, Van der Waals forces and electrostatic forces were mainly responsible for the stability of platinum (II) complex-HSA [5]. In the interaction between cephalexin and calf thymus DNA, the drug interacted with the DNA helix by means of a minor groove binding mode [6]. Hamishehkar et al. observed conformational change of bovine serum albumin (BSA) due to the interaction [7]. Since the drug-protein interaction may result either in desired therapeutic or ad-

* Corresponding author.
E-mail address: bhawani.joshi@snsc.tu.edu.np (B.D. Joshi).

https://doi.org/10.1016/j.molstruc.2021.130594
0022-2860/

verse effects, it is necessary to explore the interactions of drugs with different human proteins [5–7]. In the literature, few studies had been conducted on cephalexin-protein interactions using various spectroscopic and molecular modeling techniques [5–7]. Further, some similar works had also been performed on the other cephalosporins like cefradoxil and cefradine [8,9].

Ganeshvar et al., using polarized function with a double zeta function, computed different properties of cephalexin [3]. On the other hand, to explain the weak interaction like hydrogen bonding, inclusion of diffused function is mandatory, for the heavy atoms, with B3LYP functional [10, 11]. So, the present work has been conducted using DFT/B3LYP/6-311++G(d,p) which contains both the diffused and the polarized function with the triple zeta function to provide a broad and deep understanding of the structural and spectroscopic properties including the biological activity of the title molecule along with the spectroscopic techniques (FT-IR and Raman). In addition to the former work, the present work deals with the detailed conformational study, Fukui function analysis, the quantum theory of atoms in molecule (QTAIM), biological activity with Leukotriene A-4 hydrolase and matrix carbonic anhydrase II and the comparison of optimized geometry with the related crystal structure [12]. The comparative study of all stable conformers have been performed. The potential energy distribution (PED) has been assigned to the calculated wavenumbers and chemical reactivity has been analyzed. Further, natural bond orbital (NBO) analysis has been performed to determine the stability of the molecule based on hyperconjugative interaction. The QTAIM study has been performed to understand the nature and strength of intra-molecular hydrogen bonding. Ultimately, for understanding the biological activity of the title molecule, the docking study has also been conducted.

2. Experimental details

The investigated compound, cephalexin, in the solid form of purity level more than 98% was purchased from the Merck & Co., multinational pharmaceutical company, USA. The spectra (Infrared and Raman) were recorded without making any further purification. The Bruker Vertex 70 FT-IR spectrometer having a spectral resolution of 4 cm^{-1} was used to record infrared spectra in the region 400-4000 cm^{-1}. The sample pellet was prepared using a hydraulic press from a mixture of KBr and cephalexin in 200:1. Further, baseline corrections were performed by using multi-tasking OPUS software. Raman spectra was recorded in the range 50-4000 cm^{-1} with the help of RAM II module using diode-pumped Nd:YAG laser at a laser power not greater than 100 mW. The excitation wavelength of radiation produced by the laser was 1064 nm.

3. Computational details

Gaussian 09 program [13] was used to perform the computational study on structural and spectroscopic properties of cephalexin with DFT [14] employing B3LYP functional [15–17]. The functional B3LYP consists of Becke's three parameters (local, non-local and Hartree-Fock) hybrid exchange functional with Lee-Yang-Parr correlation functional. The geometry optimization and vibrational frequency calculation were performed using 6-311++G(d,p) basis set [18]. The potential energy distribution (PED) was assigned to the calculated wavenumbers using GAR2PED software package [19]. GaussView 05 [20] was used to visualize optimized geometry, the highest occupied molecular orbital (HOMO) and the lowest unoccupied molecular orbital (LUMO) and the distribution of charges in MEP map. Further, the hyperconjugative interaction in the molecule, the natural bond orbital (NBO) analysis was performed by implementing NBO 3.0 program [21] included in Gauss 09 program. The electron density function was analyzed by the QTAIM method using AIMALL and AIM 2000 software [22,23]. Molecular docking study of the title molecule was performed by implementing AutoDock Vina [24] and visualization of active sites and non-covalent bonding interactions were done by using Discovery studio Visualizer software [25].

4. Results and discussion

4.1. Conformational studies

The same molecule at room temperature may exist in different positions [26]. So, to predict the possible stable conformers of the title molecule having 2D-chemical structure as shown in Fig. 1a, the optimization has been performed with B3LYP/6-311++G(d,p). To obtain the minimum energy structure of the title molecule one-dimensional potential energy surface (PES) scan has been performed across eight flexible bonds C19-C18, C18-C15, C15-C7, C7-C10, C12-C17, C17-C4, C14-C16, C18-C8 as shown in Fig. 1b. Further, on the basis of local and global minima in PES scan graph, the eight conformers of the title molecule have been observed on the basis of self-consistent field (SCF) energy. The structure obtained corresponding to global and local minima was again optimized at the same level of theory. Fig. S1 (Supplementary material) shows the relative energy variation across the flexible bonds along the bond axis at each 10° variation of dihedral angle in the range 0-360° corresponding to the dihedral angles τ_1, τ_2, τ_3, τ_4, τ_5, τ_6, τ_7 and τ_8. The optimized geometry of all eight conformers has been presented in Fig. S2 (Supplementary material).

The conformers having relative energy less than 0.56 kcal/mol (equivalent to kT) are only likely to exist at room temperature [9]. The ground state optimized energy of all possible conformers along with their relative energy (energy differences) have been presented in Table 1. Among the eight conformers, only conformers A and B (ground state optimized energies: −930983.638252 and −930983.102415 kcal/mol, respectively) have a relative energy less than 0.56 kcal/mol, whereas conformers C, D, E, F, G and H have a relative energy greater than 0.56 kcal/mol. Hence, only the conformers A and B can exist at room temperature. Further, the conformer A being in the global minimum energy state it is more stable than the conformer B. Therefore, further study has been carried out with these stable conformers A and B.

4.2. The Geometry optimization and AIM analysis

The optimized structure of conformers A and B with the related crystal structure have been overlapped using a least-square algorithm that measures the minimum deviations of corresponding non-hydrogen atoms. Also, on superimposition with the crystal structure, the root mean square deviation (rmsd = 0.80 Å) obtained for conformer A is lower than the root mean square deviation (rmsd = 2.16 Å) obtained for conformer B. Hence, the conformer A is matched well compared with the conformer B as shown in Fig. S3 (Supplementary material). For the comparative study, the optimized parameters: bond length, bond angle and dihedral angle of A and B conformers have been tabulated in Table S1 (Supplementary material). The optimized parameters of both the conformers are almost similar except some of them vary with a small value. The bond length N8-C18 in conformer B is elongated by 0.012Å than in conformer A. Similarly, the angles A(C10-N7-H27), A(C15-N7-H27), A(C18-N8-H35) and A(H34-N8-H35) differ by 1.955°, 2.391°, 1.862° and 1.847°, respectively. This confirms the intra-molecular hydrogen bonding H27…N8 in conformer B as shown in Fig. 2. Also, due to the blueshift in hydrogen bonding X-H…Y, the bond length X-H contracts instead of increasing [27]. Hence, the bond length N7-H27 (0.880Å) in crystal form is less than the calculated bond length

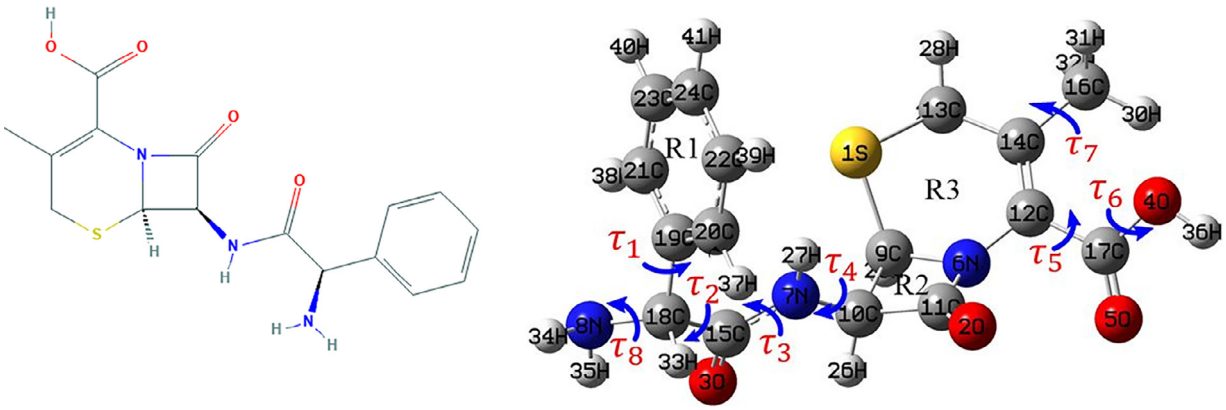

a. Chemical structure of cephalexin

b. Initial optimized structure of cephalexin with atom numbering scheme showing possible rotational bonds

Fig. 1. a. Chemical structure of cephalexin
b. Initial optimized structure of cephalexin with atom numbering scheme showing possible rotational bonds.

Table 1
Ground state optimized energy predicted at B3LYP/6-311++G(d,p) level and relative energy of all possible conformers.

Dihedral angles	Conformers	Energy (Hartree)	Energy (kcal/mol)	Relative Energy (ΔE) kcal/mol
τ_5(N6–C12–C17–O4)	A	−1483.6156	−930983.6383	0.0000
τ_2(N7–C15–C18–C19)	B	−1483.6148	−930983.1024	0.5358
τ_2(N7–C15–C18–C19)	C	−1483.6135	−930982.2996	1.3387
τ_7(C13–C14–C16–H32)	D	−1483.6130	−930982.0148	1.6235
τ_8(C19–C18–N8–H34)	E	−1483.6109	−930980.6598	2.9785
τ_6(C12–C17–O4–H36)	F	−1483.6057	−930977.3812	6.2570
τ_3(C10–N7–C15–O3)	G	−1483.6039	−930976.2796	7.3586
τ_4(C11–C10–N7–C15)	H	−1483.6038	−930976.2451	7.3931

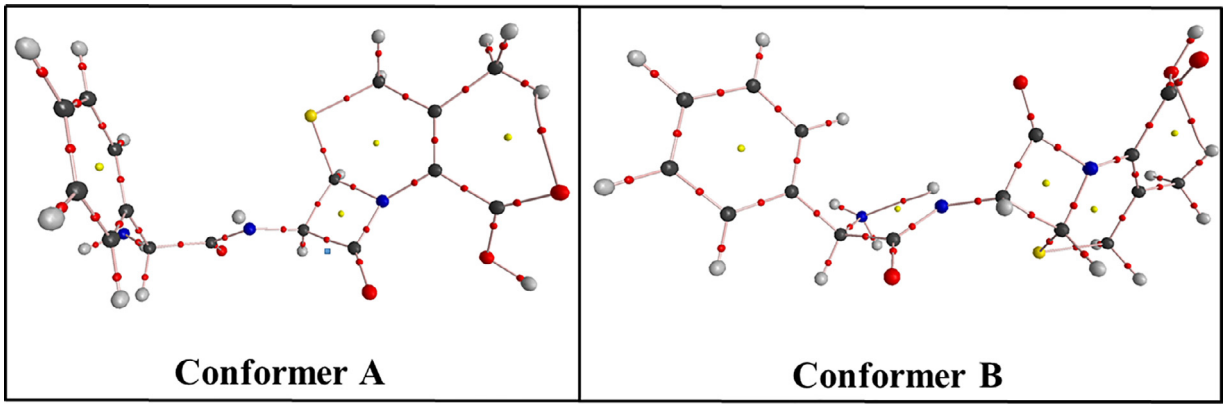

Fig. 2. Molecular graph of conformers A and B of cephalexin.

(1.010 Å) by 0.130 Å. This is also justified by a prominent peak in IR spectra explained in Section 4.3.2. As the X-rays diffraction is dependent on the atomic mass of an element, the bonds associated with the hydrogen atom generally suffer a low scattering effect [28]. Consequently, the experimental bond lengths C-H (0.949Å–1.001Å) are found to be lower than the calculated bond length C-H (1.083Å-1.096 Å). Further, the calculated and experimental torsional angles vary in sign due to either a mirror image or a conformational isomer [29]. Since, the study has been carried out by optimizing the molecule in an isolated gaseous state, there are still small discrepancies in some optimized parameters of crystal and optimized structure which is due to inter-molecular hydrogen bonding and crystal packing interaction in the crystal structure.

Further, to analyze structural changes of both conformers, due to possible intra-molecular interactions, quantum theory of atoms in molecule (QTAIM) [30] has been analyzed. QTAIM, which defines properly an atom as an open system, is used to explain numerous physical, chemical and biological processes [31,32]. It analyses the nature of intra and inter-molecular hydrogen bonding on the basis of electron density (ρ_{BCP}), Laplacian electron density ($\nabla^2\rho_{BCP}$) and total electron energy density (H_{BCP}) at bond critical point (BCP). The total electron energy density is expressed as the sum of kinetic (G_{BCP}) and potential energy density (V_{BCP}) [32]. According to Koch and Popelier, existence of hydrogen bonds is only possible if electron density and Laplacian of electron density at BCP are in the range 0.002–0.040 a.u. and 0.024–0.139 a.u., respectively [31]. Further, to explain the strength of hydrogen bond interaction, Roza

Table 2
Topological parameters for intra-molecular interaction in cephalexin are tabulated as follows.

Interactions	Bond Length(Å)	ρ_{BCP} (a.u.)	$\nabla^2\rho_{BCP}$ (a.u.)	G_{BCP} (a.u.)	V_{BCP} (a.u.)	H_{BCP} (a.u.)	E_{int} (kcal/mol)
Conformer A							
H30...O5	2.2983	0.0152	0.0559	−−0.0021	−−0.0098	−−0.0119	−−3.0748
Conformer B							
H30...04	2.3311	0.0215	0.0832	−−0.0029	−−0.0150	-0.0179	−−4.7094
H27...N8	2.1751	0.0215	0.0531	−−0.0019	−−0.0094	−−0.0113	−−2.9528

Table 3
Geometrical parameters (bond length (Å), bond angle (°) and the sum of van der Waal radii of interacting atoms ($r_H + r_A$) for intra-molecular hydrogen bonds of cephalexin are given below.

D-H...A	D-H (Å)	H...A (Å)	D-H...A (°)	($r_H + r_A$) (Å)
Conformer A				
C16-H30...O5	1.0862	2.2983	115.92052	2.72
Conformer B				
C16-H30...O4	1.0861	2.3311	113.4029	2.72
N7-H27...N8	1.0137	2.1751	108.8464	2.75

et al. [33] has categorized hydrogen bond interaction as weak hydrogen bond [if $(\nabla^2\rho_{BCP}) > 0$ and $(H_{BCP}) > 0$; electrostatic in nature], medium hydrogen bond [if $(\nabla^2\rho_{BCP}) > 0$ and $(H_{BCP}) < 0$; partially covalent in nature] and strong hydrogen bond [if $(\nabla^2\rho_{BCP}) < 0$ and $(H_{BCP}) < 0$; covalent in nature]. Also, if the sum of Van der Waals radii of interacting atoms ($r_H + r_A$) is greater than the distance between interacting atoms, the interactions are characterized by Van der Waals interaction.

The molecular graph of conformers A and B of the title molecule have been calculated using the AIM2000 program at B3LYP/6-311++G(d,p) level and is presented in Fig. 2. The topological and geometrical parameters of both conformers are illustrated in Tables 2 and 3, respectively. From the molecular graph, we observed only a single hydrogen bonding C16-H30...O5 in conformer A and two hydrogen bonding C16-H30...O4 and N7-H27...N8 in conformer B. These all observed interactions between proton and acceptor atom satisfy all the criteria to be considered as hydrogen bond interaction. Further, for each hydrogen bond of both conformers, $(\nabla^2\rho_{BCP}) > 0$ and $(H_{BCP}) < 0$. Therefore, according to the criteria of Roza et al., all hydrogen bonds are of medium type that is partially covalent in nature.

4.3. Vibrational assignment

The vibrational analysis of cephalexin has been performed by employing 6-311++G(d,p) basis sets combined with experimental IR and Raman spectra. A cephalexin molecule is a non-linear molecule with 41 atoms, so it has 117 (3N-6) fundamental modes of vibration. Complete potential energy distribution (PED) was assigned to every wavenumber using the GAR2PED software package. Due to the assumptions of simple harmonic vibrations in vibrational analysis, the calculated wavenumbers have usually higher value than the observed one. So, the calculated wavenumbers were scaled down using the WLS factor, $\nu_{observed} = (1.008700 - 0.0000163 \times \nu_{calculated})\nu_{calculated}$ given by Yoshida et al. [34]. Also, as the Raman intensity varies with the Raman Scattering cross-section [35,36], it is determined by evaluating Raman scattering amplitude and predicted wavenumbers. Finally, the potential energy distribution (PED) % assignment of all possible modes of vibration of conformers A and B have been presented in Table S2 (Supplementary material).

The calculated and observed vibrational wavenumbers of conformers A and B with potential energy distribution are presented in Table S2 (Supplementary material). The comparison of calculated and observed FT-IR and Raman spectra for both conformers is demonstrated in Fig. 3a and 3b, respectively. The linear fit between calculated and observed wavenumbers were obtained as $R^2 = 0.9997$, SD = 15.33/$R^2 = 0.9999$, SD = 7.82 for conformer A and $R^2 = 0.9995$, SD = 20.42/$R^2 = 0.9998$, SD = 10.77 for conformer B as shown in Fig. S4 (Supplementary material). The conformer A shows comparatively a good correlation and a minimum deviation value. Hence, the further vibrational study has been mainly focused on the conformer A.

4.3.1. O-H and CHO vibration

The cephalexin molecule consists of a carboxylic acid group in which the stretching vibration of the hydroxyl group with 100 PED% was calculated at 3570 cm^{-1}. Moreover, stretching bands for a non-bonded O-H group in different compounds occurs in the range 3530–3645 cm^{-1}, whereas the stretching bands for an H-bonded O-H group in the carboxylic acid typically occurs in the C-H characteristic region 3300–2500 cm^{-1} [37]. In the FT-IR spectrum, a broad peak confirming O-H stretching has been observed in the region 2800-3300 cm^{-1}. The lowering of stretching bands with a broad peak indicates the prevalence of strong hydrogen bonding in the crystal form. Deformation of CHO with a low PED contribution was detected at 1152 cm^{-1} and assigned at 1157/1156 cm^{-1} in the IR/Raman spectra.

4.3.2. N-H vibration

Generally, the primary and secondary amine suffer stretching vibration in the region 3460–3325 cm^{-1} and 3490–3310 cm^{-1}, respectively [37]. In the primary amine NH_2, the symmetric stretching of amine was calculated at 3412 cm^{-1} and observed at 3356 cm^{-1} in the IR spectra. Similarly, the asymmetric stretching calculated at 3333 cm^{-1} was observed at 3331 cm^{-1} in the IR spectra. The redshift in the symmetric vibration indicates the intermolecular hydrogen bonding of amine group in the crystal form. Further, scissoring vibration at 1601 cm^{-1} reported at 1600 cm^{-1} in the Raman spectra falls within the range of literature value 1638-1575 cm^{-1} [38,39]. Again, waging vibration of NH_2 at 817 cm^{-1} was observed at 819 cm^{-1} in the Raman spectra.

The stretching band of secondary amine was calculated at 3421 cm^{-1} and observed at 3480 cm^{-1} in the FT-IR spectra. According to Barnes, in the hydrogen bonding due to weakly interacting bases, the blueshift with decreased intensity is observed, whereas for strongly interacting bases the redshift with increased intensity is observed [27]. Hence, the contraction of bond N7-H27 and blue shift in the vibration is due to hydrogen bonding among weakly interacting bases. Further, a rocking vibration of secondary amine N7H27 detectable at 1229 cm^{-1} was found at the absorption band 1227 cm^{-1} in the Raman spectra.

4.3.3. C-H vibration

The characteristic region for C-H stretching bands in aromatic structure typically falls in the region 3100-3000 cm^{-1} [40, 41]. In the molecule, the ring R1 has five CH moieties exhibiting five stretching modes of vibration within the range 3018-3058 cm^{-1}. For R1[ν(CH)], calculated bands at 3054, 3048, 3041 were observed at 3057, 3049, 3047 cm^{-1} in the Raman spectrum. The stretching of R2[ν(CH)] at 2977 cm^{-1} was observable in both IR and Raman

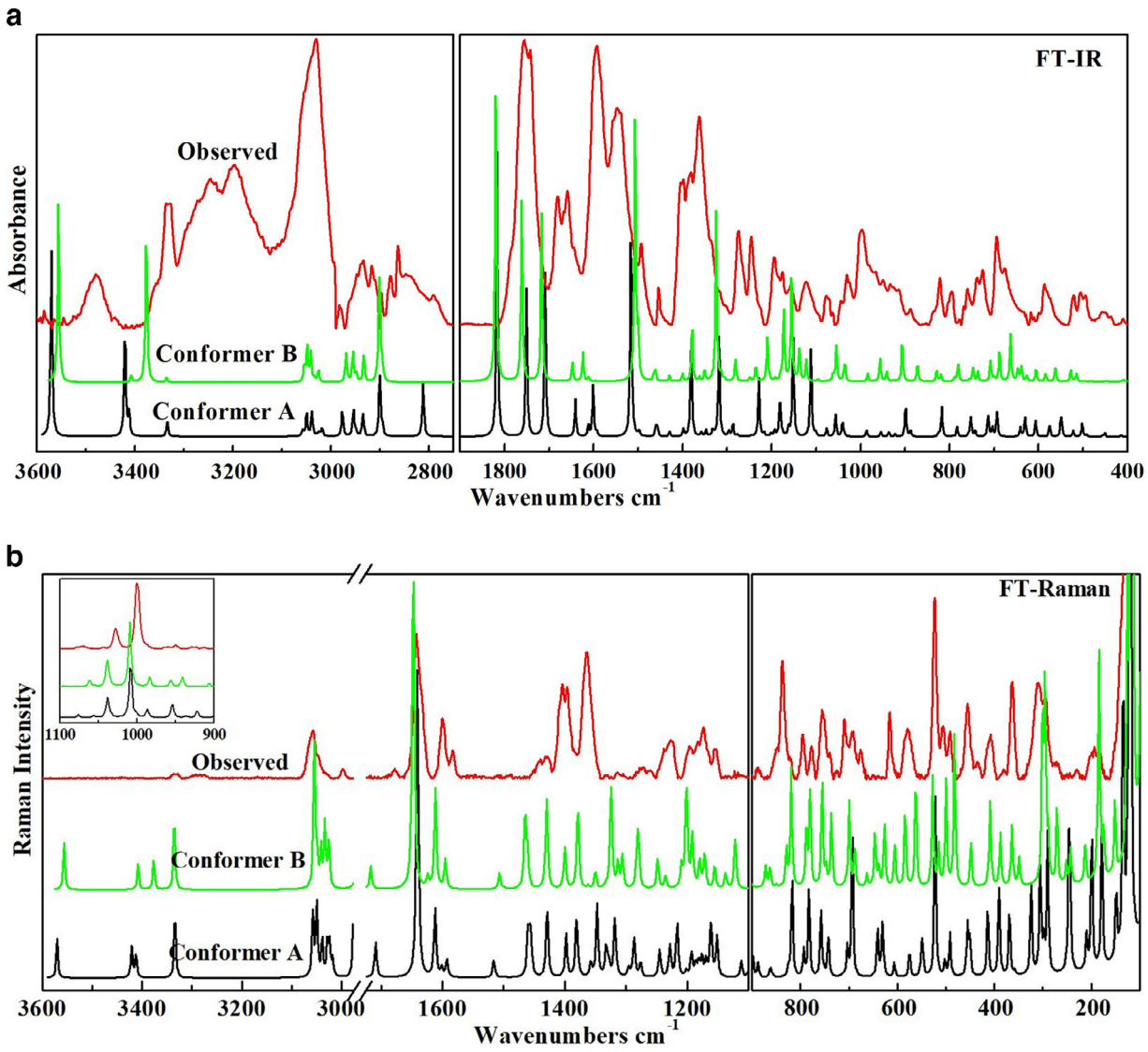

Fig. 3. a. Observed and calculated FT-IR spectra of conformers A and B of cephalexin.
b. Observed and calculated Raman spectra of conformers A and B of cephalexin.

at frequency 2983 cm^{-1} and 2967 cm^{-1}, respectively. The aromatic CH in-plane bending vibrations and the CH out-of-plane bending vibrations almost appear in the range 1350-950 cm^{-1} and 1100–600 cm^{-1}, respectively [40, 42]. The rocking of methine moieties of ring R2, was very prominent at frequency 1245 cm^{-1} and also was observed at 1246/1245 cm^{-1} in the IR/Raman spectra. The out of plane bending of CH in the ring R1 was observed in the region 713-1001 cm^{-1}.

The asymmetric and symmetric stretching band of methyl group (CH_3) is expected in the region 3000-2905 cm^{-1} and 2870-2860 cm^{-1} [43, 44]. The asymmetric stretching calculated at 2935 cm^{-1} was observed at 2934/2933 cm^{-1} in the IR/Raman spectra and symmetric stretching at 2895 cm^{-1} was observed at 2897/2884 cm^{-1} in the IR/Raman spectra. The asymmetric deformation was assigned at 1454 cm^{-1} in the IR and symmetric deformation at 1398/1397 cm^{-1} in the IR/Raman spectrum, were in the given range of asymmetric (1465-1440 cm^{-1}) and symmetric deformation (1390-1370 cm^{-1}) [45]. The corresponding wavenumbers were calculated at 1456 and 1398 cm^{-1}, respectively. The rocking vibration of CH_3 calculated at 1041 cm^{-1} was well matched with the experimental values.

The asymmetric and symmetric stretching of CH_2 usually occur in the range 3000-2900 cm^{-1} and 2900-2800 cm^{-1}, respectively [40]. The asymmetric stretching band associated with ring R3 was calculated at 2949 cm^{-1} and observed at 2947/2942 cm^{-1} in the IR /Raman Spectra and symmetric stretching at 2900 cm^{-1} was observed at 2910/2912 cm^{-1} in IR/ Raman. The scissoring vibration (in-plane bending) calculated at 1429 cm^{-1} was observed at the same frequency in Raman spectra, and twisting vibration at 1193 cm^{-1} was observed at 1194/1994 cm^{-1} in the IR/Raman spectrum. Also, waging vibration with a low intensity was detected at 1286 cm^{-1} in the Raman and 863 cm^{-1} in the IR spectra, respectively.

4.3.4. C=O, C-C and C=C vibration

The carbonyl group (C=O) generally exhibits strong stretching bands in the region 1870–1550 cm^{-1} [46]. The stretching bands of carbonyl groups (C11=O, C17=O and C15=O) were calculated at 1817, 1751 and 1709 cm^{-1} and observed at 1756, 1743 and 1681 cm^{-1} in the experimental IR spectra with very intense peak. The region 1750–1600 cm^{-1} is identified as the characteristic region for C=O stretching in carboxylic acid [45]. The observed frequency of C15=O is slightly lower than the calculated frequency due to the

intra-molecular hydrogen bonding (C15-O5...H30) between electronegative atom O and electron donor group CH_3 in the aromatic system as shown in Fig 2. Further, as represented in ESP, the intense red region over the oxygen atoms associated with the carbonyl groups indicate oxygen as a highly electronegative region. So, lowering of the wavenumbers of C11=O and C15=O is due to either the inter or intra-molecular hydrogen bonding. Further, the deformation of C17=O takes place at calculated frequency 783 cm^{-1} and observed at 788 cm^{-1} and 766 cm^{-1} in the IR and Raman spectra. Also, at very low calculated wavenumbers 693 cm^{-1}, the rocking vibration of C17=O was detected and the corresponding value was assigned at 694 /693 cm^{-1} in the IR/Raman spectra.

Generally, the stretching vibration of C-C takes place in the region 1650–1100 cm^{-1} [47]. In this study, stretching bands of C-C calculated at 1056, 1076 and 1593 cm^{-1} was reported at 1063/1058 cm^{-1}, 1077/1077 cm^{-1} and 1593/1583 cm^{-1} in the IR/Raman spectra. On the other hand, the stretching wave number of C12=C14 was calculated at 1648 cm^{-1} was observed at 1645 cm^{-1} in FT-IR and 1643 cm^{-1} in the Raman spectra.

4.4. Natural bond orbital analysis

The natural bond orbital (NBO) analysis is a useful method to study the interactions between filled Lewis-type (donor) NBOs and unfilled Lewis-type (acceptor) NBOs orbitals within the molecule. The interaction between the interacting orbitals is more intense with the increase of stabilization energy E(2) [48]. The stabilization energy E(2) is associated with the donor and acceptor orbitals and is determined by second-order perturbation theory given as [49,50]:

$$E(2) = E_{ij} = q_i \frac{\langle \sigma_i \hat{F} \sigma_j^* \rangle^2}{\varepsilon_j - \varepsilon_i} = q_i \frac{F(i,j)^2}{\varepsilon_j - \varepsilon_i}$$

where q_i represents donor orbital occupancy, $\varepsilon_{j=} \langle \sigma_i \hat{F} \sigma_i \rangle$ and $\varepsilon_i = \langle \sigma_j^* \hat{F} \sigma_j^* \rangle$ are diagonal elements representing donor and acceptor energies, respectively and $F(i, j)$ is the off-diagonal Fock matrix element (Kohn–Sham matrix element).

The NBO analysis of the title molecule has been performed at the B3LYP/6-311++G(d,p) level to study the stability of the molecule due to charge transfer and hyper-conjugative interaction within the molecule. In the conformer A, the lone pair interactions, LP(1)N7 $\rightarrow$ π^*(O3-C15), LP(1)N6 $\rightarrow$ π^*(O2-C11) and LP(2)O4 $\rightarrow$ π^*(O5-C17) stabilize the molecule with the maximum stabilization energies of 46.73, 45.86 and 43.68 kcal/mol, respectively. Furthermore, the hyper-conjugative interaction occurring due to overlapping between bonding π and anti-bonding π specifies have stronger charge delocalization than the hyper-conjugative interaction occurring due to overlapping between bonding σ and anti-bonding σ. This is due to the less occupancy of π bonds than the occupancy of σ bonds, the donating capacity of π bond is comparatively higher than the σ bonds [51]. As shown in Table S3 (Supplementary material), occupancy of π bonds and π^* bonds that lie in the range 1.65572–1.87072 and 0.24695–0.36109, respectively leads to the maximum charge delocalization energy of 21.47 kcal/mol. On the other hand, occupancy of σ bonds (1.96401–1.97714) and σ^* bonds (0.01838–0.04590) lead to the maximum delocalization energy of 7.21 kcal/mol.

4.5. Chemical reactivity

4.5.1. Analysis of HOMO, LUMO and energy gap

The molecular reactivity can be predicted by analyzing the highest occupied molecular orbital (HOMO) and the lowest occupied molecular orbital (LUMO). The corresponding energies of HOMO and LUMO orbitals are represented as ionization potential and electron affinity which demonstrate electron donating and accepting nature of a molecule [52]. The molecules with lower HOMO and LUMO energy gap (ΔE_{L-H}) are more reactive and more polarizable whereas the molecules with higher energy gap indicate less reactive and less polarizable [52, 53]. The calculated LUMO energy values of conformer A and B are -1.8784 eV and -1.7608 eV, respectively. The higher LUMO energy value of conformer A indicates its higher electron affinity than B. The energy gap of conformer A (4.81 eV) is found to be slightly lower than that of the conformer B (4.96 eV), which shows that the conformer A is less stable and more reactive than the conformer B. The HOMO and LUMO plot for both conformers are presented in Fig. 4. Further, plots of some other frontier orbitals ((HOMO-1, LUMO+1, HOMO-2, LUMO+2, HOMO-3 and LUMO+3) with their respective energy gaps for conformer A have been presented in Fig. S5 (supplementary material) as well.

4.5.2. Molecular electrostatic potential surface

The molecular electrostatic potential (MEP) is a firmly established computational technique for the prediction of reactive sites for nucleophilic and electrophilic attack of molecules. This also confirms to the possible sites for intra and inter-molecular hydrogen bonding in molecules [54,55]. In the molecular system having electron density $\rho(\vec{r})$, the electrostatic potential $V^{ES}(\vec{r})$ at a point $\vec{r}$ is obtained as [56]:

$$V^{ES}(\vec{r}) = \sum_A \frac{Z_A}{\left|\overrightarrow{R_A} - \vec{r}\right|} - \int \frac{\rho(\vec{r}')d\vec{r}'}{\left|\overrightarrow{r'} - \vec{r}\right|}$$

where, Z_A is the charge of nucleus A at position $\overrightarrow{R_A}$ and first term and second terms on the right represents nuclear and electronic contributions, respectively. On the MEP map, the electrostatic potential increases in the order as red < orange < yellow < green < blue.

So, from Fig. 5 the region over atoms O2, O3, O5 is specified as a low electrostatic potential region (red region) and the region over H36, H34 and H35 (blue region) is specified as a high electrostatic potential region. This may be due to the presence of lone pairs in the oxygen atom of the carbonyl group which increases electron density across oxygen and hence increases the nucleophilic character across oxygen. On the other hand, due to the high electronegativity of oxygen in carboxylic acid, electrons are attracted from H36 and increase the electrophilic character across H36. Also, the region across H34 and H35 is found to be electrophilic in nature which is due to the electronegative character of the nitrogen atom. Further, these predicted nucleophilic and electrophilic sites in the molecule acted as proton acceptor and proton donor in protein-ligand interaction are explained in the Section 4.6.2.

4.5.3. Global reactivity descriptor

The Global reactivity descriptors HOMO and LUMO energy are used to define global reactivity descriptors like softness (S), hardness (η), chemical potential (μ), electronegativity (χ), and electrophilicity index (ω) using the following relations [57]:

$$\text{Electronegativity } (\chi) = -0.5(E_{LUMO} + E_{HOMO})$$

$$\text{Chemical potential } (\mu) = -\chi = 0.5(E_{LUMO} + E_{HOMO})$$

$$\text{Global hardness } (\eta) = 0.5(E_{LUMO} - E_{HOMO})$$

$$\text{Softness } (S) = \frac{1}{2\eta}$$

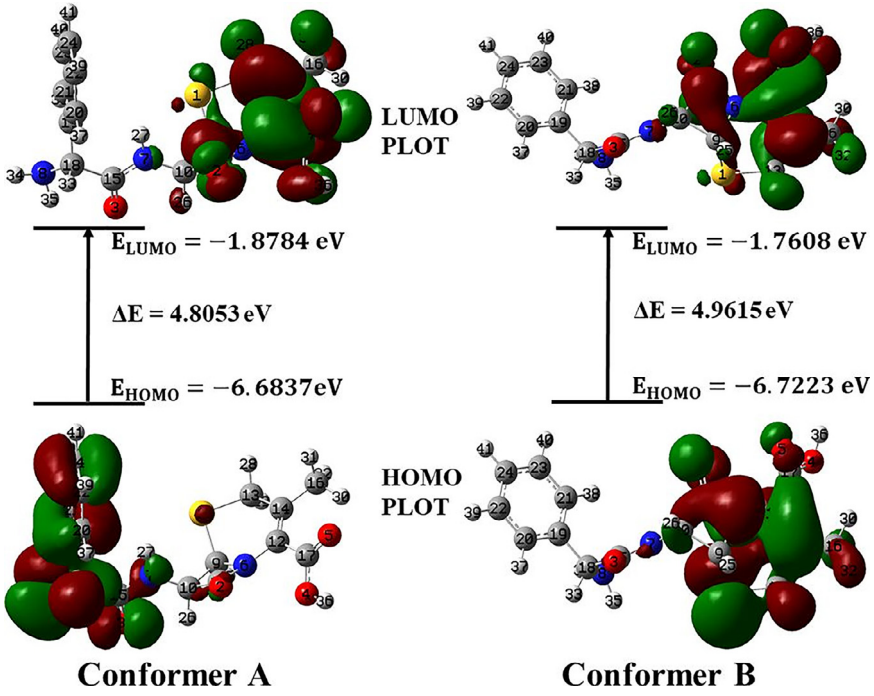

Fig. 4. HOMO-LUMO plot with an energy gap of conformers A and B of cephalexin.

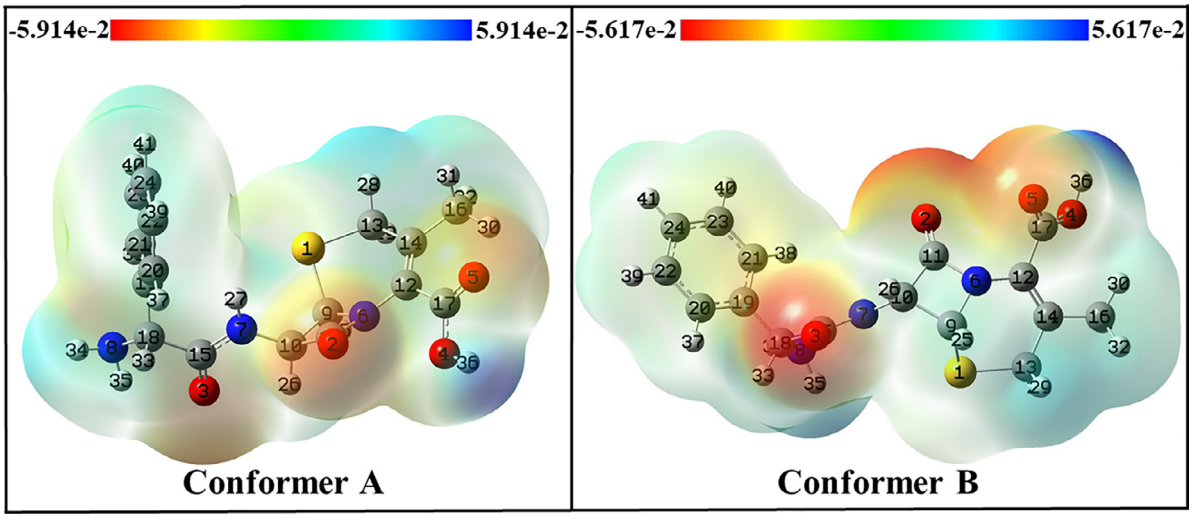

Fig. 5. Molecular electrostatic potential surface formed by mapping of total density over electrostatic potential for conformers A and B of cephalexin.

Table 4
Calculated E_{HOMO}, E_{LUMO}, energy gap (ΔE_{L-H}), chemical potential (μ), electronegativity (χ), global hardness (η), global softness (S) and global electrophilicity index (ω) for conformers A and B of cephalexin.

Conformer	E_{HOMO} (eV)	E_{LUMO} (eV)	ΔE_{L-H}	χ	μ	η	S	ω	ΔNmax
A	−6.6837	−1.8784	4.8053	4.2810	−4.2810	2.4026	0.2081	3.8140	1.7818
B	−6.7223	−1.7608	4.9615	4.2416	−4.2416	2.4807	0.2016	3.6261	1.7098

Here, the global electrophilicity index calculated as $(\omega) = \frac{\mu^2}{2\eta}$ measures the stabilization energy of a system after electrophile gains the extra charge (ΔN) from others [58]. The maximum electron gain by electrophile is denoted by ΔNmax, where $\Delta Nmax = -\frac{\mu}{\eta}$.

The global reactivity descriptors for conformers A and B are presented in Table 4. The tendency of accepting electrons from donors increases with the increasing value of ω. As the value of ω for conformer A is higher than the conformer B it has a higher tendency to attract electrons than conformer B. Also, the global hardness (η) of conformer A is slightly lower than the conformer B. This indicates that conformer A is comparatively more reactive. Further, the negative value of the chemical potential (μ) of both conformers specifies the stability of both the conformers.

4.5.4. Local reactivity descriptors

Fukui function (FF) is widely used to explain the quantitative analysis of charge in terms of local reactivity parameters that explains the chemical activity and specific sites in a molecular sys-

Table 5
Drug likeness properties of cephalexin.

Drug likeness parameters	Value	Range expected
Molecular weight	347.39 g/mol	<500
Molar refractivity	92.05	40-130
AlogP	0.67	<5
Number of rotatable bonds	5	<10
Polar surface area (PSA)	138.03 Å^2	<140
H-bond donors	3	<5
H-bond acceptors	5	<10

tem. Fukui function (FF) predicts reactive sites for nucleophilic and electrophilic attack and radial attack in a molecule. The Fukui function is defined as [59]:

$$f(r) = \left(\frac{\partial \rho(r)}{\partial N}\right)_{V(r)}$$

where, $\rho(r)$ is electron density, V(r) is potential on an electron due to all nuclei and N is the total number of electrons of that system. Further, for an atom k in a molecule, depending upon the nature of electron transfer in the atom k, the value of condensed Fukui function may be f_k^+, $f_k^-(r)$ or $f_k^0(r)$. According to Parr and Yang [60], the reactivity of atomic sites increases with the increasing value of condensed Fukui function. Here, f_k^+, $f_k^-(r)$ and $f_k^0(r)$ which are associated with nucleophilic, electrophilic and radial attack, respectively can be estimated from the given equations:

For nucleophilic attack, $f_k^+(r) = [q_k(N+1) - q_k(N)]$

For electrophilic attack, $f_k^-(r) = [q_k(N) - q_k(N-1)]$

For radial attack, $f_k^0(r) = [q_k(N+1) - q_k(N-1)]$

where, q_k is atomic charge associated with neutral(N), anionic (N+1), or cationic (N-1) chemical species.

Also, local softness, electrophilicity indices are determined using the following equation

local softness, $s_k^+ = Sf_k^+$, $s_k^- = Sf_k^-$ and $s_k^0 = Sf_k^0$

local electrophilicity indices, $\omega_k^+ = \omega f_k^+$, $\omega_k^- = \omega f_k^-$ and $\omega_k^0 = \omega f_k^0$

The selected value of Fukui functions, local softness, and local electrophilicity of conformers A and B are illustrated in Table S4 (Supplementary material). For conformers A and B, the most susceptible local site for the nucleophilic attack is N8 and C17 is the most susceptible site for the electrophilic attack.

4.6. Study of biological activity of cephalexin

4.6.1. Molecular characterization

The biological activity and nontoxic nature of a drug molecule can be evaluated by studying the drug-likeness parameters like molecular weight, molar refractivity, number of H-bond acceptors and H-bond donors, number of rotatable bonds, Polar surface area and AlogP of the molecule [61]. Here, the parameter AlogP is used to visualize the molecular hydrophobicity maps and to evaluate local hydrophobicity and hydrophobic interactions in protein-ligand complexes [62]. Further, a drug molecule which obeys the Lipinski's five rule is biologically active and nontoxic in nature [63,64].

In this study, the drug-likeness parameters of cephalexin have been predicted using the Swiss ADME web tool as shown in Table 5 [65]. Since, all the predicted drug-likeness parameters of cephalexin fall under the range of Lipinski's five rule, it is a nontoxic and biologically active molecule.

4.6.2. Molecular Docking simulation

Bioactive molecule binds with several proteins or macromolecular targets to modulate its activity [66]. So, molecular docking simulation of cephalexin has been performed to predict its binding sites and biological activity to explore its cross-reactivity and novel potentiality against secondary targets. Molecular docking is a fundamental tool used to predict the non-covalent binding of the ligand with the receptor along with the determination of binding affinity [67]. For docking analysis, the probable target proteins for the title molecule have been predicted using online Swiss Target Prediction [68]. Further, the PDB files of target human proteins Leukotriene A-4 hydrolase (PDB code; 3B7R, 3CHP) and matrix carbonic anhydrase II (PDB code; 3IBN, 5L9E) with resolution in the range 1.81–2.90 Å were downloaded from the RSCBPDB database. The Ramchandran Plots in Fig. S7 (supplementary material) show that maximum residues of proteins are lying under the allowed region (inside blue line) which specifies the stability of proteins.

Further, the most stable conformer A of cephalexin, corresponding to the minimum ground state energy, was taken as a ligand molecule for the docking study. The partial charges were calculated using Geistenger method [69]. The co-crystallized ligand and water molecules were removed from the receptor (protein), with the help of auto-dock tools. Polar hydrogen and Kollman charges were added to the proteins and the Lamarckian Genetic Algorithm (LGA) [70] was implemented for the overall docking process. The docking was performed using AutoDock Vina software [24] under the predicted active site of protein in the grid box of size 60Å × 60Å × 60Å. Further, the result of AutoDock Vina was visualized using the Biovia Discovery studio [25]. The interaction of proteins with the ligand is shown in Fig. 6 and the different types of interactions (binding affinity, binding residues, bond lengths, inhibition constants and rmsd value with respect to initial structure) are tabulated in Table 6. In this study, the rmsd value of all docked ligand structures for each protein is found to be less than 2 Å which strengthens the validation of docked structure [71]. Besides, all the important bonded residues of proteins lie within the allowed region. As there are different modes of binding confirmation for each docked ligand, the best mode of binding conformation with lb (lower bound) rmsd corresponding to the minimum binding affinity has been selected for further analysis.

4.6.2.1. Docking of cephalexin and Leukotriene A-4 hydrolase (PDB code; 3B7R, 3CHP). The target protein Leukotirence A-4 hydralase, a bifunctional zinc dependent metalloenzyme which belongs to a class of metallohydroses, is a precursor of Leukotrine B4 (LTB4) that acts as a pro-inflamamatory activator for several inflammatory diseases like asthma, arthritis, obstructive pulmonary diseases, bowl diseases, atherosclerosis, psoriasis [72]. To find the inhibitory potentiality of cephalexin with this protein, the docking study has been performed taking predicted binding sites centered at x = 34.96 Å, y = 8.69 Å, z = 11.29 Å and x = 10.32 Å, y = 39.95 Å, z = 68.05 Å for PDB code 3B7R and 3CHP, respectively. The protein code 3B7R and 3CHP on binding with cephalexin possess very low binding affinity as -8.3 kcal/mol and –8.6 kcal/mol, respectively. In 3B7R bound structure, atoms O2, O3 and O4 and H36 form six hydrogen bonds with residues SER352, SER380 and THR355 having bond lengths in the range 2.52-3.04 Å. Similarly, with 3CHP atoms O2, O3 and O4, O5 and H35 bound with residues ASN291, ARG326, ASN341 and GLU325 to form five strong hydrogen bonds with the bond lengths 2.06-2.81 Å. Also, Cephalexin on binding with 3B7R and 3CHP also possesses very less inhibition coefficient 0.82 μM and 0.49 μM, respectively. Hence, cephalexin shows the good inhibitory potentiality towards the protein Leukotriene A-4 hydrolase.

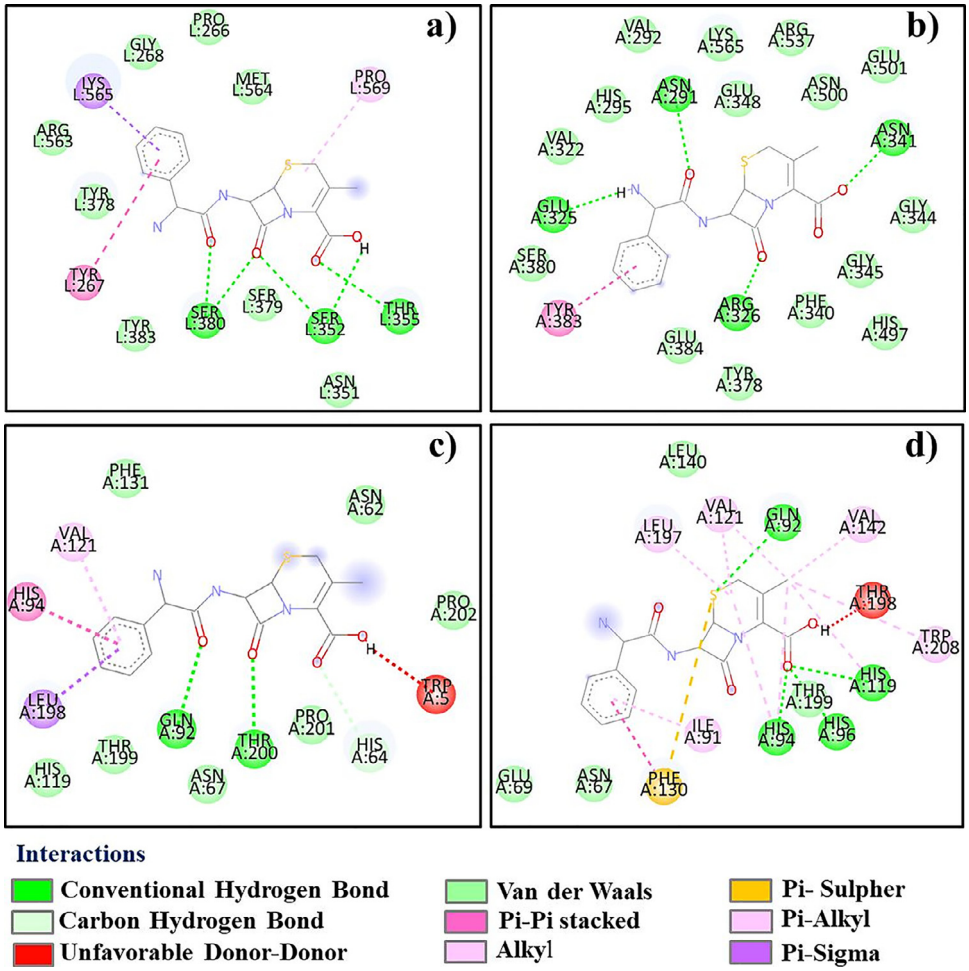

Fig. 6. Interactions of cephalexin with (a) 3B7R, (b) 3CHP, (c) 3K7K and (d) 5L9E.

Table 6
Docking parameters of cephalexin docked with the given protein targets.

Protein	PDB code	Binding affinity (kcal/mol)	Bond length(Å)	H-Bonded Residues	Inhibition constant (μM)	Rmsd Value (Å)
Leukotriene A-4 hydrolase	3B7R(1.81Å)	−8.3	3.04	SER352	0.82	1.14
			2.98	THR355		
			3.00	SER380		
			2.85	SER380		
			3.04	SER380		
			2.52	SER352		
	3CHP(2.10Å)	−8.6	2.41	ASN291	0.49	0.84
			2.81	ARG326		
			2.O6	ARG326		
			2.58	ASN341		
			2.09	GLU325		
Carbonic anhydraseII	3K7K(1.90Å)	−7.3	3.05	GLN92	4.42	2.18
			2.85	THR200		
			3.43	HIS64		
	5l9E(2.90**Å**)	−8.0	3.08	GLN92	1.37	0.65
			3.07	GLN92		
			2.11	HIS94		
			2.21	HIS96		
			2.45	HIS119		

4.6.2.2. Docking of cephalexin and matrix carbonic anhydrase II (PDB code; 3K7K, 5L9E). The second target protein is a carbonic anhydrase II, a second isoform, which is expressed in most of the tissues catalyzes the reversible hydration of carbon dioxide to carbonic acid [73]. To explore the biological activity of cephalexin with it, the docking study was performed with 3K7K and 5L9E taking binding sites centered at x = -9.584 Å, y = -1.752, z = 15.901 Å and x = 52.16 Å, y = 26.84 Å, z = 67.41 Å respectively. The docked conformation of 3IBN and 5LNE shows good binding affinity -7.3 and −8.0 kcal/mol with inhibition coefficient 4.42 μM and 1.37 μM, respectively. The bound structure of 3K7K shows two conventional and one carbon hydrogen bonds associated with atoms O2,

O3 and O5 and residues GLN92, THR200 and HIS64. On the other hand, in the bound structure of 5L9E, three strong conventional hydrogen bonds (2.11–2.45 Å) and two Pi-Sulphur bonds (3.07–3.08 Å) were found bonded with the residues GLN92, HIS94, HIS96 and HIS199. Finally, the drug molecule cephalexin also shows potent binding activities with the protein matrix carbonic anhydrase II.

5. Conclusion

Ultimately, using quantum chemical computation along with spectroscopic technique and molecular docking simulation the most stable structure, chemical reactivity and biological activity of cephalexin has been studied. The title molecule possesses only two stable conformers A and B. The analysis of observed and theoretical FT-IR and Raman spectra indicate some redshift in vibrational bands of C=O, NH_2 and O-H functional groups and blueshift in secondary amine (N7H27) due to either the intra or inter-molecular hydrogen bonding. Further, lone pair interactions LP(1)N7 $\rightarrow$ π^*(O3-C15), LP(1)N6 $\rightarrow$ π^*(O2-C11) and LP(2)O4 $\rightarrow$ π^*(O5-C17) has a maximum contribution for stabilizing the molecule. QTAIM analysis depicts one intra-molecular hydrogen bonding in conformer A and two in conformer B, which are partially covalent in nature. The smaller HOMO and LUMO energy gap and greater value of softness indicated that conformer A is comparatively more reactive than conformer B. Also, from the MEP map the atoms O2, O3, O5 and H34, H35, H36 were found to be nucleophilic and electrophilic in nature, respectively. Further, Fukui function's analysis shows that N8 atom is the most favorable site for nucleophilic attack while C17 for electrophilic attack. The molecular docking displays that the binding sites of cephalexin were mainly associated with carbonyl group, primary amine, and hydroxyl group in carboxylic acid. These sites were also justified by MEP surface and Fukui function. Cephalexin exhibits good inhibitory potentiality against both proteins Leukotriene A-4 hydrolase and carbonic anhydrase II. So, the information regarding the interaction of cephalexin with these proteins may be useful in further research.

Declaration of Competing Interest

The authors declare that they have no known competing financial interests or personal relationships that could have appeared to influence the work reported in this paper.

CRediT authorship contribution statement

Tarun Chaudhary: Writing – original draft, Formal analysis. **Manoj Kumar Chaudhary:** Writing – original draft, Formal analysis. **Bhawani Datt Joshi:** Supervision, Writing – review & editing. **Maria Silmara Alves de Santana:** Data curtion. **Alejandro Pedro Ayala:** Supervision, Writing – review & editing.

Acknowledgments

We sincerely acknowledge to Prof Poonam Tandon, HoD, Department of Physics, Lucknow University, India, for providing software facilities including Gaussian 09 program as well as sharing research concepts during whole study period.

Supplementary materials

Supplementary material associated with this article can be found, in the online version, at doi:10.1016/j.molstruc.2021.130594.

References

[1] T.M. Speight, R.N. Brogden, G.S. Avery, Cephalexin: a review of its antibacterial, pharmacological and therapeutic properties, Drugs 3 (1-2) (1972) 9–78, doi:10.2165/00003495-197203010-00002.
[2] A. Bailey, A. Hadley, A. Walker, D.G. James, Cephalexin-a new oral antibiotic, Postgrad. Med. J. 46 (533) (1970) 157–158, doi:10.1136/pgmj.46.533.157.
[3] P.S. Ganeshvar, S. Gunasekaran, T. Gnanasambandan, K. Viswanathan, Cefalexin: molecular structure, vibrational spectroscopy, natural bond orbital analysis and HOMO, LUMO studies, Int. J. Sci. Res. 4 (10) (2015) 182–189, doi:10.36106/ijsr.
[4] J.R. Anacona, I. Rodriguez, Synthesis and antibacterial activity of cephalexin metal complexes, J. Coord. Chem. 57 (15) (2004) 1263–1269, doi:10.1080/00958970410001721411.
[5] N. Shahabadi, S. Hashempour, A. Taherpour, F. Mohsenzadeh, Synthesis, characterization, HSA interaction, and antibacterial activity of a new water-soluble Pt (II) complex containing the drug cephalexin, J. Coord. Chem. 71 (22) (2018) 3708–3730, doi:10.1080/00958972.2018.1525488.
[6] N. Shahabadi, S. Hashempour, DNA binding studies of antibiotic drug cephalexin using spectroscopic and molecular docking techniques, Nucleos. Nucleot. Nucl. 38 (6) (2019) 428–447, doi:10.1080/15257770.2018.1562071.
[7] H. Hamishehkar, S. Hosseini, A. Naseri, A. Safarnejad, F. Rasoulzadeh, Interactions of cephalexin with bovine serum albumin: displacement reaction and molecular docking, BioImpacts: BI 6 (3) (2016) 125, doi:10.15171/bi.2016.19.
[8] K. Muthu, K. Gunasekaran, A. Kala, P. Govindasamy, P. Rajesh, P.P. Moorthi, Spectroscopic (FT-IR, FT-Raman & UV-Vis) and density functional theory studies of Cefadroxil, Int. J. Curr. Microbiol. App. Sci. 4 (11) (2015) 211–225 http://www.ijcmas.com.
[9] M.K. Chaudhary, T. Karthick, B.D. Joshi, P. Prajapati, M.S.A. de Santana, A.P. Ayala, V.S.J. Reeda, P. Tandon, Molecular structure and quantum descriptors of cefradine by using vibrational spectroscopy (IR and Raman), NBO, AIM, chemical reactivity and molecular docking, Spectrochim. Acta A Mol. Biomol. Spectrosc. 246 (2020) 118976, doi:10.1016/j.saa.2020.118976.
[10] J. Hutter, J. VandeVondele, Gaussian basis sets for accurate calculations on molecular systems in gas and condensed phases, J. Chem. Phys. 127 (11) (2007) 114105, doi:10.1063/1.2770708.
[11] G.I. Csonka, Proper basis set for quantum mechanical studies of potential energy surfaces of carbohydrates, J. Mol. Struct. THEOCHEM. 584 (1-3) (2002) 1–4, doi:10.1016/S0166-1280(02)00096-9.
[12] A.R. Kennedy, M.O. Okoth, D.B. Sheen, J.N. Sherwood, S.J. Teat, R.M. Vrcelj, Cephalexin: a channel hydrateacta crystallogr, Acta. Cryst. C. (Struct. Chem.) 59 (11) (2003) 0650–0652, doi:10.1107/S0108270103022649.
[13] M.J. Frisch, G.W. Trucks, H.B. Schlegel. G.E. Scuseria, J.R. Cheeseman, M.A. Robb, G. Scalmani, V. Barone, B. Mennucci, G.A. Petersson, H. Nakatsuji, M. Caricato, X. Li, H.P. Hratchian, A.F. Izmzylov, J. Bloino, G. Zheng, J.L. Sonnenberg, M. Hada, M. Ehara, K. Toyota, R. Fukuda, J. Ishida, M. Hasegawa, T. Nakajima, Y. Honda, O. Kitao, H. Nakai, T. Vreven, J.A. Montgomery, J.E. Peralta, F. Ogliaro, M. Bearpark, J.J. Heyd, E. Brothers, K.N. Kudin, V.N. Staroverov, R. Kobayashi, J. Normand, A. Raghavachari, A. Rendell, J.C. Burant, S.S. Iyengar, J. Tomasi, M. Cossi, N. Rega, J.M. Millan, M. Klene, J.E. Knox, J.B. Cross, V. Bakken, C. Adamo, J. Jaramillo, R. Gomperts, R.E. Stratmann, O. Yazyev, A.J. Austin, R. Cammi, C. Pomelli, J.W. Ochterski, R.L. Martin, K. Morokuma, V.G. Zakrzewski, G.A. Voth, P. Salvador, J.J. Dannerberg, S. Dapprich, A.D. Daniels, J. Farkas, B. Foresman, J.V. Ortiz, J. Cioslowski, D.J. Fox, GAUSSIAN 09, Revision, Gaussian, Inc., Wallingford CT, (2009).
[14] P. Hohenberg, W. Kohn, Inhomogeneous electron gas, Phys. Rev. B. 136 (1964) 864–871, doi:10.1103/PhysRev.136.B864.
[15] C. Lee, W. Yang, R.G. Parr, Development of the colle-salvetti correlation-energy formula into a functional of the electron density, *Phys. Rev. B.* 37 (2) (1998) 785–789, doi:10.1103/PhysRevB.37.785-789.
[16] R.G. Parr, W. Yang, in: Density Functional Theory of Atoms and Molecules, Oxford University Press, New York, 1989, pp. 1–325.
[17] A.D. Becke, Densityfunctional thermochemistry. III. The role of exact exchange, J. Chem. Phys. 98 (1993) 5648–5652, doi:10.1063/1.464913.
[18] T.H. Dunning, Gaussian basis sets for use in correlated molecular calculations. The atoms boron through neon and hydrogen, J. Chem. Phys. 90 (1989) 1007–1023, doi:10.1063/1.456153.
[19] J.M.L. Martin, C. Van Alsenoy, Gar2ped University of Antwerp, 1995.
[20] A. Frisch, A.B. Nielson, A.J. Holder, GaussView User Manual, Gaussian Inc, Pittsburgh, PA, 2005.
[21] E.D Glendening, A.E. Reed, J.E. Carpenter, F. Weinhold, NBO 3.0 Program manual, Theoretical Chemistry Institute, University of Wisconsin, Madison, WI, 1996.
[22] T.A. Keith, AIMALL Version 090201 TK Gristmill Software Overland Park, KS.USA, 2009.
[23] R.F.W. Bader, S.G. Anderson, A.J. Duke, Quantum topology of molecular charge distributions, J. Am. Chem. Soc. 101 (1979) 1389–1395, doi:10.1021/ja00500a006.
[24] O. Trott, A.J. Olson, AutoDock Vina: improving the speed and accuracy of docking with a new scoring function, efficient optimization and multithreading, J. Comput. Chem. 31 (2010) 455–461, doi:10.1002/jcc.21334.
[25] Discovery Studio 4.5 Guide, Accelrys Inc., San Diego, 2009. http://www.accelrys.com.
[26] K. Srivastava, A. Srivastava, P. Tandon, K. Sinha, J. Wang, Spectroscopic, quantum chemical calculation and molecular docking of dipfluzine, J. Mol. Struct. 1125 (2016) 751–762, doi:10.1016/j.molstruc.2016.07.078.

[27] A.J. Barnes, Blue-shifting hydrogen bonds-are they improper or proper? J. Mol. Struct. 704 (1-3) (2004) 3–9, doi:10.1016/j.molstruc.2004.02.040.
[28] R. Kumar, T. Karthick, V. Parol, P. Rawat, P. Tandon, A. Gupta, A.N. Prabhu, V. Upadhyaya, Spectroscopic characterization and structural insights of 4-[(1E)-3-(4-methoxyphenyl)-3-oxoprop-1-en-1-yl]phenyl 4-methylbenzene-1-sulfonate using vibrational, electronic spectra and quantum chemical calculations, J. Mol. Struct. 1225 (2021) 129144, doi:10.1016/j.molstruc.2020.129144.
[29] R. Swamy, C. Ravikumar, Crystal structure determination, Hirshfeld surface analysis and quantum computational studies of (3E, 5E)-1-ethyl-3, 5-bis (naphthalen-1-yl-methylidene) piperidin-4-one: A novel RORc inhibitor, J. Mol. Struct. 1225 (2021) 129313, doi:10.1016/j.molstruc.2020.129313.
[30] R.F.W. Bader, Atoms in Molecules: A Quantum Theory, Oxford University, New York, 1990.
[31] U. Koch, P. Popelier, Characterization of CHO hydrogen bonds on the basis of the charge density, J. Phys. Chem. 99 (24) (1995) 9747–9754, doi:10.1021/j100024a016.
[32] S.J. Grabowski, Red-and blue-shifted hydrogen bonds: the Bent rule from quantum theory of atoms in molecules perspective, J. Phys. Chem. A. 115 (45) (2011) 12789–12799, doi:10.1021/jp203908n.
[33] I. Rozas, I. Alkorta, J. Elguero, Behavior of ylides containing N, O, and C atoms as hydrogen bond acceptors, J. Am. Chem. Soc. 122 (45) (2000) 11154–11161, doi:10.1021/ja0017864.
[34] H. Yoshida, K. Takeda, J. Okamura, A. Ehara, H. Matsurra, A new approach to vibrational analysis of large molecules by density functional theory: wavenumber-linear scaling method, J. Phys. Chem. A. 106 (14) (2002) 3580–3586, doi:10.1021/jp013084m.
[35] P.L. Polavarapu, Ab initio vibrational Raman and Raman optical activity spectra, J. Phys. Chem. 94 (21) (1990) 8106–8112, doi:10.1021/j100384a024.
[36] G.A. Guirgis, P. Klaboe, S. Shen, D.L. Powell, A. Gruodis, V. Aleksa, C.J. Nielsen, J. Tao, C. Zheng, J.R. Durig, Spectra and structure of silicon-containing compounds. XXXVI—Raman and infrared spectra, conformational stability, ab initio calculations and vibrational assignment of ethyldibromosilane, J. Raman Spectrosc. 34 (2003) 322–336, doi:10.1002/jrs.989.
[37] J. Coates, Interpretation of infrared spectra, a practical approach. Encyclopedia of analytical chemistry: applications, theory and instrumentation (2006), 10.1002/9780470027318.a5606.
[38] D. Lin–Vien, N.B. Colthup, W.G. Fateley, J.G. Grasselli, The Handbook of Infrared and Raman Characteristic Frequencies of Organic Molecules, Academic Press, Boston, MA, 1991.
[39] M.Cinar Karabacak, Z. Unal, M. Kurt, FT-IR, UV spectroscopic and DFT quantum chemical study on the molecular conformation, vibrational and electronic transitions of 2-aminoterephthalic acid, J. Mol. Struct. 982 (1-3) (2010) 22–27, doi:10.1016/j.molstruc.2010.07.033.
[40] S. Muthu, J.U. Maheswari, Quantum mechanical study and spectroscopic (FT-IR, FT-Raman, 13C, 1H, UV) study, first order hyperpolarizability, NBO analysis, HOMO and LUMO analysis of 4-[(4-aminobenzene) sulfonyl] aniline by ab initio HF and density functional method, Spectrochim. Acta A Mol. Biomol. Spectrosc 92 (2012) 154–163, doi:10.1016/j.saa.2012.02.056.
[41] S. Sevvanthi, S. Muthu, M. Raja, Quantum mechanical, spectroscopic studies and molecular docking analysis on 5, 5-diphenylimidazolidine-2, 4-dione, J. Mol. Struct. 1149 (2017) 487–498, doi:10.1016/j.molstruc.2017.08.015.
[42] K. Karrouchi, S.A. Brandán, Y. Sert, M. El Karbane, S. Radi, M. Ferbinteanu, Y. Garcia, Synthesis, structural, molecular docking and spectroscopic studies of (E)-N'-(4-methoxybenzylidene)-5-methyl-1H-pyrazole-3-carbohydrazide, J. Mol. Struct. 1225 (2020) 129072, doi:10.1016/j.molstruc.2020.129072.
[43] N.B. Colthup, I.H. Daly, S.E. Wiberley, Introduction to Infrared and Raman Spectroscopy, 3rd Ed., Academic Press, New York, 1990.
[44] N.L. Alpert, W.E. Keiser, H.A. Szymanski, Theory and Practice of Infrared Spectroscopy, 2nd Ed., Plenum Press, New York, 1970.
[45] B.D. Joshi, R. Mishra, P. Tandon, A.C. Oliveira, A.P. Ayala, Quantum chemical studies of structural, vibrational, NBO and hyperpolarizability of ondansetron hydrochloride, J. Mol. Struct. 1058 (2014) 31–40, doi:10.1016/j.molstruc.2013.10.062.
[46] G. Socrates, Infrared and Raman Characteristic Group Frequencies, 3nd Ed., Wiley, New York, 1981.
[47] A. Srivastava, T. Karthick, B.D. Joshi, R. Mishra, P. Tandon, A.P. Ayala, J. Ellena, Spectroscopic (far or terahertz, mid-infrared and Raman) investigation, thermal analysis and biological activity of piplartine, Spectrochim. Acta A Mol. Biomol. Spectrosc. 184 (2017) s368–s381, doi:10.1016/j.saa.2017.05.007.
[48] M.E.D. Lestard, D.M. Gil, O. Estevez-Hernandez, M.F. Erben, J. Duque, Structural, vibrational and electronic characterization of 1-benzyl-3-furoyl-1-phenylthiourea: an experimental and theoretical study, New J. Chem. 39 (9) (2015) 7459–7471, doi:10.1039/C5NJ01210D.
[49] F. Weinholdand, C.R. Landis, Valency and Bonding: A Natural Bond Orbital Donor–Acceptor Perspective, Cambridge University Press, Cambridge, 2005.
[50] F. Weinhold, C.R. Landis, Natural bond orbitals and extensions of localized bonding concepts, Chem. Educ. Res. Pract. 2 (2) (2001) 91–104, doi:10.1039/B1RP90011K.
[51] B.D. Joshi, A. Srivastava, V. Gupta, P. Tandon, S. Jain, Spectroscopic and quantum chemical study of an alkaloid aristolochic acid I, Spectrochim. Acta A Mol. Biomol. Spectrosc. 116 (2013) 258–269, doi:10.1016/j.saa.2013.07.036.
[52] B. Borah, T.G. Devi, Characterization of Zn (l-Proline) 2 complex using spectroscopic techniques and DFT analysis, J. Mol. Struct. 1210 (2020) 128022, doi:10.1016/j.molstruc.2020.128022.
[53] K. Venil, A. Lakshmi, V. Balachandran, B. Narayana, V.V. Salian, FT-IR and FT-Raman investigation, quantum chemical analysis and molecular docking studies of 5-(4-Propan-2-yl) benzylidene)-2-[3-(4-chlorophenyl)-5 [4-(propan-2-yl) phenyl-4, 5-dihydro-1H-pyrazol-1-yl]-1, 3-thiazol-4 (5H)-one, J. Mol. Struct. 1225 (2021) 129070, doi:10.1016/j.molstruc.2020.129070.
[54] M.K. Gümüş, S. Kansız, E. Aydemir, N.Y. Gorobets, N. Dege, Structural features of 7-methoxy-5-methyl-2-(pyridin-3-yl)-11, 12-dihydro-5, 11-methano [1, 2, 4] triazolo [1, 5-c][1, 3, 5] benzoxadiazocine: Experimental and theoretical (HF and DFT) studies, surface properties (MEP, Hirshfeld), J. Mol. Struct. 1168 (2018) 280–290, doi:10.1016/j.molstruc.2018.05.032.
[55] J.S. Murray, K. Sen, Molecular Electrostatic Potential, Concepts and 399 Applications, Elsevier, Amsterdam, 1996.
[56] P. Politzer, D.G. Truhlar, Chemical Applications of Atomic and Molecular Electrostatic Potentials, Plenum, New York, 1981.
[57] R.G. Parr, R.G. Pearson, Absolute hardness: companion parameter to absolute electronegativity, J. Am. Chem. Soc. 105 (26) (1983) 7512–7516, doi:10.1021/ja00364a005.
[58] R.G. Parr, L.V. Szentpaly, S. Liu, Electrophilicity index, J. Am. Chem. Soc. 121 (9) (1999) 1922–1924, doi:10.1021/ja983494x.
[59] K. Fukui, Science, Role of frontier orbitals in chemical reactions, Science 218 (4574) (1982) 747–754 https://www.jstor.org/stable/1689733.
[60] R.G. Parr, W. Yang, Density functional approach to the frontier-electron theory of chemical reactivity, J. Am. Chem. Soc. 106 (14) (1984) 4049–4050, doi:10.1021/ja00326a036.
[61] B.F. Rizwana, J.C. Prasana, S. Muthu, C.S. Abraham, Vibrational spectroscopy, reactive site analysis and molecular docking studies on 2-[(2-amino-6-oxo-6, 9-dihydro-3H-purin-9-yl) methoxy]-3-hydroxypropyl(2S)-2-amino-3-methylbutanoate, J. Mol. Struct. 1202 (2020) 127274, doi:10.1016/j.molstruc.2019.127274.
[62] A.K. Ghose, V.N. Viswanadhan, J.J. Wendoloski, Prediction of hydrophobic (lipophilic) properties of small organic molecules using fragmental methods: an analysis of ALOGP and CLOGP methods, J. Phys. Chem. A 102 (21) (1998) 3762–3772, doi:10.1021/jp980230o.
[63] C.A. Lipinski, Lead-and drug-like compounds: the rule-of-five revolution, Drug Discovery Today Technol. 1 (4) (2004) 337–341, doi:10.1016/j.ddtec.2004.11.007.
[64] J.C. Prasana, S. Muthu, C.S. Abraham, Wavefunction analysis, charge transfer and molecular docking studies on famciclovir and entecavir: potential antiviral drugs, Chemical Data Collections 26 (2020) 100353, doi:10.1016/j.cdc.2020.100353.
[65] A. Daina, O. Michielin, V. Zoete, SwissADME: a free web tool to evaluate pharmacokinetics, drug-likeness and medicinal chemistry friendliness of small molecules, Sci. Rep. 7 (1) (2017) 42717, doi:10.1038/srep42717.
[66] D. Gfeller, A. Grosdidier, M. Wirth, A. Daina, O. Michielin, V. Zoete, SwissTargetPrediction: a web server for target prediction of bioactive small molecules, Nucleic Acids Res 42 (W1) (2014) W32–W38, doi:10.1093/nar/gku293.
[67] M.K. Chaudhary, T. Chaudhary, B.D. Joshi, Simulated spectra (IR and Raman), NLO, AIM and molecular docking of carisoprodol from DFT approach, BIBECHANA 18 (2) (2021) 48–57, doi:10.3126/bibechana.v18i1.29036.
[68] A. Grosdidier, V. Zoete, O. Michielin, SwissDock, a protein-small molecule docking web service based on EADock DSS, Nucleic Acids Res. 39 (2011) W270–W277, doi:10.1093/nar/gkr366.
[69] J. Gesteiger, M. Marsili, Iterative partial equalization of orbital electronegativity—a rapid access to atomic charges, Tetrahedron 36 (22) (1980) 3219–3228, doi:10.1016/0040-4020(80)80168-2.
[70] G.M. Morris, D.S. Goodsell, R.S. Halliday, R. Huey, W.E. Hart, R.K. Belew, A.J. Olson, Automated docking using a Lamarckian genetic algorithm and an empirical binding free energy function, J. Comput. Chem. 19 (1998) 1639–1662, doi:10.1002/(SICI)1096-987X.
[71] V. Vyas, A. Jain, A. Jain, A. Gupta, Virtual screening: a fast tool for drug design, Sci. Pharm. 76 (3) (2008) 333–360, doi:10.3797/scipharm.0803-03.
[72] T.A. Kirkland, M. Adler, J.G. Bauman, M. Chen, J.Z. Haeggström, B. King, M.J. Kochanny, A.M. Liang, L. Mendoza, G.B Phillips, M. Thunnissen, Synthesis of glutamic acid analogs as potent inhibitors of leukotriene A4 hydrolase, Bioorg. Med. Chem. 16 (9) (2008) 4963–4983, doi:10.1016/j.bmc.2008.03.042.
[73] D. Krishnan, W. Pan, M.R. Beggs, F. Trepiccione, R. Chambrey, D. Eladari, E. Cordat, H. Dimke, R.T. Alexander, Deficiency of carbonic anhydrase II results in a urinary concentrating defect, Front. Physiol. 8 (2018) 1108, doi:10.3389/fphys.2017.01108.

Journal of Molecular Structure 1286 (2023) 135518

Contents lists available at ScienceDirect

Journal of Molecular Structure

journal homepage: www.elsevier.com/locate/molstr

Computational evaluation on molecular stability and binding affinity of methyldopa against Lysine-specific demethylase 4D Enzyme through quantum chemical computations and molecular docking analysis

Tarun Chaudhary [a], T. Karthick [b], Manoj Kumar Chaudhary [c,*], Poonam Tandon [d], Bhawani Datt Joshi [e,*]

[a] Central Department of Physics, Tribhuvan University, Kirtipur, Kathmandu, Nepal
[b] Department of Physics, School of Electrical and Electronics Engineering, SASTRA Deemed University, Thanjavur, Tamil Nadu 613 401, India
[c] Department of Physics, Institute of Science and Technology, Tribhuvan University, Amrit Campus, Kathmandu 44600, Nepal
[d] Department of Physics, University of Lucknow, Lucknow 226007, India
[e] Department of Physics, Tribhuvan University, Siddhanath Science Campus, Mahendranagar 10406, Nepal

ARTICLE INFO

Keywords:
Methyldopa
Reduced density graph
Natural bond orbital
Chemical activity
Molecular docking

ABSTRACT

For the complete characterization of the molecule, quantum chemical calculations utilizing density functional theory (DFT) were performed at the B3LYP/6–311++*G*(d,p) level of theory. The quantum theory of atoms in molecules (QTAIM) and the reduced density gradient (RDG) analysis were implemented to investigate non-covalent interactions. The electronic environment of each atom in a molecule was explored using an electron localization function (ELF). Molecular stability of dimer structure due to intermolecular hydrogen bonds: O29-H54···O2, O1-H26···O30, and O32-H56···O4 and their corresponding stabilization energies were predicted by natural bond orbital (NBO) analysis. The energy gap and global and local reactivity parameters were determined to predict the chemical reactivity. The molecular electrostatic potential (MEP) was used to predict the electrophilic and nucleophilic sites. The frontier molecular orbitals (FMOs) were also portrayed using a density of states (DOS). Molecular docking was performed to study the interaction of the molecule with an enzyme, Lysine-specific demethylase 4D-like, a human protein.

1. Introduction

Methyldopa, $C_{10}H_{13}NO_4$, a centrally acting antihypertensive agent is chemically known as (*S*)−2-amino-3-(3,4-dihydroxyphenyl)−2-methyl-propanoic acid [1]. Methyldopa exhibits decarboxylase-inhibiting and sedative properties [2,3]. It is a crucial drug primarily used to treat pregnancy-induced hypertension, malignant hypertension, and heart failure [4]. It works by acting as a false transmitter in the central nervous system or in peripheral adrenergic neurons [1]. It lies in class II antigens drug which is used to treat autoimmune diabetes [5]. Besides that, it has some side effects like psychological depression, decreased mental activity, gastrointestinal upset, and rarely fatal hemolytic anemia [6–8]. Methyldopa contains carboxylic group, which plays a vital role in hydrogen bonding with its neighbours. Intra- and intermolecular hydrogen bonds play a remarkable role in excited-state intramolecular proton transfer and are mainly responsible for a compound's chemical and biological activities [9]. The electron-hole distribution analysis of methyldopa shows intramolecular charge transfer [10]. Weak interactions like: H-bonding, charge transfer, hydrophobic interactions, and van der Waals forces are responsible in drug's binding with protein, enzyme and DNA [11]. In this work, we have explored the intra- and intermolecular non-covalent interactions to study the structure, chemical reactivity, and binding affinity of methyldopa.

Literature reveals that the formation of intermolecular hydrogen bonds among monomers and its effects on chemical and biological activities have not been investigated yet. The DFT approach, a useful and popular tool to characterize the electronic structure of molecular systems which reveals the results closer to the experimental one, have been employed [12–14]. In addition, the topology of electron localization function (ELF), QTAIM, non-covalent interactions (NCI), molecular orbital compositions, and chemical properties of methyldopa were studied. The presence of intra- and intermolecular hydrogen bonds, van

* Corresponding authors.
E-mail addresses: manoj.chaudhary@ac.tu.edu.np (M.K. Chaudhary), bhawani.joshi@snsc.tu.edu.np (B.D. Joshi).

https://doi.org/10.1016/j.molstruc.2023.135518
Received 21 November 2022; Received in revised form 1 March 2023; Accepted 4 April 2023
Available online 5 April 2023

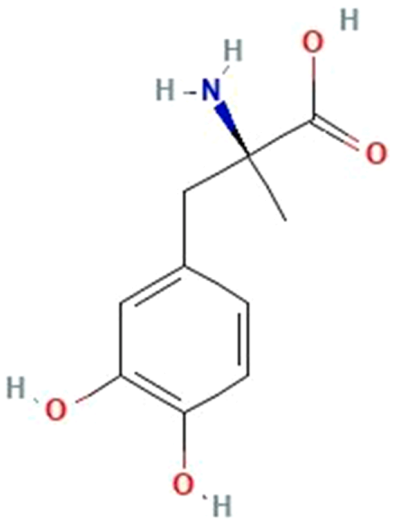

Fig. 1. Chemical structure of methyldopa.

der Waals interactions, and steric effects were investigated. Moreover, the stability of intermolecular hydrogen bonding has been analyzed by using NBO analysis. The chemical stability and active reactive sites for biological activities have been investigated on the basis of FMOs, energy gap, MEP, global, and local reactivity parameters. The total density of states (TDOS), the partial density of states (PDOS), and the overlap population density of states (OPDOS) demonstrate the MO's compositions along with their contribution to the chemical bonding and the nature of interaction among two orbitals, atoms or groups. A molecular docking study of the title molecule with Lysine-specific demethylase 4D-like has been carried out [15,16]. The chemical structure of the molecule is shown in Fig. 1.

2. Computational and theoretical details

To explore more insights into the structure and reproduce the vibrational and electronic spectra, the density functional theory computations were performed by using the Gaussian 09 package [17]. The DFT method [18] with exchange hybrid functional Becke's 3-parameters (local, nonlocal, and Hartree-Fock) and correlation functional Lee–Yang–Parr, B3LYP, and basis set consisting of triple zeta function with diffused as well as polarized function, 6–311++*G*(d,p), was employed [19,20]. GaussView 05 was used to visualize the charge distribution within the molecular geometry [21]. For the prediction of possible conformers of the molecule, a one-dimensional potential energy surface (PES) scan was performed using the B3LYP/6–31G(d,p) level of theory. However, for the accurate description of hydrogen bond interactions, flexible basis sets with diffuse and polarization functions are required [22,23]. To obtain the minimum energy structure, the geometries corresponding to the global and local minima of the molecule were further optimized at B3LYP/6–311++*G*(d,p) level of theory. The QTAIM approach was used to search for bond critical points (BCP), Nuclear attractor critical point (NACP), ring critical points (RCP), and bond paths using AIMALL and the AIM 2000 software package [24,25]. The NCI analysis was carried out to determine the nature of intra- and intermolecular non-covalent interactions. It is implemented to ascertain the types of interactions including H-bonds, van der Waals interactions and steric effects between complex systems [26]. The scattered graph between reduced density gradient (RDG) and a new function (Λ(r)) was plotted by using Multiwfn 3.8 software [27]. Further, van der Waals and steric effects were visualized by VMD 1.9.4 software [28]. RDG, the dimensionless quantity obtained from the density and its first derivative, is defined by the equation [29]:

$$\mathrm{RDG} = \frac{1}{2(3\pi^2)^{1/3}} \frac{\nabla\rho(\mathrm{r})}{\rho(\mathrm{r})^{4/3}} \tag{1}$$

The function, Λ(r) is defined as:

$$\Lambda(\mathrm{r}) = \mathrm{sign}(\lambda_2)\ \rho(\mathrm{r}) \tag{2}$$

where, λ_2 represents the second-largest Hessian matrix of electron density.

Further, exploring the electron localization region in the molecule, two-dimensional color-filled maps of electron localization function (ELF) and a 3D shaded projected map were plotted by using Multiwfn 3.8. The electron localization function (η) is defined by the equations [30]:

$$\eta = \frac{1}{1 + (D/\mathrm{D_h})^2} \tag{3}$$

where, $D = \frac{1}{2}\sum_i |\nabla\varphi_i|^2 - \frac{1}{8}\frac{|\nabla\rho|^2}{\rho}$ and $\mathrm{D_h} = \frac{3}{10}(3\pi^2)^{2/3}\rho^{5/3}$

D represents the excess of the kinetic energy density and $\mathrm{D_h}$ is the corresponding value for a uniform electron gas.

The frontier molecular orbitals and their energy gap (ΔE) were employed to obtain global reactivity descriptors like electronegativity (χ), chemical potential (μ), hardness (η), softness (S), and electrophilicity index (ω), using the following equations [31]:

$$\chi = -(E_L + E_H)/2 \tag{4}$$

$$\mu = (E_L + E_H)/2 \tag{5}$$

$$\eta = (E_L - E_H)/2 \tag{6}$$

$$S = 1/2\eta \tag{7}$$

$$\omega = \mu^2/2\eta \tag{8}$$

The stabilization energy of a system after gaining an extra charge (ΔN) from the surroundings can be measured from the electrophilicity index (ω) [31,32], where the maximum charge (ΔNmax) is calculated from the relation $(\Delta\mathrm{Nmax}) = -\mu/\eta$. The ω measures electron-accepting behavior of the molecular system. A system with a high value of ω is more electrophilic in nature and vice-versa.

The popular local reactive descriptors Fukui functions (FF) were used to determine the reactive sites in the molecule. The FF is mathematically expressed as [33]:

$$f(r) = \left(\frac{\partial\rho(r)}{\partial N}\right)_{V(r)} \tag{9}$$

where, ρ(r) is the density of the system having N electrons, whereas, V(r) is the external potential on an electron by all nuclei. On the basis of condensed FFs such as $f_k^+(r)$ or $f_k^-(r)$, the probable reactive sites for nucleophilic or electrophilic attack can be determined. The following equations can be used to evaluate $f_k^+(r)$ and $f_k^-(r)$ [21].

For reactive sites of nucleophilic attack,

$$f_k^+(r) = [q_k(N+1) - q_k(N)] \tag{10}$$

For reactive sites of electrophilic attack,

$$f_k^-(r) = [q_k(N) - q_k(N-1)] \tag{11}$$

where, q_k is the atomic charge at k^{th} atomic sites, evaluated from Hirshfeld analysis corresponding to neutral (N), anionic ($N + 1$) or cationic (N-1) chemical species. The dual descriptor (Δf_k) is used to predict the reactive sites and is given by [34]:

$$\Delta f_k = f_k^+(r) - f_k^-(r) \tag{12}$$

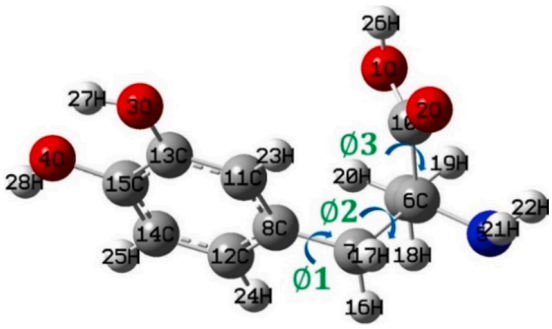

Fig. 2. Initial optimized structure of methyldopa with atom numbering scheme and possible flexible bonds.

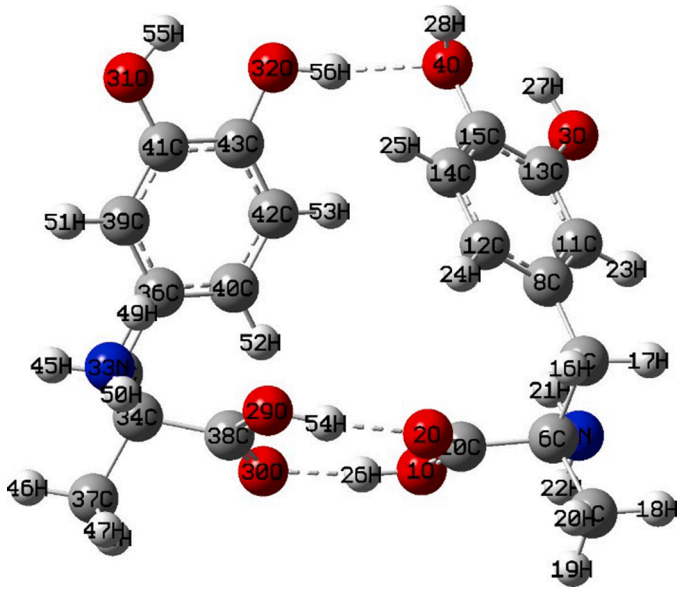

Fig. 3. Optimized structure of methyldopa dimer (C1C1) at B3LYP/6-311++*G*(d,p).

The positive value of Δf_k is favorable for a nucleophilic attack, whereas, the negative value of Δf_k is prone to an electrophilic attack.

For the study of biological activity of the molecule with the target protein, flexible-rigid docking, where the ligand is flexible and the protein is rigid, has been performed using AutoDock Vina and Discovery Studio Visualizer [35,36]. The binding affinity is determined on the basis of scoring function that includes steric terms (gauss1, gauss2, repulsion), a hydrophobic interaction term, a hydrogen bonding term and a number of rotational bonds [35,37]. For docking, the most stable conformation corresponding to the lowest ground state energy has been selected as the ligand molecule and the Geisteiger method was used to calculate the partial charges [38]. The target protein feasible to bind with the ligand was predicted from the chemical library using the SwissTargetPrediction tool [39]. The PDB files of the target protein were downloaded from the RCSB protein data bank [40].

3. Results and discussion

3.1. Conformational analysis and geometry

The methyldopa molecule consists of a carboxylic group, the most probable fragment for the formation of a cyclic dimer structure [2,22,41]. Thus, the dimer structure has been generated through carboxylic group. The one-dimensional PES scan of methyldopa has been carried out across the three flexible rotational bonds C7-C8, C6-C7, and C6-C10 which is presented in Fig. 2. Potential energy of the molecule is calculated at each of 10° variation of dihedral angle in steps of 0° to 360° and potential energy surfaces are shown in Fig. S1 (Supplementary Materials). Four possible minimum energy conformers named C1, C2, C3 and C4 were obtained as presented in Fig. S2 (Supplementary Materials). The relative energies of the conformers are presented in Table S1 (Supplementary Materials). With the aid of these four monomer structures, the dimer structures C1C1, C3C3, C4C4, C1C3, C1C4, C2C2, C1C2, C2C3, and C3C4 were generated as depicted in Fig. S3 (Supplementary Materials). The ground state energy and relative energy of each of the dimers were calculated at B3LYP/6–31G(d,p) level and are depicted in Table S2 (Supplementary Materials). Dimer C1C1 has the minimum energy, hence it is considered the most stable dimer. The dimer C1C1 was again optimized from the B3LYP/6–311++*G*(d,p) level of theory as shown in Fig. 3. Its ground state energy at this level of calculation is found to be − 934733.8112 kcal/mol. The global minimal energy, relative energy, interaction energy, and the basis-set-superimposition-error (BSSE) of dimer C1C1 are illustrated in Table 1. The interaction energy (ΔE), due to the formation of the dimer, was obtained using the relation, $\Delta E =$ Energy of dimer $- 2 \times$ Energy of monomer [42]. The BSSE corrections were found to be 0.0029 kcal/mol.

3.2. AIM and NCI analysis

The QTAIM is a widely used technique for revealing the covalent and non-covalent interactions within the molecule [43,44]. In the present work, the non-covalent interactions within the dimer structure of methyldopa were identified on the basis of topological analysis of electron density $\rho(r)$. The various topological parameters including BCP, NACP, RCP, electron density at BCP (ρ_{BCP}), Laplacian of electron density at BCP ($\nabla^2\rho_{BCP}$), electronic energy density H(r), local kinetic energy density G(r), potential energy density V(r), the ratio of the local potential and kinetic energy density at the BCP i.e. $|V|/G$ and ellipticity (ε) of methyldopa monomer and the dimer are illustrated in the Table S3 (a, b) (Supplementary Materials). The total number of NACP (3, –3) and BCP (3, –1) and RCP (3, +1) associated with monomer and its dimer are 28, 29, 2 and 56, 63, 8, respectively as shown in Fig. 4. The bonds having quantity $|V|/G$, greater than 2 and negative H(r) value are categorized as a covalent in nature [45,46]. Nevertheless, in a monomer, the value of $|V|/G$, for O2-C10 (2.0681) is very low compared to the values for C—C, C—N, C—H and N—H (3.6359 to 8.4524). In spite of being a shared shell interaction, O2-C10 shows comparatively a weak covalent effect. On the other hand, the H26-O1 (11.4021) bond shows the strongest covalent effect. Similarly, in the dimer structure, the bonds C2-C10 (2.1086) and C38-O30 (2.1099) seem weak when compared to the bonds H55-O31 (11.2593), H56-O32 (11.2535), H27-O3 (11.2402) and H28-O4 (11.0483). The electron density (ρ_{BCP}) at O2-C10 (0.4155a.u) in

Table 1
The calculated energies and the interaction energy of monomer (C1) and its dimer state (C1C1) at B3LYP /6-311++*G*(d,p) level of theory.

Energies of monomer and dimers			Relative energies of dimers (kcal/mol)	Interaction energies of methyldopa dimers		BSSE (kcal/mol)
	Hartree	kcal/mol		BSSE uncorrected ΔE (kcal/mol)	BSSE corrected ΔE (kcal/mol)	
Monomer C1	− 744.7818	− 467,357.7540	–	–	–	–
Dimer C1C1	− 1489.5928	− 934,733.8112	0	− 18.3032	− 16.4972	0.0029

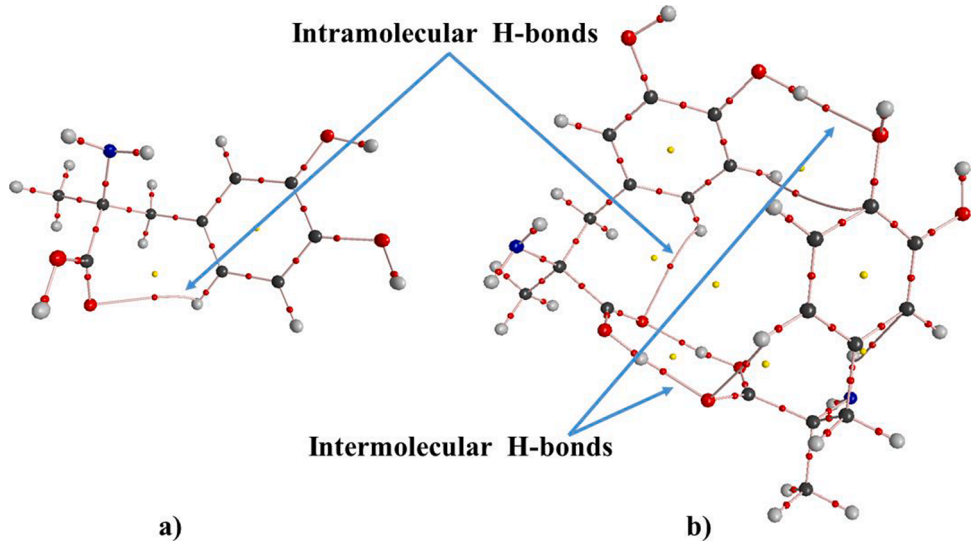

Fig. 4. The graphical representation of methyldopa (a) monomer, and (b) dimer showing bond critical points, ring critical points and bond paths.

Table 2
Geometric parameters: bond length (Å), bond angle (°) and the sum of van der Waals radii of interacting atoms ($r_H + r_A$) for intra- and intermolecular hydrogen bonds of methyldopa in monomer and the dimer forms.

D-H···A	D-H (Å)	H···A (Å)	D-H···A (°)	(r_H+ r_A) (Å)
		Monomer		
C12-H24···O2	1.0831	2.6963	118.09	2.72
		Dimer		
O29-H54···O2	0.9982	1.6955	173.39	2.72
O1-H26···O30	1.0022	1.6532	173.74	2.72
O32-H56···O4	0.9710	1.9803	158.18	2.72
C40-H52···O30	1.08319	2.7372	114.80	2.72
C12-H24···O2	1.0826	2.7675	108.52	2.72
C5-H21···C11	1.0152	2.6501	115.13	2.9
C42-H53···C15	1.0849	3.3140	113.91	2.9

monomer and O2-C10 (0.3970a.u), O38-O30 (0.3961a.u) in the dimer, are almost double that of most other electron densities with positive value of ellipticity. Thus, the electron density distribution at these BCPs is anisotropic. As, $\nabla^2\rho_{BCP} > 0$ at each of the RCPs of benzene ring corresponding to the monomer and the dimer, RCPs are associated with the charge depleted zone and hence, it is electrophilic in nature. The calculated value of bond ellipticity (ε) for C—H and C—C bonds outside of the ring lies in the range of 0.0073 to 0.0496 for monomer, 0.0073 to 0.0104 for the dimer, and 0.0199 to 0.0630 for monomer, 0.0155 to 0.0356 for dimer, respectively. These values, depict the presence of single bond between carbon atoms, since it is nearly equal to the standard value ($\varepsilon = 0$) for single C—C bonds in ethane [30]. However, the bond ellipticity of some ring C—C bonds has been found to be greater than 0.2. This shows that charge delocalization occurs in aromatic carbon atoms, which is also depicted well in the ELF plot. The molecular graph (Fig. 4) shows the presence of intra and intermolecular

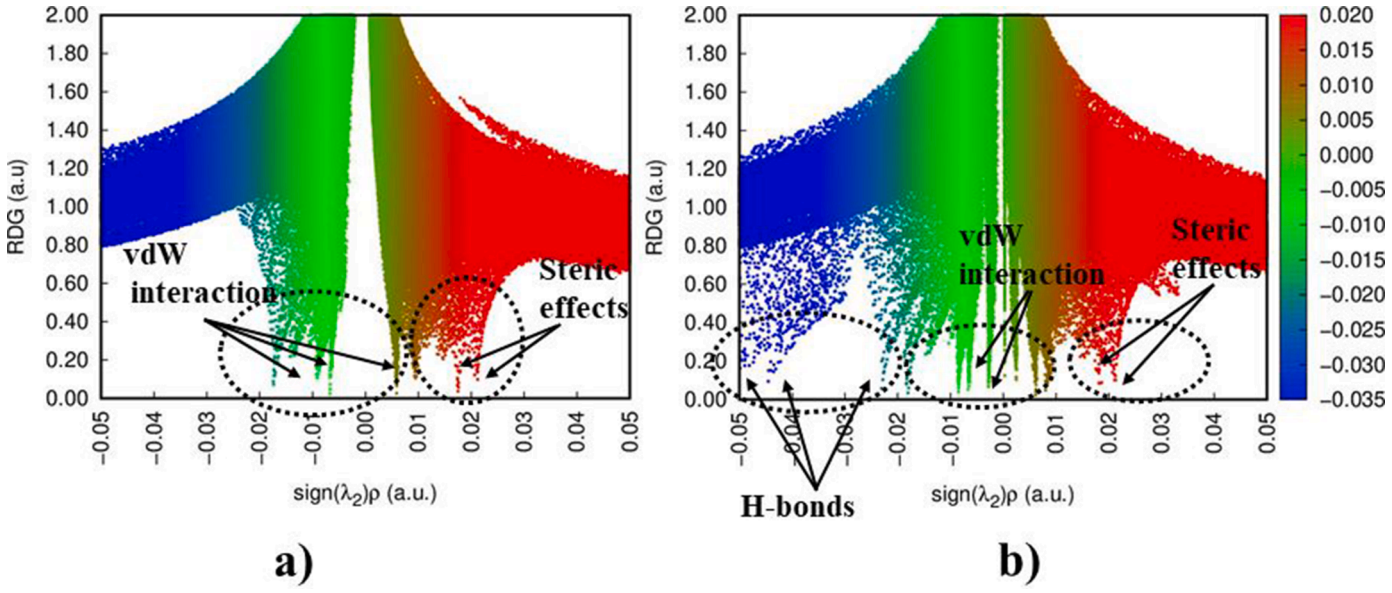

Fig. 5. RDG- scatter graph, of (a) monomer and (b) dimer of methyldopa.

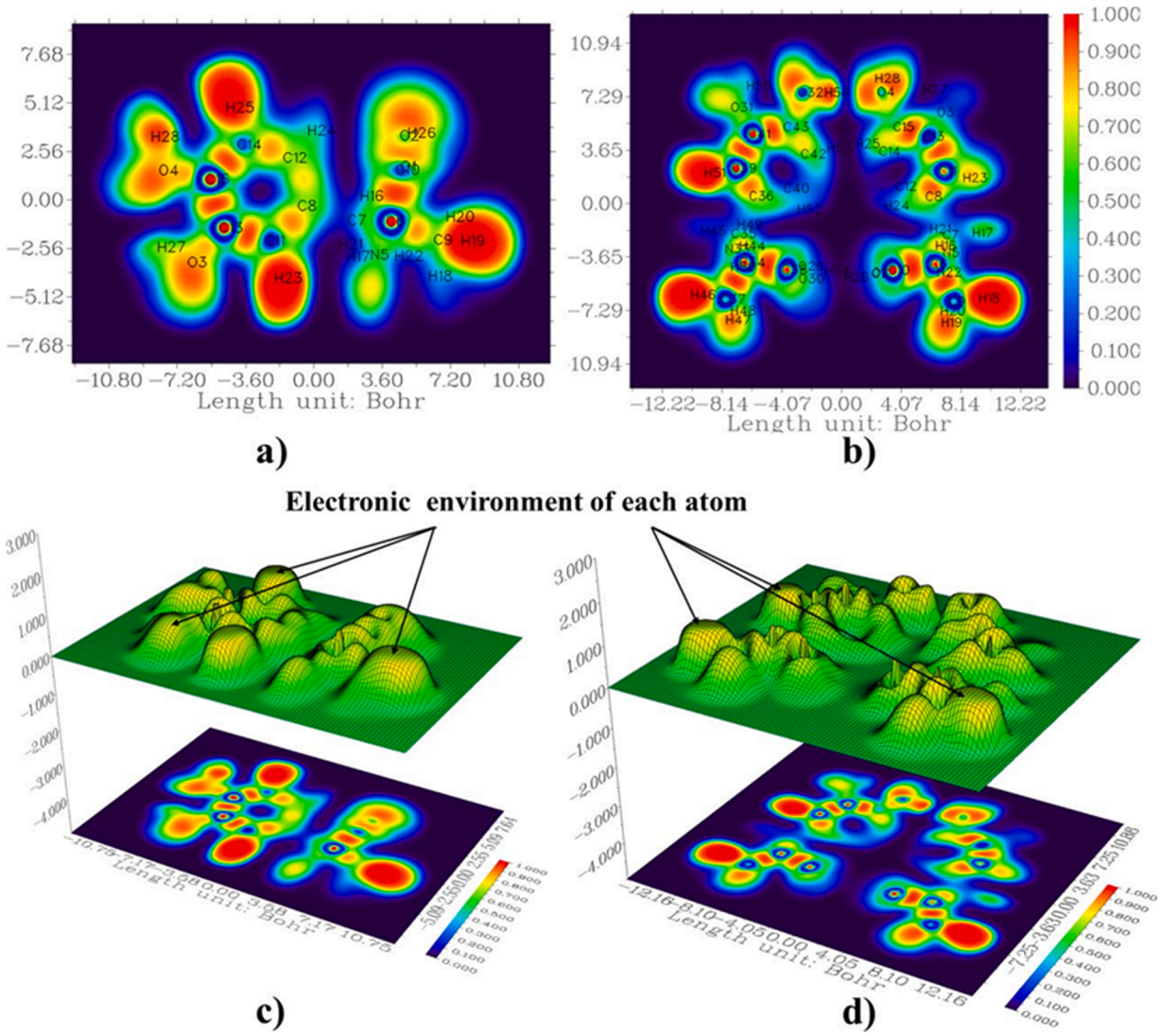

Fig. 6. 2D color filled map (a, b) and 3D projection of shaded map (c, d) of ELF of methyldopa in monomer and the dimer forms.

interactions in monomer C1 and the dimer (C1C1). Only the interactions having a bond length less than the sum of van der Waals radii (r_H+r_A) have been analyzed. Hence, the monomer exhibits only one conventional intramolecular hydrogen bond, whereas, dimer exhibits three intermolecular hydrogen bond interactions. The geometrical parameter for monomer and dimer regarding the hydrogen bonding is listed in Table 2. The nature of hydrogen bond is characterized as an strong for $\nabla^2\rho_{BCP} < 0$ and $H_{BCP} < 0$, a medium for $\nabla^2\rho_{BCP} > 0$ and $H_{BCP} < 0$ and a weak for $\nabla^2\rho_{BCP} > 0$ and $H_{BCP} > 0$ [41,47]. The topological parameters for monomer and dimer of methyldopa regarding the intra- and intermolecular interaction are listed in Table S4 (Supplementary Materials). In monomer, the intramolecular H-bond C12-H24…O2 with $\nabla^2\rho_{BCP} \sim$ 0.0228 a.u and $H_{BCP} \sim$ 0.0008 a.u is recognized as a weak hydrogen bond. Similarly, for the dimer, the intermolecular H-Bond O29-H54···O2 with $\nabla^2\rho_{BCP} \sim$ 0.1317 a.u and $H_{BCP} \sim -$ 0.0039 a.u and another H-bond O1-H26···O30 with $\nabla^2\rho_{BCP} \sim -$ 0.1397 a.u and $H_{BCP} \sim -$ 0.0062 a.u. Both are categorized as the medium hydrogen bonds. On the other hand, O32-H56···O4 with $\nabla^2\rho_{BCP} \sim$ 0.0818 a.u and $H_{BCP} \sim$ 0.0018 a.u is characterized as a weak hydrogen bond. The bond lengths and bond angles associated with hydrogen bonds fall in the range of 1.6532 Å to 1.9803 Å and 158.18° to 173.74°, respectively.

Additionally, NCI analysis method using Multiwfn 3.8 software, has been used to obtain the auxiliary information about the weak non-covalent interactions. The scattered graph between sign (λ_2)ρ and RDG monomer and the dimer of methyldopa is illustrated in Fig. 5. In the graph, a number of spikes with either a red or a blue color are observed. The large positive value of sign (λ_2)ρ corresponding to the red color indicates the repulsive interaction (steric effect), the large negative value corresponding to the blue color indicates the strong attractive interaction (hydrogen bonding) and the value nearer to zero corresponding to the green color indicates the very weak interaction (van der Waals interaction) in the monomer and the dimer form. The isosurface of RDG presented in Fig. S4 (Supplementary Materials) signifies that there are two strong hydrogen bonds H54···02 and H26···030. These are represented by intense blue colored isosurfaces, whereas a weak hydrogen bond H56···O4 is demonstrated by less intense blue colored isosurfaces in the dimer form. The presence of intermolecular hydrogen bonds in methyldopa indicates intra- and intermolecular proton transfer.

3.3. Electron localization function analysis

The ELF is a widely used function for visualizing localized and delocalized electron zones in molecules [48–50]. The ELF reveals the regions associated with the high electron-pair density [51]. The pictorial representation of ELF and its 3D projection are illustrated in Fig. 6. In

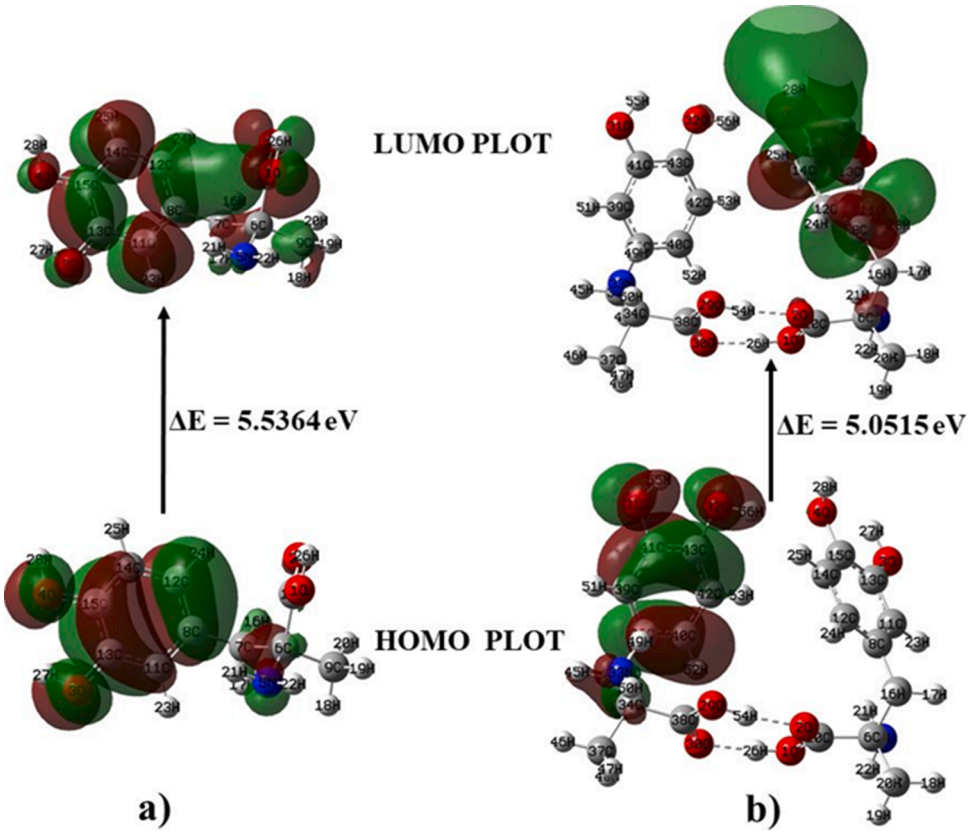

Fig. 7. HOMOs and LUMOs plot of methyldopa (a) monomer and (b) dimer in gaseous phase.

ELF color filled map, the red regions across hydrogen, oxygen and in between carbon atoms reveal either bonding or nonbonding electrons. The red colored regions between the atoms represent the bond critical point and justify the covalent nature of the bond. A pair of additional red zones associated with O4, and O32 in dimer represent the lone pair localization.

The blue ring-like structure around the nuclei of C6, C10, C11, C13, C14, and C15 in monomer and around the nuclei of C6, C9, C10, C11, C13, C34, C37, C38, C39, C41, and O32 in the dimer, shows the electron depletion region between the valence and inner shells. Furthermore, due to aromaticity, π electrons are delocalized in the ring structure. This region is depicted by the dark blue color inside the ring. Thus, the ELF plots predict the bond critical points and the chemically active region associated with charge transfer. The electronic environment in monomer and dimer is represented by the raised parts of the 3D projection map, as shown in Fig. 6(c, d).

3.4. Natural bond orbital analysis

The NBO analysis is an efficacious tool to investigate the H-bonding interactions of a variety of chemical systems [52]. The NBO analysis of methyldopa dimer has been carried out to explore the intra and intermolecular interactions between its donor (filled Lewis-type NBOs) and acceptor (unfilled Lewis-type NBOs) orbitals. The stabilization energy E (2) due to the interactions of filled (donor) and unfilled (acceptor) orbitals, is calculated by the second-order perturbation theory, defined as [53,54]:

$$E(2) = E_{ij} = q_i \frac{\left\langle \sigma_i \middle| \widehat{F} \middle| \sigma_j^* \right\rangle^2}{\varepsilon_j - \varepsilon_i} = q_i \frac{F(i,j)^2}{\varepsilon_j - \varepsilon_i} \quad (13)$$

where q_i, $\varepsilon_j = \langle \sigma_i | \widehat{F} | \sigma_i \rangle$, $\varepsilon_i = \langle \sigma_j^* \middle| \widehat{F} \middle| \sigma_j^* \rangle$ and $F(i,j)$ are donor orbital occupancy, diagonal elements representing donor energies, diagonal elements representing acceptor energies and off-diagonal Fock matrix element, respectively.

The stabilization energy of methyldopa during the interactions of filled (donor) and unfilled (acceptor) orbitals is presented in Table S5 (Supplementary Materails). The stability of the dimer is mainly due to the interactions of lone pairs and π orbitals with antibonding π orbitals. The lone pair interactions LP(2)O1→ π*(O2-C10), LP(2)O3→ π*(C11-C15), LP(2)O2→σ*(O1-C10) in unit one (C1) and LP(2)O29→π*(O30-C38), LP(2)O31→π*(C39-C41), LP(2)O30→σ*(C29-C38) in unit two (C2) stabilizes the dimer form of methyldopa with their respective stabilization energies of 46.33, 28.96, 21.14 kcal/mol and 47.63, 27.04, 20.06 kcal/mol. The maximum stabilization energy (23.55 kcal/mol) is due to π to antibonding π* orbitals interactions obtained for π(C8-C11)→ π*(C13-C15). Furthermore, the charge delocalization from lone pairs to antibonding σ orbitals, LP(1)O2 / LP(2)O2→σ*(O29-H54), LP(1)O3/ LP (2)O3→σ*(O1-H26) with the stabilization energy of 7.75 /18.04 kcal/mol, 8.83/21.36 kcal/mol confirms the hydrogen bonding interactions O29-H54···O2and O1-H26···O30. Similarly, the interaction LP(2)O4→σ* (O32-H56) with a stabilization energy of 6.39 kcal/mol gives rise to another weak hydrogen bond interaction, O32-H56…O4.

3.5. HOMO-LUMO analysis

The chemical stability and reactivity of compounds can be determined on the basis of the energy of the highest occupied molecular orbital (E_{HOMO}) and the lowest unoccupied molecular orbital (E_{LUMO}) [55,56]. The electron transition from HOMO (electron rich zone) to LUMO (electron deficient zone) is the main factor that ascertains the ease of chemical reaction and ΔE is the feasibility of electron transfer [57,58]. In the present study, the chemical behavior of methyldopa has been studied in both gaseous and aqueous media. The HOMO and LUMO

Table 3
Calculated global parameters of methyldopa monomer and its dimer in the gaseous and solvent phases.

Medium	E_{HOMO} (eV)	E_{LUMO} (eV)	ΔE (eV)	χ (eV)	μ (eV)	η (eV)	S $(eV)^{-1}$	ω (eV)	ΔNmax
				Monomer					
Gas	− 5.6379	− 0.1015	5.5364	4.2416	− 2.8697	2.7682	0.1806	1.4875	1.0367
Water	− 5.7043	− 0.2588	5.4455	2.8697	− 2.9816	2.7228	0.1836	1.6325	1.0950
Methanol	− 5.7002	− 0.2520	5.4483	2.9816	− 2.9761	2.7241	0.1835	1.6257	1.0925
Ethanol	− 5.6983	− 0.2484	5.4499	2.9761	− 2.9734	2.7249	0.1835	1.6222	1.0912
				Dimer					
Gas	− 5.4752	− 0.4237	5.0515	2.9734	− 2.9494	2.5258	0.1980	1.7221	1.1677
Water	− 5.6883	− 0.2746	5.4137	2.9494	− 2.9814	2.7069	0.1847	1.6419	1.1014
Methanol	− 5.6815	− 0.2759	5.4055	2.9814	− 2.9787	2.7028	0.1850	1.6414	1.1021
Ethanol	− 5.6779	− 0.2767	5.4012	2.9787	− 2.9773	2.7006	0.1851	1.6412	1.1025

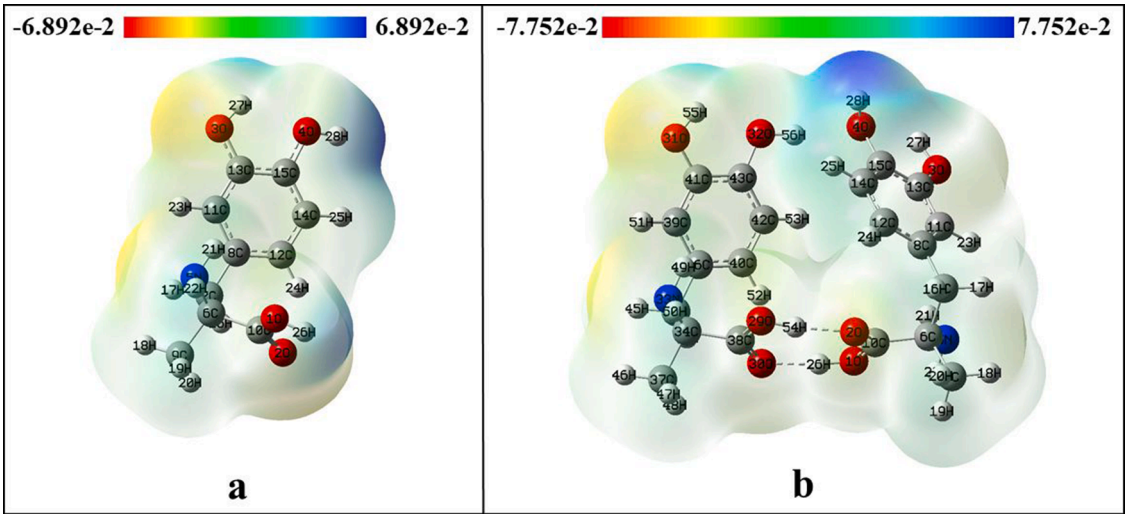

Fig. 8. Molecular electrostatic potential for methyldopa (a) monomer and (b) dimer.

plots, and their respective energy gaps in the gaseous state, are shown in Fig. 7. The calculated HOMO-LUMO energy gap values are 5.5364 eV (gas), 5.4455 eV (water), 5.4483 eV (methanol), and 5.4499 eV (ethanol) for monomer, and 5.0515 eV (gas), 5.4137 eV (water), 5.4055 eV (methanol), and 5.4012 eV (ethanol) for dimer, respectively. The lower computed energy gap of the dimer compared to the monomer confirms its lower stability.

3.6. Global reactivity

The global reactivity descriptors based on conceptual density functional theory are an efficient tool to understand the association between structure, stability and global chemical reactivity [59]. The global reactivity parameters (like:μ, S, η, χ and ω) have been determined utilizing HOMO and LUMO energy and their values are illustrated in Table 3. Similarly, the ionization potential, equivalent to HOMO energy and electron affinity (EA), equivalent to LUMO energy, in the gaseous as well as in solvent phases were calculated. The low value of softness (found to be 0.1806 eV^{-1} in monomer and 0.1980 eV^{-1} in dimer) in the gaseous state indicates the lower toxicity of the molecule [51]. The stability of molecules was determined by the value of chemical hardness, which was obtained as 2.7682 eV (monomer) and 2.5258 eV (dimer) in the gaseous state. The electrophilicity index, one of the precursor descriptor to analyze the biological activity [60], 1.4875 eV (monomer) and 1.7221 eV (dimer), represents the electrophilic character of the molecule. The molecule with a higher value of electrophilicity index behaves as an electrophile, whereas it behaves as a nucleophile for very low value electrophilicity index [61].

3.7. Molecular electrostatic potential

The charge distributions and reactivity of molecules were revealed by the MEP surface [62]. It is a widely used technique to predict the nucleophilic and electrophilic regions in the molecule as well as the possible hydrogen bonding sites in the molecule [23,63]. In the molecular system, the electrostatic potential at a point $\vec{r}$ is defined as [64]:

$$V^{ES}(\vec{r}) = \sum_{A} \frac{Z_A}{\left|\overrightarrow{R_A} - \vec{r}\right|} - \int \frac{\rho(\vec{r}')d\vec{r}'}{\left|\vec{r}' - \vec{r}\right|} \tag{14}$$

where, $\rho(\vec{r}')$ is the electron density, $\vec{r}'$ is dummy integration variable and Z_A is the charge of nucleus A situated at $\overrightarrow{R_A}$.

In the MEP map, the electrostatic potential increases in the order: red <orange < yellow < green < blue. The color code representing electrostatic potential in a monomer and dimer falls in the range of $(-6.892 \times 10^{-2}$ to $+ 6.892 \times 10^{-2})$ and $(-7.752 \times 10^{-2}$ to $- 7.752 \times 10^{-2})$ a.u, respectively, as shown in Fig. 8. It was observed that the low electrostatic potential regions (red colored) lie over oxygen and nitrogen atoms of hydroxyl and carbonyl groups and the high electrostatic potential regions (blue colored) lie over the hydrogen atoms of amine, hydroxyl and carboxylic group in the monomer. But, the effects of electro-negativity over oxygen and positivity over hydrogen of carboxylic group in dimer have significantly decreased. The electrostatic potential over atoms increases in the order: O1<N5<O3<O2 in the monomer and N5<O3<N33<O31 in the dimer. Similarly, the electrostatic potential over atoms decreases in the order:

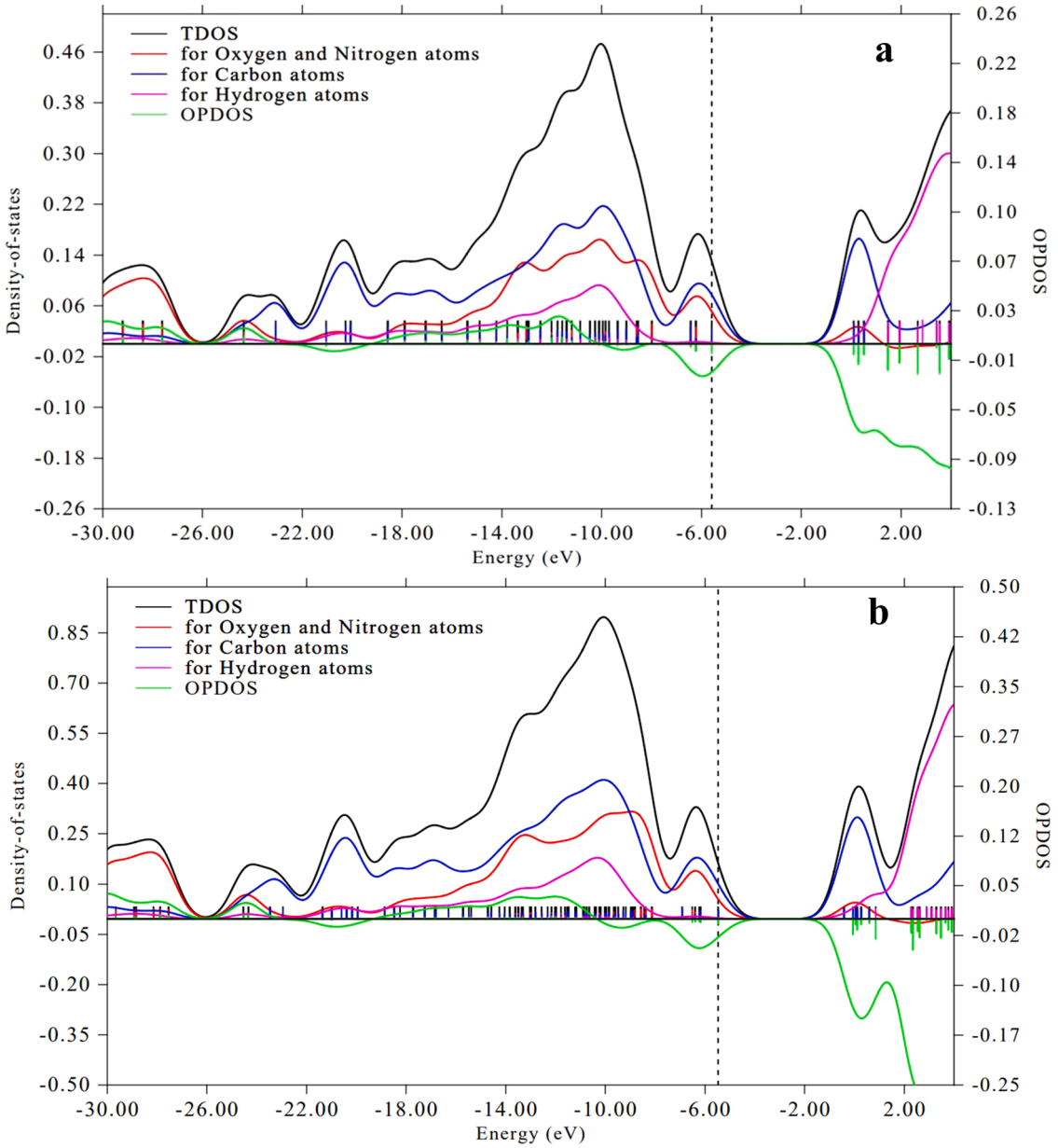

Fig. 9. TDOS, PDOS and OPDOS graphs of methyldopa in (a) monomer and (b) dimer form.

H28>H26>H27>H22>H21 in the monomer and H28>H27>H55>H22 in the dimer. Hence, the most favorable nucleophilic sites are O2 (monomer) and O31 (dimer) and electrophilic site is H28 in monomer as well as in dimer. In the molecular docking, Section 3.10, it can be observed that these predicted nucleophilic and electrophilic sites are the major sites for hydrogen bond interaction during the protein-ligand interaction.

Thus, these sites are highly responsible for the biological activities of the molecule as well as in intermolecular hydrogen bonding in a crystal packing.

3.8. Analysis of composition of molecular orbital (MO)

Moreover, neighboring orbitals in the boundary region may exhibit quasi degenerate energy levels [65]. Therefore, for a more practical description of frontier molecular orbitals (HOMO and LUMO), the graph of TDOS, PDOS and OPDOS was plotted using Multiwfn which is presented in Fig. 9. The values of OPDS may be positive, zero or negative according to the bonding, non-bonding or anti-bonding nature of the interaction of two atoms, orbitals or groups, respectively [65]. The dashed vertical lines correspond to the HOMO energy level, at − 5.6379 eV for the monomer and at − 5.4752 eV for the dimer. In the graph, the carbon and nitrogen atoms have almost equal contributions to HOMO. However, carbon atoms have dominantly high contributions to LUMO. The antibonding nature of oxygen and nitrogen with carbon atoms is found to contribute to both HOMO and LUMO. The hydrogen atoms have negligible contributions to HOMO but have significant contributions around −11.00 eV and have the highest contribution to the virtual molecular orbital LUMO+3. At this level, we can also observe the anti-bonding nature of oxygen and nitrogen atoms with carbon atoms.

3.9. Local reactivity

The global reactivity descriptors and MEP are commonly employed to forecast a molecular system's reactivity, but they are unable to portray the precise reactive sites. The FF reveals the regions, where the molecule will modify its density upon gaining or losing electrons [66]. To view the nucleophilic and electrophilic sites, Δf_k is calculated.The

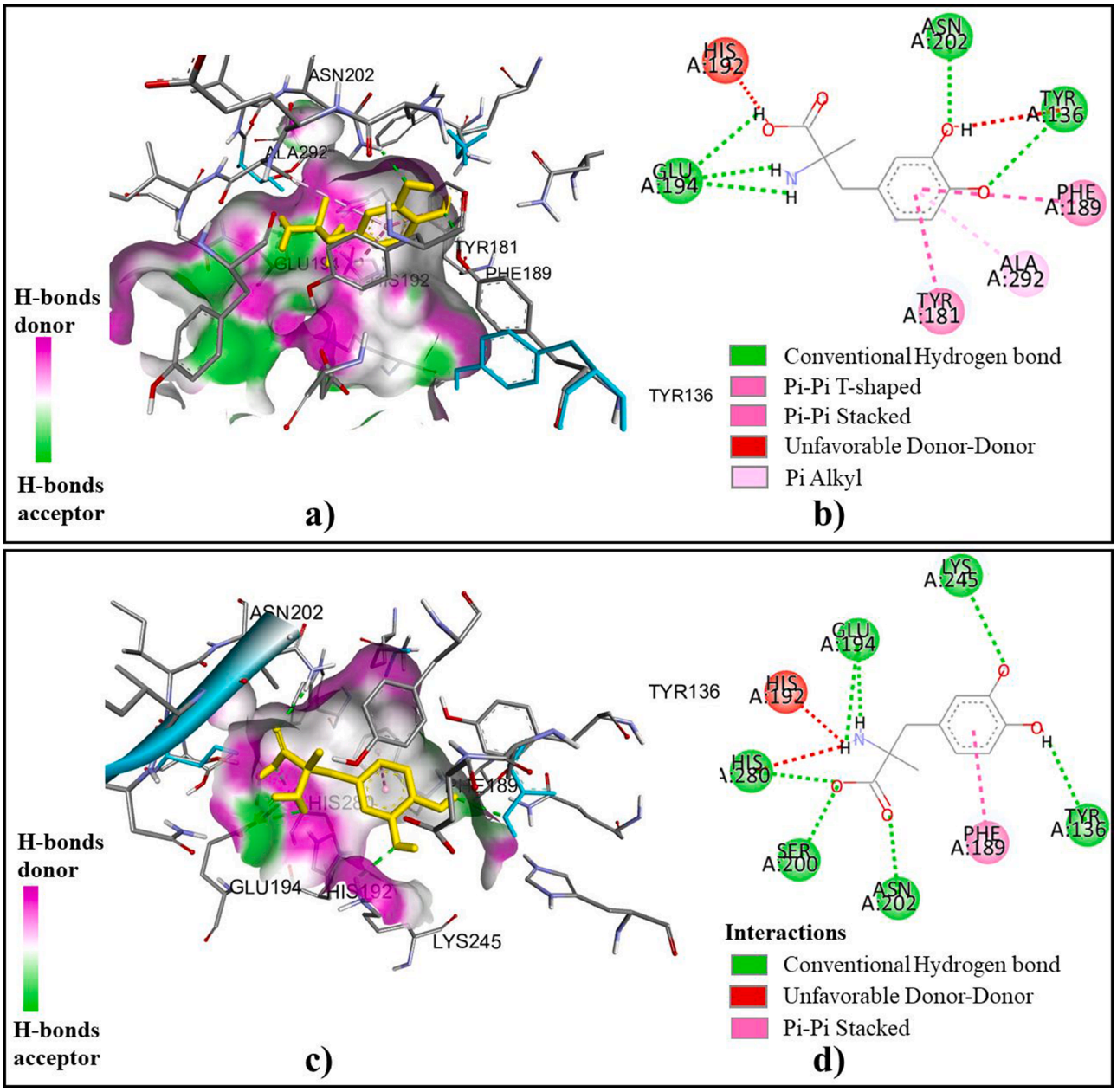

Fig. 10. Best binding mode (a, c) and interactions (b, d) of methyldopa with (5PNO, 5PNQ) protein.

Table 4
Docking parameters of methyldopa with Lysine-specific demethylase 4D-like.

Protein	PDB code	Binding affinity (kcal/mol)	Conventional H-Bond		Bond length(Å)	Inhibition constant (μM)	RMSD (Å)
			Residues	Atoms			
Lysine-specific demethylase 4D-like	5PNO (1.55 Å)	–7.6	GLU194	H22	2.79	2.67	1.18
			GLU194	H21	2.63		
			GLU194	H26	2.48		
			TYR136	O3	2.35		
			ASN202	O4	2.22		
	5PNQ (1.47 Å)	–7.4	SER200	O1	1.89	3.74	1.25
			ASN202	O2	2.34		
			LYS245	O3	2.53		
			HIS280	O1	2.09		
			GLU194	H21	2.36		
			GLU194	H22	2.45		
			TYR136	H28	2.60		

quantitative values of f_k^+or $f_k^-(r)$ and dual descriptor $\Delta f_k$for monomer and dimer states of the molecule are illustrated in Table S6 (a,b) (Supplementary Materials). For $\Delta f_k > 0$, the reactive site is favorable for nucleophilic attack and for $\Delta f_k < 0$, the reactive site is favorable for electrophilic attack [34]. The calculated Δf_k for nitrogen, oxygen and some carbon atoms have positive values in the order: C9>N5>O4>O3>O1>O2 in monomer and N5>N33>O32>O31>O4 >O3>O30>O2>O29>C9 in dimer. Hence, C9 (monomer) and N5 (dimer) are the most favorable sites for nucleophilic attack. On the other hand, all hydrogen atoms, including carbon atoms C6, C10, C15 in monomer and C10, C14, C6, C43, C15, C15, C38 in the dimer have $\Delta f_k <$ 0, whereas C10 (monomer) and C38 (dimer) have the most negative value. So, C10 (monomer) and C10 (dimer) are favorable sites for electrophilic attack.

3.10. Molecular docking

Molecular docking is a well-known and widely used tool in structural molecular biology and computer-aided drug discovery [67]. It is used to predict the binding modes of receptor proteins and ligand molecules [68–70]. In the present work, a docking study was performed to investigate the interactions of methyldopa with the predicted target. The conformation, C1 corresponding to the lowest ground state energy level, has been selected as the ligand molecule. The most probable target (receptor) for the ligand, predicted by the SwissTargetPrediction is Lysine-specific demethylase 4D-like as depicted in Fig. S5 (Supplementary Materials). The PDB files 5PNO and 5PNQ of the target protein have been used for the docking analysis. The Ramachandran plots of these proteins are demonstrated in Fig. S6 (Supplementary Materials), in which the region inside the blue line represents the allowed region for residues. The maximum residues lying under the blue line indicate the stability of the protein. The best binding mode and interactions of the docked protein structure are depicted in Fig. 10. The binding affinity, conventional hydrogen bond lengths, inhibition constants and RMSD between the docked and the initial structure of the ligand have been presented in Table 4. The AutoDock Vina estimates different binding modes of the ligand and, hence, the binding conformation corresponding to the lowest binding affinity and the minimum lower bound RMSD has been selected for docking analysis on the basis of Table S7 (Supplementary Materials).

3.10.1. Docking of methyldopa with 5PNO

The binding active sites of protein 5PNO were confined in a grid box of size 60 Å × 60 Å × 60 Å with a spacing of 0.375 Å and is centered at $x = 8.7153$, $y = -2.4944$ and $z = 19.9720$. The docked structure of the protein shows a binding affinity of –7.6 kcal/mol with an inhibition constant of 2.67 μM. The RMSD value between the docked and initial stable structure is 1.18 Å. It consists of five strong hydrogen bonds, having bond lengths in the range of (2.22 to 2.79) Å. Atoms H2, H22, H26, O3 and O4 of ligand molecule participate in the hydrogen bonding with the residues GLU194, TYR136 and ASN202 of the receptor protein. As a result, due to highly negative-valued binding affinity, low inhibition constant, large number of hydrogen bonds and small value of RMSD (< 2), the molecule have the potent inhibitor of protein, 5PNO.

3.10.2. Docking of methyldopa with 5PNQ

For predicting the possible binding modes of the molecule and its interactions with the protein, the grid box is centered at $x = 7.285$, $y = -3.881$ and $z = 19.12$. The docked complex 5PNQ shows a binding affinity of –7.4 kcal/mol with an inhibition constant of 3.74 μM. The RMSD value of the docked pose is 1.25 Å. The ligand interacts with the protein with seven hydrogen bonds, with bond lengths in the range of (1.89 to 2.60) Å. Atoms H21, H22, H28, O1, O2 and O3 of the ligand and residues GLU194, TYR136, ASN202, LYS245, HIS280 and SER200 of protein 5PNQ participate in the hydrogen bonding. Thus, from the estimated docking parameters, the molecule is also identified as a good inhibitor of 5PNQ.

4. Conclusion

The chemical and biological activities of methyldopa monomer and its dimer form have been investigated. The covalent effects of each bond were determined. It was found that methyldopa forms a dimer via three intramolecular hydrogen bonds with a low energy gap (softness), and a high electrophilicity index. The stability of intermolecular hydrogen bonds in the dimer has been confirmed by NBO analysis with the highest stabilization energy of 21.36 kcal/mol, which corresponds to P(2)→O30 σ*(O1-H26). The high degree of localization of electrons was explored across the bond critical points of C—H, oxygen, and nitrogen atoms, as well as the degree of delocalization of electrons at the RCP. The HOMO-LUMO energy gap was calculated as 5.5364 eV for monomer and 5.0515 eV for dimer. The nucleophilic sites have been explored over oxygen atoms of carbonyl groups in monomer and dimer. Similarly, electrophilic sites have been detected across the hydrogen atom of the hydroxyl group in both monomer and dimer. The binding active sites of the target proteins have been investigated. The binding affinity of the complex ranges from –7.6 to –7.4 kcal/mol. The least value of inhibition constant (2.67 μM) and RMSD (1.18 Å) of 5PNO signifies that it is a good inhibitor for the title molecule. Thus, it is computationally predicted that methyldopa has very good inhibitory properties against the protein, Lysine-specific demethylase 4D-like protein. However, further *in vitro* and preclinical trials are needed to validate the predicted results.

Declaration of Competing Interest

The authors declare that they have no known competing financial interests or personal relationships that could have appeared to influence the work reported in this paper.

Data availability

Data will be made available on request.

Acknowledgments

T. Karthick acknowledges the management of SASTRA Deemed University, Thanjavur, Tamil Nadu, India for providing necessary infrastructure and computational facilities and work was supported by Department of Science and Technology, New Delhi, India under DST-FIST project (Project No. SR/FST/PS-1/2020/135).

Supplementary materials

Supplementary material associated with this article can be found, in the online version, at doi:10.1016/j.molstruc.2023.135518.

References

[1] M. Noei, M. Holoosadi, H. Anaraki-Ardakani, Design of methyldopa structure and calculation of its properties by quantum mechanics, Arab. J. Chem. 10 (2017) S1923–S1937, https://doi.org/10.1016/J.ARABJC.2013.07.021.
[2] A. Prabakaran, S. Muthu, Normal coordinate analysis and vibrational spectroscopy (FT-IR and FT-Raman) studies of (2S)-2-amino-3-(3, 4-dihydroxyphenyl)-2-methylpropanoic acid using ab initio HF and DFT method, Spectrochim. Acta A Mol. Biomol. Spectrosc. 99 (2012) 90–96, https://doi.org/10.1016/j.saa.2012.09.014.
[3] A. Sjoerdsma, A. Vendsalu, K. Engelman, M.D. Watts, Studies on the metabolism and mechanism of action of methyldopa, Circulation 28 (4) (1963) 492–502, https://doi.org/10.1161/01.CIR.28.4.492.
[4] R. Wang, C. Chen, W. Yang, P. Zhou, F. Zhu, H. Xu, G. Hu, W. Sun, W. Shen, Y. Hu, Solubility determination, model correlation and preferential solvation of methyldopa in binary mixed solvents from 278.15 K to 323.15 K, J. Mol. Liq. 363 (2022), 119838, https://doi.org/10.1016/j.molliq.2022.119838.

[5] D.A. Ostrov, A. Alkanani, K.A. McDaniel, S. Case, E.E. Baschal, L. Pyle, S. Ellis, B. Pöllinger, K.J. Seidl, V.N. Shah, S.K. Garg, M.A. Atkinson, P.A. Gottlieb, A. W. Michels, Methyldopa blocks MHC class II binding to disease-specific antigens in autoimmune diabetes, J. Clin. Investig. 128 (5) (2018) 1888–1902, https://doi.org/10.1172/jci97739.

[6] S. Adler, Methyldopa-induced decrease in mental activity, JAMA 230 (10) (1974) 1428–1429, https://doi.org/10.1001/jama.1974.03240100046027.

[7] P.J. Toghill, P.G. Smith, P. Benton, R.C. Brown, H.L. Matthews, Methyldopa liver damage, Br. Med. J. 3 (5930) (1974) 545–548, https://doi.org/10.1136/bmj.3.5930.545.

[8] J.S. Rodman, D.J. Deutsch, S.I. Gutman, Methyldopa hepatitis: a report of six cases and review of the literature, Am. J. Med. 60 (7) (1976) 941–948, https://doi.org/10.1016/0002-9343(76)90564-7.

[9] S. Wang, Z. Wang, C. Hao, Role of intramolecular hydrogen bonding in the excited-state intramolecular double proton transfer (ESIDPT) of calix [4]arene: a TDDFT study, Open Phys. 14 (1) (2016) 602–609, https://doi.org/10.1515/phys-2016-0067.

[10] T. Chaudhary, M.K. Chaudhary, B.D. Joshi, A theoretical study on charge transfer and hyperpolarizability of (S)-2-amino-3-(3, 4-dihydroxyphenyl)-2-methyl-propanoic Acid, JNPS 8 (1) (2022) 16–21, https://doi.org/10.3126/jnphyssoc.v8i1.48280.

[11] K. Sharma, S.P. Sharma, S.C. Lahiri, Spectrophotometric, Fourier transform infrared spectroscopic and theoretical studies of the charge–transfer complexes between methyldopa [(S)-2 amino-3-(3, 4-dihydroxyphenyl)-2-methyl propanoic acid] and the acceptors (chloranilic acid, o-chloranil and dichlorodicyanobenzoquinone) in acetonitrile and their thermodynamic properties, Spectrochim. Acta A Mol. Biomol. Spectrosc. 92 (2012) 212–224, https://doi.org/10.1016/j.saa.2012.02.072.

[12] H. Nourmohamadi, M.D. Esrafili, V. Aghazadeh, A DFT investigation into the effects of As-doping on the electronic structure and electrochemical activity of pyrite (FeS2), J. Mol. Graph. Model. 110 (2022), 108040, https://doi.org/10.1016/j.jmgm.2021.108040.

[13] I. Jomaa, C. Daghar, N. Issaoui, T. Roisnel, H. Marouani, Supramolecular association of (1, 4-phenylenedimethanaminium) bis (perchlorate) monohydrate: a combined experimental and theoretical study, J. Mol. Struct. 1272 (2023), 134212, https://doi.org/10.1016/j.molstruc.2022.134212.

[14] M. Medimagh, C.B. Mleh, N. Issaoui, A.S. Kazachenko, T. Roisnel, O.M. Al-DOSSARY, H. Marouani, L.G. Bousiakoug, DFT and molecular docking study of the effect of a green solvent (water and DMSO) on the structure, MEP, and FMOs of the 1-ethylpiperazine-1, 4-diium bis (hydrogenoxalate) compound, J. Mol. Liq. 369 (2023), 120851, https://doi.org/10.1016/j.molliq.2022.120851.

[15] M. Katoh, M. Katoh, Identification and characterization of JMJD2 family genes in silico, Int. J. Oncol. 24 (6) (2004) 1623–1628.

[16] N. Rappaport, M. Twik, I. Plaschkes, R. Nudel, T. Iny Stein, J. Levitt, M. Gershoni, C.P. Morrey, M. Safran, D. Lancet, Mala Cards: an amalgamated human disease compendium with diverse clinical and genetic annotation and structured search, Nucleic Acids Res. 45 (D1) (2017) D877–D887, https://doi.org/10.1093/nar/gkw1012.

[17] M.J. Frisch, G.W. Trucks, H.B. Schlegel, G.E. Scuseria, J.R. Cheeseman, M.A. Robb, G. Scalmani, V. Barone, B. Mennucci, G.A. Petersson, H. Nakatsuji, M. Caricato, X. Li, H.P. Hratchian, A.F. Izmzylov, J. Bloino, G. Zheng, J.L. Sonnenberg, M. Hada, M. Ehara, K. Toyota, R. Fukuda, J. Ishida, M. Hasegawa, T. Nakajima, Y. Honda, O. Kitao, H. Nakai, T. Vreven, J.A. Montgomery Jr, J.E. Peralta, F. Ogliaro, M. Bearpark, J.J. Heyd, E. Brothers, K.N. Kudin, V.N. Staroverov, R. Kobayashi, J. Normand, A. Raghavachari, A. Rendell, J.C. Burant, S.S. Iyengar, J. Tomasi, M. Cossi, N. Rega, J.M. Millan, M. Klene, J.E. Knox, J.B. Cross, V. Bakken, C. Adamo, J. Jaramillo, R. Gomperts, R.E. Stratmann, O. Yazyev, A.J. Austin, R. Cammi, C. Pomelli, J.W. Ochterski, R.L. Martin, K. Morokuma, V.G. Zakrzewski, G.A. Voth, P. Salvador, J.J. Dannerberg, S. Dapprich, A.D. Daniels, J. Farkas, B. Foresman, J.V. Ortiz, J. Cioslowski, D.J. Fox, Gaussian 09, Revision, Gaussian, Inc., Wallingford CT, 2009.

[18] P. Hohenberg, W. Kohn, Inhomogeneous electron gas, Phys. Rev. B 136 (1964) 864–871, https://doi.org/10.1103/PhysRev.136.B864.

[19] A.D. Becke, A new mixing of Hartree–Fock and local density-functional theories, J. Chem. Phys. 98 (2) (1993) 1372–1377, https://doi.org/10.1063/1.464304, doi.

[20] R.G. Parr, Density functional theory of atoms and molecules. Horizons of Quantum Chemistry, Springer, 1980, pp. 5–15, pagesISBN0199878722.

[21] A. Frisch, A.B. Nielson, A.J. Holder, GaussView User Manual, Gaussian Inc., Pittsburgh, PA, 2000, p. 556.

[22] S.S. Malaganvi, J. Tonannavar, J. Tonannavar, Experimental, DFT dimeric modeling and AIM study of H-bond-mediated composite vibrational structure of Chelidonic acid, Heliyon 5 (5) (2019) e01586, https://doi.org/10.1016/j.heliyon.2019.e01586.

[23] T. Chaudhary, M.K. Chaudhary, B.D. Joshi, M.S.A. de Santana, A.P. Ayala, Spectroscopic (FT-IR, Raman) analysis and computational study on conformational geometry, AIM and biological activity of cephalexin from DFT and molecular docking approach, J. Mol. Struct. 1240 (2021), 130594, https://doi.org/10.1016/j.molstruc.2021.130594.

[24] T.A. Keith, AIMALL version 090201 TK Gristmill software Overland Park, KS.USA (2009). http://aim.tkgristmill.com/.

[25] R.F.W. Bader, S.G. Anderson, A.J. Duke, Quantum topology of molecular charge distributions.1, J. Am. Chem. Soc. 101 (1979) 1389–1395, https://doi.org/10.1021/ja00500a006.

[26] V. Saravanan, A. Rajamani, M. Subramani, S. Ramasamy, Exploring two-dimensional graphene and boron-nitride as potential nanocarriers for cytarabine and clofarabine anti-cancer drugs, Comput. Biol. Chem. 88 (2020), 107334, https://doi.org/10.1016/j.compbiolchem.2020.107334.

[27] T. Lu, F. Chen, Multiwfn: a multifunctional wavefunction analyzer, J. Comput. Chem 33 (5) (2012) 580–592, https://doi.org/10.1002/jcc.22885.

[28] W. Humphrey, A. Dalke, K. Schulten, VMD: visual molecular dynamics, J. Mol. Graph. 14 (1) (1996) 33–38, https://doi.org/10.1016/0263-7855(96)00018-5.

[29] E.R. Johnson, S. Keinan, P. Mori-Sánchez, J. Contreras-García, A.J. Cohen, W. Yang, Revealing non-covalent interactions, J. Am. Chem. Soc. 132 (18) (2010) 6498–6506, https://doi.org/10.1021/ja100936w.

[30] Y. Yang, Hexacoordinate bonding and aromaticity in silicon phthalocyanine, J. Phys. Chem. A 114 (50) (2010) 13257–13267, https://doi.org/10.1021/jp109278v.

[31] R.G. Parr, R.G. Pearson, Absolute hardness: companion parameter to absolute electronegativity, J. Am. Chem. Soc. 105 (26) (1983) 7512–7516, https://doi.org/10.1021/ja00364a005.

[32] R.G. Parr, L.V. Szentpály, S. Liu, Electrophilicity index, J. Am. Chem. Soc. 121 (9) (1999) 1922–1924, https://doi.org/10.1021/ja983494x.

[33] K. Fukui, Science, role of frontier orbitals in chemical reactions, Science 218 (4574) (1982) 747–754, https://doi.org/10.1126/science.218.4574.747.

[34] C. Morell, A. Grand, A. Toro-Labbe, New dual descriptor for chemical reactivity, J. Phys. Chem. A 109 (1) (2005) 205–212, https://doi.org/10.1021/jp046577a.

[35] O. Trott, A.J. Olson, AutoDock Vina: improving the speed and accuracy of docking with a new scoring function, efficient optimization and multithreading, J. Comput. Chem. 31 (2010) 455–461, https://doi.org/10.1002/jcc.21334.

[36] Discovery Studio 4.5 Guide, Accelrys Inc., San Diego, 2009. www.accelrys.com.

[37] V.Y. Tanchuk, V.O. Tanin, A.I. Vovk, G. Poda, A new, improved hybrid scoring function for molecular docking and scoring based on AutoDock and AutoDockVina, Chem. Biol. Drug Des. 87 (4) (2016) 618–625, https://doi.org/10.2174/1570163812666150825110208.

[38] J. Gesteiger, M. Marsili, Iterative partial equalization of orbital electronegativity-a rapid access to atomic charges, Tetrahedron 36 (22) (1980) 3219–3228, https://doi.org/10.1016/0040-4020(80)80168-2.

[39] D. Gfeller, A. Grosdidier, M. Wirth, A. Daina, O. Michielin, V. Zoete, SwissTargetPrediction: a web server for target prediction of bioactive small molecules, Nucleic Acids Res. 42 (W1) (2014) W32–W38, https://doi.org/10.1093/nar/gku293.

[40] P.W. Rose, B. Beran, C. Bi, W.F. Bluhm, D. Dimitropoulos, D.S. Goodsell, A. Prlić, M. Quesada, G.B. Quinn, J.D. Westbrook, J. Young, The RCSB protein data Bank: redesigned website and web services, Nucleic Acids Res. 39 (2010) D392–D401, https://doi.org/10.1093/nar/gkq1021.

[41] A. Sagaama, O. Noureddine, S.A. Brandán, A. Jarczyk-Jędryka, H.T. Flakus, H. Ghalla, N. Issaoui, Molecular docking studies, structural and spectroscopic properties of monomeric and dimeric species of benzofuran-carboxylic acids derivatives: DFT calculations and biological activities, Comput. Biol. Chem. 87 (2020), 107311, https://doi.org/10.1016/j.compbiolchem.2020.107311.

[42] N. Issaoui, H. Ghalla, S. Muthu, H.T. Flakus, B. Oujia, Molecular structure, vibrational spectra, AIM, HOMO–LUMO, NBO, UV, first order hyperpolarizability, analysis of 3-thiophenecarboxylic acid monomer and dimer by Hartree-Fock and density functional theory, Spectrochim. Acta A Mol. Biomol. Spectrosc. 136 (2015) 1227–1242, https://doi.org/10.1016/j.saa.2014.10.008.

[43] R.F.W. Bader, Atoms in Molecules: A Quantum Theory, Oxford University Press, Oxford, U.K., 1990. ISBN: 9780198558651.

[44] P.S.V. Kumar, V. Raghavendra, V. Subramanian, Bader's theory of atoms in molecules (AIM) and its applications to chemical bonding, J. Chem. Sci. 128 (10) (2016) 1527–1536, https://doi.org/10.1007/s12039-016-1172-3.

[45] E. Espinosa, I. Alkorta, J. Elguero, E. Molins, From weak to strong interactions: a comprehensive analysis of the topological and energetic properties of the electron density distribution involving X–H··· F–Y systems, J. Chem. Phys. 117 (12) (2002) 5529–5542, https://doi.org/10.1063/1.1501133.

[46] D. Cremer, E. Kraka, Chemical bonds without bonding electron density-does the difference electron-density analysis suffice for a description of the chemical bond? Angew. Chem. Int. Ed. Engl. 23 (38) (1984) 627–628, https://doi.org/10.1002/anie.198406271, 23.

[47] I. Rozas, I. Alkorta, J. Elguero, Behavior of ylides containing N, O, and C atoms as hydrogen bond acceptors, J. Am. Chem. Soc. 122 (45) (2000) 11154–11161, https://doi.org/10.1021/ja0017864.

[48] M. Salah, M.E. Belghiti, A.O. Aitouna, A. Zeroual, S. Jorio, H.E.A. Abdellaoui, H. E. Hadki, K. Marakchi, N. Komiha, MEDT study of the 1, 3-DC reaction of diazomethane with psilostachyin and investigation about the interactions of some pyrazoline derivatives with protease (Mpro) of nCoV-2, J. Mol. Graph. Model. 102 (2021), 107763, https://doi.org/10.1016/j.jmgm.2020.107763.

[49] A.D. Becke, K.E. Edgecombe, A simple measure of electron localization in atomic and molecular systems, J. Chem. Phys. 92 (9) (1990) 5397–5403, https://doi.org/10.1063/1.458517.

[50] H.L. Schmider, A.D. Becke, Chemical content of the kinetic energy density, J. Mol. Struct. THEOCHEM. 527 (1–3) (2000) 51–61, https://doi.org/10.1016/s0166-1280(00)00477-2.

[51] J.C. Prasana, S. Muthu, C.S. Abraham, Wavefunction analysis, charge transfer and molecular docking studies on famciclovir and entecavir: potential anti-viral drugs, Chem. Data Collect. 26 (2020), 100353, https://doi.org/10.1016/j.cdc.2020.100353.

[52] S. Celik, E. Tanıs, Toxic potential of poly-hexamethylenebiguanide hydrochloride (PHMB): a DFT, AIM and NCI analysis study with solvent effects, Comput. Theor. Chem. 1212 (2022), 113709, https://doi.org/10.1016/j.comptc.2022.113709.

[53] F. Weinhold, C.R. Landis, Natural bond orbitals and extensions of localized bonding concepts, Chem. Edu. Res. Pract. 2 (2) (2001) 91–104, https://doi.org/10.1039/b1rp90011k.
[54] F. Weinhold, C.R. Landis, Valency and Bonding: A Natural Bond Orbital Donor-Acceptor Perspective, Cambridge University Press, 2005, https://doi.org/10.5860/choice.43-4035.
[55] M.M. Kadhim, E.A. Mahmood, V. Abbasi, M.R.P. Heravi, S. Habibzadeh, S. Mohammadi-Aghdam, S.M. Shoaei, Theoretical investigation of the titanium-nitrogen heterofullerenes evolved from the smallest fullerene, J. Mol. Graph. Model. 117 (2022), 108269, https://doi.org/10.1016/j.jmgm.2022.108269.
[56] F. Basha, F.L.A. Khan, S. Muthu, M. Raja, Elaborated molecular structure, molecular docking and vibrational spectroscopic investigation of N-((4-aminophenyl) sulfonyl) benzamide with Density functional theory, Chem. Data Collect. 31 (2021), 100609, https://doi.org/10.1016/j.cdc.2020.100609.
[57] B.D. Joshi, A. Srivastava, P. Tandon, S. Jain, A.P. Ayala, A combined experimental (IR, Raman and UV–Vis) and quantum chemical study of canadine, Spectrochim. Acta A Mol. Biomol. Spectrosc. 191 (2018) 249–258, https://doi.org/10.1016/j.saa.2017.10.008.
[58] A. Hanif, R. Kiran, R.A. Khera, A. Ayoub, K. Ayub, J. Iqbal, Tuning the optoelectronic properties of superalkali doped phosphorene, J. Mol. Graph. Model. 107 (2021), 107973, https://doi.org/10.1016/j.jmgm.2021.107973.
[59] R. Vijayaraj, V. Subramanian, P.K. Chattaraj, Comparison of global reactivity descriptors calculated using various density functionals: a QSAR perspective, J. Chem. Theory Comput. 5 (10) (2009) 2744–2753, https://doi.org/10.1021/ct900347f.
[60] V. Vidhya, A. Austine, M. Arivazhagan, Experimental approach, theoretical investigation and molecular docking of 2-chloro-5-fluoro phenol antibacterial compound, Heliyon 6 (11) (2020) e05464, https://doi.org/10.1016/j.heliyon.2020.e05464.
[61] A. Shafi, R.D.T. Sathyamurthy, J. Seetharaman, M. Sambanthan, R. Murugesan, S. Sundaram, R.B. Ramarathinam, Molecular docking, quantum chemical computational and vibrational studies on bicyclic heterocycle "6-nitro-2, 3-dihydro-1, 4-benzodioxine: anti-cancer agent, Comput. Biol. Chem. 86 (2020), 107226, https://doi.org/10.1016/j.compbiolchem.2020.107226.
[62] A.S.L.I. Eşme, S.G. Sağdınç, Spectroscopic (FT–IR, FT–Raman, UV–Vis) analysis, conformational, HOMO-LUMO, NBO and NLO calculations on monomeric and dimeric structures of 4–pyridazinecarboxylic acid by HF and DFT methods, J. Mol. Struct. 1147 (2017) 322–334, https://doi.org/10.1016/j.molstruc.2017.06.110.
[63] A. Rasool, S. Zahid, N. Alfryyan, A.R. Ayub, K. Ayub, M.S. Akhter, J. Iqbal, M.S. Al-Buriahi, Remarkable nonlinear optical properties of gold cluster doped graphyne (GY): a DFT study, J. Mol. Graph. Model. 114 (2022), 108204, https://doi.org/10.1016/j.jmgm.2022.108204.
[64] J.S. Murray, K.D. Sen, Molecular electrostatic potentials: concepts and applications. Theoretical and Computational Chemistry, Elsevier, 1996. ISBN: 0444823530.
[65] S. Muthu, E.I. Paulraj, Spectroscopic and molecular structure (monomeric and dimeric structure) investigation of 2-[(2-hydroxyphenyl) carbonyloxy] benzoic acid by DFT method: a combined experimental and theoretical study, J. Mol. Struct. 1038 (2013) 145–162, https://doi.org/10.1016/j.molstruc.2013.01.043.
[66] A. Bendjeddou, T. Abbaz, A. Gouasmia, D. Villemin, Molecular structure, HOMO-LUMO, MEP and Fukui function analysis of some TTF-donor substituted molecules using DFT (B3LYP) calculations, Int. Res. J. Pure Appl. Chem. 12 (1) (2016) 1–9, https://doi.org/10.9734/IRJPAC/2016/27066.
[67] G.M. Morris, M. Lim-Wilby, Molecular docking. Molecular Modeling of Proteins, Humana Press, 2008, pp. 365–382. ISBN: 978-1-58829-864-5.
[68] B.K. Shoichet, I.D. Kuntz, D.L. Bodian, Molecular docking using shape descriptors, J. Comput. Chem. 13 (3) (1992) 380–397, https://doi.org/10.1002/JCC.540130311.
[69] R. Srivastava, S.K. Gupta, F. Naaz, P.S.S. Gupta, M. Yadav, V.K. Singh, A. Singh, M. K. Rana, S.K. Gupta, D. Schols, R.K. Singh, Alkylated benzimidazoles: design, synthesis, docking, DFT analysis, ADMET property, molecular dynamics and activity against HIV and YFV, Comput. Biol. Chem. 89 (2020), 107400, https://doi.org/10.1016/j.compbiolchem.2018.05.021.
[70] M.K. Chaudhary, A. Srivastava, K.K. Singh, P. Tandon, B.D. Joshi, Computational evaluation on molecular stability, reactivity, and drug potential of frovatriptan from DFT and molecular docking approach, Comput. Theor. Chem. 1191 (2020), 113031, https://doi.org/10.1016/j.comptc.2020.113031.

Journal of Institute of Science and Technology, 27(1), 83-92 (2022)
ISSN: 2467-9062 (print), e-ISSN: 2467-9240
https://doi.org/10.3126/jist.v27i1.46361

Research Article

ELECTRONIC, THERMODYNAMIC PROPERTIES, NONLINEAR OPTICAL RESPONSES, AND MOLECULAR DOCKING STUDIES ON CEPHALEXIN

Tarun Chaudhary[1], Bhawani Datt Joshi[2]
[1]Central Department of Physics, Tribhuvan University, Kirtipur, Kathmandu, Nepal
[2]Department of Physics, Tribhuvan University, Siddhanath Science Campus, Mahendranagar, 10406, Nepal
**Corresponding author: bhawani.joshi@snsc.tu.edu.np, pbdjoshi@gmail.com*
*(**Received**: September 18, 2021; **Revised**: April 02, 2022; **Accepted**: May 26, 2022)*

ABSTRACT
The topology analysis of electron localization function (ELF), localized orbital locator (LOL), the study of nonlinear optical properties, thermal properties, and biological activities of cephalexin have been performed using DFT/B3LYP and employing 6-311++G(d,p) basis sets. The Mulliken atomic charge on atoms has been calculated. The quantities describing nonlinear optical (NLO) properties like molecular polarizability (α), first hyperpolarizability (β), and second hyperpolarizability (γ) were comparable to the values of urea. The computed value of the second hyperpolarizability was found to be negative, which is an important feature for the system of controllable NLO devices. The thermodynamic properties like heat capacity (S), enthalpy (H), and entropy (S) are positively correlated with the temperature. Further, the title molecule shows good potentiality for binding with the selected target protein matrix metalloproteinase-2.

Keywords: Cephalexin, ELF, LOL, nonlinear optical properties, thermodynamics, molecular docking

INTRODUCTION
Cephalexin,C16H17N3O4S, is an antibiotic from the first-generation cephalosporin (Nguyen and Graber, 2020). It is active against most gram-positive and many gram-negative bacteria (Speight *et al.*, 1972). Cephalexin, a white to cream-colored crystalline powder, is stable below a mild acidic condition (Manelli, 1975). It is used to treat respiratory tract infections, Gonorrhoea, urinary tract infections, and several infections due to susceptible organisms (Bailey *et al.*, 1970; Speight *et al.*, 1972).

The recent work on cephalexin reflects the DFT study on structural, chemical, and spectroscopic properties. Cephalexin at normal temperature has two stable conformers (Chaudhary *et al.*, 2021). Moreover, organic molecules exhibit significant non-linear optical properties (NLO) (Kariper, 2017) and compounds with nitrogen and Sulphur contribute to various biological activities (Joshi *et al.*, 2018). Thus, the present work deals with non-linear optical properties, topology analysis, thermal properties, and biological activities. The electron localization function (ELF) and localized orbital locator (LOL) have been plotted to depict the electron localization. The quantities like static dipole moment, molecular polarizability, first hyperpolarizability, and second hyperpolarizability have been calculated. Further, these properties are also compared with the value of standard, conventional molecule, urea.

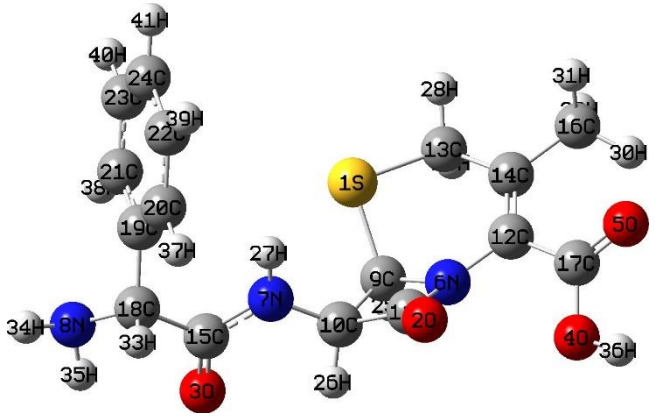

Figure 1 Optimized structure of cephalexin.

The correlation of thermodynamic properties like heat capacity, enthalpy, entropy, and temperature is studied. Ultimately, the non-covalent interaction of cephalexin with matrix metalloproteinase-2 has been investigated using a molecular docking approach. The optimized structure of cephalexin is shown in Fig. 1.

MATERIALS AND METHODS

Computational and theoretical details

The software package Gaussian 09 (Frisch *et al.*, 2009) was used for various computational studies in the present work. The density functional theory (DFT) using the B3LYP exchange correlation function with a basis set 6-311++(d,p) has been used for the calculation (Becke, 1993;Parr, 1980). Further, GaussView 05 (Dennington *et al.*, 2009) was used for visualizing the optimized structure of the title molecule. The topology study, Electron Localization Function (ELF), and Localized Molecular Orbital (LOL) have been performed using Multiwfn 3.4.1 software (Lu and Chen, 2012). The ELF function is defined by the equation (Silvi & Savin, 1994; Yang, 2010).

$$\text{ELF}=\frac{1}{1+\left(\frac{\text{D}}{\text{D}_\text{h}}\right)^2} \quad (1)$$

With $\text{D}=\frac{1}{2}\sum_i|\nabla\varphi_i|^2-\frac{1}{8}\frac{|\nabla\rho|^2}{\rho}$

and $\text{D}_\text{h}=\frac{3}{10}(3\pi^2)^{2/3}\rho^{5/3}$

Where, D and D_h represent excess kinetic energy and reference value, respectively.

The molecular polarizability, electric dipole moment, first hyperpolarizability, and second hyperpolarizability have been computed using a finite field approach employing a 6311++G(d,p) basis set. Using the finite field, the energy in the static electric field is expanded in terms of the Taylors series (Kumar *et al.*, 2017).

$$\text{E(F)}=\text{E(0)}-\sum_i\mu_i F_i-\frac{1}{2}\sum_{i,j}\alpha_{ij}F_iF_j-\frac{1}{6}\sum_{i,j}\beta_{i,j,k}F_iF_jF_k-\frac{1}{24}\sum_{i,j,k,l}\gamma_{ijkl}F_iF_jF_kF_l\ldots \quad (2)$$

Here, E(0) is the total energy in the absence of an electrical field, and the quantities $\mu_i, \alpha_{ij}, \beta_{ijk} and \gamma_{ijkl}$ represent the dipole moment, the polarizability, the first hyperpolarizability, and the second hyperpolarizability, respectively. The subscripts i, j, k, and l represent the Cartesian coordinates. The subscripts i, j, k, and l represent the Cartesian coordinates. The total static dipole moment(μ_0), mean polarizability ($|\alpha_0|$), anisotropy of polarizability ($\Delta\alpha$), first hyperpolarizability (β_0), and second hyperpolarizability (γ_0) that describe the non-linear optical phenomena of the molecule can be determined by the equations (Kumar *et al.*, 2017; Joshi *et al.*, 2013) as follows:

$$\mu_0=\left(\mu_x^2+\mu_y^2+\mu_z^2\right)^{1/2} \quad (3)$$

$$|\alpha_0|=\frac{1}{3}\left(\alpha_{xx}+\alpha_{yy}+\alpha_{zz}\right) \quad (4)$$

$$\Delta\alpha=2^{-1/2}\left[\left(\alpha_{xx}-\alpha_{yy}\right)^2+\left(\alpha_{yy}-\alpha_{zz}\right)^2+(\alpha_{zz}-\alpha_{xx})^2+6\alpha_{xx}^2\right]^{1/2} \quad (5)$$

$$\beta_0=\left[\left(\beta_{xxx}+\beta_{xyy}+\beta_{xzz}\right)^2+\left(\beta_{yyy}+\beta_{xxy}+\beta_{yzz}\right)^2+\left(\beta_{zzz}+\beta_{xxz}+\beta_{yyz}\right)^2\right]^{1/2} \quad (6)$$

$$\gamma_0=\frac{1}{5}\left[\gamma_{xxxx}+\gamma_{yyyy}+\gamma_{zzzz}+2(\gamma_{xxyy}+\gamma_{yyzz}+\gamma_{zzxx})\right] \quad (7)$$

The dipole moment, molecular polarizability, first hyperpolarizability, and second hyperpolarizability are first rank (vector), second rank, third rank, and fourth rank tensors, respectively.

The Gaussian 09 at the B3LYP/6-311+G(d,p) level, has been used to compute thermodynamic quantities like entropy, heat capacity, and enthalpy in the gas phase. The thermodynamic contributions of translational motion, rotational motion, electronic motion, and vibrational motion are obtained in terms of the partition function, q(V,T). The given equations (Ochterski, 2000) are used to determine the various thermodynamic quantities.

$$Total\ entropy\ , S_{total}=S_{translational}+S_{rotational}+S_{vibrational}+S_{electronic} \quad (8)$$

$$Total\ internal\ energy, E_{total}=E_{translational}+E_{rotational}+E_{vibrational}+E_{electronic} \quad (9)$$

$$Total\ heat\ capacity, C_{total}=C_{translational}+C_{rotatonal}+C_{vibrational}+C_{electronic} \quad (10)$$

$$Corrected\ enthalpy, H_{corrrected}=E_{total}+k_BT \quad (11)$$

where, different entropy contributions from translational, rotational, vibrational and electronic motion are

$$S_{translational}=R\left(lnq_t+1+\frac{3}{2}\right),$$

$$S_{rotational}=R(lnq_r+\frac{3}{2}), S_{vibrational}=R\sum_K\left(\frac{\Theta_{v,K/T}}{e^{\Theta_{v,K/T}}-1}-\ln\left(1-e^{-\Theta_{v,K/T}}\right)\right)$$

and $E_{electronic}=(\ln q_e+0)$.

Similarly, internal thermal energy and heat capacity contributions due to different motions are

$$E_{translational}=\frac{3}{2}RT, \quad E_{rotatonal}=RT,$$

$$E_{vibrational}=R\sum_K\Theta_{v,K/T}\left(\frac{1}{2}-\frac{1}{e^{\Theta_{v,K/T}}-1}\right)$$

and $C_{translational}=\frac{3}{2}R, \quad C_{rotatonal}=R,$

$$C_{vibrational}=R\sum_K\Theta_{v,K/T}\left(\frac{\Theta_{v,K/T}}{e^{-\Theta_{v,K/T}}-1}\right)^2.$$

The electronic contribution term for both thermal energy and heat capacity is zero.

The study of intermolecular non-covalent interactions between target proteins and cephalexin, the flexible-rigid blind docking, has been performed using AutoDockVina software (Trott and Olson, 2010). The result of AutoDockVina has been visualized and interpreted with the help of bio visualizer software (Studio, 2009) Generally, the binding affinity of a docked complex is determined on the basis of the scoring function. The scoring function for AutoDockVina can be obtained using the equation (Tanchuk *et al.*, 2016).

$$\Delta G_{\text{binding}}=\Delta G_{\text{H-bond}}+\Delta G_{\text{hydrophobic}}+\Delta G_{\text{repulsion}}+\Delta G_{gauss}+\Delta G_{\text{AutoDock Vina score}} \quad (12)$$

whereΔG_{H-bond} represents the change in the binding energy due to hydrogen bond, $\Delta G_{hydrophobic}$, due to hydrophobic interaction,ΔG_{gauss} ($gauss_1(d) = e^{-(d/0.5)^2}$ and $gauss_2(d) = e^{-((d-3)/2)^2}$), due to steric effects, $\Delta G_{repulsion}$, due to repulsion and $\Delta G_{AutoDock\ Vina\ score}$, due to rotational bonds penalty.

RESULTS AND DISCUSSION

ELF and LOL

Electron localization function (ELF) and localized orbital locator (LOL) are described on the basis of electron density by Becke and Edgecombe (Becke and Edgecombe, 1990; Schmider and Becke, 2002). The ELF and LOL display similar interpretations, however, ELF is based on kinetic energy density and the LOL on gradients of localized orbital locators (Chaudhary *et al.*, 2021). ELF measures Pauli repulsion effects (Abraham *et al.*, 2019).

The quantitative values of ELF and LOL come down in the range of 0-1 where the degree of localization for electrons is high for values greater than 0.5 and the degree of delocalization is high for the value less than 0.5 (Chaudhary *et al.*, 2021). The Multiwfn software has been used to plot the ELF and LOL maps of the title molecule. The ELF and LOL plot of the title molecule have been shown in Figs. 2 and 3. In the ELF and LOL, the red region represents the localized electrons, and the Blue region represents the delocalized electrons. The red zone between every two atoms represents the bond critical point (BCP).

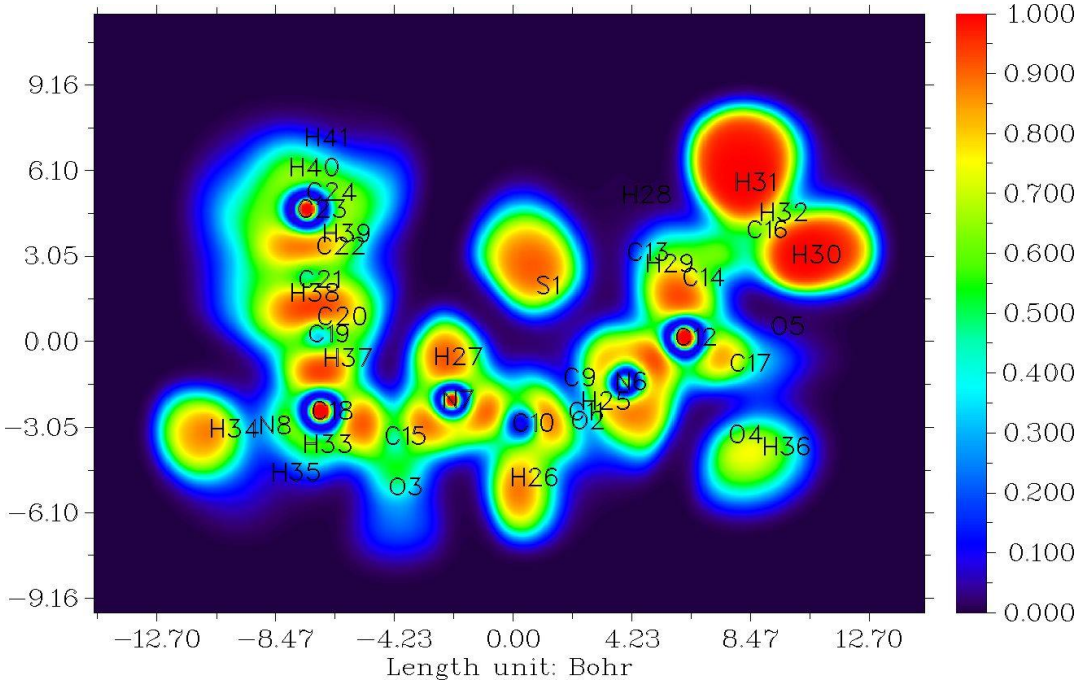

Figure 2 Electron localization function (ELF) of cephalexin.

The red zone across nitrogen and oxygen represents the lone pair associated with them. Similarly, high electron localization is depicted across hydrogen atoms due to maximum Pauli repulsion. On the other hand, a blue color zone is found across non-hydrogen heavy atoms. The blue color, at the center of the atoms, represents the atomic shell and the ring-like structures indicate the electron delocalization of electrons between core and valence electrons.

Mulliken charges

Mulliken population analysis is complementary to molecular electrostatic potential (MEP) and it provides the net atomic population in the molecule (Kumar *et al.*, 2017). Atomic charges affect different molecular properties, including dipole moment, polarizability and hyperpolarizability, and further help in understanding ionization potential and chemical potential (Abraham *et al.*, 2017). The Mulliken charge associated with various atoms of cephalexin has been obtained using the B3LYP/6-311++G(d,p) level of theory. The calculated Mulliken charges of various atoms of the title compound is illustrated in Table 1 and presented by a simple bar diagram in Fig. 4. The atomic charge on all hydrogen atoms and atoms N6, N7, C9, C12, C14, C19, and C21 have positive charges (0.1596-0.5247|e|) and all the remaining atoms have negative charges. The carbon atom C13 has the highest magnitude of negative atomic charge (–0.9247|e|) since it is attached to less electronegative atom S1. The other atoms like O2, O3, O4, O5 have atomic charges in the range of –0.1704|e| to –0.3149|e| and N8 has –0.3104|e|. The net negative charge on oxygen atoms (electron donor) and the positive charge on hydrogen atoms have a significant role in intermolecular hydrogen bonding as observed in the section on molecular docking.

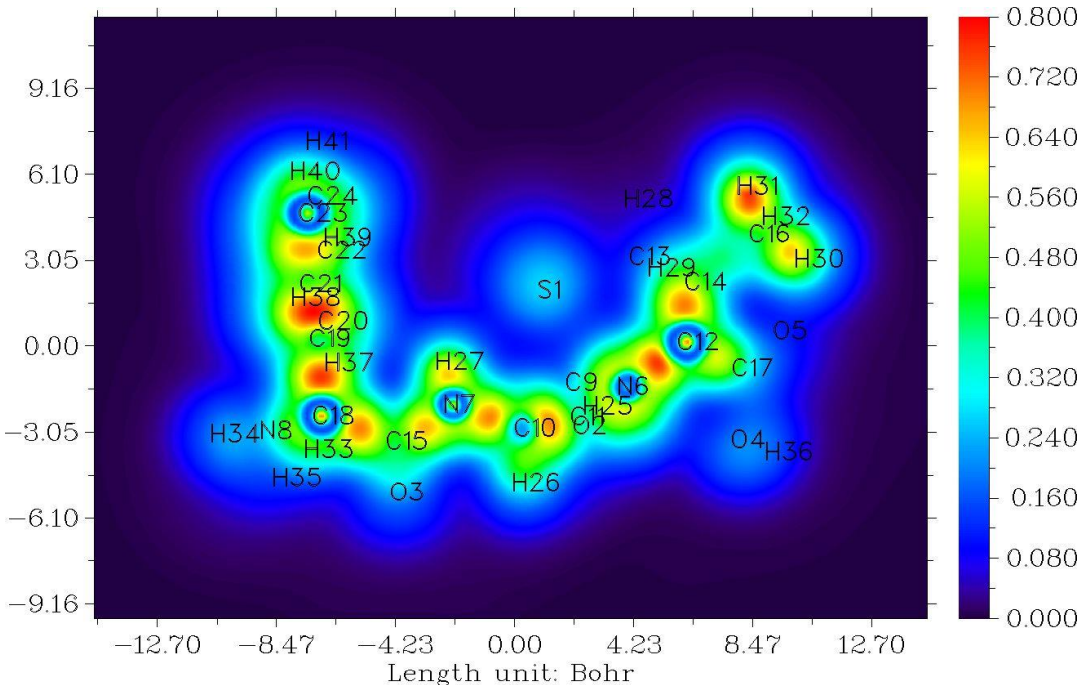

Figure 3 Orbital localization function (LOL) of cephalexin.

Mulliken population analysis is complementary to molecular electrostatic potential (MEP) and it provides the net atomic population in the molecule (Kumar *et al.*, 2017). Atomic charges affect different molecular properties, including dipole moment, polarizability and hyperpolarizability, and further help in understanding ionization potential and chemical potential (Abraham *et al.*, 2017). The Mulliken charge associated with various atoms of cephalexin has been obtained using the B3LYP/6-311++G(d,p) level of theory. The calculated Mulliken charges of various atoms of the title compound is illustrated in Table 1 and presented by a simple bar diagram in Fig. 4. The atomic charge on all hydrogen atoms and atoms N6, N7, C9, C12, C14, C19, and C21 have positive charges (0.1596-0.5247|e|) and all the remaining atoms have negative charges. The carbon atom C13 has the highest magnitude of negative atomic charge (–0.9247|e|) since it is attached to less electronegative atom S1. The other atoms like O2, O3, O4, O5 have atomic charges in the range of –0.1704|e| to –0.3149|e| and N8 has –0.3104|e|. The net negative charge on oxygen atoms (electron donor) and the positive charge on hydrogen atoms have a significant role in intermolecular hydrogen bonding as observed in the section on molecular docking.

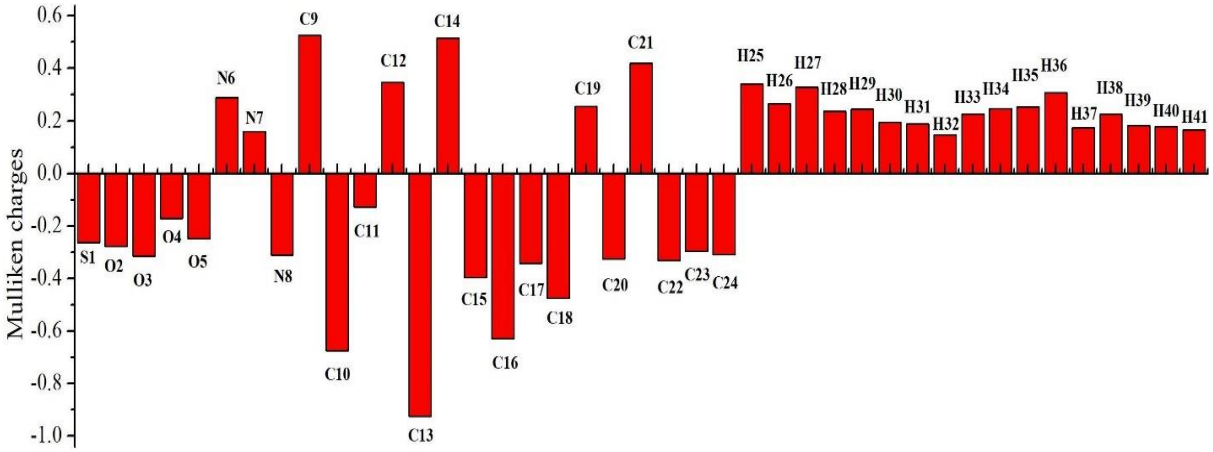

Figure 4 Calculated Mulliken charges of cephalexin.

Table 1: Mulliken charges calculated at B3LYP/6-311++G(d,p) level of theory.

Atom	Charges |e|	Atom	Charges |e|	Atom	Charges |e|	Atom	Charges |e|
S 1	–0.2627	C 12	0.3474	C 23	–0.2968	H 34	0.2467
O 2	–0.2766	C 13	–0.9247	C 24	–0.3093	H 35	0.2539
O 3	–0.3149	C 14	0.5152	H 25	0.3406	H 36	0.3076
O 4	–0.1704	C 15	–0.3956	H 26	0.2647	H 35	0.2539
O 5	–0.2480	C 16	–0.6283	H 27	0.3280	H 36	0.3076
N 6	0.2893	C 17	–0.3411	H 28	0.2361	H 37	0.1741
N 7	0.1596	C 18	–0.4754	H 29	0.2440	H 38	0.2266
N 8	–0.3104	C 19	0.2556	H 30	0.1944	H39	0.1815
C 9	0.5247	C 20	–0.3248	H 31	0.1888	H40	0.1780
C 10	–0.6755	C 21	0.4194	H 32	0.1468	H41	0.1664
C 11	-0.1275	C 22	-0.3326	H 33	0.2252		

NLO properties

The nonlinear optics, in the presence of electromagnetic fields give rise to new magnetic fields with different frequency, phase and other physical properties (Joshi *et al.*, 2013). The energy of the system in the presence of an electric field is the function of the electric fields (Issaoui *et al.*, 2015). The delocalization of π electrons in the molecule deals with the NLO properties of the system (Kariper, 2017). In the last few years, NLO properties have been of great interest due to their potential applications in telecommunication, data storage, optical signal processing, etc. (Koparir, 2013; Joshi, 2016). The dipole moment (μ_0), mean polarizability $|\alpha_0|$, anisotropy of polarizability ($\Delta\alpha$), first hyperpolarizability (β_0), and second hyperpolarizability (γ_0) of cephalexin are illustrated in Table 2. The calculated value of μ_0, $|\alpha_0|$, $\Delta\alpha$, β_0, and γ_0 are 3.1362 Debye, 3.1362 Debye, 21.4940 $*10^{-24}$esu, 36.0946$*10^{-24}$esu, 0.4440$*10^{-30}$esu and –0.12849$*10^{-35}$esu. Urea is the standard, conventional molecule which is used to institute the threshold value for the comparative study of NLO properties of different molecules (Abraham *et al.*, 2017). The dipole moment of the title molecule is higher than the value of urea (1.3732 Debye). However, the first hyperpolarizability (β_0) is comparable to the value of urea (($0.3728*10^{-30}$esu), so the molecule exhibits significant NLO properties. On the other hand, the value of second hyperpolarizability(γ_0) is negative. In quantum optics, the negative value of $\gamma_0$is very important because it causes a defocusing effect of an incident beam and such molecular systems can be good candidates for systems of controllable nonlinear properties (Nakano *et al.*, 1996; Kumar *et al.*, 2017).

Table 2: The calculated dipole moment (μ_0), mean polarizability$|\alpha_0|$, anisotropy of polarizability ($\Delta\alpha$) first hyperpolarizability (β_0),and second hyperpolarizability(γ_0)of cephalexin.

Dipole moment (Debye)	Polarizability ($*10^{-24}$esu)	First Hyperpolarizability ($*10^{-30}$esu)	Second hyperpolarizability ($*10^{-35}$esu)
μ_x =0.5882	α_{xx} = –140.4955	β_{xxx} = 14.7286	γ_{xxxx} = –9060.7026
μ_y =2.9643	α_{xy}= –2.4790	β_{xxy}= –40.9736	γ_{yyyy}= –2271.7508
μ_z =–0.8380	α_{yy}= –143.0230	β_{xyy}= 22.0851	γ_{zzzz} = –1421.9954
μ_0 =3.1362	α_{xz}= –17.9694	β_{yyy}= 32.0184	γ_{xxyy} = –1683.9580
μ_0(Urea) =1.3732	α_{yz}= –5.6946	β_{xxz}= –7.2215	γ_{xxzz} = –1756.0085
	α_{zz}= –151.5867	β_{xyz}= –17.3457	γ_{yyzz} = –611.3782
	$\|\alpha_0\|$ = 21.4940	β_{yyz}= 12.7285	γ_0 = –0.12849
	$\Delta\alpha$ =36.0946	β_{xzz}= 12.0654	
	$\Delta\alpha$(Urea) = 9.7710	β_{yzz}= 6.9303	
		β_{zzz}=10.2229	
		β_0= 0.4440	
		β_0(Urea) = 0.3728	

Thermodynamic properties

The temperature has a direct effect on the chemical reactivity and the mechanism of drug action (Basha *et al.*, 2019; Choudhary *et al.*, 2014). The thermodynamic parameters are estimated from the Boltzmann distribution and partition function (Singh *et al.*, 2016). Thermodynamic properties like heat capacity, enthalpy,

entropy, zero-point energy, total energy, and rotational constant of cephalexin have been illustrated in Table 3. To study the thermal behavior of cephalexin, the temperature varied from 50 K to 600k, and the respective values of thermodynamic quantities are noted. Hence, the quadratic equations, from 13 to15 have been obtained from the second-order polynomial fit between the thermodynamic quantities (a dependent variable) and the temperature (an independent variable). The graph showing quadratic fit in Fig. 5 demonstrates the positive correlation of enthalpy (H_m^o), heat capacity ($C_{p,m}^o$), entropy (S_m^o), and temperature. The value of R^2 for H_m^o, $C_{p,m}^o$ and S_m^o is obtained as 1, 0.9996, and 0.9994, respectively. The quantitative value of the thermodynamic parameters increases with the increase in temperature, which is due to the increase in vibrational motion with an increase in temperature. Furthermore, the specific heat capacity of the title compound at room temperature (298.15 K) has been calculated to be 1022.07J/kg-K (355.06 J/Mol-K), which is slightly smaller than the value, 1322.77 J/kg-K of amino acid, glycine (Spink & Wadsö, 1975). However, the specific heat capacity of cephalexin is very close to the estimated value (960.36 J/kg-K) of a biologically active molecule, alkaloid aristolochic acid I (Joshi *et al.*, 2013).

$$H_m^o = 833.7112 + 0.0629T + 4.7996 \times 10^{-4}T^2 \ (R^2 = 1) \quad (13)$$

$$C_{p,m}^o = 31.7992 + 1.2119T - 4.1214 \times 10^{-4}T^2 \quad (R^2 = 0.9996) \quad (14)$$

$$S_m^o = 269.5741 + 1.5674T - 5.1161 \times 10^{-4}T^2 \quad (R^2 = 0.9994) \quad (15)$$

The above equations can also be further utilized during the study of the interaction of the title molecule with another compound. They help to predict the Gibbs free energy and then the spontaneity of the reaction. In addition, these give useful details that can be used for the analysis of thermodynamic energies and can be used to estimate the direction of chemical reaction using the second law of thermodynamics in the thermochemical field (Joshi *et al.*, 2013).

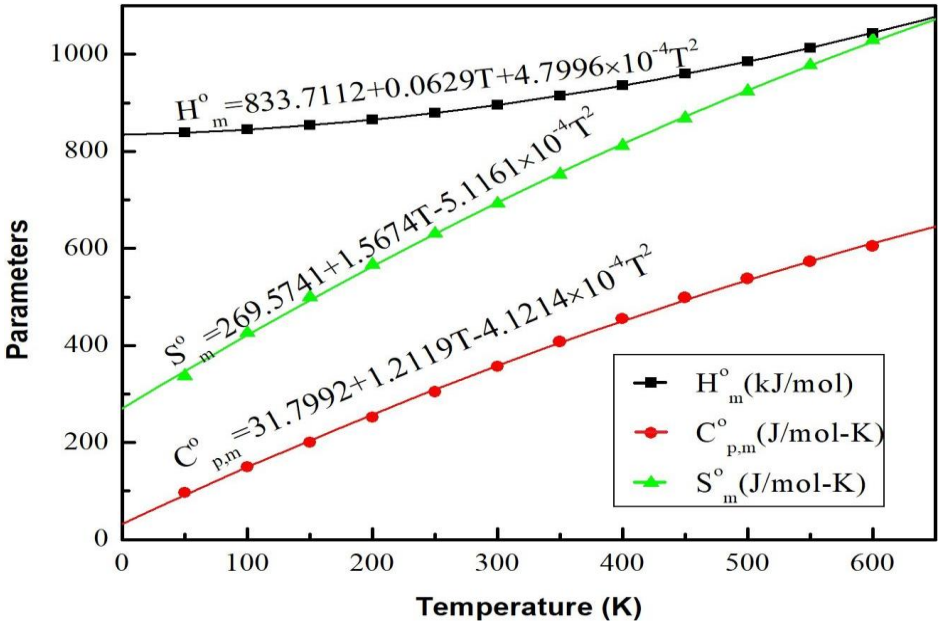

Figure 5 Correlation of enthalpy, heat capacity, entropy and temperature for cephalexin.

Table 3: Thermodynamic parameters of cephalexin at various temperature.

Temperature (K)	Enthalpy (kJ/mol)	Heat capacity (J/mol-K)	Entropy (J/mol-K)	Zero-point energy (Joules/mol)	Total energy (eV)
50	838.6870	97.00186	336.72	835576	–40371.2566
100	844.8877	149.9211	426.3036	835576.1	–40371.2566
150	853.6448	200.4513	500.0298	835576	–40371.2566
200	864.9458	251.7471	567.0743	835576.1	–40371.2566
250	878.8450	304.2981	630.7296	835576.1	–40371.2566
300	895.3760	356.8952	692.3934	835576.1	–40371.2566
350	914.5011	407.7141	752.5635	835574.9	–40371.2566
400	936.0947	455.2778	811.2483	835576	–40371.2566
450	959.9644	498.8081	868.4059	835576	–40371.2566
500	985.9052	538.0959	923.7895	835580.2	–40371.2566
550	1013.7037	573.3293	977.6627	835576.1	–40371.2566
600	1043.1758	604.8725	1029.641	835576.1	–40371.2566

Molecular docking

In medicinal chemistry, for entire potential drug targets, the study of drug-protein interaction can be performed either using an experimental method or a computational method. Molecular docking conducted on AutoDockVina is a popular computational technique that is used to calculate the quantitative parameters of ligand and protein interaction (Ferreira da Costa *et al.*, 2018). It helps to anticipate the binding mode and affinity between ligand and receptor protein interactions. In the present work, for the docking analysis, the target protein (matrix metalloproteinase-2) (MMP-2) has been predicted with the help of online software, the Swiss Target Prediction (Daina *et al.*, 2019). The invasive features of certain human malignancies, such as colon and breast tumors, are influenced by matrix metalloproteinases (Kanayama *et al.*, 1998) MMP-2 has a key role in the pathophysiology of inflammatory and cancerous disorders in a variety of organs, including the lungs(Chakrabarti and Patel, 2005). Hence, docking analysis has been performed with this particular protein to know the biological activities of cephalexin with this protein. The PDB code was downloaded from the RSCB protein data bank (Rose *et al.*, 2010).

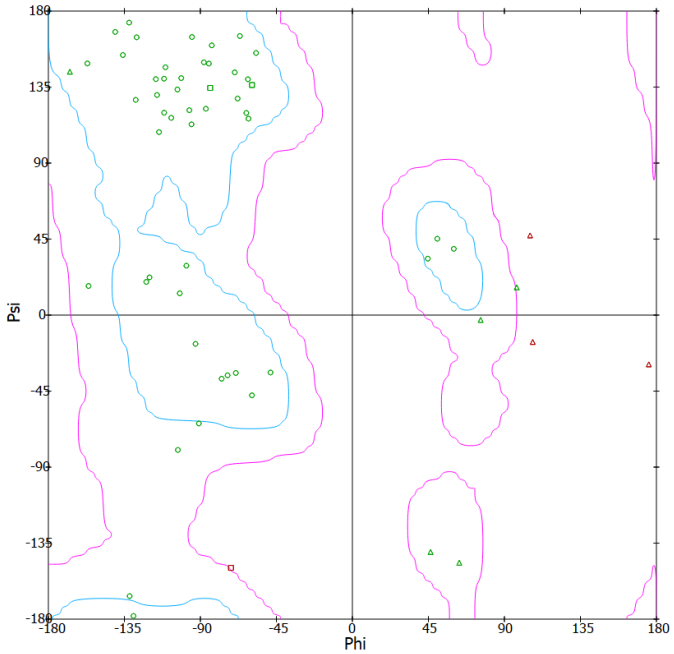

Figure 6 Ramachandran plots of protein 1J7M

The Ramachandran plots in Fig. 6 demonstrate the phi-psi torsional angles of the residues of the protein. It shows that maximum residues lie inside the blue line the, allowed region. The ligand molecule cephalexin was prepared by optimizing it using Gaussian 09 at B3LYP/6-311++G(d,p) level. Thus, the most stable state corresponding to the minimum ground state energy is obtained. Water was removed and the polar hydrogen was added to the receptor protein with the help of AutoDock. A docking simulation has been formed using AutoDockVina. The Discovery studio was used to observe the ligand protein interactions. The center of the binding active sites is located at –0.044, y=0.009, z=–0.151 and it is limited in the grid box of size 40 Å ×40 Å ×40 Å of spacing 0.375 Å. The docked structure of cephalexin-1J7M is presented in Fig. 7. The various docking parameters are displayed in Table 4. The title molecule is strongly bound to the protein 1J7M protein with a binding affinity –5.9 kcal/mol. The electropositive atoms H35, H27, and the electronegative atom O2 interact non-covalently with residues GLU27, SER28, LYS25, and GLU27 of the proteins.

Thus, the formation of a total of four hydrogen bonds takes place and the length of these bonds falls in the range of 1.8814 Å to 2.5723 Å. Further, the root mean square deviation (RMSD) between the docked structure and its initial structure is less than 1.2 Å which is less than 2 Å. Hence, in general, cephalexin shows good binding activity with the protein matrix metalloproteinase-2 (PDB code: 1J7M).

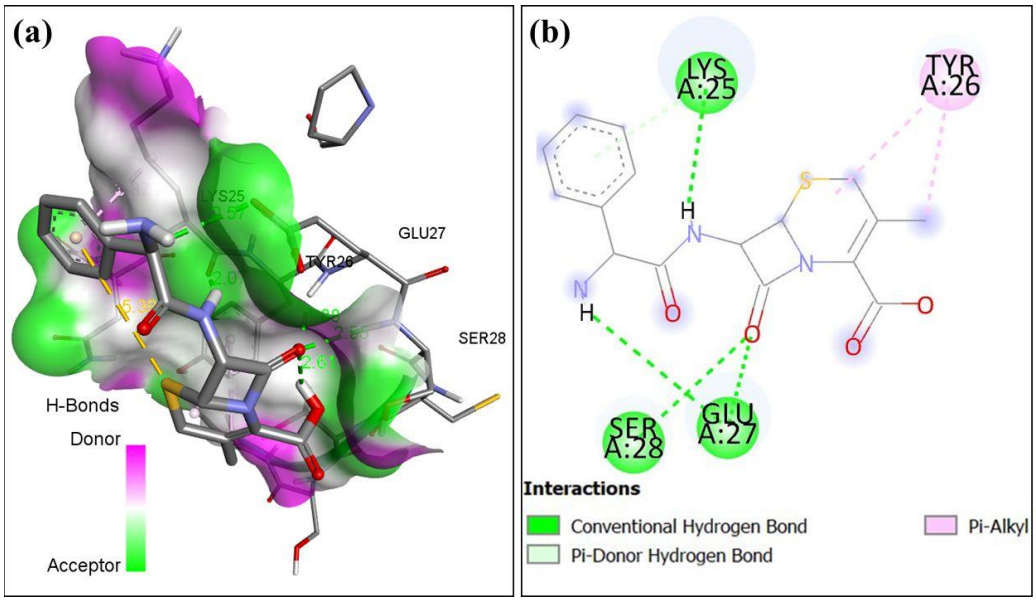

Figure 7 (a) Docked structure and (b) interactions of cephalexin with protein 1J7M.

Table 4: Docking parameters of cephalexin against the protein matrix metalloproteinase-2.

Protein	PDB code	Binding affinity (kcal/mol)	Bond length(Å)	H-Bonded Residues	Rmsdvalue (Å)	Inhibition constant (μM)
Matrixmetall-oproteinase-2	1J7M	–5.9	1.8814	GLU27	1.2	47.06
			2.5530	SER28		
			2.0745	LYS25		
			2.5723	GLU27		

CONCLUSIONS

In the present work, the analysis of electron localization function (ELF) and localized orbital locator (LOL) and non-linear optical properties, thermal properties, as well as biological activities of cephalexin has been performed using DFT/B3LYP employing 6-311++G(d,p) basis sets. The ELF and LOL map show that the localization of electrons is higher across oxygen, nitrogen and hydrogen, and carbon atoms. The calculated Mulliken atomic charges associated with carbon atoms C13 and C9 are found to be −0.9247|e| and 0.5247|e|, which are the highest negative charge and the highest positive charges, respectively. The nonlinear optical properties (NLO) have been computed. The estimated value of first hyperpolarizability ($0.4440*10^{-30}$esu) is comparable to the value of the standard molecule, urea. These properties represent the significant NLO properties. In addition, the molecule has negative second hyperpolarizability ($-0.12849*\ 10^{-35}$esu) which is very important for constructing controllable NLO devices. Furthermore, the quadratic fits, demonstrating the nature of the correlation between enthalpy, heat capacity, entropy, and temperature, are useful for the thermodynamic energies analysis. Furthermore, the binding sites of the title molecule and the protein matrix metalloproteinase-2 have been predicted. The binding affinity of the protein-molecule complex was predicted to be −5.9 kcal/mol. Thus, the molecular docking study theoretically proves that the title molecule has a good binding potential against the protein 1J7M.

ACKNOWLEDGEMENTS

We sincerely acknowledge Prof. Poonam Tandon, HOD, Department of Physics, Lucknow University, India, for providing software facilities, including the Gaussian 09 program, as well as sharing research concepts during the whole study period.

AUTHOR CONTRIBUTIONS

Both authors contributed equally.

CONFLICT OF INTERESTS

The authors declare no conflict of interests.

DATA AVAILABILITY STATEMENT

The data that support the findings of this study are available from the corresponding author, upon reasonable request.

REFERENCES

Abraham, C.S., Muthu, S., Prasana, J.C., Armaković, S., Armaković, S.J., & Geoffrey, B. (2019). Computational evaluation of the reactivity and pharmaceutical potential of an organic amine: A DFT, molecular dynamics simulations and molecular docking approach. *Spectrochimica Acta Part A: Molecular and Biomolecular Spectroscopy*, *222*, 117-188.

Abraham, C.S., Prasana, J.C., & Muthu, S. (2017). Quantum mechanical, spectroscopic and docking studies of 2-amino-3-bromo-5-nitropyridine by density functional method. *Spectrochimica Acta Part A: Molecular and Biomolecular Spectroscopy, 181*, 153-163.

Bailey, A., Hadley, A., Walker, A., & James, D.G. (1970). Cephalexina new oral antibiotic. *Postgraduate Medical Journal, 46*(533), 157.

Basha, S.J., Chamundeeswari, S.V., Muthu, S., & Raajaraman, B. (2019). Quantum computational, spectroscopic investigations on 6-aminobenzimidazole by DFT/TD-DFT with different solvents and molecular docking studies. *Journal of Molecular Liquids, 296*, 111787.

Becke, A.D. (1993). A new mixing of hartree-fock and local density-functional theories. The *Journal of Chemical Physics, 98*(2), 1372–1377.

Becke, A.D., & Edgecombe, K.E. (1990). A simple measure of electron localization in atomic and molecular systems. *The Journal of Chemical Physics, 92*(9), 5397-5403.

Chakrabarti, S., & Patel, K.D. (2005). Matrix metalloproteinase-2 (MMP-2) and MMP-9 in pulmonary pathology. *Experimental Lung Research*, *31*(6), 599-621.

Chaudhary, T., Chaudhary, M.K., & Joshi, B.D. (2021). Topological and reactivity descriptor of carisoprodol from DFT and molecular docking approach. *Journal of Institute of Science and Technology, 26*(1), 74-82.

Choudhary, N., Agarwal, P., Gupta, A., & Tandon, P. (2014). Quantum chemical calculations of conformation, vibrational spectroscopic, electronic, NBO and thermodynamic properties of 2, 2-dichloro-n-(2, 3-dichlorophenyl) acetamide and 2, 2-dichloro-n-(2, 3-dichlorophenyl) acetamide. *Computational and Theoretical Chemistry, 1032,* 27-41.

Daina, A., Michielin, O., & Zoete, V. (2019). Swiss Target Prediction: updated data and new features for efficient prediction of protein targets of small molecules. *Nucleic Acids Research, 47*(W1), W357-W364.

Dennington, R., Keith, T., & Millam, J. (2009). GaussView, version 5.

Ferreira da Costa, J., Silva, D., Caaman˜o, O., Brea, J.M., Loza, M.I., Munteanu, C.R., Pazos, A., Garc´ıa-Mera, X., & Gonz´alez-D´ıaz, H. (2018). Perturbation theory/machine learning model of chembl data for dopamine targets: docking, synthesis, and assay of new l-prolyl-l-leucyl-glycinamide peptidomimetics. *ACS Chemical Neuroscience, 9*(11), 2572-2587.

Frisch, M., Trucks, G., Schlegel, H.B., Scuseria, G.E., Robb, M.A., Cheeseman, J.R., Scalmani, G., Barone, V., Mennucci, B., Petersson, G., et al. (2009*).* Gaussian 09, revision d. 01, Gaussian. *NC., Wallingford CT, 201.*

Issaoui, N., Ghalla, H., Muthu, S., Flakus, H., & Oujia, B. (2015). Molecular structure, vibrational spectra, AIM, HOMO-LUMO, NBO, UV, first order hyperpolarizability, analysis of 3-thiophenecarboxylic acid monomer and dimer by hartree-fock and density functional theory. *Spectrochimica Acta Part A: Molecular and Biomolecular Spectroscopy, 136*, 1227-1242.

Joshi, B.D. (2016). Chemical reactivity, dipole moment and first hyperpolarizability of aristolochic acid I. *Journal of Institute of Science and Technology, 21*(1), 1-9.

Joshi, B.D., Khadka, J.B., & Bhatt, A. (2018). Structure, electronic and vibrational study of 7-methyl-2, 3-dihydro-(1, 3) thiazolo (3, 2-a) pyrimidin-5-one by using density functional theory. *Journal of Institute of Science and Technology, 22*(2), 1-11.

Joshi, B.D., Srivastava, A., Gupta, V., Tandon, P., & Jain, S. (2013). Spectroscopic and quantum chemical study of an alkaloid aristolochic acid I. *Spectrochimica Acta Part A: Molecular and Biomolecular Spectroscopy*, *116*, 258-269.

Kanayama, H.O., Yokota, K.Y., Kurokawa, Y., Murakami, Y., Nishitani, M., & Kagawa, S. (1998). Prognostic values of matrix metalloproteinase-2 and tissue inhibitor of metalloproteinase-2 expression in bladder cancer. *Cancer: Interdisciplinary International Journal of the American Cancer Society*, *82*(7), 1359-1366.

Kariper, S.E. (2017). Spectroscopic and quantum chemical studies on some β-lactam inhibitors. *Turkish Computational and Theoretical Chemistry, 1*(2), 13-26.

Koparir, M. (2013). 7, 7-bis [(aza-18-crown-6) carbonyl] thioindigo: Synthesis, experimental, theoretical characterization and biological activities. *Medicine Science, 2*(1), 386-402

Kumar, A., Kumar, R., Gupta, A., Tandon, P., & D'silva, E.D. (2017). Molecular structure, nonlinear optical studies and spectroscopic analysis of chalcone derivative (2e)-3-[4-(methylsulfanyl) phenyl]-1-(3-bromophenyl) prop-2-en-1-one by DFT calculations. *Journal of Molecular Structure, 1150*, 166-178.

Lu, T., & Chen, F. (2012). Multiwfn: a multifunctional wavefunction analyzer. *Journal of Computational Chemistry, 33(*5), 580-592.

Manelli, L.P. (1975). Cephalexin. In *Analytical profiles of drug substances* (Vol. 4, pp. 21-46). Academic Press.

Nakano, M., Kiribayashi, S., Yamada, S., Shigemoto, I., & Yamaguchi, K. (1996). Theoretical study of the second hyperpolarizabilities of three charged states of pentalene. a consideration of the structure-property correlation for the sensitive second hyperpolarizability. *Chemical Physics Letters, 262*(1-2), 66-73.

Nguyen, H.M., & Graber, C.J. (2020). A critical review of cephalexin and cefadroxil for the treatment of acute uncomplicated lower urinary tract infection in the era of bad bugs, few drugs. *International Journal of Antimicrobial Agents*, page 106085.

Ochterski, J.W. (2000). Thermochemistry in gaussian. *Gaussian Inc*, *1*, 1-19.

Parr, R.G. (1980). Density functional theory of atoms and molecules. *In Horizons of Quantum Chemistry*, pages 5-15. Springer.

Rose, P.W., Beran, B., Bi, C., Bluhm, W.F., Dimitropoulos, D., Goodsell, D.S., Prli´c, A., Quesada, M., Quinn, G.B., Westbrook, J.D., et al. (2010). The RSCB protein data bank: redesigned web site and web services. *Nucleic Acids Research, 39*(suppl 1), D392-D401.

Schmider, H.L., & Becke, A.D. (2002). Two functions of the density matrix and their relation to the chemical bond. *The Journal of Chemical Physics, 116*(8), 3184-3193.

Silvi, B., & Savin, A. (1994). Classification of chemical bonds based on topological analysis of electron localization functions. *Nature, 371*(6499), 683-686.

Singh, S., Singh, H., Karthick, T., Agarwal, P., Erande, R. D., Dethe, D. H., & Tandon, P. (2016). Combine experimental and theoretical investigation on an alkaloid–dimethylisoborreverine. *Journal of Molecular Structure, 1103*, 187-201.

Speight, T., Brogden, R., & Avery, G. (1972). Cephalexin: a review of its antibacterial, pharmacological and therapeutic properties. *Drugs, 3*(1), 9-78.

Spink, C.H., & Wadsö, I. (1975). Thermochemistry of solutions of biochemical model compounds. 4. The partial molar heat capacities of some amino acids in aqueous solution. *The Journal of Chemical Thermodynamics*, *7*(6), 561-572.

Studio, D. (2009). version 2.5. *Accelrys Inc.: San Diego, CA, USA*.

Tanchuk, V.Y., Tanin, V.O., Vovk, A.I., & Poda, G. (2016). A new, improved hybrid scoring function for molecular docking and scoring based on autodock and autodockvina. *Chemical Biology and Drug Design, 87*(4), 618-625.

Trott, O., & Olson, A.J. (2010). Autodockvina: improving the speed and accuracy of docking with a new scoring function, efficient optimization, and multithreading. *Journal of Computational Chemistry, 31*(2), 455-461.

Yang, Y. (2010). Hexacoordinate bonding and aromaticity in silicon phthalocyanine. *The Journal of Physical Chemistry A, 114*(50), 13257-13267.

A Theoretical Study on Charge Transfer and Hyperpolarizability of (S)-2-amino-3-(3,4-dihydroxyphenyl)-2-methyl-propanoic Acid

Tarun Chaudhary, Manoj Kumar Chaudhary and Bhawani Datta Joshi

Journal of Nepal Physical Society
Volume 8, No 1, 2022
(Special Issue: ICFP 2022)
ISSN: 2392-473X (Print), 2738-9537 (Online)

JNPS, **8** (1), 16-21 (2022)
DOI: http://doi.org/10.3126/jnphyssoc.v8i1.48280

Published by: Nepal Physical Society
P.O. Box: 2934
Tri-Chandra Campus
Kathmandu, Nepal
Email: nps.editor@gmail.com

ICFP 2022
ISSN: 2392-473X (Print)
2738-9537 (Online)

Research Article ©Nepal Physical Society
DOI: http://doi.org/10.3126/jnphyssoc.v8i1.48280

A Theoretical Study on Charge Transfer and Hyperpolarizability of (S)-2-amino-3-(3,4-dihydroxyphenyl)-2-methyl-propanoic Acid

Tarun Chaudhary,[1, a)] Manoj Kumar Chaudhary,[2, b)] and Bhawani Datta Joshi[3, c)]

[1)] *Central Department of Physics, Tribhuvan University, Kirtipur, Kathmandu, Nepal*
[2)] *Department of Physics, Tribhuvan University, Amrit Campus, Institute of Science and Technology, Kathmandu 44600, Nepal*
[3)] *Department of Physics, Tribhuvan University, Siddhanath Science Campus, Mahendranagar, 10406, Nepal*

[a)] *Electronic mail: chaudharytarun167@gmail.com*
[b)] *Electronic mail: manojkc054@gmail.com*
[c)] *Corresponding Author: bhawani.joshi@snsc.tu.edu.np, pbdjoshi@gmail.com*

Abstract. The DFT approach was used to investigate the antihypertensive molecule (S)-2-amino-3-(3,4-dihydroxyphenyl)-2-methyl-propanoic acid at the B3LYP/6-311++G(d,p) level of theory. The electron-hole analysis of three excited states has been performed, in which the maximum charge transfer length (2.727Å) has been calculated for the first excited state and the minimum for the third excited state (1.626 Å). On the other hand, the electron-hole overlap is found to be almost negligible for the first excited state and it is found to be maximum for the second excited state. The variation of thermodynamic properties with temperature is studied. The correlation graphs are obtained between the thermodynamic quantities (heat capacity, enthalpy, entropy) and temperature with a very high value of R^2 (>0.99). The values of dipole moment, mean polarizability, anisotropy of polarizability, first hyperpolarizability and second hyperpolarizability are found to be 3.5250 Debye, 12.6980×10-24esu, 19.8162×10^{-24}esu, 0.9017×10^{-30}esu and -0.0412×10^{-35}esu, respectively. These values are higher than the value of urea.

Keywords: Charge transfer, Nonlinear optical (NLO) properties, Thermodynamic properties

Received:20 March 2022; **Revised**:15 April 2022; **Accepted**:5 May 2022.

1. INTRODUCTION

Methyldopa, also known as (S)-2-amino-3-(3,4-dihydrox yphenyl)-2-methyl-propanoic acid, is a centrally acting antihypertensive medication [1]. Methyldopa consists of an amino acid skeleton with a pyrocatechol group and a methyl group. It contains amine, carboxylic acid and hydroxyl functional groups. It lowers blood pressure by acting through a central mechanism involving the biotransformation of methyl norepinephrine [2]. Methyldopa is the most preferred medicine for the treatment of preeclampsia and gestational hypertension [3]. However, it has some side effects like impairment of renal function, depression, sedation and bad dreams [3, 4]. Since methyldopa has fewer side effects on infants, it is considered a safer medicine to use by a breast feeding mother [5]. The literature review reveals combined density functional theory (DFT) studies on structures in different solvents, molecular electrostatic surface potential (MEP), natural bond orbital (NBO) analysis and vibrational studies on the title molecule [2, 6, 7] Methyldopa exhibits an electropositive region over oxygen atoms and a negative region over hydrogen atoms of hydroxyl groups [6]. The study on frontier molecular orbitals and energy gaps indicates intramolecular charge transfer in the molecule [7]. The energy gap of methyldopa is generally found to be lower than the energy gap of its derivatives [6, 8]. The majority of the previous work on the title molecule was done with small basis sets. On the other hand, higher basis sets with polarized and diffused functions are required for more accurate and reliable results [9]. Hence, the present work has been conducted using B3LYP/6-311++G(d,p). The electron-hole distribution has been analysed, which provides additional verification of the intramolecular charge transfer. The variation of thermodynamic properties with varying temperatures has been

studied and essential thermodynamic relations have been deduced. Furthermore, methyldopa, being an organic molecule, should possess significant nonlinear optical (NLO) properties [10]. Thus, the quantities like dipole moment, mean polarizability, anisotropy of polarizabilty, first hyperpolarizability and second hyperpolarizability has been determined. The optimized structure of the methyldopa at B3LYP/6-311++G(d,p) has been shown in Fig. 1.

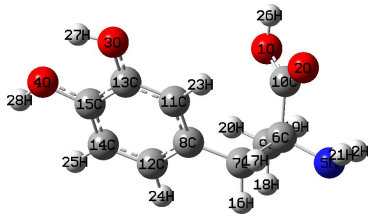

FIGURE 1: Optimized structure of methyldopa at B3LYP/6-311++G(d,p).

2. MATERIALS AND METHODS

2.1 Computational Aspects

The computational study of methyldopa monomer has been performed using density functional theory (DFT) [11] employing the Gaussian 09 program [12]. The molecule's geometry was optimized using the B3LYP/6-311++(d,p) level of theory [13, 14]. Gaussview 05 software [15] was used to visualize and interpret the output data of Gaussian-09. The electron-hole distribution in the molecule has been analysed using Multiwfn 3.8 [16]. The non-linear optical properties and thermal properties have been computed at the B3LYP/6-311++(d,p) level of theory.

For the characterization of a charge transfer (CT) due to excitation in a molecule, the electron-hole overlapping and charge transfer lengths are calculated using the given relations [17].

The electron hole overlapping

$$S_r = \int \sqrt{\rho^{hole}(r)\rho^{ele}(r)} \tag{1}$$

Charge Transfer length

$$D = \sqrt{D_X^2 + D_y^2 + D_z^2} \tag{2}$$

where, $D_x = X_{ele} - X_{hole}$, $D_y = Y_{ele} - Y_{hole}$ and $D_Z = Z_{ele} - Z_{hole}$.

Here, X_{ele}, Y_{ele} and Z_{ele} represents X, Y and Z coordinates of centroid of electron and X_{hole}, Y_{hole} and Z_{hole} represents X, Y and Z coordinates of centroid of hole.

The quantity describing NLO properties like first hyperpolarizabilty (β_0) and second hyperpolarizability (γ_0) alongwith dipole moment (μ_0), mean polarizability ($|\alpha_0|$) and anisotropy of polarizability ($\Delta\alpha$), can be calculated using
the equations [18, 19]:

$$\mu_0 = (\mu_X^2 + \mu_y^2 + \mu_z^2)^{1/2} \tag{3}$$

$$|\alpha_0| = \frac{1}{3}(\mu_{xx} + \mu_{yy} + \mu zz) \tag{4}$$

$$\Delta\alpha = 2^{-1/2}[(\alpha_{xx} - \alpha_{yy})^2 + (\alpha_{yy} - \alpha_{zz})^2 + (\alpha_{zz} - \alpha_{xx})^2 + 6\alpha_{xx}^2]^{1/2} \tag{5}$$

$$\beta_0 = [(\beta_{xxx} + \beta_{xyy} + \beta_{xzz})^2 + (\beta_{yyy} + \beta_{xxy} + \beta_{yzz})^2 + (\beta_{zzz} + \beta_{xxy} + \beta_{yyz})^2]^{1/2} \tag{6}$$

$$\gamma_0 = \frac{1}{5}[\gamma_{xxxx} + \gamma_{yyyy} + \gamma_{zzzz} + 2(\gamma_{xxyy} + \gamma_{yyzz} + \gamma_{zzxx})] \tag{7}$$

The thermodynamic properties of a system are determined by the Boltzmann distribution and the partition function q(V, T) [20].The contributions to entropy, enthalpy, and heat capacity result from translational, rotational, electronic and vibrational motion. The partition functions used for different motions can be stated as below [21]. Translational partition function,

$$q_t = \left(\frac{2\pi m k_B T}{h^2}\right)^{3/2} V \tag{8}$$

Rotational partition function,

$$q_r = \frac{1}{\sigma_r}\left(\frac{T}{\theta_r}\right) \tag{9}$$

Electronic partition function

$$q_e = \omega_0^{-\varepsilon_0/k_B T} + \omega_1^{-\varepsilon_1/k_B T} + \omega_2^{-\varepsilon_2/k_B T} + \ldots \tag{10}$$

Vibrational partition function

$$q_k = \Pi_k \frac{1}{1 - e^{\Theta_{v,k/T}}} \tag{11}$$

where, k_B represents Boltzmann constant, ω represents degeneracy of the energy level, ε_n is the energy of the n-th level and $\Theta = h^2/8^2 I k_B$.

3. RESULT AND DISCUSSIONS

3.1 Electron-Hole Distribution

The charge transfer (CT) due to excitation in the molecule, is scrutinized by analyzing the CT due to excitation using Multiwfn. In the only case, in which the excitation is directly represented by the HOMO-LUMO transition, the hole and electron are equivalent to HOMO and LUMO, respectively [17]. The plots of electron-hole (green-blue) distribution for different excited states and their respective electron-hole overlap (S) have been shown in Fig. 2. The values for electron-hole overlap integral (S), charge transfer length (D) and Δr for all three excitation modes are presented in Table 1. The charge transfer-length (D) represents the distance between the centroid of electrons and the centroid of holes, and Δr represents the quantitative electron excitation mode [22].The overlap integral for the first, second and third excited states is found to be 0.2706, 0.5825, 0.4500 and their charge transfer length is found to be 2.727 Å, 1.831 Å and 1.626 Å, respectively. The electron-hole analysis showed that, first and third excited states have large value of Δr index (>2Å) hence, the CT is probable in these two states. However, the overlap integral (S) of electron-hole is higher for the third excited state than the first excited state, the charge transfer is less probable in the third excited state. Besides this, the charge transfer length (D) is also high in the first excited state, which means the charge transfer is more probable in the first excited state. Therefore, on the basis of overlap integral and charge transfer length, it is concluded that the first excited state corresponds to strong intra molecular charge transfer due to excitation.

TABLE I: Overlap integral of electron-hole, charge transfer length (D), Δr and excitation energy of first, second and third excited states of methyldopa.

Excitation states	Overlap integral (S)	Charge transfer length (D)(Å)	Δ r (Å)	Excitation energy(E)eV
First	0.2706	2.727	2.7642	4.612
Second	0.5825	1.831	1.8493	4.705
Third	0.4500	1.626	2.9874	4.995

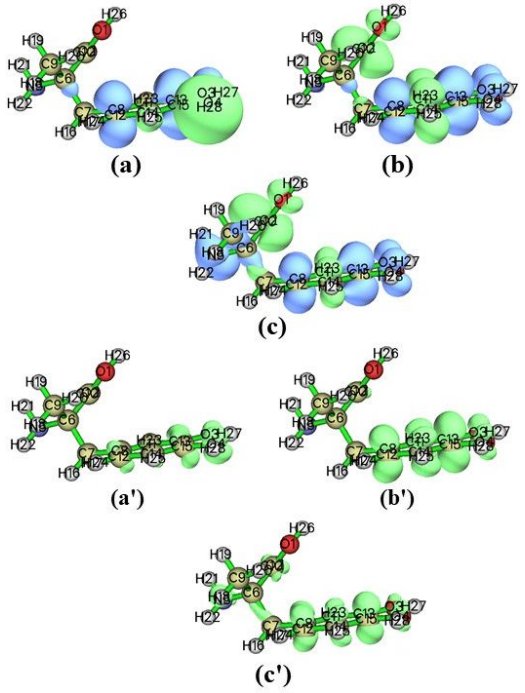

FIGURE 2: Electron-hole excitation of (a) first, (b) second (c) third excited states and overlap for (a') first, (b') second, (c') third excited states.

3.2 NLO Properties

The molecules that have π- conjugated interaction between donor-acceptor group can exhibit significant nonlinear optical (NLO) properties [23, 24]. NLO properties are applicable for optical signal processing, telecommunication, optical computing, etc [24]. The estimated value of the quantity The dipole moment (μ_0), mean polarizability ($|\alpha_0|$), anisotropy of polarizability ($\Delta\alpha$),first hyperpolarizability (β_0) and second hyperpoarizabilty(γ_0) describing the NLO phenomena of methyldopa has been delineated in Table 2. The estimated value of first hyperpolarizability 0.9017×10^{-30} esu is slightly greater than the value of reference molecule urea 0.3728×10^{-30} esu). But, the value of first hyperpolarizability calculated by Prabakaran and Muthu using the 6-31G(d,p) basis set was 3.782×10^{-30} esu [7]. This difference in the value may be due to use of different basis sets for the calculation. The value of μ_0, $|\alpha_0|$, $\Delta\alpha$, β_0 and γ_0 is found to have the negative value, -0.0412×10^{-35} esu. The negative value of γ_0 is one of the important factors that can be utilized in constructing NLO devices with controllable NLO properties [24, 25]. Hence, the molecule could be a potential candidate for studying NLO properties in the future.

3.3 Thermodynamic Properties

Thermodynamic properties are used to assess the drug molecule's stability and chemical reactivity [26, 27]. Boltzmann distribution and partition function are used to evaluate the thermodynamic parameters. In the literature, the variation of thermodynamic quantities of methyldopa have been studied at each interval of 100K [7]. How-

TABLE II: The estimated dipole momentμ_o, mean polarizability $|\alpha_o|$, anisotropy of polarizability $\Delta\alpha_o$, first hyperpolarizability β_o and second hyperpolarizability γ_o of methyldopa.

Dipole moment Debye	Polarizability ($\times10^{-24}$esu)	First hyperpolarizability ($\times10^{-30}$esu)	Second hyperpolarizabilty ($\times10^{-35}$esu)
μ_x= 1.6148	α_{xx} = -76.8156	β_{xxx} = 54.7143	γ_{xxxx}= -2741.6992
μ_y= -1.8569	α_{xy} = -6.6647	β_{xxy} = -12.4652	γ_{yyyy}= -911.8254
μ_z= 2.5238	α_{yy} = -89.8383	β_{xyy} = 24.8604	γ_{zzzz}= -432.5846
μ_o= 3.5250	α_{xz} = 0.1714	β_{yyy} = 4.2333	γ_{xxyy}= -676.5233
μ_o(Urea)= 1.3732	α_{yz} = 1.3593	β_{xxz} = 37.0746	γ_{xxzz}= -605.0103
	α_{zz} = -90.3878	β_{xyz} = -6.741	γ_{yyzz}= -611.3782
	$\|\alpha_o\|$ = 12.6980	β_{yyz} = 12.7285	γ_o= -211.7205
	$\Delta\alpha_o$ = 19.8162	β_{xzz} = 12.0654	
	$\Delta\alpha_o$(Urea) = 9.7710	β_{yzz} = 6.9303	
		β_{yzz} = 10.2229	
		β_o = 0.4440	

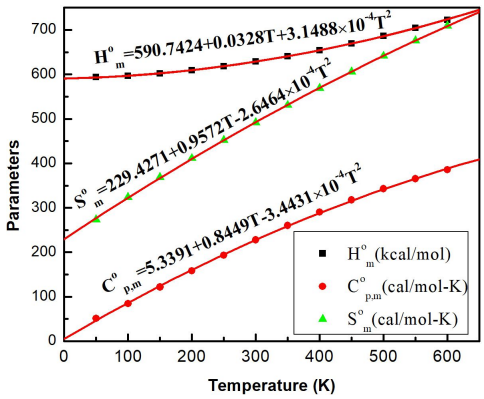

FIGURE 3: Correlation of enthalpy, heat capacity, entropy and temperature for methyldopa.

ever, to study the behavior of thermodynamic quantities more precisely, we have studied these properties even at a smaller interval of 50K.The variation of thermodynamic properties has been observed in the range of 50 K to 600 K. The estimated values of thermodynamic parameters are tabulated in Table 3. The graph representing variation of heat capacity, enthalpy and entropy with respect to temperature has been depicted in Fig. 3. As stated by an earlier study, these three quantities are positively correlated with temperature. The values of R^2 were found to be 1, 0.9995 and 0.9999 for enthalpy, heat capacity and entropy. The positive value of R^2 states that all the thermodynamic properties increase with the increasing temperature due to the reason that vibrational energy of the molecules increases with the temperature [28]. The given equations represent the correlation of enthalpy (H^o_m), heat capacity $(C^o_{p,m})$, entropy (S^o_m) and temperature.

$$H^o_m = 590.7424 + 0.0328T + 3.1488 \times 10^{-4}T^2 \quad (12)$$

$$C^o_{p,m} = 1.2755 + 0.2019T - 8.2253 \times 10^{-4}T^2 \quad (13)$$

$$S^o_m = 229.4271 + 0.9572T - 2.6464 \times 10^{-4}T^2 \quad (14)$$

Further, utilizing the above equations, the Gibbs free energy can be determined, which further helps to judge the spontaneity of the reactions. In addition, these thermodynamic relations are helpful for studying the thermodynamic energies and estimating the direction of the reaction according to the second law of thermodynamics[18].

4. CONCLUSION

The intramolecular charge transfer, thermal properties and non-linear optical properties of methyldopa have been determined using DFT method at the B3LYP/6-311++G(d,p) level of approximation. In the electron-hole analysis of three excited states, the first excited state, was found to have the highest charge transfer length (2.727Å) and a negligible electron-hole overlap (S=0.2706). Hence, the intramolecular charge transfer due to excitation corresponds to the first excited states. The thermodynamic relations of heat capacity, enthalpy, and entropy have been obtained, which is useful in determining the spontaneity and direction of the reaction. A very high positive correlation is found be-

TABLE III: Thermodynamic parameters of methyldopa at various temperature.

Temperature (K)	Enthalpy (Kcal/Mol)	Heat capacity Cal/Mol-Kelvin)	Entropy (Cal/Mol-Kelvin)	Zero-point energy (Joules/Mol)	Total energy (eV)
50	141.863	12.223	65.349	591651.1	-20260.7940
100	142.661	20.173	77.474	591651.1	-20260.7940
150	143.894	29.130	88.159	591651.1	-20260.7940
200	145.569	37.794	98.304	591651.1	-20260.7940
250	147.670	46.210	108.089	591651.1	-20260.7940
300	150.186	54.369	117.603	591651.1	-20260.7940
350	153.100	62.136	126.879	591651.1	-20260.7940
400	156.390	69.369	135.920	591651.1	-20260.7940
450	160.027	75.984	144.713	591651.1	-20260.7940
500	163.978	81.964	153.243	591651.1	-20260.7940
550	168.213	87.339	161.501	591651.1	-20260.7940
600	172.703	92.167	169.484	591651.1	-20260.7940

tween the thermodynamic properties and the temperature. This indicates that the thermodynamic properties increase with the increase in temperature due to the increase of molecular vibrations. The title molecule has a higher dipole moment (3.5250 Debye), mean polarizabilty (12.6980×10^{-24}esu), and the first hyperpolarizability (0.9017×10^{-30}esu) than urea. In addition, it has a negative value of second hyperpolarizability (-0.0412×10^{-35}esu), which makes it more suitable for constructing NLO devices. Hence, methyldopa exhibits significant NLO properties and could be a good candidate for NLO devices.

ACKNOWLEDGEMENT

We sincerely acknowledge Prof Poonam Tandon, former HoD, Department of Physics, Lucknow University, India, for providing software facilities, including the Gaussian 09 program.

REFERENCES

1. Mah, G. T.; Tejani, A. M.; and Musini, V. M. Methyldopa for primary hypertension. Cochrane Database of Systematic Reviews, (4) (2009).

2. Noei, M.; Holoosadi, M.; and Anaraki-Ardakani, H. Design of methyldopa structure and calculation of its properties by quantum mechanics. Arabian Journal of Chemistry, 10, S1923-S1937 (2017).

3. Wiciński, M.; Malinowski, B.; Puk, O.; Socha, M.; and Słupski, M. Methyldopa as an inductor of postpartum depression and maternal blues: A review. Biomedicine Pharmacotherapy, 127: 110196 (2020).

4. Oparil, S. Review of therapeutic modalities acting directly via central pathways. Clinical and Experimental Hypertension. Part A: Theory and Practice, 4(4-5): 579-593 (1982).

5. Amro, F. H.; Moussa, H. N.; Ashimi, O. A.; and Sibai, B. M. Treatment options for hypertension in pregnancy and puerperium. Expert Opinion on Drug Safety, 15(12), 1635-1642(2016).

6. Merza, M. M.; Hussein, F. M.; and AL-ani, R. R. Physical properties and biological activity of methyldopa drug carrier cellulose derivatives. Theoretical study. Egyptian Journal of Chemistry, 64(8), 4081-4090(2021).

7. Prabakaran, A.; and Muthu, S. Normal coordinate analysis and vibrational spectroscopy (FT-IR and FT-Raman) studies of (2S)-2-amino-3-(3, 4-dihydroxyphenyl)-2-methylpropanoic acid using ab initio HF and DFT method. Spectrochimica Acta Part A: Molecular and Biomolecular Spectroscopy, 99: 90-96, (2012).

8. da Silva Gomes, D.; de Lima, J. D. M.; Frazão, N. F.; and Sarmento, R. G. A quantum biochemical study on optoelectronic and vibrational properties of the peripheral inhibitor l-alpha-methyldopa hydrazine. Educação, Ciência e Saúde, 4(1)(2017).

9. Chaudhary, T.; Chaudhary, M. K.; Joshi, B. D.; de Santana, M. S. A.; and Ayala, A. P. Spectroscopic (FT-IR, Raman) analysis and computational study on conformational geometry, AIM and biological activity of cephalexin from DFT and molecular docking approach. Journal of Molecular Structure, 1240: 130594 (2021).

10. Kariper, S. E. Spectroscopic and quantum chemical studies on some -lactam inhibitors. Turkish Computational and Theoretical Chemistry, 1(2), 13-26(2017).

11. Hohenberg, P.; and Kohn, W. Inhomogeneous electron gas. Physical review, 136(3B) 864–871 (1964).

12. Frisch, M.J.; Trucks, G.W.; Schlegel, H.B.; Scuseria, G.E.; Cheeseman, J.R.; Robb, M.A.; Scalmani, G.;

Barone, V.; Mennucci, B.; Petersson, G.A.; Nakatsuji, H.; Caricato,M.; Li, X.; Hratchian, H.P.; Izmzylov, A.F.; Bloino, J.; Zheng, G.; Sonnenberg, J.L.; Hada, M.; Ehara, M.; Toyota, K.; Fukuda, R.; Ishida, J.; Hasegawa, M.; Nakajima, T.; Honda, Y.; Kitao, O.; Nakai, H.; Vreven, T.; Montgomery Jr.; J.A.; Peralta, J.E.; Ogliaro, F.; Bearpark, M.; Heyd, J.J.; Brothers, E.; Kudin, K.N.; Staroverov, V.N.; Kobayashi, R.; Normand, J. , Raghavachari, A.; Rendell, A.; Burant, J.C.; Iyengar, S.S.; Tomasi, J.; Cossi, M.; Rega, N.; Millan, J.M.; Klene, M.; Knox, J.E.; Cross, J.B.; Bakken, V.; Adamo, C.; Jaramillo, J.; Gomperts, R.; Stratmann, R.E.; Yazyev, O.; Austin, A.J.; Cammi, R.; Pomelli, C.; Ochterski, J.W.; Martin, R.L.; Morokuma, K.; Zakrzewski, V.G.; Voth, G.A.; Salvador, P.; Dannerberg, J.J.; Dapprich, S.; Daniels, A.D.; Farkas, J.; Foresman, B.; Ortiz, J.V.; Cioslowski, J.; Fox, D.J. GAUSSIAN 09, Revision, Gaussian, Inc.; Wallingford CT, (2009).

13. Becke, A. D. A new mixing of Hartree–Fock and local density-functional theories. The Journal of chemical physics, 98(2), 1372-1377 (1993).

14. Parr, R. G. Density functional theory of atoms and molecules. In Horizons of Quantum Chemistry, pages 5-15. Springer, (1980).

15. Frisch, A.; Nielson, A. B.; and Holder, A. J. Gaussview user manual. Gaussian Inc., Pittsburgh, PA, 556 (2000).

16. Lu, T.; and Chen, F. Multiwfn: a multifunctional wavefunction analyzer. Journal of Computational Chemistry, 33(5) 580-592 (2012).

17. Liu, Z.; Lu, T.; and Chen, Q. (2020). An sp-hybridized all-carboatomic ring, cyclo [18] carbon: Electronic structure, electronic spectrum, and optical nonlinearity. Carbon, 165, 461-467.

18. Joshi, B. D.; Mishra, R.; Tandon, P.; Oliveira, A. C.; and Ayala, A. P. Quantum chemical studies of structural, vibrational, NBO and hyperpolarizability of ondansetron hydrochloride. Journal of Molecular Structure, 1058: 31-40 (2014).

19. Kumar, A.; Kumar, R.; Gupta, A.; Tandon, P.; and D'silva, E. D. Molecular structure, nonlinear optical studies and spectroscopic analysis of chalcone derivative (2e)-3-[4-(methylsulfanyl) phenyl]-1-(3-bromophenyl) prop-2-en-1-one by DFT calculations. Journal of Molecular Structure, 1150:166-178 (2017).

20. Singh, S.; Singh, H.; Karthick, T.; Agarwal, P.; Erande, R. D.; Dethe, D. H.; and Tandon, P. Combine experimental and theoretical investigation on an alkaloid–dimethylisoborreverine. Journal of Molecular Structure, 1103: 187-201 (2016).

21. Ochterski, J. W. Thermochemistry in gaussian. Gaussian Inc, 1, 1-19 (2000).

22. Guido, C. A.; Cortona, P.; Mennucci, B.; and Adamo, C. On the metric of charge transfer molecular excitations: a simple chemical descriptor. Journal of chemical theory and computation, 9(7), 3118-3126(2013).

23. Venkatesan, P.; Thamotharan, S.; Ilangovan, A.; Liang, H.; and Sundius, T. Crystal structure, Hirshfeld surfaces and DFT computation of NLO active (2E)-2-(ethoxycarbonyl)-3-[(1-methoxy-1-oxo-3-phenylpropan-2-yl) amino] prop-2-enoic acid. Spectrochimica Acta Part A: Molecular and Biomolecular Spectroscopy, 153: 625-636 (2016).

24. Pandey, M.; Muthu, S.; and Gowda, N. N. Quantum mechanical and spectroscopic (FT-IR, FT-Raman, 1H, 13C NMR, UV-Vis) studies, NBO, NLO, HOMO, LUMO and Fukui function analysis of 5-Methoxy-1H-benzo [d] imidazole-2 (3H)-thione by DFT studies. Journal of Molecular Structure, 1130: 511-521 (2017).

25. Nakano, M.; Kiribayashi, S.; Yamada, S.; Shigemoto, I.; and Yamaguchi, K. Theoretical study of the second hyperpolarizabilities of three charged states of pentalene. a consideration of the structure-property correlation for the sensitive second hyperpolarizability. Chemical Physics Letters, 262(1-2): 66-73 (1996).

26. Bhuvaneswari, M.; Santhakumari, R.; Usha, C.; Jayasree, R.; and Sagadevan, S. Synthesis, growth, structural, Spectroscopic, optical, Thermal, DFT, HOMO–LUMO, MEP, NBO analysis, and Thermodynamic properties of vanillin isonicotinic hydrazide single crystal. Journal of Molecular Structure, 130856 (2021).

27. Chaudhary, M. K.; Prajapati, P.; and Joshi, B. D. Quantum Chemical Calculation and DFT Study of Sitagliptin: Insight from Computational Evaluation and Docking Approach. Journal of Nepal Physical Society, 6(1): 73-83 (2020).

28. Abraham, C. S.; Muthu, S.; Prasana, J. C.; Armaković, S. J.; Armaković, S.; and AS, B. G. Spectroscopic profiling (FT-IR, FT-Raman, NMR and UV-Vis), autoxidation mechanism (H-BDE) and molecular docking investigation of 3-(4-chlorophenyl)-N, N-dimethyl-3-pyridin-2-ylpropan-1-amine by DFT/TD-DFT and molecular dynamics: A potential SSRI drug. Computational biology and chemistry, 77: 131-145(2018).

Journal of Institute of Science and Technology, 26(1), 74-82 (2021)
ISSN: 2469-9062 (print), 2467-9240 (e)
https://doi.org/10.3126/jist.v26i1.37828

Research Article

TOPOLOGICAL AND REACTIVITY DESCRIPTOR OF CARISOPRODOL FROM DFT AND MOLECULAR DOCKING APPROACH

Tarun Chaudhary[1], **Manoj Kumar Chaudhary**[1,2], **Bhawani Datt Joshi**[3*]

[1]*Central Department of Physics, Tribhuvan University, Kirtipur, Kathmandu, Nepal*
[2]*Department of Physics, University of Lucknow, Lucknow-226007, India*
[3]*Department of Physics, Siddhanath Science Campus, Tribhuvan University, Mahendranagar, 10406, Nepal*
[*]*Corresponding author: bhawani.joshi@snsc.tu.edu.np, pbdjoshi@gmail.com*

(***Received**: February 05, 2021; **Revised**: June 01, 2021; **Accepted**: June 08, 2021)*

ABSTRACT

This study aims to investigate the optimized structure and optimized parameters of carisoprodol from the DFT/B3LYP/6-31G(d,p) level of theory. The molecular electrostatic potential (MEP) map signifies that the positive potential across hydrogen of the amine group (NH_2) and the negative potential around the carbonyl groups (C=O). HOMO-LUMO energy gap was found to be 8.1064 eV. The global and local reactivity parameters describe the possible chemical reactive sites in the molecule. The topological analysis of the electron localization function (ELF) and localized orbital locator (LOL) revealed that the charge localization around hydrogen atoms. The hyper-conjugative interaction between donor and acceptor orbital showed that the interaction LP(2) O4→ σ*(O2-C16) plays a vital role in the molecular stability. The molecular docking simulation encircles that the carisoprodol behaves as a good inhibitor with the target protein, Tyrosine-protein kinase ABL.

Keywords: Carisoprodol, Electrostatic potential, Energy gap, Orbital locator, Molecular docking

INTRODUCTION

Carisoprodol ($C_{12}H_{24}N_2O_4$), chemically known as (RS)-2-{[(aminocarbonyl)oxy]methyl}-2-methyl pentyl isopropyl carbamate is a centrally acting muscle-skeletal relaxant (Reeves *et al.*, 1999). It is used to treat a craniomandibular disorder, sciatica, lumbago, and other lower back syndromes (Kumar *et al.*, 2017; Horio *et al.*, 2004). Literature reveals that the recent works on carisoprodol were mainly focused on its physical, chemical, and biological properties. Bolattin *et al.* (2016) studied biomolecular interactions of carisoprodol with bovine serum albumin by fluorescence and UV-visible spectroscopy along with a molecular docking approach. Further, the thermal behavior and dynamic fragility in its amorphous state were studied by Diogo *et al.* (2018).

Recently, Liu *et al.* (2020) studied the binding activity of carisoprodol on GABA (Gamma-Aminobutyric Acid) receptor by both docking and molecular dynamics (MD) simulation methods. Chaudhary *et al.* (2021a) performed AIM analysis and investigated vibrational spectra and the nonlinear optical (NLO) properties of the title molecule. However, the structural and spectroscopic properties like calculation of optimized parameters, NBO analysis, HOMO and LUMO energies, MEP, global and local reactivity, the electron localization function (ELF), and the localized orbital locator (LOL) have not been conducted so far. Hence, the present work is mainly concentrated to explore these properties to study the chemical and biological activities of the molecule. The calculations have been performed by using the functional B3LYP/6-31G (d,p) and the result is closer to the experimental one (Horio *et al.*, 2004).

MATERIALS AND METHODS

The quantum mechanical study of carisoprodol was performed using the Gaussian 09 program package (Frisch *et al.*, 2009). The geometry was optimized through density functional theory (DFT) calculation by employing the functional B3LYP/6-31G(d,p) (Becke, 1993; Parr & Yang, 1989). The GaussView 05 program was used to visualize and interpret the output data of Gaussian 09. It was used to plot HOMO, LUMO, and MEP maps. Furthermore, Multiwfn 3.4.1 (Lu & Chen, 2012) and VMD 1.9.1 (Humphrey *et al.*, 1996) program packages were used for computation and visualization of ELF (electron localization function) and LOL (localized molecular orbital). The molecular docking of carisoprodol has been carried out with AutoDock-Vina software (Trott & Olson, 2010) and ligand-protein interaction has been visualized with bio visualizer software (Studio, 2009).

To determine the chemical reactivity of carisoprodol, molecular electrostatic potential map, the energy of the highest occupied molecular orbital (E_H) and the lowest occupied molecular orbital (E_L), energy gap (E_L–E_H), global reactivity, and local reactivity descriptors have been calculated. The molecular electrostatic potential V(r) (Sjoberg *et al.*, 1990) which is used to generate MEP was calculated using the equation (1).

$$V(r) = \sum_A \frac{Z_A}{|\overrightarrow{R_A} - \vec{r}|} - \int \frac{\rho(\overrightarrow{r'})}{|\overrightarrow{r'} - \vec{r}|} \quad (1)$$

Where, Z_A and $\rho(\vec{r'})$ are nuclear charge and electron density respectively.

The chemical potential (μ) of a system is the first-order partial derivatives of energy (E) for the number of electrons (N) at constant external potential V(r).

$$\mu = \left(\frac{\partial E}{\partial N}\right)_{V(r)} = -\chi \quad (2)$$

The words hardness (η) and softness (S) were first introduced by Pearson to check the direction of the acid-base reaction as well as to gain the stability of the product. From the Koopmans theorem, η is half of the energy gap between HOMO and LUMO which signifies to bear the resistance of the system to take or give up electrons. The global hardness which is the inverse of softness is the second-order derivative of energy (E) concerning the number of electrons (N) at constant external potential V(r).

$$\eta = \frac{1}{2}\left(\frac{\partial^2 E}{\partial N^2}\right)_{V(r)} = \frac{1}{2}\left(\frac{\partial \mu}{\partial N}\right)_{V(r)} \quad (3)$$

Electrophilicity index (ω) is introduced by Parr and Pearson (1983) which is a global reactivity descriptor. It is the characteristics of atoms that include the reduction of energy procedure during the absorption of electrons from the donors. The chemical reactivity of the molecule is analyzed in terms of electrophilicity index (ω). It measures the stabilization in energy as the molecule gain external electronic charge from neighboring donor species.

Global reactivity descriptor is used to determine the reactivity of a molecule. Koopman's theorem described the global reactivity parameters like electronegativity (χ), chemical potential (μ), hardness (η), electrophilicity index (ω) and softness (S) are estimated using the equations (4)-(9) (Parr & Pearson, 1983; Joshi, 2016).

$$\chi = -\frac{1}{2}(E_L + E_H) \quad (4)$$

$$\mu = -\chi = \frac{1}{2}(E_L + E_H) \quad (5)$$

$$\eta = \frac{1}{2}(E_L - E_H) \quad (6)$$

$$S = \frac{1}{2\eta} \quad (7)$$

$$\omega = \frac{\mu^2}{2\eta} \quad (8)$$

$$\Delta Nmax = -\frac{\mu}{\eta} \quad (9)$$

Here, ω measures the stabilization energy after the system gains the extra charge (ΔN) from neighboring molecules and ΔN_{max} is the maximum charge gained by electrophile (Parr *et al.*, 1999). Fukui functions help to predict the particular site for the chemical activity. The high values of Fukui functions f(r) indicate the high reactivity (Yang & Parr., 1985). The Fukui functions $f_A^+(r)$, $f_A^-(r)$ and $f_A^0(r)$ corresponds to the nucleophilic, electrophilic, and radial attacks respectively. The given Fukui equations for the nucleophilic, electrophilic, and radial attack are:

$$f_A^+(r) = [q_A(N+1) - q_A(N)] \quad (10)$$

$$f_A^-(r) = [q_A(N) - q_A(N-1)] \quad (11)$$

$$f_A^0(r) = \frac{1}{2}[q_A(N+1) - q_A(N-1)] \quad (12)$$

Where, q_A is an atomic charge of the A^{th} atomic site corresponding to neutral (N), anionic (N+1), or cationic (N-1) chemical state of the molecule.

To interpret the charge delocalization in a molecule, NBO analysis had been performed using the same level of theory. The given equation which is based on second-order perturbation theory was used to compute the stabilization energy (E2) between the donor and the acceptor groups (Prajapati *et al.*, 2016; Reed *et al.*, 1988):

$$E(2) = E(i,j) = q_i \frac{F_{ij}^2}{(E_j - E_i)} \quad (13)$$

Where, q_i, E_i, E_j, and F_{ij} are donor orbital occupancy, donor orbital energy, acceptor orbital energy, and off-diagonal elements of the Fock-matrix, respectively.

RESULTS AND DISCUSSION

Geometrical parameters

The geometry of carisoprodol was fully optimized at the DFT-B3LYP level using a 6-31G(d,p) basis set. The optimized structure of carisoprodol is shown in Fig. 1. The comparative study of optimized parameters (bond lengths, bond angles, and dihedral angles) with the geometry of crystal structure (Horio *et al.*, 2004) has been presented in Table 1. Almost all the calculated values are approximately equal to its crystal structure parameters.

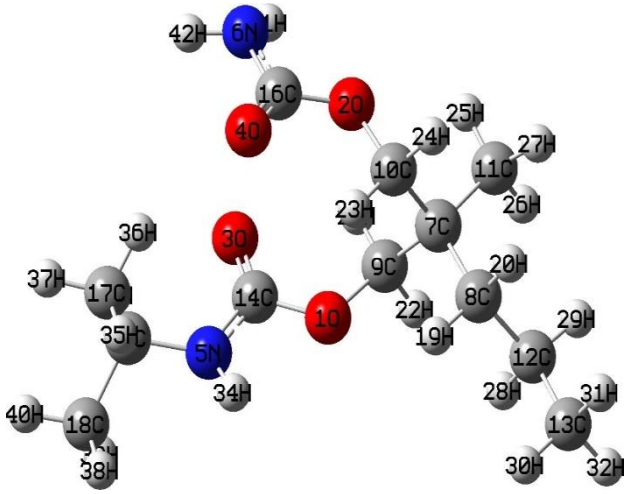

Fig. 1. Optimized structure of carisoprodol

The calculated values of bond lengths N5-H34, N6-H41, and N-H42 are 0.891, 0.966, and 0.779 Å, whereas their respective crystal structure values are 1.011, 1.010, and 1.009 Å. Similarly, the optimized bond angles (C14-N5-H34), (C15-N5-H34), and (C16-N6-H41) are calculated as 116.16°, 118.46° and 116.38°, and the crystal structure values are 113.07°, 107.86° and 119.34°, respectively. The difference in structural parameters is due to the intermolecular hydrogen bonding in solid form. However, this work is based on computational evaluation for a single isolated molecule in the gaseous state.

Molecular electrostatic potential

The molecular electrostatic potential (MEP) map is an important tool to explain the chemical reactivity, hydrogen bonding, and structural activity of different biomolecules including drugs (Joshi *et al.*, 2014). Based on the mapped potential energy surface, the relative polarity of molecule, chemically reactive sites can be predicted. On the MEP, the red surface shows the most electronegative region and the blue surface shows the most positive region.

Table 1. Selected optimized parameters of carisoprodol

Bond length (Å)	Crystal	Calculated	Bond angles (°)	Crystal	Calculated
(O1,C9)	1.448	1.440	(C9,O1,C14)	115.06	116.91
(O1,C14)	1.360	1.369	(C14,N5,C15)	121.70	122.16
(O2,C10)	1.450	1.440	(C14,N5,H34)	113.07	116.16
(O2,C16)	1.343	1.362	(C15,N5,H34)	107.86	118.46
(O3,C14)	1.214	1.221	(C16,N6,H41)	119.34	116.38
(O4,C16)	1.222	1.218	(C16,N6,H42)	115.86	113.88
(N5,C14)	1.379	1.359	(H41,N6,H42)	124.73	115.72
(N5,C15)	1.445	1.465	(O2,C10,C7)	108.71	110.30
(N5,H34)	0.891	1.011	(O2,C10,H23)	107.56	108.72
(N6,C16)	1.348	1.368	(O1,C13,O3)	124.93	124.62
(N6,H41)	0.966	1.010	(O1,C13,N5)	109.66	109.58
(N6,H42)	0.779	1.009	(O3,C13,N5)	125.35	125.78
(C7,C9)	1.550	1.539	(N5,C15,C17)	110.85	111.24

Dihedral Angles (°)	Crystal	Calculated
(C8,C12,C13,H30)	58.53	59.7365
(C8,C12,C13,H31)	-50.69	-60.066
(H28,C12,C13,H31)	177.50	177.8358
(H29,C12,C13,H31)	66.77	62.1842
(C18,C15,C17,H35)	63.98	59.0411
(C18,C15,C17,H36)	178.09	179.0676
(C18,C15,C17,H37)	-56.33	-60.0656
(C18,C15,C17,H35)	63.98	59.0411

Further, the lighter color or almost white surface explains the non-polar nature of molecules. The MEP counter map of carisoprodol is shown in Fig. 2 which demonstrates negative regions over O3 and O4 and positive regions over H34, H41, and H42. The region over oxygen of carbonyl groups, C14=O3 and C16=O4 are almost equal whereas the region over hydrogen (H41 and H42) of primary amine are comparatively more positive than the region over hydrogen of secondary amine (H34). The molecular docking analysis shows that the atoms O1, O2, O3, and O4 actively participated in hydrogen bonding with the protein during the ligand-protein interaction.

HOMO-LUMO analysis

The chemical stability of molecules depends upon the energy of the highest occupied molecular orbital (HOMO) and the lowest unoccupied molecular orbital (LUMO). The orbital energy HOMO (E_H) acts as the electron donor and the orbital energy LUMO (E_L) acts as the electron acceptor and their energy gap (E_L-E_H) determines the

chemical reactivity of the molecule (Chaudhary *et al.*, 2021b; Joshi *et al.*, 2018). The probability of electronic transition activity increases with the increase in the energy gap and vice-versa (Fukui, 1982). To understand the chemical stability of carisoprodol, time-dependent DFT calculations have been performed employing the B3LYP/6-31G (d, p) level of theory. The energy gap for carisoprodol is obtained as 8.1064 eV. The HOMO-LUMO plot of the molecule shown in Fig. 3 signifies that the electron density in HOMO is concentrated on O1, C14=O3, and N5H34 whereas the charge diverges on C16=O4 and $N6H_2$ in LUMO.

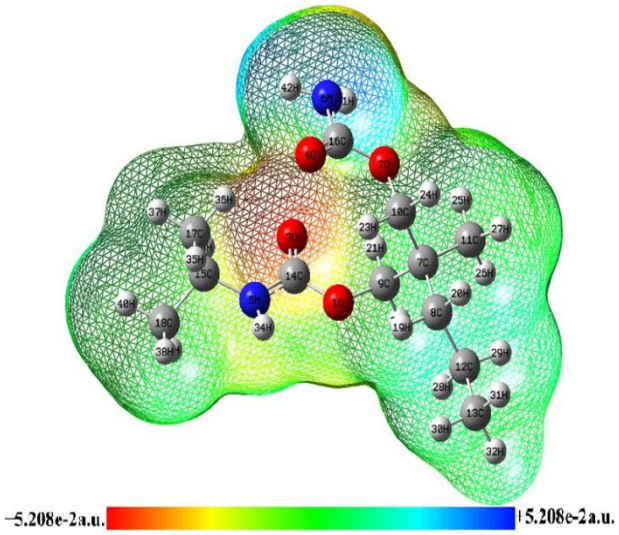

Fig. 2. Molecular electrostatic potential map of carisoprodol

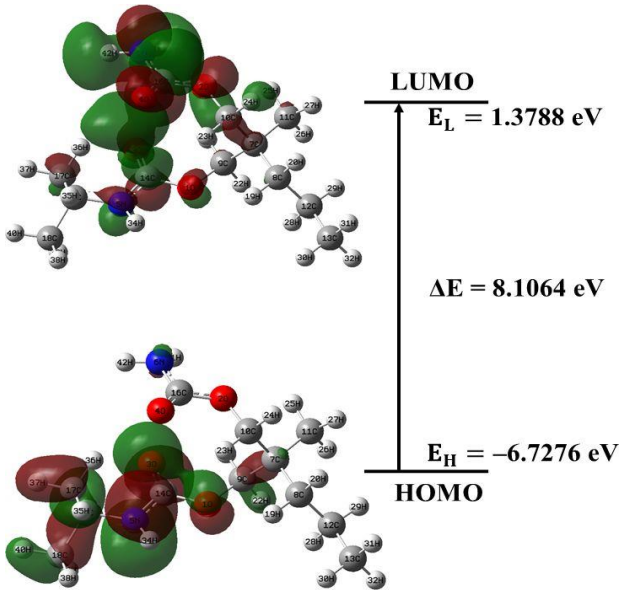

Fig. 3. HOMO and LUMO plot of carisoprodol

Global reactivity

The high value of μ and ω indicates good electrophilic behavior and low-value μ and ω indicates nucleophilic behavior of the molecules, respectively (Chaudhary *et al.*, 2020; Joshi, 2017). The electrophilicity index (ω) and softness (S) describes the stability of the molecules. The chemical activity increases with a decrease of the energy gap ($E_L - E_H$) and vice-versa. The values of frontier molecular orbitals (FMOs) energies with their energy gap ($E_L - E_H$) and parameters; χ, μ, η, ω and S are illustrated in Table 2.

Table 2. Calculated E_H, E_L energy, band gap (E_L–E_H), chemical potential (μ), electronegativity (χ), global hardness (η), global softness (S), and global electrophilicity index (ω) for carisoprodol

E_H (eV)	E_L (eV)	$E_L - E_H$ (eV)	χ (eV)	μ (eV)	η (eV)	S $(eV)^{-1}$	ω (eV)
–6.7276	1.3788	8.1064	2.6744	–2.6744	4.0532	0.1234	0.8823

Local reactivity

To explore the quantitative reactive site, the local reactivity descriptors parameters have been calculated. Fukui functions help to predict the particular site for the chemical reactivity. To investigate the particular sites for nucleophilic and electrophilic attack more precisely, we have performed Fukui function analysis. The local reactivity descriptors of the title molecule have been presented the Table 3. The analysis of local reactivity descriptors shows that the most probable nucleophilic and electrophilic sites of the molecule are C16 and C14, respectively.

Topological analysis (ELF and LOL)

The density-based description of chemical bonding, the electron localization function (ELF), and the localized orbital locator (LOL) were introduced in literature (Becke & Edgecombe, 1990; Schmider & Becke, 2002). The ELF and LOL exhibit similar interpretations based on kinetic energy density in which, electron pair density is considered in ELF, and gradients of localized orbitals were recognized in LOL (Schmider & Becke, 2000; Rizwana *et al.*, 2020). The values of ELF and LOL fall within the range 0-1, whereas values greater than 0.5 indicate the region of localized electrons and the values smaller than 0.5 indicate the region for delocalized electrons. The value of ELF is high if Pauli's repulsion is high and vice versa. The localized electrons represent the atomic shells, chemical bonds, and lone pair electrons (Abraham *et al.*, 2018).

The Topological analysis of ELF and LOL of the title molecule based on covalent bonds has been performed

using Multiwfn software. The ELF and LOL map of electrons are presented in Figs. 4(a) and 4(b), respectively. The region around the hydrogen atom is depicted by the red region (high LOL values) which is due to maximum Pauli repulsion. The red region around O2 and N5 indicates the presence of localized electron lone pairs. Similarly, the covalent bond region between carbon atoms is characterized by red color showing a high degree of electron localization in that place. On the other hand, the blue ring (low LOL values) region is obtained around the nucleus of O2, C7, C12, C15, and N5 which is the region between the inner shell and valence shell showing a very low degree of electron localization in that zones.

Table 3. Calculated local reactivity properties of the selected atoms using Hirshfeld [B3LYP/6-31G (d,p)] derived charges of carisoprodol

Site	f_k^+	Site	f_k^-	Site	f_k^0
N5	0.71809	C14	0.45364	C16	0.484545
N6	0.54164	C16	0.4298	C14	0.462195
O4	0.47303	C15	-0.03689	C15	-0.03287
O3	0.44081	C7	-0.05088	C7	-0.04419
C17	0.39192	C10	-0.06599	C10	-0.05063
C18	0.36003	C9	-0.06719	C9	-0.05111
O1	0.35283	C12	-0.24017	N5	-0.15244
C11	0.34618	C8	-0.24339	C12	-0.2241
C13	0.33921	O2	-0.28615	C8	-0.22981
O2	0.31333	O1	-0.29079	O1	-0.26587
C8	0.23454	O4	-0.32017	O4	-0.26713
C12	0.23021	O3	-0.33656	O2	-0.28333
C9	0.06022	N5	-0.34209	O3	-0.28569
C7	0.05691	C13	-0.34877	C17	-0.32884
C10	0.05691	C18	-0.3557	C18	-0.33597
C15	0.02592	C11	-0.35806	C13	-0.3382
C16	-0.49487	C17	-0.36145	C11	-0.34277
C14	-0.51843	N6	-0.44489	N6	-0.38874

Natural bond orbital (NBO) analysis

NBO analysis is the fundamental tool to interpret the delocalization of charge from donor Lewis type (occupied) orbitals to acceptor Lewis type (unoccupied) orbitals or lone pair to acceptor orbital, within the molecule, to check the stability of the molecular system (Chaudhary *et al.*, 2021c). The stabilization energy E(2) is determined by the second-order perturbation theory. Higher the value of E(2), the stronger the interaction between donor and acceptor orbital, and vice versa. For carisoprodol, the NBO analysis has been carried out by B3LYP/6-31G(d,p) and the selected hyper-conjugative interaction of stabilization energy E(2) greater than 5 kcal/mol is presented in Table 4.

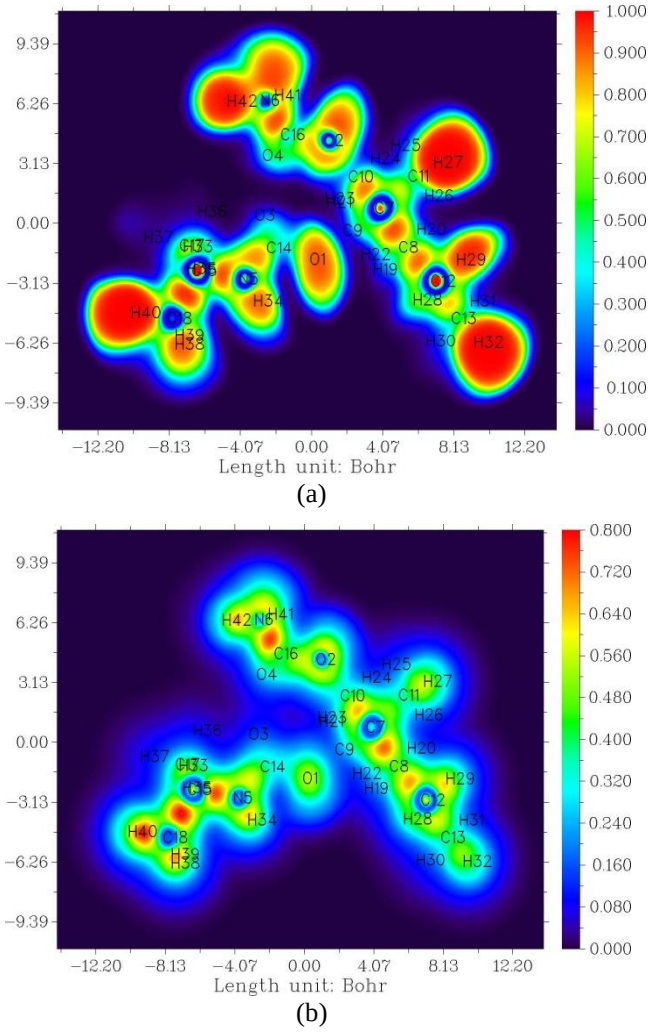

Fig. 4. ELF color-filled map of carisoprodol (a) and LOL color-filled map of carisoprodol (b)

In the carisoprodol the donor orbitals are generally associated with O1, O2, O3, O4, N5, and N6 whereas the acceptor orbitals are mainly concentrated across (O3-C14), (O2-C16), and (O4-C16). The transition from LP(2)O1 → σ*(O3-C14)/ π*(O3-C14) stabilizes the molecule with respected energies 6.12/19.32 kcal/mol. Similarly, the strongest interaction LP(2)O4 → σ*(O2-C16) gives the highest stabilization energy 33.19 kcal/mol. Moreover, the transition which participates for the stability of a molecule is LP(2)O3 → σ*(O1-C14), LP(1)N5 → π*(O3-C14), LP(2)O2 → π*(O4-C16), and LP(2)O4 → σ*(N6-C16), with the corresponding stabilization energy 33.02, 26.12, 23.95, and 22.37 kcal/mol. Also, the overlapping of σ(N6-H42) → σ*(O2-C16) and LP(1)N5 → σ*(O3-C14) stabilizes the molecule to some extent with interaction energy 5.05 and 9.01 kcal/mol, respectively.

Molecular docking of carisoprodol

The molecular docking simulation is a very popular tool to study ligand-protein interaction and to investigate the insight properties of the drug molecule (Chaudhary *et al.*, 2021d). In the present work, to study the biological activities of carisoprodol (ligand), the docking analysis has been conducted by using AutoDock-Vina software. The target protein, Tyrosine-protein kinase ABL has been predicted with the help of Swiss Target Prediction (Gfeller *et al.*, 2014). It is a human protein that is known to be essential for transforming activity (Buchdunger *et al.*, 1996). The PDB structure of this protein (1awo) has been downloaded from the RSCB PDB data bank (Rose *et al.*, 2010). Further, the Ramchandran Plots of the protein have been presented in Fig. 5.

Table 4. Second-order perturbation theory analysis of Fock matrix in NBO basis of carisoprodol

Donor NBO(i)	ED (i)/e	Acceptor NBO(j)	ED(j)/e	E(2)[a] kcal/mol	E(j)-E(i)[b] a.u.	F(i,j)[c]a.u.
σ(N6-H42)	1.98354	σ*(O2-C16)	0.10895	5.05	1.02	0.065
LP(1)O1	1.96128	σ*(O3-C14)	0.13671	6.99	0.97	0.075
LP(2)O1	1.83349	σ*(O3-C14)	0.13671	6.12	0.73	0.060
LP(2)O1	1.83349	π*(O3-C14)	0.27031	19.32	0.51	0.091
LP(2)O2	1.82575	π*(O4-C16)	0.26555	23.95	0.49	0.099
LP(2)O3	1.82617	σ*(O1-C14)	0.10898	33.02	0.60	0.128
LP(2)O3	1.82617	σ*(N5-C14)	0.06741	22.12	0.73	0.116
LP(2)O4	1.83134	σ*(O2-C16)	0.10895	33.19	0.61	0.129
LP(2)O4	1.83134	σ*(N6-C16)	0.06426	22.37	0.70	0.115
LP(1)N5	1.73537	σ*(O3-C14)	0.13671	9.01	0.67	0.072
LP(1)N5	1.73537	π*(O3-C14)	0.27031	26.12	0.45	0.097
LP(1)N5	1.73537	σ*(C15-C17)	0.02192	6.20	0.64	0.060
LP(1)N6	1.79977	σ*(O4-C16)	0.11244	8.03	0.74	0.070
LP(1)N6	1.79977	π*(O4-C16)	0.26555	20.26	0.46	0.088

[a]E(2) means the energy of hyper conjugative interaction (stabilization energy); [b]Energy difference between the donor (i) and acceptor (j) NBO orbitals and [c]F(i,j) is the Fock matrix element between i and j NBO orbitals

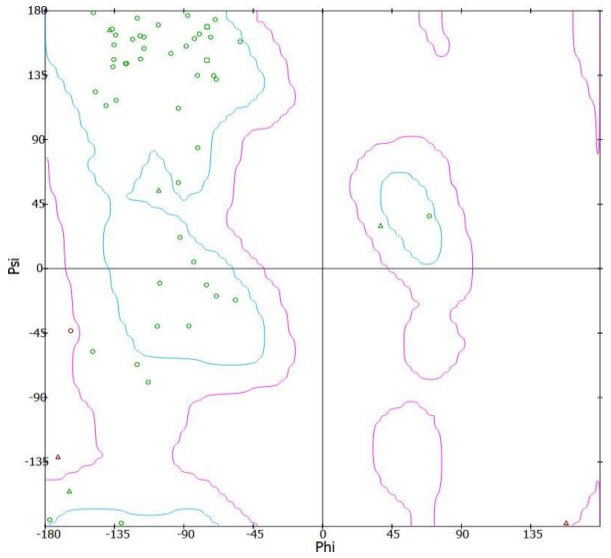

Fig. 5. Ramchandran plot of 1wao

The regions inside the first blue line indicate allowed ones and those outside it indicate disallowed regions, respectively. Hence, the maximum number of residues lies within the allowed region. The optimized structure of carisoprodol (ligand) obtained at B3LYP/6-31G(d,p) has been used for the docking analysis. The protein (receptor) was prepared by removing water molecules and co-crystallized ligand from the protein and further, the polar hydrogen and Kollman charges were added. The grid box of size 60 Å × 60 Å × 60 Å has been used for studying the binding activities.

The discovery studio was used for the visualization of ligand-protein interaction. The ligand-protein interaction and LiGPLOT are shown in Figs. 6(a) and 6(b). The binding affinity, bond length, bonded residues, and inhibition constant of the docked complex of carisoprodol and 1wao have been presented in Table 5. The atoms O1, O2, O3, and O4 form six hydrogen bonds with the amino acids SER75, GLY76, ASN78, THR79, THR79, and

THR79. The binding energy of docked structure of the investigated molecule with the protein was found to be -5 kcal/mol. Hence, carisoprodol shows strong binding activity with the protein 1wao.

Table 5. The docking parameters of docked structure of carisoprodol and 1wao

Protein	PDB code	Binding affinity (kcal/mol)	Bond length(Å)	Bonded Residues	Types of H-bond	Inhibition constant (μM)
Tyrosine-protein kinase ABL	1awo	-5.0	2.7604	SER75	H-bond	215.16
			2.8959	GLY76	H-bond	
			2.3335	ASN78	H-bond	
			2.3037	THR79	H-bond	
			2.2572	THR79	H-bond	
			2.7032	THR79	H-bond	

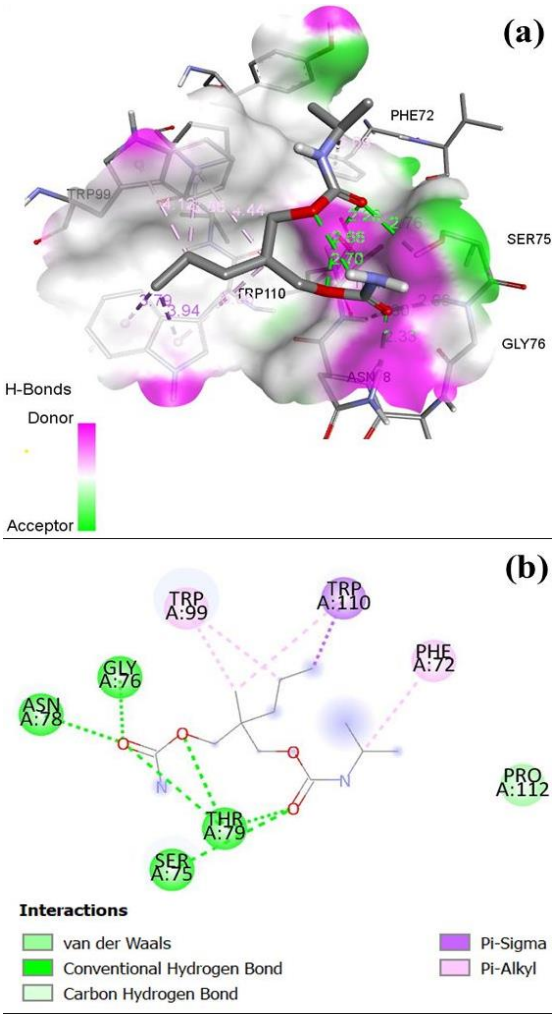

Fig. 6. (a) Docking of carisoprodol with 1wao and (b) LIGPLOT of docking of carisoprodol with 1wao

CONCLUSION

The optimized geometrical parameters and crystal geometrical parameters of carisoprodol were almost in resonance. The energy gap between HOMO and LUMO was found to be 8.1064 eV. Due to the high value of Fukai functions, the nucleophilic and electrophilic sites are predicted as C16 and C14, respectively. The molecular electrostatic potential map explorers are the negative and positive potentials associated with the carbonyl and amine groups, respectively. ELF and LOL topological analysis signifies that most of the localized electrons were predicted around hydrogen, oxygen, nitrogen, and between carbon atoms.

Further, the NBO analysis demonstrates the intramolecular charge transfer between lone pair LP(2)O4 and σ*(O2-C16), which contribute the highest value of stabilization energy 33.19 kcal/mol. The molecular docking simulation revealed that the carisoprodol strongly binds with the protein 1wao. Also, the oxygen atom of all carbonyl groups actively participated in hydrogen bonding to form a complex.

ACKNOWLEDGEMENT

Authors sincerely acknowledge to Prof. Poonam Tandon, HOD Physics and Dean Student Welfare, University of Lucknow, India for providing software facilities including Gaussian 09 as well as sharing research ideas during the project.

REFERENCES

Abraham, C. S., Prasana, J. C., Muthu, S., & Raja, M. (2018). Quantum computational studies, spectroscopic (FT-IR, FT-Raman, and UV-Vis) profiling, natural hybrid orbital, and molecular docking analysis on 2, 4 Dibromoaniline. *Journal of Molecular Structure*, *1160*, 393-405.

Becke, A. D. (1993). A new mixing of Hartree–Fock and local density-functional theories. *The Journal of Chemical Physics*, *98*(2), 1372-1377.

Becke, A. D., & Edgecombe, K. E. (1990). A simple measure of electron localization in atomic and

molecular systems. *The Journal of Chemical Physics*, *92*(9), 5397-5403.

Bolattin, M. B., Nandibewoor, S. T., Joshi, S. D., Dixit, S. R., & Chimatadar, S. A. (2016). Interaction between carisoprodol and bovine serum albumin and effect of β-cyclodextrin on binding: insights from molecular docking and spectroscopic techniques. *RSC Advances*, *6*(68), 63463-63471.

Buchdunger, E., Zimmermann, J., Mett, H., Meyer, T., Müller, M., Druker, B. J., & Lydon, N. B. (1996). Inhibition of the Abl protein-tyrosine kinase in vitro and in vivo by a 2-phenylaminopyrimidine derivative. *Cancer Research*, *56*(1), 100-104.

Chaudhary, M. K., Chaudhary, T., & Joshi, B. D. (2021a). Simulated spectra (IR and Raman), NLO, AIM, and molecular docking of carisoprodol from DFT approach. *Bibechana*, *18*(1), 48-57.

Chaudhary, M. K., Karthick, T., Joshi, B. D., Prajapati, P., de Santana, M. S. A., Ayala, A. P., Reeda, V. S. J., & Tandon, P. (2021b). Molecular structure and quantum descriptors of cefradine by using vibrational spectroscopy (IR and Raman), NBO, AIM, chemical reactivity, and molecular docking. *Spectrochimica Acta Part A: Molecular and Biomolecular Spectroscopy*, *246*, 118976. https://doi.org/10.1016/j.saa.2020.118976

Chaudhary, M. K., Prajapati, P., Srivastava, K., Silva, K. F., Joshi, B. D., Tandon, P., & Ayala, A. P. (2021c). Molecular interactions and vibrational properties of ricobendazole: Insights from quantum chemical calculation and spectroscopic methods. *Journal of Molecular Structure*, *1230*, 129889. https://doi.org/10.1016/j.molstruc.2021.129889

Chaudhary, M. K., Srivastava, A., Singh, K. K., Tandon, P., & Joshi, B. D. (2020). Computational evaluation on molecular stability, reactivity, and drug potential of frovatriptan from DFT and molecular docking approach. *Computational and Theoretical Chemistry*, *1191*, 113031. https://doi.org/10.1016/j.comptc.2020.113031

Chaudhary, T., Chaudhary, M. K., Joshi, B. D., de Santana, M. S. A., & Ayala, A. P. (2021d). Spectroscopic (FT-IR, Raman) analysis and computational study on conformational geometry, AIM and biological activity of cephalexin from DFT and molecular docking approach. *Journal of Molecular Structure*, *1240*, 130594. https://doi.org/10.1016/j.molstruc.2021.130594

Diogo, H. P., Ramos, J. J. M., & Piedade, M. F. M. (2018). Thermal behavior and dynamic fragility in amorphous carisoprodol. Correlation between the dynamic and thermodynamic fragilities. *Thermochimica Acta*, *663*, 99-109.

Frisch, M. J., Trucks, G. W., Schlegel, H. B., Scuseria, G. E., Cheeseman, J. R., Robb, M. A., & Fox, D. J., (2009). GAUSSIAN 09, revision, Gaussian, Inc., Wallingford CT.

Fukui, K. (1982). Role of frontier orbitals in chemical reactions. *Science*, *218*(4574), 747-754.

Gfeller, D., Grosdidier, A., Wirth, M., Daina, A., Michielin, O., & Zoete, V. (2014). Swiss target prediction: a web server for target prediction of bioactive small molecules. *Nucleic Acids Research*, *42*(1), W32-W38

Horio, K., Tanaka, R., Akama, H., Haramura, M., Tanaka, A., Akimoto, T., & Hirayama, N. (2004). Crystal structure of carisoprodol. *Analytical Sciences: X-ray Structure Analysis Online*, *20*, x43-x44.

Humphrey, W., Dalke, A., & Schulten, K. (1996). VMD: visual molecular dynamics. *Journal of Molecular Graphics*, *14*(1), 33-38.

Joshi, B. D. (2016). Chemical reactivity, dipole moment and first hyperpolarizability of aristolochic acid I. *Journal of Institute of Science and Technology*, *21*(1), 1-9.

Joshi, B. D. (2017). Structural, electronic and vibrational study of 4, 6-dichloro-5-methyl pyrimidine: A DFT approach. *Journal of Institute of Science and Technology*, *22*(1), 51-60.

Joshi, B. D., Khadka, J. B., & Bhatt, A. (2018). Structure, electronic and vibrational study of 7-methyl-2, 3-dihydro-(1, 3) thiazolo (3, 2-A) pyrimidine-5-one by using density functional theory. *Journal of Institute of Science and Technology*, *22*(2), 1-11.

Joshi, B. D., Mishra, R., Tandon, P., Oliveira, A. C., & Ayala, A. P. (2014). Quantum chemical studies of structural, vibrational, NBO and hyperpolarizability of ondansetron hydrochloride. *Journal of Molecular Structure*, *1058*, 31-40.

Kumar, K. A., Lakshmipathi, V. S., Meenakshi, S., & Balakrishnan, M. H. (2017). Synthesis and characterization of potential impurity of muscle relaxant drug carisoprodol. *Journal Chemistry and Chemical Sciences*, *7*(4), 352-360.

Liu, J., Huang, R., & Claudio, M. (2020). Determining the binding site of carisoprodol on GABAA receptor. https://hdl.handle.net/20.500.12503/30337

Lu, T., & Chen, F. (2012). Multiwfn: a multifunctional wave function analyzer. *Journal of Computational Chemistry*, *33*(5), 580-592.

Parr, R. G., & Pearson, R. G., (1983). Absolute hardness: companion parameter to absolute electronegativity. *Journal of the American Chemical Society. 105*(26), 7512-7516.

Parr, R. G., & Yang, W. (1989). *Density-functional theory of atoms and molecules*. Oxford University Press, New York Oxford. https://doi.org/10.1002/qua.560470107

Parr, R. G., Szentpály, L. V., & Liu, S. (1999). Electrophilicity index. *Journal of the American Chemical Society*, *121*(9), 1922-1924.

Prajapati, P., Pandey, J., Shimpi, M. R., Srivastava, A., Tandon, P., Velaga, S. P., & Sinha, K. (2016). Combined spectroscopic and quantum chemical studies of ezetimibe. *Journal of Molecular Structure*, *1125*, 193-203.

Reed, A. E., Curtiss, L. A., & Weinhold, F. (1988). Intermolecular interactions from a natural bond orbital, donor-acceptor viewpoint. *Chemical Reviews*, *88*(6), 899-926.

Reeves, R. R., Carter, O. S., Pinkofsky, H. B., Struve, F. A., & Bennett, D. M. (1999). Carisoprodol (Soma) abuse potential and physician unawareness. *Journal of Addictive Diseases*, *18*(2), 51-56.

Rizwana, B. F., Prasana, J. C., Muthu, S., & Abraham, C. S. (2020). Vibrational spectroscopy, reactive site analysis and molecular docking studies on 2-[(2-amino-6-oxo-6, 9-dihydro-3H-purin-9-yl) methoxy]-3-hydroxypropyl (2S)-2-amino-3-methyl butanoate. *Journal of Molecular Structure*, *1202*, 127274.

Rose, P. W., Beran, B., Bi, C., Bluhm, W. F., Dimitropoulos, D., Goodsell, D. S., Prlic, A., Quesada, M., Quinn, G. B., Westbrook, J. D., Young, J., Yukich, B., Zardecki, C., Berman, H. M., & Bourne, P. E. (2010). The RCSB protein data bank: redesigned website and web services. *Nucleic Acids Research*, *39*(sup. l 1), D392-D401.

Schmider, H. L., & Becke, A. D. (2000). Chemical content of the kinetic energy density. *Journal of Molecular Structure: Theochem*, *527*(1-3), 51-61.

Schmider, H. L., & Becke, A. D. (2002). Two functions of the density matrix and their relation to the chemical bond. *The Journal of Chemical Physics*, *116*(8), 3184-3193.

Sjoberg, P., Murray, J. S., Brinck, T., & Politzer, P. (1990). Average local ionization energies on the molecular surfaces of aromatic systems as guides to chemical reactivity. *Canadian Journal of Chemistry*, *68*(8), 1440-1443.

Studio, D. (2009). *Version 2.5 guide*. San Diego, CA: Accelrys Inc., *p. 92121.*

Trott, O., & Olson, A. J., (2010). AutoDock Vina: Improving the speed and accuracy of docking with a new scoring function, efficient optimization, and multithreading. *Journal of Computational Chemistry*, *31*, 455-461.

Yang, W., & Parr, R. G. (1985). Hardness, softness, and the Fukui function in the electronic theory of metals and catalysis. *Proceedings of the National Academy of Sciences*, *82*(20), 6723-6726.

iCiAST-2021

5th International Conference on
Innovative Approaches in Applied Sciences and Technologies
03-05 December 2021

Jointly-Organized by :

Scientific Educational Research Society
Meerut 250004 (U.P.) India

Babasaheb Bhimrao Ambedkar University
(A Central Univ.) Lucknow (U.P.) India

In Collaboration with

Ch. Charan Singh University,
Meerut (U.P.) India

Scientific and Applied Research Center
Meerut (U.P.) India

Certificate

This is to certify that Dr./Mr./Mrs./Ms. Tarun Chaudhary

Research Scholar, Tribhuvan University, Kirtipur, Nepal

presented a paper in Online mode (Oral) *Spectroscopic and quantum chemical studies on cephalexin*

in an International Conference (iCiAsT-2021) during 03-05 December 2021 at Babasaheb Bhimrao Ambedkar University (A Central University), Lucknow (U.P.) India

Dr. Hemant K. Gautam
Chief Scientist & Professor
CSIR-IGIB, New Delhi, India

Prof. Sanjay Kumar
Dean, School of Agril. Sci. & Tech.
BBAU, Lucknow (U.P.) India

Prof. Vijay Garg
Principal, Kisan (P.G.) College
Simbhaoli, Hapur (U.P.) India

Nepal Physical Society

Ghantaghar, Kathmandu, Nepal

International Conference on Frontiers of Physics -2022

(ICFP-2022)

This Certificate of appreciation is awarded to

Tarun Chaudhary

from IOST, Tribhuvan University, Nepal for his oral presentation on the

"Topology (ELF, LOL) analysis, chemical activity and hyperpolarizability study of aldomet: Antihypertensive drug." in the

International Conference on Frontiers of Physics -2022

held on January 22-24, 2022 via virtual platform.

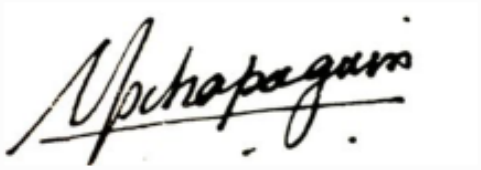

Prof. Dr. Narayan P. Chapagain

Conference Chair, ICFP-2022

President, Nepal Physical Society

February 1, 2022

Certificate of Appreciation

THIS CERTIFICATE IS PRESENTED TO

MR. TARUN CHAUDHARY

Central Department of Physics, Nepal

FOR YOUR PRESENTATION DURING THE ANPA CONFERENCE 2021

Nmalakar

DR. NABIN MALAKAR
CONVENER, ANPA CONFERENCE 2021

DR. JAGAN DEVKOTA
PRESIDENT, ANPA

St. Xavier's College

Maitighar, Kathmandu, Nepal

Department of Physics

This e-certificate of appreciation is awarded to **Mr. Tarun Chaudhary** of Central Department of Physics, Kritipur, Nepal for oral presentation on the title **"Spectroscopic and computational study of structural, chemical, AIM, AND molecular analysis on CEPHALEXIN"** in the

"International Conference on Material Science and Characterization Technology (ICMSCT)"

held on **September 26-28, 2021**

Mr. Drabindra Pandit	Fr. Dr. Augustine Thomas, S.J.	Prof. Dr. Bhim Prasad Subedi
Head,	Principal	Chairperson, University
Department of Physics	St. Xavier's College	Grants Commission Nepal

Nepal Physical Society

Ghantaghar, Kathmandu

Certificate of Participation

This certificate is awarded to

Mr. Tarun Chaudhary **from**

Central Department of Physics, TU, Nepal, for his presentation entitled

The structural, quantum mechanical and molecular docking studies of carisoprodol

On Scientific Session of 37th Annual Convention, February 6, 2021.

Prof. Dr. Narayan Prasad Chapagain	**Dr. Sunil Babu Shrestha**	**Prof. Dr. Leela Pradhan Joshi**
President	Chief Guest	Chair, Scientific Committee
Nepal Physical Society	Vice – Chancellor, NAST	37th Annual Convention, NPS

February 6, 2021

Regional Seminar on

Research Methodology, Project Selection and Scientific Writing

(RMPSW-2077)

Organized by

NEPAL PHYSICAL SOCIETY SUDURPASCHIM CHAPTER

CERTIFICATE

This is to certify that

Mr. Tarun Chaudhary, Bardiya

Delivered keynote Lecture/ Invited Lecture/ Presented/ Participated

at RMPSW-2077.

Dr. Gopi Chandra Kaphle
Secretary
NPS, Central Committee

Prof. Dr. Choodamani Joshi
Chief Guest

Dr. Bhawani Datt Joshi
Chairman
Organizing Committee

ALTEM TECHNOLOGIES

DDU GORAKHPUR UNIVERSITY

BIOVIA

This is to certify that

Tarun Chaudhary

Tribhuvan University, Kirtipur, Kathmandu, Nepal

participated in ***Online Workshop on Computer Aided Drug Design using BIOVIA Discovery Studio*** *organized by Department of Physics, Deen Dayal Upadhyaya Gorakhpur University, Gorakhpur, during 13 & 14 August 2020.*

(Dr. Ambrish K. Srivastava)	(Prof. Shantanu Rastogi)	(Prof. S. N. Tiwari)
Organizing Secretary	Convener	Chairperson

Nepal Academy of Science and Technology (NAST)

Khumaltar, Lalitpur

CERTIFICATE

Awarded to

Tarun Chaudhary

for active participation/paper presentation/poster presentation

in the

CONFERENCE ON SCIENCE AND TECHNOLOGY

"Science and Technology for Prosperous Federal Nepal"

May 21-22, 2018

Mahendranagar, Kanchanpur

Ramila

Mrs. Ramila Shrestha Raut
Chief
Promotion Division

Buddhi

Dr. Buddhi Ratna Khadge
Secretary
NAST

Prof. Dr. Jiba Raj Pokharel
Vice-Chancellor
NAST